Poly(ethylene glycol)-based Hydrogel to Support Endothelialization and Vascularization by Endothelial Progenitor Cells

by

Wen Jun Seeto (Aaron)

A Dissertation Submitted to the Graduate Faculty of
Auburn University
in Partial Fulfillment of the
Requirements for the Degree of
Doctor of Philosophy

Auburn, Alabama
December 13, 2014

Keywords: Hydrogels, Endothelial Progenitor Cells

Approved by

Elizabeth A. Lipke, Chair, Assistant Professor of Chemical Engineering
Mark E. Byrne, Daniel F. & Josephine Breeden Associate Professor
of Chemical Engineering
Steve R. Duke, Associate Professor of Chemical Engineering
Jiangzhong Shen, Associate Professor of Pharmacology,
Department of Drug Discovery and Development
Anne A. Wooldridge, Associate Professor of Clinical Sciences
College of Veterinary Medicine

Abstract

Endothelial progenitor cells (EPCs) have the potential to become a reliable source of autologous cells for endothelialization of intravascular devices and vascularization of tissue engineered constructs. Endothelial colony forming cells (ECFCs) are one type of EPCs; ECFCs are highly proliferative and are capable of forming mature and functional endothelial cells for vessel repair and postnatal angiogenesis. However, currently little is known about the homing of these circulating ECFCs. This research investigated the rolling of ECFCs on peptide-grafted hydrogels using a parallel plate flow chamber in order to mimic the dynamic adhesion of ECFCs under conditions simulating physiological arterial flow. Poly(ethylene glycol) diacrylate (PEGDA) was chosen to be the hydrogel backbone. Due to the ability of PEGDA to inhibit protein adsorption, it can be used as a "blank slate" to examine the specific interactions of cells with the covalently incorporated peptides. To assess the specific interactions required for ECFCs to interact with material coatings under shear, peptides including RGDS, REDV, YIGSR, and RGES were coupled to acryloyl-PEG and grafted onto the surface of PEG hydrogels. To study the effect of shear on cell rolling, the ECFC cell suspension was sheared over the hydrogels at rates of 20 s^{-1}, 40 s^{-1}, 80 s^{-1}, and 120 s^{-1}. ECFC rolling was significantly slower on REDV-grafted hydrogels. Further investigation of integrin-specific novel peptides has shown that ECFC capture under shear can be enhanced by the combination of REDV and CRRETAWAC. These

results can be applied in the future for modification of biomaterial surfaces to enhance endothelialization. Isolation of ECFCs from horse and encapsulation of equine ECFCs using fibrinogen-modified PEG hydrogels have also been pursued to illustrate the potential application of ECFCs in veterinary medicine.

Acknowledgments

I would like to thank my advisor, Dr. Elizabeth Lipke, for her guidance and support throughout my research. I would also like to thank my committee members, Dr. Mark Byrne, Dr. Steve Duke, Dr. Jianzhong Shen, Dr. Anne Wooldridge, and University Reader, Dr. Xinyu Zhang for their time and knowledge in the preparation and critical review of this manuscript. In addition, I would like to thank Dr. Mike Meadows and Dr. Yonnie Wu for providing advice on NMR and Mass Spectrometry. I would like to give special thanks to Stephen Hicks who has been my greatest partner since the start of the lab. I would also like to acknowledge the help of my colleagues Dr. David Dunn, Alex Hodge, Sam Chang, Shantanu Pradhan, and Petra Kerscher. I would like to express my appreciation to Dong Chen, Isabel Tian, Shasta Rizzi, Margaret Salter, Blake DeWitt, Sarah Hashimi, Ashley Sharpe, and Randolph Winter for doing research together.

Most importantly, I express gratitude to my uncle, William Sun, my aunt, Berginia Lee-Sun and my cousins, Nikke Sun, Mani Sun and Orion Sun, who have loved me so much during my time in the US. I would also like to thank Brian Lilly for enriching my life with indelible memories at Auburn University. I am extremely grateful to Teng Xu for her greatest support and love for me.

Table of Contents

List of Figures

List of Tables

List of Abbreviations

6HRGDS	HHHHHHRGDSG
A5-1	VILVLFG
Ac-LDL	Acetylated low density lipoprotein
AHA	American Heart Association
bFGF	Basic fibroblast growth factor
BMS	Bare metal stent
BSA	Bovine serum albumin
C=C	Carbon---carbon double bond
CABG	Coronary artery bypass grafting
CAD	Coronary artery disease
CB-EPC	Umbilical cord blood derived endothelial progenitor cell
CFU	Colony-forming unit
CVD	Cardiovascular diseases
DES	Drug-eluting stent
DMPA	2,2-dimethoxy-2-phenylacetophenone
DiI	1,1'-dioctadecyl-3,3,3',3'-tetramethyl-indocarbocyanine perchlorate
ECFC	Endothelial colony forming cells
EHS	Engelbreth-Holm-Swarm
EPC	Endothelial progenitor cell
FDA	Food and Drug Administration
FN	Fibronectin
HSC	Hematopoietic stem cell
KOH	Potassium hydroxide

LDL	Low-density lipoprotein
LST	Late stent thrombosis
MI	Myocardial infarction
MNC	Mononuclear cell
MW	Molecular weight
NMR	Nuclear magnetic resonance
P11	HSDVHK
PAD	Peripheral artery disease
PCI	Percutaneous coronary intervention
PEG	Poly(ethylene glycol)
PEGDA	Poly(ethylene glycol) diacrylate
PES	Paclitaxel-eluting stent
PR_b	-(C_{16})$_2$-Glu-C2-KSSPHSRNSGSGSGSGSGRGDSP
PRb	PHSRNSGSGSGSGSGRGDSG
PVA	Poly(vinyl alcohol)
PVD	Peripheral vascular disease
SES	Sirolimus-eluting stent
SMC	Smooth muscle cell
ST	Stent thrombosis
SVA	Succinimidyl valerate
TLR	Target lesion revascularization
TRIAS	TRI-stent Adjudication Study
VEGF	Vascular endothelial growth factor

Introduction

Cardiovascular disease (CVD) is the major cause of death worldwide and the most common form of CVD is atherosclerosis where plaque is formed within the arterial wall. This restricts blood supply to the downstream tissues and can cause ischemia or heart attack. To remove the plaque and restore blood flow, angioplasty and stents are the most common treatment. However, this treatment damages the endothelium, which is the inner lining of blood vessel. Without an intact and complete endothelium, complications will be developed over a period of time and blood flow is then again restricted. Complications include restenosis, neointimal hyperplasia, and late-stent thrombosis (LST). Therefore, this research studies the potential methods for re-endothelialization to avoid the development of these complications after angioplasty and stent treatment.

Numerous strategies have been attempted to prevent thrombosis and neointimal proliferation. However, regardless of the advances in blood compatible materials, the endothelium remains the ideal blood contacting surface. Endothelial progenitor cells (EPCs), which derived from bone marrow and circulate in blood, hold promise in restoring endothelium due to their regenerative capacity. Endothelial colony forming cells (ECFCs) are a subset of EPCs with a differentiative and highly proliferative nature. They can be an easily obtainable autologous cell source for use in cell therapy (Dimmeler & Zeiher, 2004; Sen, McDonald, Coates, & Bonder, 2011). Therefore, we are interested in developing a biomaterial that promotes re-endothelialization by ECFCs.

To specifically test cell-ligand interactions on biomaterials, we have employed a poly(ethylene glycol) diacrylate (PEGDA) base. PEGDA is biocompatible and it resists

protein adsorption, which is critical in serving as a blank slate to allow us to study specific interaction of our peptides with the cells. Furthermore, PEGDA hydrogels have been previously studied for intraluminal interfacial polymerization, making them a potential coating for vascular grafts and next generation stenting material.

As PEG hydrogels do not support cell adhesion, peptides are chosen as the adhesion molecules to support EPC adhesion. The peptides are short segments of extracellular matrix (ECM) protein and they can be easily synthesized. Therefore, they have advantages over natural ECM proteins, including, lower batch-to-batch variability, higher molecular concentration per mass, and lower cost. This research focuses on peptides that interact with integrins, cell surface receptors.

Shear stress has been identified to be critical in endothelial cells (ECs) behaviors. *In vivo* studies have shown that EPCs roll along the blood vessel wall while circulating in blood and eventually stay adhered. In order to develop a biomaterial that promotes ECFC re-endothelialization, interaction between ECFCs and the peptides under shear is examined through static and dynamic adhesion assays. To conclude, the result of this research could benefit future synthetic biomaterial design for vascular repair in tissue engineering.

Chapter Summary

CHAPTER 1

Cardiovascular disease (CVD) is a major cause of death worldwide and atherosclerosis is one of the most common forms of CVD. Although drug-eluting stents have reduced the mortality rate due to restenosis, complications including stent thrombosis and late lumen loss have emerged. This chapter presents the importance of recovering the endothelium and the motivation to develop a biomaterial that can perform re-endothelialization.

CHAPTER 2

To avoid redundancy, this chapter is a collection of materials and methods that are used throughout the study. Specific treatments or additional methods that are used in each projects are mentioned within the corresponding chapters.

CHAPTER 3

In vitro investigation on endothelial cell rolling under shear conditions provides valuable information on the cell-biomaterial interaction. A flow system together with rolling cell tracking algorithm was, therefore, developed to perform cell rolling, image acquisition and cell tracking analysis.

CHAPTER 4

The use of a parallel plate flow chamber system has successfully aided in studying the effect of peptides on ECFC rolling velocity under shear stress. The three bioactive peptides RGDS, REDV, and YIGSRG that were grafted on the cell resistant PEG hydrogels have shown to support ECFC rolling. Furthermore, REDV-grafted hydrogels reduced ECFC rolling velocity to a significantly greater extent than RGDS- and YIGSRG-grafted hydrogels.

CHAPTER 5

Novel peptides are proposed to be evaluated to identify their capabilities in slowing and capturing ECFCs. PepBank was used to identify potential peptides that have high affinity and/or selectivity for the integrins $\alpha_5\beta_1$ and $\alpha_v\beta_3$. Although these peptides have been shown to have great promise in cell adhesion, the performance in cell rolling and capture under shear is yet to be evaluated. This chapter evaluates their potentials in supporting ECFC rolling and compares the result to the peptides used in previous chapter. Results showed that CRRETAWAC, which has high affinity and selectivity for $\alpha_5\beta_1$, have the most promising capability in capturing ECFCs under shear.

CHAPTER 6

Besides the clinical relevance of ECFCs in human, the benefits of ECFCs may also be used in veterinary animals. Isolation of equine ECFCs was established using a media and substrate culture method. DiI-Ac-LDL uptake and Matrigel tubule formation assays

were performed to confirm the endothelial nature of the isolated cells. Based on evidence from multiple characterization assays, these cells are believed to be ECFCs.. Immunostaining and flow cytometry for ECFC surface marker has also supported their ECFC identity. Encapsulation of equine ECFCs using fibrinogen-modified PEG hydrogels have also been pursued to illustrate the potential application of ECFCs in veterinary medicine to treat common diseases that lack vasculature.

Chapter 1 Background

1.1 Current Treatments for Vascular Diseases Lack Rapid Re-endothelialization

For years, cardiovascular disease (CVD) has been a major cause of death worldwide, and 82 million American adults have CVD according to the 2012 statistical update by the American Heart Association (AHA) (Roger et al., 2011). Atherosclerosis is one of the most common forms of CVD. In atherosclerosis, a patient's blood vessel wall, typically in an artery, is thickened by the buildup of plaque. This results in the narrowing of the blood vessel lumen, or stenosis, and thereby restricts blood supply to the body. When atherosclerosis occurs in an artery of the heart, heart attack could occur and the result could be fatal. In these cases, surgical treatment is necessary to physically restore the blood supply. However, current treatments prevented the regeneration of the innermost layer of vessel blood, which is the endothelium, and led to the re-occurrence of narrowed blood vessels. This section of the chapter will focus in describing the current standard treatments to atherosclerosis and summarizing some research that have been done to improve these treatments.

1.1.1 Atherosclerosis

Stenosis is a vascular disease where narrowing of blood vessels occurs. The blood vessel narrowing causes restriction of blood flow and reduces the supply of nutrients and oxygen to the body. Stenosis can theoretically occur in any blood vessel. When it occurs in a coronary artery, this refers to coronary artery disease (CAD). Similarly, a stroke may result in patients having carotid artery disease when there is a narrowing in carotid artery.

The narrowing of vessels in the other parts of the body is called peripheral vascular disease (PVD). One specific type of PVD is peripheral artery disease (PAD).

One of the most common forms of stenosis is atherosclerosis, which refers to the constriction of blood flow and is caused by a buildup of plaque in the arterial wall. Plaque formation is initiated during an inflammation process where low-density lipoprotein (LDL) cholesterol initially accumulates within the artery wall, followed by the attachment of lipid-laden monocytes, macrophages, and leukocytes as a result of an immune response. Smooth muscle cell migration into the area results in the formation of a fibrous cap. Hence, the artery wall is thickened and hardened. The fibrous cap covers the cells and lipids underneath, eventually making the tissue necrotic and leading to plaque formation. In PAD, this plaque formation may cause a number of adverse effects due to reduced blood supply. When gangrene sets in, amputation of limbs is sometimes necessary. In addition, the plaque may rupture resulting in thrombosis. When the thrombus is separated and falls into the blood stream, blockage of smaller vessels may result causing ischemia, tissue damage, and possibly death. Therefore, atherosclerosis is very dangerous.

Atherogenesis is the development of atherosclerosis and is not yet completely understood. The hypothesis was first made that the endothelium was denuded, allowing the lesion site to accumulate lipid (Russell Ross & Glomset, 1973), but later there was another hypothesis suggesting that endothelium dysfunction is the initial step (Russel Ross, 1999). When the function of the endothelium is compromised, the adhesiveness and permeability to leukocytes or platelets is increased which initiates the buildup of plaque. There are multiple risk factors that affect the endothelium including elevated LDL level, smoking,

hypertension, diabetes, genetics, plasma homocysteine concentrations, and infectious microorganisms. Hence, the mechanism of atherogenesis remains to be exclusively determined.

1.1.2 Current Treatments

Angioplasty and Coronary Artery Bypass Grafting

Surgical treatment is necessary when stenosis or atherosclerosis cannot be controlled by change of life style or medication. The most common treatment is percutaneous coronary intervention (PCI), also known as balloon angioplasty or simply "angioplasty". In PCI, a guide wire is used to move a balloon catheter through blood vessel and the balloon catheter is inflated at the site of stenosis to open up the narrowed vessel. Coronary artery bypass grafting (CABG) is another option in restoring blood supply. Although studies have shown that CABG has the advantage of lower death and myocardial infarction rates, angioplasty is more common due to several reasons. CABG is a more invasive surgery comparing to angioplasty, surgical risk and cost are much higher than angioplasty. In small diameter vessel grafting, the grafts usually have limited lifespan and causing rapid occlusion. In addition, CABG uses autologous artery from other part of the body to restore blood flow, 60% of patients with vascular disease do not have suitable vessel for autografting (Ruoslahti, 1996). As a result, patients have a much slower recovery and more discomfort. Therefore, angioplasty is a more common treatment in terms of improving the quality of life.

Angioplasty

Angioplasty coupled with stenting is the most common and efficient surgical procedure to treat a narrowed vessel. In this procedure, a balloon catheter is inflated to physically open the narrowed vessel. In the 1970's, some patients who underwent angioplasty experienced immediate collapsing or negative remodeling of their arteries, so stents were developed to be used to correct this issue. Depending on the artery size and blockage location, stents are now often used together with angioplasty to prevent the artery from collapsing. However, there are other complications associated with the use of stents due to the material design of stents.

Bare Metal Stents Causes Restenosis

The BMS is the first generation stent developed to prevent the artery from collapsing after angioplasty. The first BMS that was approved by Food and Drug Administration (FDA) was the Palmaz-Schatz stent in 1994. This stent is a metal mesh wire tube which is expandable upon inflating the balloon catheter and stays expanded within the artery. The BMS had success in increasing the luminal diameter following placement and maintaining a larger luminal diameter six months after treatment comparing to balloon angioplasty (Fischman et al., 1994; Serruys, Jaegere, & Kiemeneij, 1994). Comparing to angioplasty, patients with BMS implantation have a decreased rate of target lesion revascularization (TLR) which is defined as any repeat revascularization procedure of the original target lesion site (Kiemeneij et al., 2001). Several other designs have been subsequently developed to improve their flexibility and ease of surgical use. However, results of clinical studies have shown that some patients with implanted BMS have

restenosis, or re-narrowing of the blood vessel after surgery. According to a study by Hoffmann *et al.*, 37% of lesions treated with BMS were restenotic at follow-up six months after stent implantation and required repeat treatments. They concluded that neointimal tissue proliferation contributed to in-stent restenosis (Hoffmann et al., 1996). On the other hand, the outcome of stenting procedures may also be influenced by the geometric design of the stent. For example, a study has shown that slotted-tube stents may have a significantly lower rate of restenosis than coiled stents as determined at a six-month follow-up (S.-W. Park et al., 1998). Therefore, solutions are needed to prevent neointimal tissue proliferation and therefore avoid in-stent restenosis with the BMS. This is due impart to the over proliferation of smooth muscle cells (SMCs) which is known as neointimal hyperplasia (Hoffmann et al., 1996).

Drug-Eluting Stents

To prevent the growth of SMCs, pharmaceutical companies have developed drug-eluting stents (DES) which are simply BMS with coatings that release drugs which inhibit cell growth. Although there are various types and numbers of layers of coatings, the fundamental design of DES are very similar. There are usually two coatings consisting a polymer coating that releasing the drug and another coating that keeps the drug releasing layer on the stent. In some designs, a third coating exists on top of the outer layer to slow down drug release. The most common drugs being released to inhibit neointimal proliferation are Sirolimus and Paclitaxel. Everolimus, which is a derivative of sirolimus, and heparin are also used in some clinical studies. Unfortunately, in some cases, patients

with DES developed a condition called late-stent thrombosis (LST) where a blood clot is formed after all the drug in the DES has been released (Stone et al., 2007).

Sirolimus-eluting stents (SES) release sirolimus, also known as rapamycin, which is an immunosuppressant drug used to prevent rejection in organ transplantation. Paclitaxel-eluting stents (PES) release paclitaxel, which is a mitotic inhibitor used in cancer chemotherapy. Both drugs are able to be released from a polymer system coated on DES to inhibit cell growth. Patients with DES are required to be pretreated with anti-platelet therapy in order to prevent stent thrombosis. Pre-treatments prior to stent placement include ticlopidine or clopidogrel and aspirin. After implantation, aspirin was continued indefinitely, and ticlopidine or clopidogrel is given at least for another 3 months for SES implantation or 6 months for PES implantation respectively.

From a world-wide pooled analysis with respect to four trials (RAVEL, SIRIUS, E-SIRIUS, and C-SIRUIS) comparing SES to BMS and five trials (TAXUS I, II, IV, V and VI) comparing PES to BMS, a reduced TLR was shown after 4 years in both DES comparing to BMS. However, DES caused stent thrombosis (ST) and delayed neointimal proliferation. Thrombosis often causes myocardial infarction (MI) or even death in some situations, and the cause of thrombosis has been determined to be the inability of the vessel to reform the endothelium while the drug is being released. According to an observational cohort study on stent implantation between April 2002 and January 2004, there was a higher number of ST events in both SES and PES than in BMS after both 1 and 4-year time points, where ST was found in 29 patients with either SES or PES at 9-month follow-up and caused 13 deaths(Stone et al., 2007). On the other hand, Carter *et al.* performed an *in*

vivo study using porcine model where histological analysis found a delayed neointimal proliferation using SES and the result was similar to BMS at day 90 and 180 (Carter et al., 2004). From these results, DES and anti-platelet therapy have not only inhibited the cell proliferation that causes restenosis, but also the re-formation of the endothelium which is critical in preventing thrombosis. Thrombosis can cause acute blockage of arteries and lead to myocardial infarction which is fatal. Therefore, alternatives to promote endothelialization of the target stent are desired.

Genous Stent for Endothelial Progenitor Cells

Endothelium serves as a lining for blood vessels to prevent neointimal hyperplasia. To more rapidly re-form a functional endothelium, the Genous stent was developed. This stent is designed to use an antibody that targets the endothelial progenitor cells (EPCs) surface marker CD34 so that the surface of the stent can capture EPC for endothelialization. More details of EPC will be discussed in the following section. Nevertheless, several studies have shown that the Genous stent causes late lumen loss, which is defined as the decrease in minimum lumen diameter. This is due to the fact that CD34 is not specific to EPCs. As a result, the stent not only captures EPCs, but also other cell types (Garg, Duckers, & Serruys, 2010). Therefore, endothelium did not re-form completely over the surface of the stent.

1.2 Endothelial Progenitor Cell as Blood-Vessel Wall Interface

In the field of regenerative medicine, more evidence has been shown in using EPCs as a potential candidate for tissue repair since their discovery (Asahara et al., 1997). As a precursor for endothelial cells (ECs), EPCs show an endothelial-like phenotype with high

proliferative capability (especially late EPCs). It can be differentiated into mature endothelial cells that form the endothelium. Hence, potential clinical applications of EPCs include vessel repair (Asahara et al., 1997), neovascularization of ischemic organs, and coating of vascular grafts (Hristov, Erl, & Weber, 2003). This section provides more details of EPCs characterization and biology.

Discovery and Identity of EPC

EPCs were discovered by Asahara *et al.* in 1997 who postulated that angioblasts and hematopoietic stem cells (HSCs) exist in circulating adult blood and contribute to vasculogenesis. Since both angioblasts and HSCs share the surface marker CD34, they isolated the CD34+ mononuclear cells (MNCs), which are a type of leukocytes, using magnetic beads coated with the antibody for CD34. After isolating the CD34+ MNCs from adult blood, they found that the CD34+ cells were able to form cellular networks and tube-like structures on fibronectin-coated plates. Furthermore, using ischemic hindlimb model in both mice and rabbits, CD34+ MNCs were able to incorporate into capillary vessel walls whereas CD34- MNCs did not. Although later studies have shown that not all CD34+ cells are EPCs, these cells do possess proangiogenic capabilities and contribute to neoangiogenesis.

In addition to CD34, EPCs generally co-express the surface markers AC133 and VEGFR-2 (or KDR) (Avci-Adali, Ziemer, & Wendel, 2010; Peichev et al., 2000; Yoder et al., 2007), and they can be separated into two types: early and late outgrowth EPCs. Different methods are used for isolating early and late EPCs (Hirschi, Ingram, & Yoder,

2008; Yoder et al., 2007). The early EPCs, or colony forming units (CFUs), are isolated by first seeding MNCs onto fibronectin-coated plates and, after 48 hours, the nonadherent cells are then re-plated. At day 5 to 7, CFU colonies are identified as elongated sprouting cells (Figure 1.1A). On the other hand, the late EPCs, which are commonly referred to endothelial colony forming cells (ECFCs), are isolated by first seeding MNCs on collagen-coated plates, and the nonadherent cells are then discarded. After 1 to 2 weeks, ECFCs colonies are identified based on their cobblestone morphology (Figure 1.1B) (Avci-Adali, Paul, Ziemer, & Wendel, 2008; Hirschi et al., 2008; Yoder et al., 2007). Both types of EPCs have been shown to contribute equally to endothelialization through separate mechanisms. While CFUs enhance angiogenesis through secretion of angiogenic cytokines to induce survival and proliferation of mature endothelial cells, ECFCs contribute by providing a relevant number of endothelial cells due to their highly proliferative capability (Hur et al., 2004).

It remains in question whether the CFUs and ECFCs are derived from the same parent cell, but Yoder *et al* has reported that the CFUs are clonally distinct from ECFCs using clonal analysis (Yoder et al., 2007). They determined that both CFUs and ECFCs express endothelial antigens including CD31, CD105, CD144, CD146, vWF, KDR, and UEA-1, but only CFUs express the hematopoeitic-specific cell surface antigen, CD45, and the macrophage cell surface antigen CD14, and CD115 (Yoder et al., 2007) (Table 1.1). This proves that CFUs are derived from HSCs, whereas ECFCs are not derived from HSCs. Furthermore, CFUs were shown to function as macrophages and did not possess the ability to form vascular structures *in vivo*. On the other hand, ECFCs formed functional human-

murine chimeric vessels *in vivo*. Therefore, based on the phenotypic and functional properties of ECFCs, Yoder *et al.* have determined ECFCs to be the true EPCs (Hirschi et al., 2008; Yoder et al., 2007).

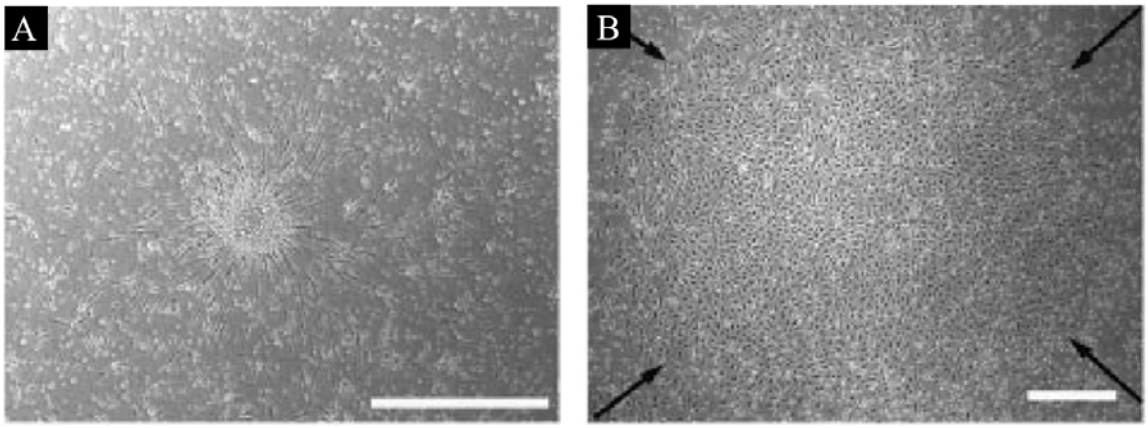

Figure 1.1 Morphology of early and late outgrowth EPCs. A) CFU colonies are identified as elongated sprouting cells while B) ECFCs colonies are identified based on their cobblestone morphology. Reprinted with permission from Ref (Yoder et al., 2007). Scale bars are 500 μm.

Table 1.1 Cell surface antigen expression and Ac-LDL uptake by CFUs and ECFCs. Adapted from Ref (Yoder et al., 2007).

Antigen	CFU-ECs	ECFCs
CD31	92.31 ± 5.47	92.29 ± 1.32
CD105	74.36 ± 6.32	96.73 ± 1.79
CD144	34.80 ± 8.74	99.15 ± 0.85
CD146	56.52 ± 10.00	94.21 ± 3.71
KDR	99.19 ± 0.81	68.61 ± 11.26
vWF	67.21 ± 12.78	97.09 ± 2.05
Ac-LDL	73.68 ± 9.05	99.75 ± 0.25
CD14	98.53 ± 1.04	1.20 ± 0.74
CD45	98.15 ± 1.85	0.37 ± 0.37
CD115	94.42 ± 2.52	0.28 ± 0.21

Advantage of using EPC as Cell Therapy for Re-endothelialization

Aside from the clinical outcome and safety issues of the Genous EPC capture stent, the idea of implementing EPCs for stent endothelialization as a preventative for restenosis remains robust as EPCs have several decisive advantages over mature ECs for cell therapy. Mature ECs, in general, have low proliferative potential and limited ability to regenerate damaged endothelium, whereas EPCs have highly proliferative and angiogenic potentials that can provide an abundant quantity of functional endothelial cells for vascular repair. In addition, autologous EPCs are readily obtainable from the blood compared to mature ECs which would be isolated from tissue. The number of ECs in circulating blood is very low and ECs that have shed off from the vessel wall are commonly damaged (Mutin et al., 1999), so patients' circulating ECs are not suitable for re-endothelialization. Also, EPCs have also been shown to be a strong candidate for endothelialization due to the fact that they can withstand superphysiological shear stress up to 250 dyn/cm^2 (Brown, Wallace, Angelos, & Truskey, 2009; Stroncek et al., 2009). When EPCs were seeded on titanium surfaces for implantable devices, thrombosis was shown to be significantly minimized in a porcine model (Achneck et al., 2011; Jantzen et al., 2011). Therefore, EPCs are an excellent source of cells for cell therapy to promote rapid endothelialization. Figure 1.2 shows a schematic that summarizes the idea of implementing EPCs in cell therapy with the use of biomaterials like hydrogels.

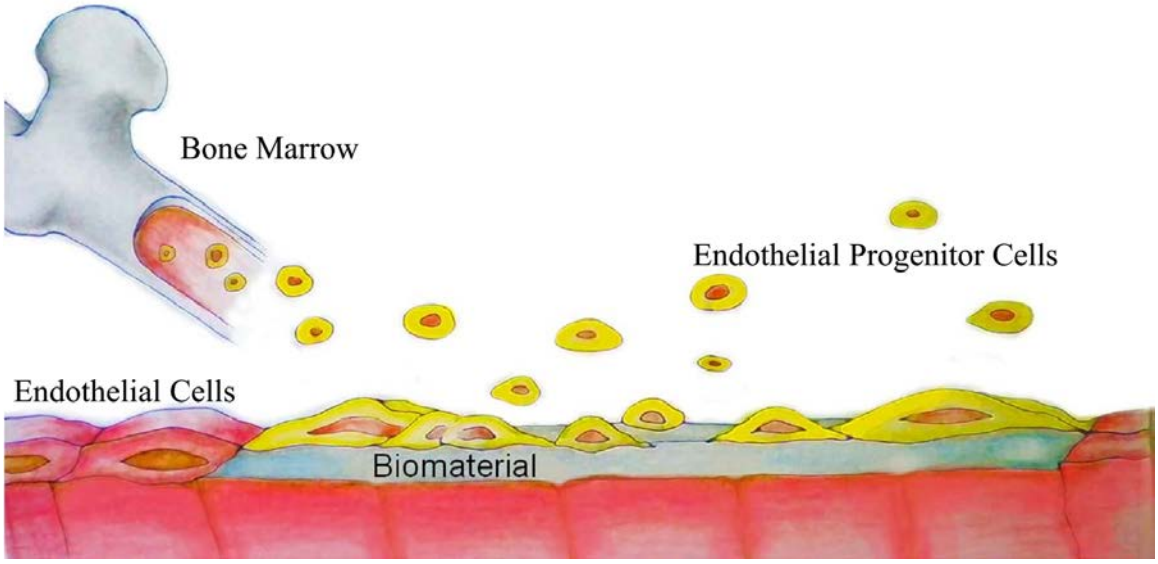

Figure 1.2 Schematic of using EPC capturing biomaterial for vessel repair. The ultimate goal of this study is to develop a EPC specific hydrogel as biomaterial to capture EPCs and support EPC rolling, adhesion, and migration for endothelialization of injured vessel. Reprinted with permission from Ref (W J Seeto, Tian, & Lipke, 2013).

1.3 Design of Biomaterials to Support Endothelial Progenitor Cells

1.3.1 Hydrogels as Potential Biomaterial for EPCs

Hydrogels are a network of polymer chains forming a hydrophilic scaffold and are widely studied and used in tissue engineering due to their various advantageous properties. Since hydrogels are very hydrophilic, they absorb water and swell to form a very flexible material that is similar to natural tissue. Most precursor polymers can form hydrogels under physiological pH and temperature which gives its significant clinical relevance. Synthetic hydrogels are highly reproducible materials that have low batch-to-batch variability compared to hydrogels made from natural materials, like ECM proteins. They can also be readily modified with natural materials to form hybrid scaffolds to suit different purposes. In tissue engineering, hydrogels also play a key role as an interfacial biomaterial for various applications including drug delivery, microencapsulation, coatings for vascular grafts, and diagnostic devices (Peppas, Hilt, Khademhosseini, & Langer, 2006; Slaughter, Khurshid, Fisher, Khademhosseini, & Peppas, 2009).

Hydrogels have potential to serve as a better material for capture EPC over traditional metal stents. *In vivo* studies have shown that hydrogel can be crosslinked and formed *in situ* within blood vessel simply by injection of polymer precursor solution and UV radiation through the skin (West & Hubbell, 1996). This significantly reduces the need for invasive surgery and decreases the complexity of surgery. Unlike metal stents, hydrogels can be produced rapidly by photopolymerization. With the low batch-to-batch variability due to the intrinsic properties of synthetic polymers, quality of the biomaterials can be tightly controlled for use in medical devices. Therefore, hydrogel provides as an alternative for metal stents.

1.3.2 Poly(ethylene glycol) (PEG) as Hydrogel Backbone

Poly(ethylene glycol) (PEG) is a unique synthetic polymer that forms PEG hydrogels with excellent properties for use in tissue engineering. It is well known for its biocompatibility and minimal protein adsorption due to the steric hindrance by water absorbed (Hill-West et al., 1994). As a result of this lack of protein adsorption, it is non-thrombogenic and non-inflammatory due to the high resistance against platelet and macrophage adhesion. Molecular weight (MW) of PEG was found to affect the cytotoxicity where MW less than 400 is cytotoxic due to oxidation of PEG *in vivo* forming diacid and hydroxyacid metabolites (Herold, Keil, & Bruns, 1989), and a MW of 1,000 or above have been proven to be safe (Working, Newman, Johnson, & Cornacoff, 1997). Therefore, the PEG chosen for use in this study have a molecular weights of 3,400, 6,000 and 10,000.

PEG is acrylated to form poly(ethylene glycol) diacrylate (PEGDA) providing the ability to crosslink it into PEG hydrogels. This also provides the capability for conjugation of the PEG hydrogels with cell adhesion ligands. The crosslinking is a rapid photopolymerization process adapting a free radical chemistry together with photoinitiator and long wavelength ultraviolet light. The chemical structure of PEGDA is shown in Figure 1.3. Poly(vinyl alcohol) (PVA) is another major synthetic polymer in forming hydrogel that can be crosslinked using physical, chemical or irradiative methods, but these methods may be time consuming comparing to the photopolymerization of PEGDA (C R Nuttelman, Mortisen, Henry, & Anseth, 2001; Charles R Nuttelman, Henry, & Anseth, 2002; Peppas & Merrill, 1977; Schmedlen, Masters, & West, 2002).

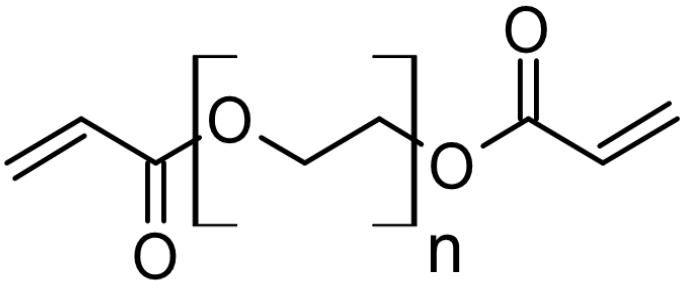

Figure 1.3 The chemical structure of poly(ethylene glycol) diacrylate. Figure was produced using ChemSketch.

PEGDA Crosslinking/Free Radical Chemistry

PEGDA is crosslinked into hydrogel networks by photopolymerization using photoinitiator, and photopolymerization consists of the initiation, propagation, and termination steps. There are three major types of photoinitiation: photocleavage, hydrogen abstraction, and cationic photopolymerization (Nguyen & West, 2002), where photocleavage is one of the most commonly used approach in crosslinking PEGDA. As an example of photocleavage shown in Figure 1.4, 2,2-dimethoxy-2-phenylacetophenone (DMPA) is a photoinitiator where a methyl free radical $CH_3\cdot$ is generated when DMPA is exposed to UV light. Then, the methyl radical attacks the carbon-carbon double bond (C=C) in the acrylate groups of PEGDA to form $—CH_2\cdot$ on PEGDA. Hence, the $—CH_2\cdot$ propagates to other PEGDA until termination of the reaction (Mellott, Searcy, & Pishko, 2001). Figure 1.5 shows the propagation of PEGDA after being attacked by the methyl radical. Other than the concentrations of PEGDA and photoinitiator being used, the crosslinking time needed also depends upon the choice of photoinitiator and the power of the UV light. For example DMPA varies from 3 s under 20 W/cm^2 to 30 min under 1 W/cm^2 (Mellott et al., 2001; Scott & Peppas, 1999).

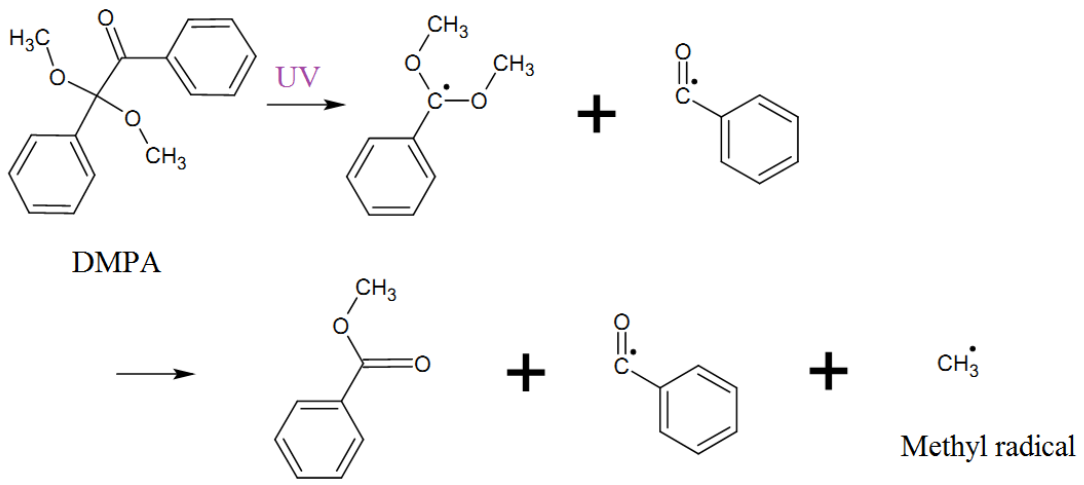

Figure 1.4 The photoinitiation of DMPA started by exposure to UV light to generate reactive methyl free radical. Figure was produced using ChemSketch.

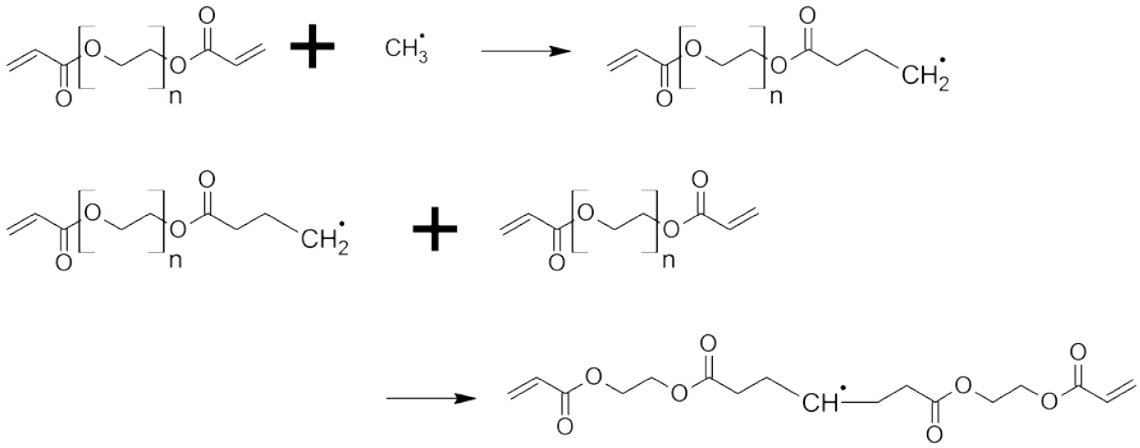

Figure 1.5 The propagation of PEGDA by reactive methyl free radical generated by DMPA under exposure to UV. Figure was produced using ChemSketch.

1.3.3 Peptide as Ligand for EPC Surface Receptors

Peptide and Integrin

A peptide is a short sequence of amino acids joined by peptide bond. Depending on the sequence of the amino acids, a peptide may or may not be recognized by the cell surface receptors. As an example, the amino acid sequence RGD is recognized by half of the over twenty known integrins (Ruoslahti, 1996) whereas the sequence RGE has been shown to be not recognized by any integrins. Moreover the length of the peptide may alter the availability of the active portion of the sequence. Most of the short peptides are considered linear and longer peptides are not, and this is due to the tendency of longer peptides to form secondary structure. For example, a bend within a longer peptide occurs when there is a formation of hydrogen bond or disulfide bond. Therefore, peptide sequence is critical in terms of providing specificity for ligand-receptor recognition.

The study and use of peptides as a biomaterial has been growing rapidly because they possess excellent advantages over proteins. Unlike ECM proteins, peptides are able to be synthesized in a much more rapid manner with fewer logistical challenges, so this allows the identification of the critical peptide sequence within a protein as a specific ligand. On the other hand, an increasing number of novel peptides that are specific to their receptors have been discovered which leads to a better understanding of the role of these receptors in cellular activities. Also, with the improved technology in peptide synthesis, the batch-to-batch variations that commonly occur in protein production is very minimal in peptide production. Therefore, peptide is chosen in this study as biomaterial to study ECFCs homing due to its great potential.

Integrins are a family of proteins present on the cell surface that play a key role in cell adhesion. An integrin is a heterodimeric protein that has an α and a β subunit where nineteen α and eight β subunits have been discovered in mammals (Humphries, 2000). Specificity of integrin binding is determined by different combinations of α and β subunits. Figure 1.6 shows the known integrin subunit combinations (Ruoslahti, 1991). Although integrins also possess signal transduction ability in modulating numerous cellular activities that affect cell proliferation and differentiation (Chan et al., 2011; Giancotti, 1999), their role in cell adhesion is the primary concern in this study in terms of cell rolling and capture.

Integrins Found on EPCs

Some recent studies have explored the involvement of integrins in EPC adhesion. *In vivo* studies have shown that β_2 integrins are important in both EPC homing to site of ischemia and neovascularization (Emmanouil Chavakis et al., 2005). Integrins also play an important role in EPC capture on EC or ECM proteins *in vitro* (Hristov, Zernecke, Liehn, & Weber, 2007). Although the types and distribution of integrin receptors are not well identified on EPCs, Angelos *et al.* have estimated the number of $\alpha_5\beta_1$ and $\alpha_v\beta_3$ integrin receptors present on umbilical cord-blood derived EPC using flow cytometry (Angelos et al., 2010). Besides flow cytometry, investigation of EPC migration has shown that blocking $\alpha_5\beta_1$ decreases EPC migration (Wijelath et al., 2004). Until now, knowledge of integrins present on the membrane surface of EPCs is still very limited and needs to be further explored.

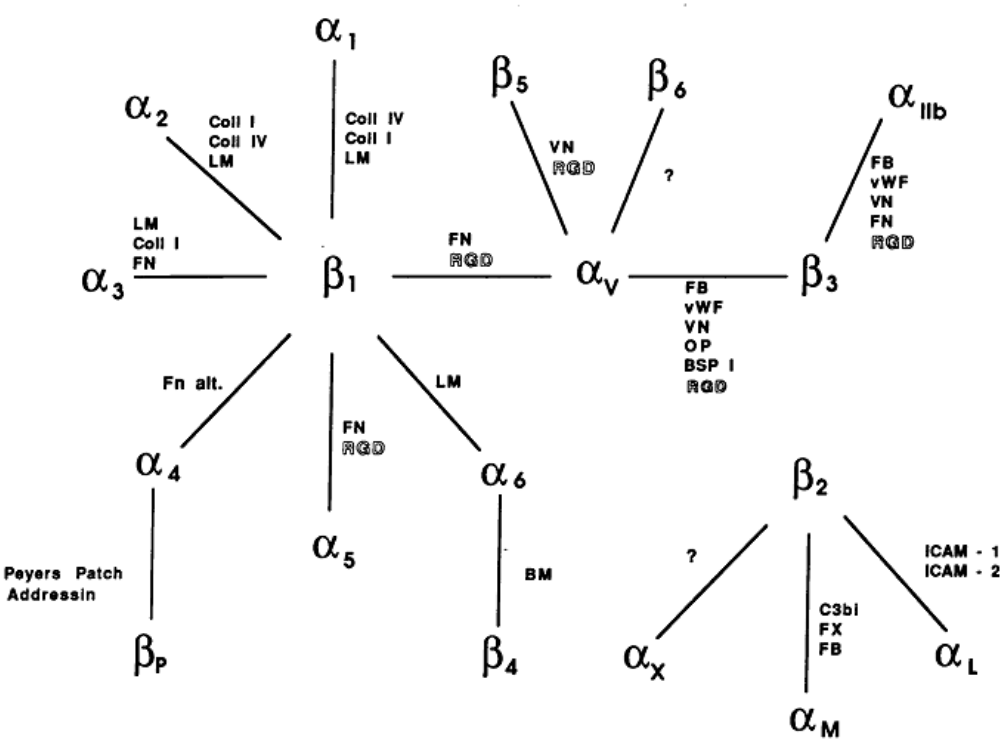

Figure 1.6 Integrin map showing the combinations of α and β subunits, and their ligands. Reprinted with permission from Ref (Ruoslahti, 1991). This article Copyright © 1991, The American Society for Clinical Investigation.

1.4 Importance of Fluid Shear on Biomaterial Design for Endothelial Progenitor Cells

1.4.1 Blood Vessels Fluid Dynamics

Fluid dynamics in blood vessel is extremely complex, so simplified mathematical models can only be used to aid in understanding the flow in blood vessels. One of the major challenges is due to the fact that blood contains cells, which exist in various sizes, types, and amounts. Although blood is generally considered as Newtonian in most arteries, it appears to be non-Newtonian in the microcirculatory system where low shear rates and clumping of red blood cells occurs. In addition to cells, blood contains blood serum which has a large amount of various concentrations and types of proteins resulting in blood viscosity being approximated to be four times of that of water (Ku, 1997). Another challenge is the peristaltic nature of blood flow causing the change in diameter of blood vessels. Therefore, the bulk values for properties, e.g. shear rate, shear stress, Reynolds number, and pressure, are typically considered to be estimates of the fluid dynamics for blood vessels. Reynolds number range from 1 in small arterioles to 4000 in largest artery, which is the aorta, so blood flow is generally considered to be laminar (Ku, 1997). Since blood vessels are generally approoximated to have a cylindrical structure, the equation of Reynolds number for blood vessels is essentially that for cylindrical conduits and is shown in Equation (1) where ρ is the density of the fluid (kg/m^3), v is the average velocity (m/s), D is the diameter of the blood vessel (m), and μ is the viscosity (kg/(m·s)). Similarly, wall shear stress and shear rate of tubes are shown in Equations (2) and (3) respectively. Wall shear stress for most arteries is reported to be approximately 15 dyn/cm^2 (Glagov, Zarins, Giddens, & Ku, 1988).

$$Re = \frac{\rho v D}{\mu} \quad (1)$$

$$\tau_{wall} = \frac{32\mu Q}{\pi D^3} \quad (2)$$

$$\dot{\gamma}_{wall} = \frac{4Q}{\pi r^3} \quad (3)$$

1.4.2 Fluid Dynamics in Parallel Plate Flow Chamber

The parallel plate flow chamber has been a standard apparatus used for studying the effect of blood vessel like flow on cells (Frangos, Eskin, McIntire, & Ives, 1985). Although the flow geometry is different from the flow in blood vessels, parallel plate flow chamber has the benefit to provide an easy observation under microscope. The advantage of using parallel plate flow chamber is that it is simple to model and, also, able to capture the fluid-solid interfacial shear phenomenon. It has been used in studying various cell types, such as platelets, leukocytes, epithelial cells, and endothelial cells. Fluid shear can be altered by flow rate, dimension of flow chamber, and viscosity. A fluid pump, like a syringe pump, is commonly used in controlling the flow rate. Gravity driven flow and peristaltic pumps are usually applied in cycling flow system for long-term studies. The vertical dimension (height) of a flow chamber is typically controlled by a silicone gasket while viscosity of the fluid is usually determined by temperature and the type of flow media.

Assumptions and Equations

To describe the fluid dynamics within the flow chamber, several assumptions were made. Figure 1.7 shows a schematic of the side view of a flow chamber with the Cartesian

coordinates specified. The width and the length of the flow chamber are about 15 and 150 times larger than the height respectively, so it is assumed to be much larger than the height. Hence, end effects are neglected. The density of the flow media was assumed to be a constant and the flow was at steady state and steady flow. The steady flow assumption produces Equation (4), so only flow in the *x*-direction was considered. Together, these satisfy the equation of continuity (Equation (5)) and give Equation (6).

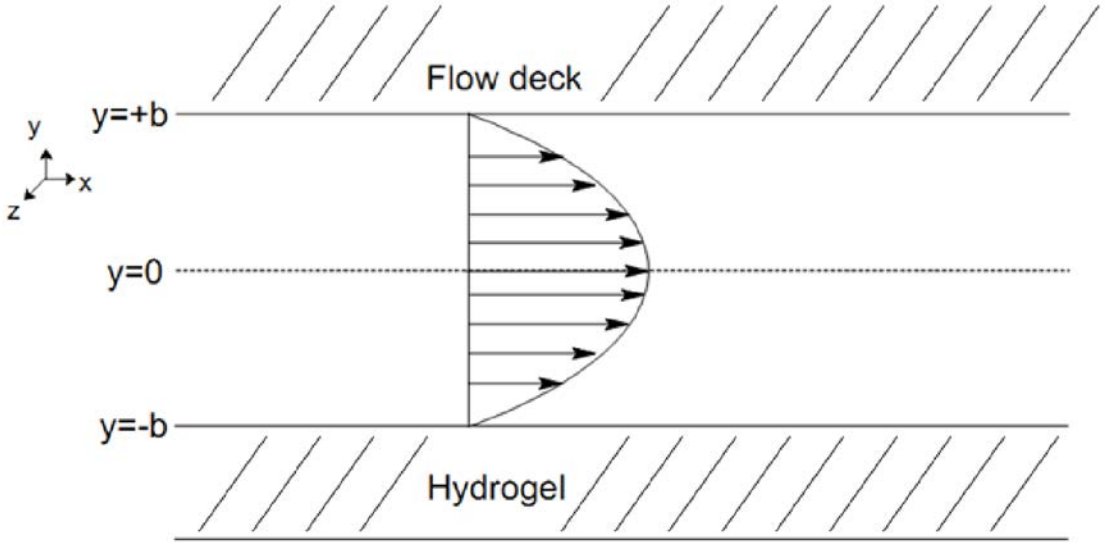

Figure 1.7 Qualitative velocity profile in parallel plate flow chamber. Using assumptions discussed in this section, parallel plate flow chamber shows a parabolic velocity profile.

$$v_y = 0,\ v_z = 0, v_x = v_x(y) \tag{4}$$

$$\frac{\partial \rho}{\partial t} + \frac{\partial}{\partial x}\rho v_x + \frac{\partial}{\partial y}\rho v_y + \frac{\partial}{\partial z}\rho v_z = 0 \tag{5}$$

$$\frac{\partial}{\partial x}\rho v_x = 0 \tag{6}$$

The walls of the flow chamber consist of the flow deck, the silicone gasket and the surface of the hydrogel. The rigid walls assumption is applied meaning that the walls, which include the surface of the hydrogel, are assumed to be uninfluenced by the flow. The no-slip boundary assumption is also applied.

$$y = \pm b, v_x = 0 \tag{7}$$

The flow chamber was placed horizontally, so gravitational effects can be neglected (g_x = 0). The flow medium was assumed incompressible and Newtonian. The flow is laminar and Reynolds number is low. These satisfy the laminar flow requirements, so equation of motion in the *x*-direction (Equation (8)) simplifies to Equation (9).

$$\rho\left(\frac{\partial v_x}{\partial t} + v_x\frac{\partial v_x}{\partial x} + v_y\frac{\partial v_x}{\partial y} + v_z\frac{\partial v_x}{\partial z}\right) \tag{8}$$

$$= -\frac{\partial p}{\partial x} + \mu[\frac{\partial^2 v_x}{\partial x^2} + \frac{\partial^2 v_x}{\partial y^2} + \frac{\partial^2 v_x}{\partial z^2}] + \rho g_x$$

$$0 = -\frac{\partial p}{\partial x} + \mu\frac{\partial^2 v_x}{\partial y^2} \tag{9}$$

Equation (9) can be written in terms of shear stress, τ_{yx}, and is shown in Equation (10). Taking the pressure of the inlet as P_0 and outlet as P_L, the difference between the inlet and outlet pressure is ΔP. The length of the flow chamber is L, so Equation (9) becomes Equation (11) and the shear stress τ_{yx} can be found. To solve Equation (10), the boundary conditions shown in Equation (13) are used to obtain the constant C_1 to be 0.

$$\tau_{yx} = -\mu \frac{\partial v_x}{\partial y} \tag{10}$$

$$\frac{d\tau_{yx}}{dy} = \frac{\Delta P}{L} \tag{11}$$

$$\tau_{yx} = \frac{\Delta P}{L} y + C_1 \tag{12}$$

$$at\ y = 0, \tau_{yx} = 0, C_1 = 0 \tag{13}$$

To further solve for v_x, integration of Equation (12) gives Equation (14). Using the boundary conditions in Equation (7), C_2 is solved and v_x is shown in (16).

$$v_x = -\frac{\Delta P}{2\mu L} y^2 + C_2 \tag{14}$$

$$0 = -\frac{\Delta P}{2\mu L} b^2 + C_2, C_2 = -\frac{\Delta P}{2\mu L} b^2 \tag{15}$$

$$v_x = \frac{\Delta P}{2\mu L} (b^2 - y^2) \tag{16}$$

Besides the velocity in the *x*-direction as a function of *y*, the average fluid velocity can also be found by integrating Equation (16) and gives Equation (17).

$$\langle v_x \rangle = \frac{1}{2b}\int_{-b}^{+b} \frac{\Delta P}{2\mu L}(b^2 - y^2)dy \tag{17}$$

$$= \frac{\Delta P}{2\mu L}(b^2 y - \frac{1}{3}y^3)|_{-b}^{+b} \tag{18}$$

$$= \frac{\Delta P b^2}{2\mu L} \tag{19}$$

For parallel plate flow chamber, the shear rate, $\dot{\gamma}$, is shown in Equation (20), where *Q* is the volumetric flow rate (mL/s), w is the width of the chamber and *h* is the height of the chamber (Truskey, Yuan, & Katz, 2004). To evaluate shear stress, τ_{yx}, Equation (21) was used.

$$\dot{\gamma} = \frac{6Q}{wh^2} \tag{20}$$

$$\tau_{yx} = \mu\dot{\gamma} \tag{21}$$

Due to the fact that there was a lack of ability to measure pressure drop, ΔP, average fluid velocity was estimated with Equation (22). Using the estimated average fluid velocity, ΔP was estimated and v_x was determined.

$$v_{avg} = \frac{Q}{w2b} \tag{22}$$

Chapter 2 Materials and Methods

To avoid redundancy, this chapter is a collection of materials and methods that are used throughout the study. Specific treatments or additional methods that are used in each projects are mentioned within the corresponding chapters.

2.1 Cell culture

ECFC

Human umbilical cord blood derived ECFCs (Poietics Human Endothelial Colony Forming Cells, Lonza) were expanded in collagen (BD)-coated tissue culture polystyrene flasks using EGM-2 growth media (Lonza). When ECFCs reached 80-90% confluency, they were subcultured using trypsin (0.025%, Lonza) at 37°C for 1.5 min. Trypsin was neutralized by the addition of ECFC media, followed by centrifugation at 200 g for 5 min. Cells were resuspended in ECFC media and subcultured at a ratio of 1:3 or used for experiments (ECFCs were received at passage 6 and used at passage 8 through 16).

BAEC

BAECs were expanded in collagen (BD)-coated tissue culture polystyrene flasks using general cell culture media. When BAECs reached 80-90% confluency, they were subcultured using trypsin (0.05%, Lonza) at room temperature for 5 min. Trypsin was neutralized by the addition of media, followed by centrifugation at 200 g for 5 min. Cells were resuspended in media and subcultured at a ratio of 1:8 or used for experiments.

Mouse 3T3 cells

Mouse 3T3 cells were expanded in tissue culture polystyrene flasks using general cell culture media. When mouse 3T3 cells reached 80-90% confluency, they were

subcultured using trypsin (0.05%, Lonza) at room temperature for 5 min. Trypsin was neutralized by the addition of media, followed by centrifugation at 200 g for 5 min. Cells were resuspended in media and subcultured at a ratio of 1:8 or used for experiments.

2.2 PEG Acrylation

Poly(ethylene glycol) (PEG, 6kDa; Sigma) was acrylated to form PEGDA following methods that have been previously described (DeLong, Gobin, & West, 2005). In brief, PEG was first lyophilized at -50°C and 0.03 mbar overnight before reaction. Each batch of polyethylene glycol diacrylate (PEGDA) was prepared by reacting 24 g of the lyophilized PEG with 0.016 mol of acryloyl chloride (0.4 M, Alfa Aesar) and 0.008 mol of triethyl amine (0.2 M, TEA, Sigma) in up to 40 mL of anhydrous dichloromethane (DCM, Acros) under argon (Airgas) for at least 12 hr or overnight. Two moles of 1.5 M K_2CO_3 (Fisher) were added per initial mole of acryloyl chloride with vigorous shaking and the mixture was allowed to separate for at least 3 days. The organic phase was collected and anhydrous $MgSO_4$ (Fisher) was added to remove the trace amount of aqueous solution. Vacuum filtration was performed to filter out the $MgSO_4$ in the solution. The PEGDA in the organic solution was precipitated by adding into 1.6 L of cold ethyl ether and stirred for 10 min to move TEA into the organic solution. Then, PEGDA was collected by vacuum filtration and air dried thoroughly to allow most of the ethyl ether (EMD) to evaporate. The PEGDA was further dried by lyophilization or dried under vacuum. PEGDA was then aliquoted and stored under argon at –20°C. The extent of acrylation was estimated by NMR analysis.

2.3 NMR Analysis

After each batch of PEG-DA was prepared, the acrylation percentage was estimated by NMR analysis to characterize the yield of the acrylation process. Sample of PEG-DA was dissolved in 50 mg per 0.75 mL in deuterium oxide (D_2O, Acros) and injected into NMR tube (VWR) that was pre-cleaned with acetone (Macron). Analysis was done by Bruker 400 MHz NMR. Parameters in refining the analysis were used according to the suggested equipment protocol. By setting the D_2O peak at 4.8 ppm, peaks for acrylate single protons were found at around 6.00, 6.20, and 6.45 ppm while the peak representing PEG was found at 3.70 ppm. Integrated intensity peaks were found and used in estimating acrylation percentage and were shown in sample calculations shown in Appendix A.1.

2.4 Peptide Synthesis

An automated peptide synthesizer APEX396 SC (aapptec, Louisville, KY) was used to synthesize the peptides applying solid phase chemistry at room temperature with continuous nitrogen supply that served as an inert atmosphere. Fmoc-Gly-Wang resin and amino acids were first thawed to reach the room temperature before measuring the needed quantity. 600 mg of resin was placed in each chemically resistant Teflon reactor block. Each amino acid solution was prepared in 0.4 M in reagent bottles. After synthesis was completed, peptides were cleaved off from resin in the cleavage block. The cleavage solution was prepared by mixing 95% TFA, 2.5% TIPS, 2.5% ultrapure DI water by volume and used at 10 mL/g of resin. Peptides were collected in the glass collection vessels and poured into centrifuge tubes for air drying. After most of the cleavage solution was evaporated, the peptides were washed three times with cold ether under centrifugation at

4,000X g for 2 min each to remove the left over TFA. After the ether was discarding, the peptides were air dried and prepared for lyophilization. Peptides were then aliquoted into brown glass vials and stored under argon at -80°C.

2.5 Characterization of Peptides by Mass Spectrometry

Peptide synthesis was confirmed by mass spectrometry. A small amount of peptide (<1 mg) was dissolved in 10% acetonitrile and 0.1% formic acid injection solution. Result mass was obtained using Q-TOF Premier (Waters, Milford, MA) and shown in Appendix D .

2.6 PDMS Mold Formation

PDMS spacers and seeding molds were created with Sylgard 184 silicone elastomer kit (Dow Corning) in aiding migration study. Base and curing agent were measured in a 10:1 weight ratio on a disposable weighing dish and mixed vigorously for 3 min. De-gassing of the mixture was done by pulling vacuum in a desiccator. The mixture was then poured into either glass or polystyrene molds, and baked in an oven at 75°C for 1.5 hours. After curing, desired shape was removed from the PDMS using a punch or a blade. Then, PDMS molds were cleaned by sonication in 70% ethanol for 1 hour to remove uncured molecules. After each use, PDMS molds were cleaned and stored in 70% ethanol.

2.7 Hydrogel Formation

Hydrogel precursor solution was prepared and crosslinked in biosafety cabinet to keep the hydrogel sterile. First, precursor solution was prepared by adding sterilized PBS to PEGDA to a concentration of 200 mg/mL. Since clumps of PEGDA were present after

adding PBS, PEGDA is dissolved by first vortexing for 15 s and then a short centrifugation for 10 s. The dissolved PEGDA solution was filter sterilized by passing through a syringe filter (Millipore) having a pore size of 0.22 μm. Photoinitiator was prepared by dissolving 2,2-dimethoxy-2-phenylacetophenone (DMPA, Acros) in N-vinylpyrrolidinone (NVP, Aldrich) at a concentration of 300 mg/mL. The photoinitiator was added to PEGDA solution at 10 μL/mL, where vortexing and centrifugation were also performed, to form the hydrogel precursor solution. The precursor solution was used immediately after it was prepared.

Hydrogel precursor solution was crosslinked with the use of a hydrogel crosslinking mold that consists of three components, including a 0.5 mm thick PDMS spacer, two pieces of rectangular microscope glass slides, and binder clips. Before use, the PDMS spacer was dried completely with nitrogen gun while the glass slides were soaked in a base bath prepared with 1M potassium hydroxide (KOH, Fisher) in ethanol for at least 3 hours and then rinsed with DI water following air drying. All components were setup together and shown in Figure 2.1.

Hydrogel precursor solution was injected into the mold and placed horizontally under a pre-warmed 365 nm UV lamp (Cole-Parmer) with an average intensity of 3 mW/cm^2 at a distance of 2.5 cm for 5 min as shown in Figure 2.2. After the PEG hydrogel was formed, it was rinsed with sterile PBS and briefly dried using a nitrogen gun before peptide grafting. For use as a control, PEG hydrogel was placed in sterile PBS to swell before use.

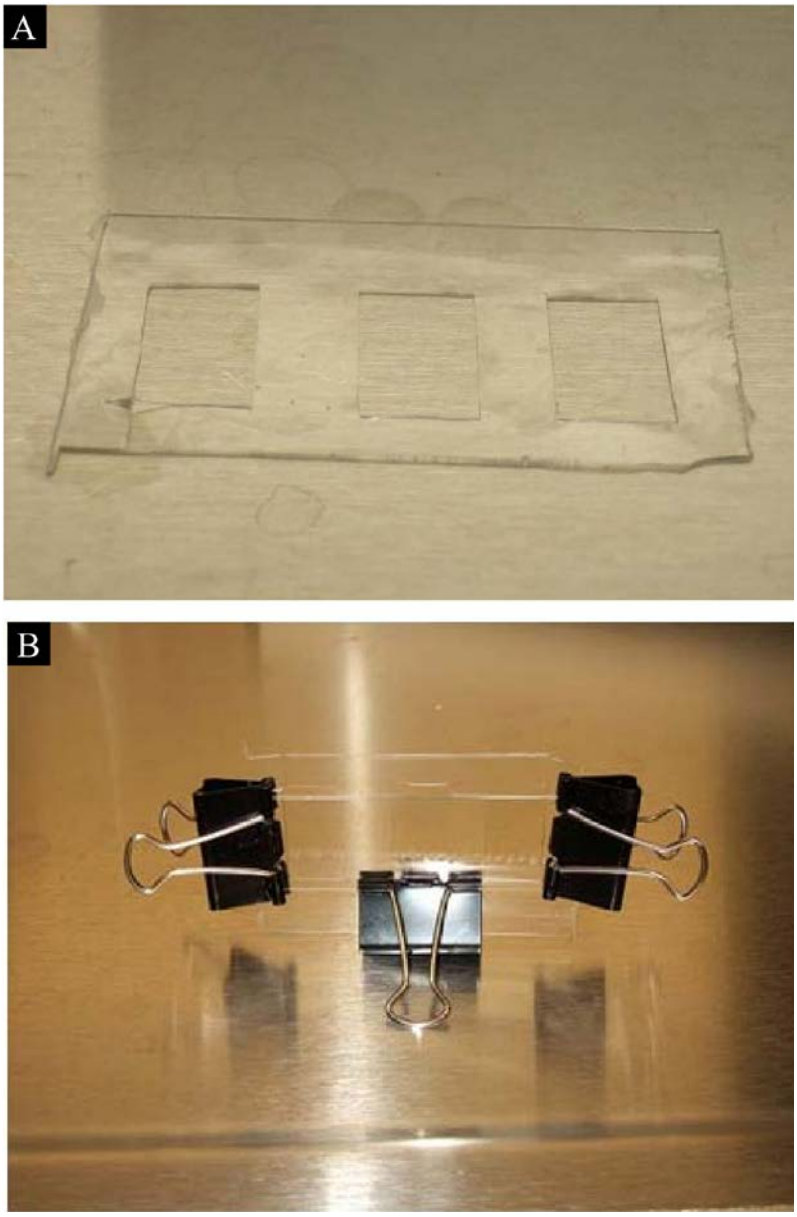

Figure 2.1 Hydrogel crosslinking molds. A) 0.5 mm thick PDMS spacer for crosslinking hydrogel. B) PDMS spacer was placed in between two pieces of glass slides and binder clips were used to hold them together. Polymer precursor solution was injected into the gap created by the spacer for crosslinking.

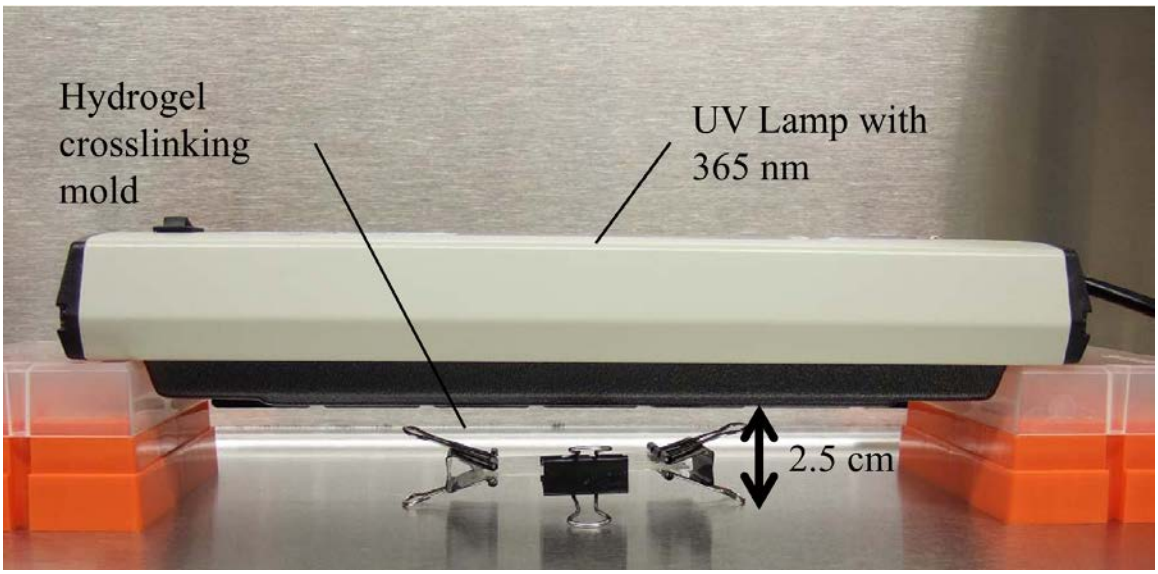

Figure 2.2 Hydrogel crosslinking setup. Hydrogel crosslinking mold was placed at a distance of 2.5 cm away under a UV lamp.

2.8 PEG-peptide Conjugation

Peptides, either synthesized or purchased (American Peptide), were first conjugated to acryloyl-PEG-succinimidyl valerate (acryloyl-PEG-SVA, 3400Da; Laysan Bio) and then grafted onto PEGDA hydrogels. Peptides, including RGDS, RGES, RGDSHHHHHHG, YIGSRG, and REDV, were first dissolved in sodium bicarbonate buffer (0.04 mg/μL, pH 8.5). Acryloyl-PEG-SVA was then dissolved in 1 mL of 50 mm sodium bicarbonate buffer (pH 8.5) for every 10 mg of peptide to be reacted. The final peptide:acryloyl-PEG-SVA molar ratio was 1.2:1. The peptide solution was immediately added dropwise to the acryloyl-PEG-SVA solution with mild vortexing. The mixture was allowed to react for 4 hrs at room temperature in the dark with constant mixing. The resulting acryloyl-PEG-peptide was then dialyzed (molecular weight cutoff 500-1,000, Spectrum Labs) and lyophilized for storage under argon at -80°C in a brown glass vial.

2.9 Hydrogel Grafting with Peptides

To form the PEG-peptide grafting solution, the acryloyl-PEG-peptide was first dissolved in sterile PBS at the desired concentration (ranging from 0.7 mM to 5.6 mM) and the photoinitiator was added as described above. After each PEGDA hydrogel was photocrosslinked, the top plate of the mold was removed. The hydrogels were rinsed with sterile PBS and briefly dried with a stream of nitrogen to remove excess PBS on the surface of the hydrogel. The mold's 0.5 mm PDMS spacers were replaced with 0.7 mm PDMS spacers and a clean glass slide was placed on top. Then the PEG-peptide grafting solution was injected between the hydrogel and the new piece of glass and photocrosslinked to the

top of the PEGDA hydrogel under the UV lamp for 7 min. PEG-peptide grafted hydrogels were then rinsed and swollen in sterile PBS for experiments.

2.10 Cell Adhesion on Peptide-grafted Hydrogels

The ability of the PEG-RGDS grafted hydrogels to support cell adhesion study was tested. Ungrafted PEGDA hydrogels were used as a control. After the hydrogels were formed and swollen, ECFCs were seeded on the hydrogels at a seeding density of 30,000 cells/cm^2 and incubated at 37°C and 5% CO_2. After 1 hour of incubation, the hydrogels were rinsed with sterile PBS and images were acquired using photomicroscopy.

2.11 ECFC Rolling on Hydrogels

For the ECFC dynamic adhesion experiments, the parallel plate flow chamber setup was the same as that for the strength of adhesion experiments. When ECFCs reached 90% confluence, they were detached from the culture flask and resuspended at a final concentration of 1 x 10^6 cells/mL in cell culture media. The cell suspension reservoir was controlled at 37°C using a heated water jacket and was stirred constantly at 150 rpm before the start of the flow and between runs to minimize cell settling and aggregation. A low-flow syringe pump was used to generate the tested shear rates by withdrawing cell suspension from the cell reservoir through the parallel plate flow chamber. ECFC movement was visualized using a 20X objective and images were acquired at 70 fps (time interval between frames is 0.014 s) using an Andor Luca S high speed camera. To determine the instantaneous velocity, cells in the focal plane of the hydrogel were tracked across the field of view. Recordings were taken 10 s after the onset of laminar flow for 2 min. A customized data analysis system to track ECFCs and quantify ECFC velocity was

developed and validated (Wen J Seeto, 2012). Briefly, image processing was first done in ImageJ on a frame by frame basis to identify the centroid of every cell. After all of the centroids were identified, MATLAB was used to correlate the position data for each cell between the frames. Finally, these tracked cell position data sets were analyzed to calculate instantaneous and average rolling velocity. A minimum of three PEG-peptide grafted hydrogels, each prepared separately, were tested for each condition with 30-200 total cells tracked across the field of view. Average cell velocities on each of the three separately prepared hydrogels for each condition were calculated and used for statistical analysis.

2.12 Statistical Analysis

Results were presented as average of three or more replicates for each experiment if not specifically mentioned. Statistical analysis was done by analyzing datasets using two-way analysis of variance (ANOVA), followed by Tukey's test for multiple comparisons. The normality assumption for ANOVA was verified for each condition using the Anderson-Darling Normality Test. Taking all individually tracked rolling cells together, skewness was determined; rolling velocities were considered significantly skewed for a given condition when skewness was larger than two times the standard error of skewness (SES) (Tabachnick & Fidell, 1996) where $SES = \sqrt{\frac{6}{No.of\ Rolling\ cell}}$. Error bars reflect standard deviations. P-values less than 0.05 were considered statistically significant.

Chapter 3 Development of a Flow Chamber System to Investigate Cell Rolling on Hydrogels

3.1 Introduction

EPCs are thought to act similarly to other monocytes in that they roll along the vessel wall. More introduction of EPC rolling will be discussed in Section 5.1. To evaluate cell rolling, a flow chamber system was developed to perform image acquisition of cell rolling on hydrogel.

3.1.1 Hydrogel Formation

Glass slides are commonly used as a mold to form hydrogel sheets or discs. It is critical to ensure the glass slides are clean before use in hydrogel formation. In preliminary studies, unexpected events of ungrafted PEG hydrogels supporting cell adhesion and spreading were observed. It was suspected that glass slides that have been used to graft RGDS peptides on PEG hydrogels contained residual RGDS and, hence, the RGDS were transferred to new PEG hydrogels. Therefore, an investigation was undertaken to determine an appropriate glass cleaning method. Three glass cleaning methods were compared including ethanol cleaning, glass soap brushing, and base bath soaking. The results obtained from this investigation were implemented in choosing the proper glass cleaning method and used in all hydrogel formation experiments.

Taite *et al.* was using a similar PEG-peptide grafting technique to modify the surface of PEG hydrogels. The PEG-peptides were grafted onto the surface of PEG hydrogels by crosslinking the grafting solution under a UV of 365 nm for 1 min with a UV lamp rated at 10 mW/cm^2 (Taite et al., 2006). However, the UV lamp used in this study was rated at 3 mW/cm^2. Since the success of PEG-peptide grafting depends on UV lamp

intensity and crosslinking time, the UV intensity was first confirmed and the effect of crosslinking time on PEG-peptide grafting was then studied. The effect was evaluated through cell adhesion assay. Results showed that crosslinking time affected the success of PEG-peptide grafting. Therefore, evaluation of the effect of crosslinking time was essential for successful PEG-peptide grafting.

Besides crosslinking time, the concentration of the PEG-peptide precursor solution (grafting solution) was considered to be an important factor that affects PEG-peptide grafting. To study the dependency of the final amount of grafted PEG-peptides on the concentration of grafting solution, a HHHHHH-tagged RGDS peptide (HHHHHHRGDSG) was employed and detected by immunolabeling. This allowed us to verify the success of PEG–peptide grafting and to determine the relationship between PEG–peptide concentration in the grafting solution and the amount of grafted PEG–peptide on the PEGDA hydrogel surface.

3.1.2 ECFC Rolling

Cell rolling is a phenomenon that has been historically observed in the recruitment of leukocytes, during inflammation. When a leukocyte comes in contact with the endothelium, surface receptors on the leukocyte interact adhesively with the ligands present on the endothelium. However, this adhesion is transient due to the shear force exerted on the cells by flowing blood. This force causes the leukocyte to roll along the endothelium with the flow stream until the overall cellular adhesiveness, or avidity, is strong enough to withstand the shear forces and support firm adhesion (Ley et al., 1991). The strength of the adhesion depends on the number and types of bonds formed between

the leukocyte and the endothelium. Cell rolling is the result of balanced bond formation and breakage, and it seems to be a necessary step before leukocytes are firmly adhered to the endothelium. Cell rolling velocity can be used to characterize cell rolling (Rinker, Prabhakar, & Truskey, 2001) and it is determined by finding the mean of instantaneous velocity during rolling.

EPCs are thought to act similarly to other monocytes in that they originate from the bone marrow, circulate in the blood, roll along the vessel wall, and eventually firmly adhere (Fadini, Losordo, & Dimmeler, 2012). EPCs can then participate in local repair of the vascular endothelium (Zeng et al., 2012) or extravasate and participate in neovascularization (Asahara et al., 1997). Although EPC rolling has not been widely investigated, EPC rolling has been observed both *in vitro* on extracellular matrix (ECM) proteins (Angelos et al., 2010) and *in vivo* on the endothelium (Vajkoczy et al., 2003). An *in vitro* study by Angelos *et al.* has shown that umbilical cord blood derived EPCs (CB-EPCs) roll on fibronectin and bovine serum albumin (BSA) coated surfaces (Angelos et al., 2010). An *in vivo* study has provided evidence of embryonic EPC (eEPC) moves along the vessel wall within seconds (Vajkoczy et al., 2003). Figure 3.1 showed sequential intravital microscopic images of two labeled eEPCs, 1 and 2. eEPC 1 was firmly captured to the vessel wall under flow and eEPC 2 was moving along the vessel wall from Figure 3.1B to Figure 3.1D in 4 s. Figure 3.1E showed that eEPC 2 was sheared away from the vessel wall at the end of the 4 s. Therefore, EPC rolling was observed in both *in vivo* and *in vitro*. For tissue engineering applications, designing materials which exploit the natural mechanisms for EPC rolling and capture could substantially advance the ability of these materials to be

endothelialized intravascularly as illustrated in Figure 1.2. Ideally, ECFCs would be able to be injected into the blood vessel upstream of a location needing endothelialization and captured on the intravascular material surface. Even if the risk of angiogenesis-mediated tumor growth (Kopp, Ramos, & Rafii, 2006; Mellick et al., 2010; Urbich & Dimmeler, 2004) or other logistical considerations preclude distal injection of ECFCs, designing materials that support firm ECFC adhesion in a relatively short time will still be highly advantageous for use in enhancing endothelialization.

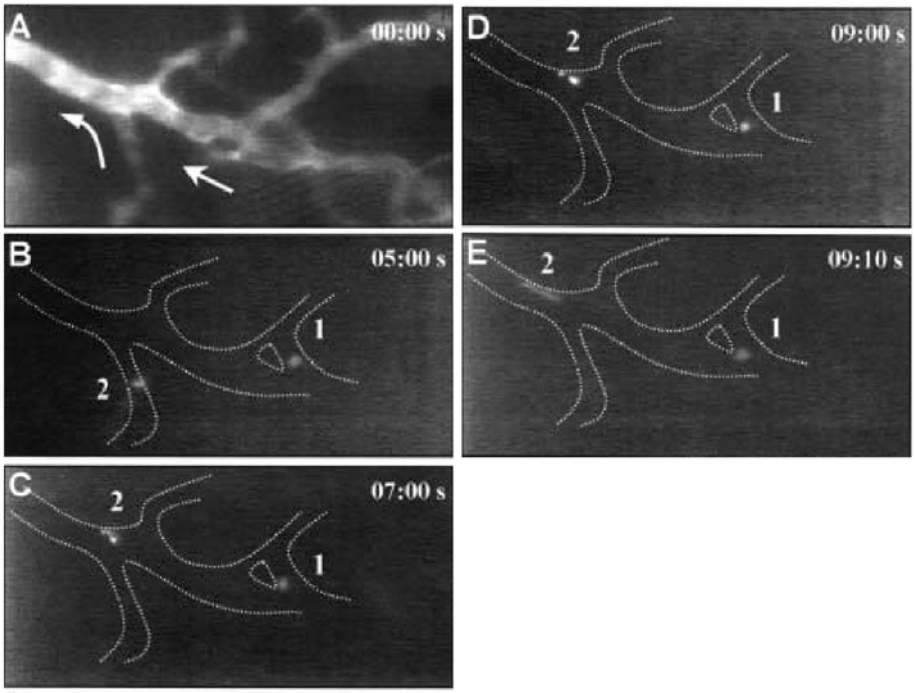

Figure 3.1 Sequential intravital microscopic images of two labeled eEPCs. A) Arrows indicate the direction of blood flow in the tumor blood vessel of the skinfold chamber of nude mice. B) eEPC 1 and 2 were fluorescently labeled and eEPC 1 was captured at bifurcation while eEPC 2 was transiently adhering onto the tumor endothelium. C) eEPC 1 did not move and was shown to be firmly adhered, whereas eEPC 2 reached another location of the endothelium at 2 seconds later. D) Both eEPC 1 and 2 continued to be captured at the same location. E) eEPC 1 remained adhered and eEPC 2 was washed away by the blood flow. Reprinted from Vajkoczy et al., 2003 (copyrighted). Originally published in *The Journal of Experimental Medicine*. Vol:197–12.

EPC Rolling on Hydrogel

As seen in the *in vivo* and *in vitro* examples mentioned above, EPCs possess the ability to roll on either endothelium or ECM proteins. To develop a biomaterial that is suitable for supporting EPCs, the investigation of ECFC rolling provides strong insight in understanding the interaction between ligands and EPC surface receptors. As mentioned in Section 1.3, PEG hydrogels have great potential in serving as vascular graft coatings, especially with respect to their ability to limit protein absorption and their flexibility which is similar to natural tissue. Using the grafting technique, peptides of interest can be immobilized on PEG hydrogels to evaluate the potential of these peptides-grafted hydrogels as biomaterial for ECFCs. Therefore, characterizing rolling velocity of EPCs on a hydrogel material is essential. To my knowledge, all studies investigating EPC rolling have been limited to the use of ECM proteins which bind a wide range of cell surface receptors. This study is robust and unique in that it investigates EPC rolling on a biomaterial surface and examines individual receptor interactions.

3.2 Flow Chamber Setup

3.2.1 Flow Chamber

As mentioned in Section 1.4, parallel plate flow chamber is a standard piece of apparatus in studying the effect of blood vessel like flow on cells. The flow chamber used in this study was purchased from Glycotech (Gaithersburg, MD). The flow chamber consists of a flow deck, silicone gasket and a flat surface that serves as the bottom plate as shown in Figure 3.2. The flow deck has the inlet, outlet and a vacuum port. The silicone gasket in light green color defines the width, length and height of the chamber. Hydrogels

are placed underneath the flow deck and silicone gasket to serve as the bottom plate of the chamber. Since the flow chamber was initially designed to be used on solid surface that serves as the bottom plate of the chamber, it requires a vacuum to keep the flow deck and silicone gasket to stay firmly on the solid surface. However, hydrogels that were used in this study were too soft for this approach; the vacuum suction was found to deform the hydrogel sheet and was not able to form a tight seal. Therefore, a modification was implemented to improve the sealing of the chamber. Each piece of hydrogel was first placed on a glass slide. Then, the flow deck and silicone gasket were placed on top of the hydrogel. A PMDS ring was placed glass slide that surrounds the hydrogels and the flow chamber to contain any potential leaks. Lastly, the flow deck, silicone gasket, the hydrogel and glass slide were hold together by using a custom made metal plates and screws as a clamp as shown in Figure 3.3

Figure 3.2 Image of Glycotech flow chamber. Chamber dimension is determined by the silicone gasket in light green color.

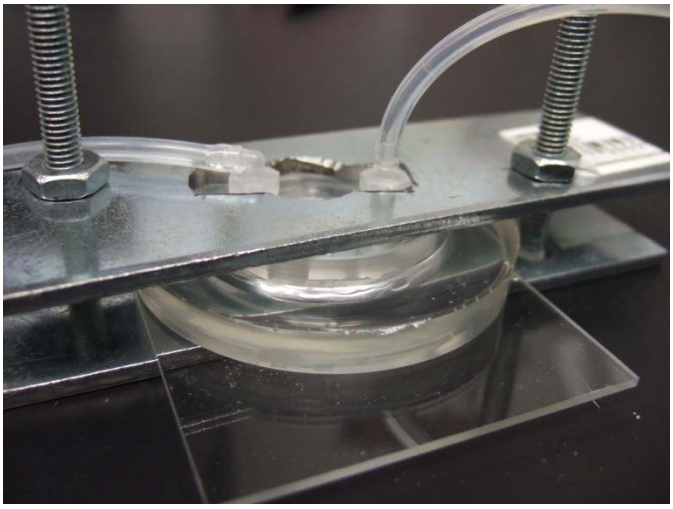

Figure 3.3 Modified flow chamber setup. Flow chamber is clamped with two metal plates and screws in order to hold the flow deck on top of the hydrogel. Holes were drilled in the center of the metal plates for viewing under microscopes. A PDMS ring was placed around the flow deck to keep flow media from leaking, if any, into the microscope.

3.2.2 Syringe Pump

Two syringe pumps were compared for use in flow chamber setup (Figure 3.4). While the syringe pump KDS-100 has a high performance-to-price ratio, it could not deliver a smooth continuous flow at low flow conditions. Suspended cells were observed to "hopping" across the chamber at the shear rates tested (20 – 120 s^{-1}). This was due to a large step size of 0.529 μm/step. As a result, a higher end model KDS Legato 180 that has a step size of 0.031 μm/step was chosen. This pump was able to deliver a smooth flow all the way down to 10 s^{-1}. Therefore, KDS Legato 180 was chosen.

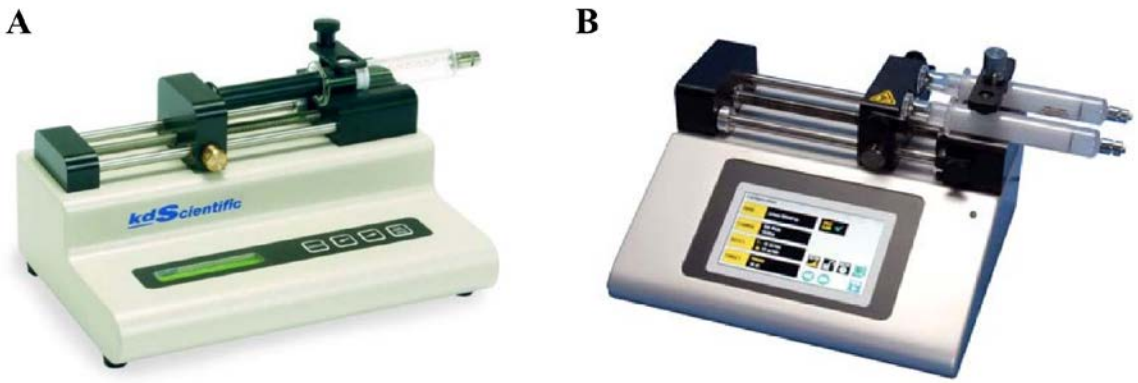

Figure 3.4 Syringe pumps that were compared for cell rolling experiment. A) Syringe pump KDS-100 advances 0.529 μm/step. B) KDS Legato 180 advances 0.031 μm/step. KDS-100 has a much larger step size than KDS Legato 180. Therefore, KDS Legato 180 was chosen as the syringe pump to provide smooth flow. Images adapted from http://www.kdscientific.com.

3.2.3 Cell Reservoir

To eliminate the variability on cell and viscosity of the flow media due to temperature change, a cell reservoir was custom made as shown in Figure 3.5. A 10 mL syringe without the plunger was used as a container to store cell suspension. A 50 mL centrifuge tube was modified as a water jacket to control the temperature at 37°C. Water jacket inlets were connected to a temperature controlled water bath that was cycled using a peristaltic pump. A stir bar and a portable stirrer were used to reduce cell aggregation over time.

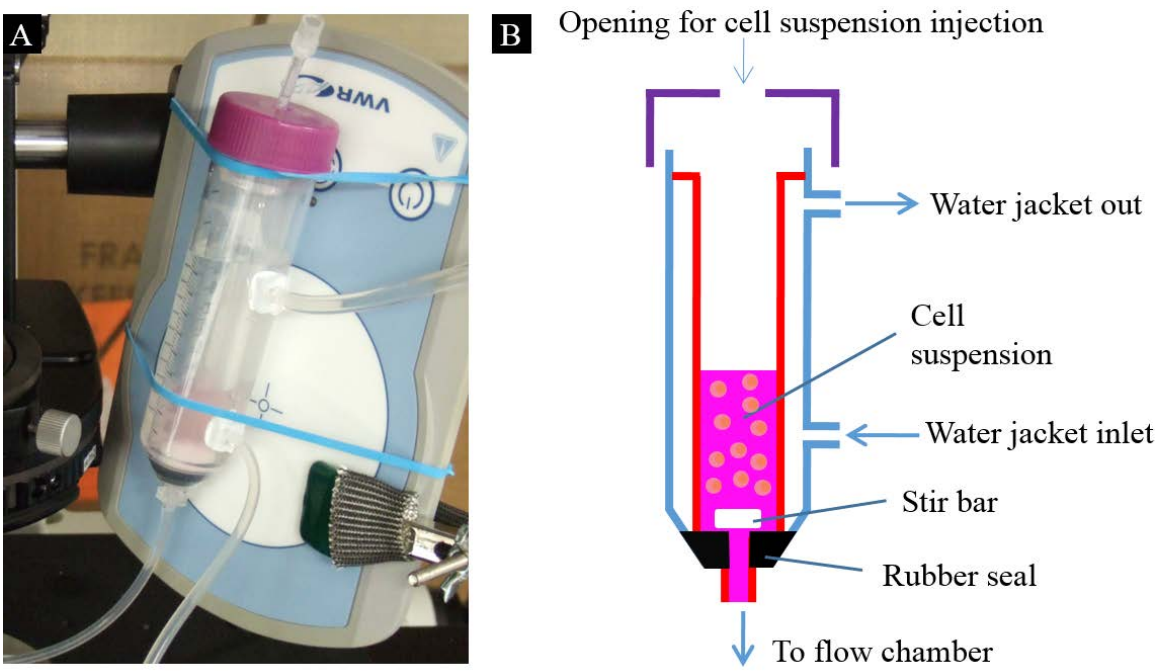

Figure 3.5 Image of cell reservior to maintain temperature and reduce cell aggregation. A) Image of cell reservior. B) Schematic of cell reservior.

3.2.4 Imaging of Cell Rolling

To investigate cell rolling, a suitable camera is required to complete the flow chamber setup. Besides the capability to record the fast action of cell rolling phenomena, several other factors are also essential in choosing a camera for studying cell rolling. Figure 3.6 shows the cameras that I have tested. Cohu 1322, as shown in Figure 3.6A, is a traditional CCD camera. Although it is capable of providing a good resolution of 768 x 494, it is an analog output camera which means that a converter is required to convert the analog signal into the more commonly used digital signal format. The converter that was suggested has a non-user-friendly user interface (UI). The limited codec support also hinders the process of importing to ImageJ and MATLAB. Another critical disadvantage of this camera is that it runs on an interlaced video format. Images from this format are almost impossible for most cell-tracking software to identify cells. Representative image from this camera is shown in Figure 3.7A. AVT Guppy F-033 is a camera that has a high frame rate of 60 fps, but it has a very unique image quality that is also difficult for cell-tracking software to identify cells (Figure 3.6B).

Andor DU-897 and Photometrics Evolve (Figure 3.6C and D) are very similar to each other. Both have high pixel size which is beneficial to recording at low light conditions. In addition, both have a good resolution of 512 x 512 and their images are capable to be binned to increase the frame rate. However, the resolution was significantly decreased when using the binning feature to obtain a high frame rate of 95 fps. As shown in Figure 3.7C, cells are very blurry even using a 20X objective.

Hamamatsu Flash 2.8 (Figure 3.6E)is a camera that has a combination of high speed (45.4 fps) and ultra-high resolution (1920 x 1440) features, but the camera software

does not support instant saving. This camera works in a way that it temporarily saves the video into RAM and then transfers to hard disk for storage at the end of the recording. This mechanism is very time consuming. For example, a 1 minute video is first recorded into RAM and then the video takes 7 minutes to be saved to hard disk. Similarly, pco.pixelfly (Figure 3.6F) has a very similar mechanism to Hamamatsu Flash 2.8 where it saves the video into RAM and then transfer to hard disk for storage. This camera only works with 32-bit Windows which means RAM is limited to 3GB. After the consumption of RAM by Windows OS and other software, the remaining RAM available is sufficient for about 30 sec of recording. As a result, both of these cameras were determined to be not appropriate for the purpose of this study.

Finally, the Andor Luca S (Figure 3.6G) that I have tested was found to be sufficient for cell rolling study. It has a good resolution of 658 x 496 and it is able to be adjusted to 500 x 240 in order to achieve a high frame rate of 70 fps. It is capable to be used with the user friendly and efficient Nikon NIS Elements image acquisition software. Furthermore, it is relatively inexpensive compared to the cameras that I have tested. Therefore, I have chosen the Andor Luca S for cell rolling study due to its high performance-to-price ratio. A summary of comparison between the cameras is shown in Table 3.1. The complete flow chamber system is assembled and shown in Figure 3.8.

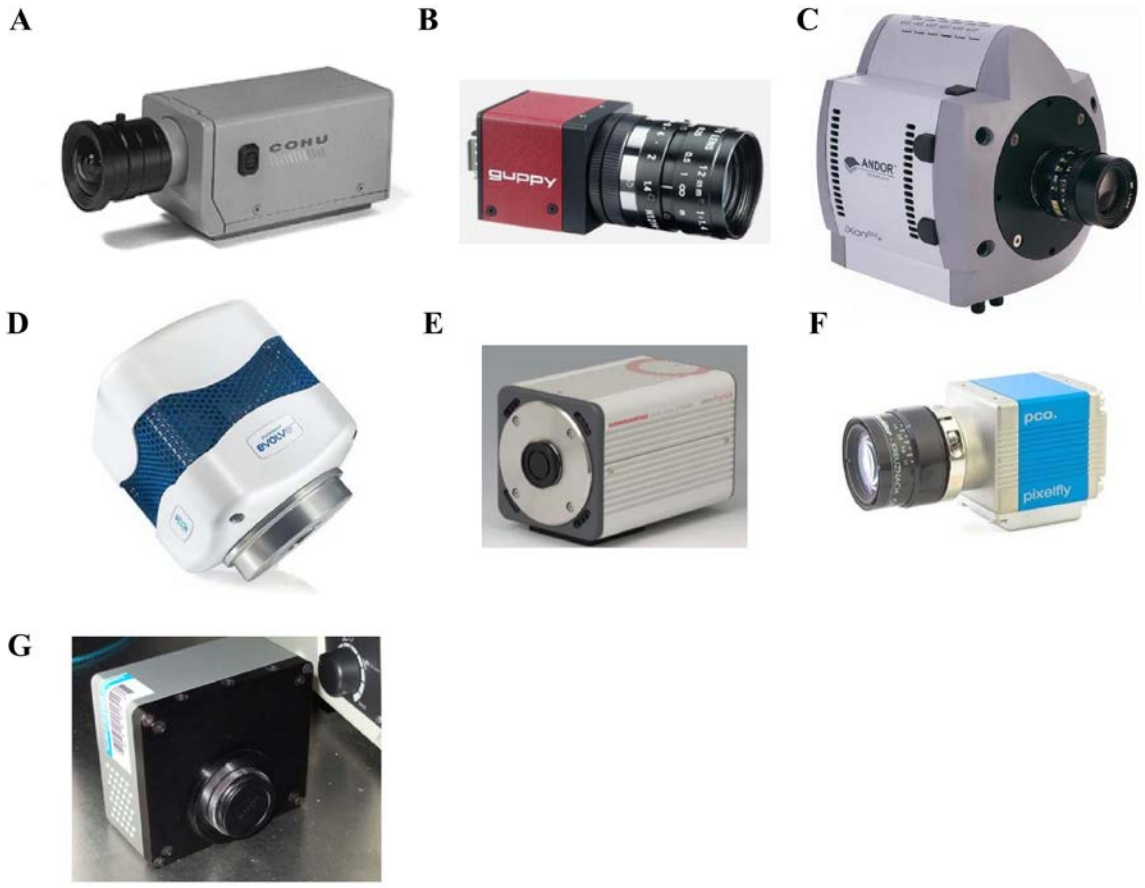

Figure 3.6 Cameras that were compared for use in the investigation of cell rolling. A) Cohu 1322 (B) AVT Guppy F-033 (C) Andor DU-897(D) Photometrics Evolve 512 (E) Hamamatsu Flash 2.8 (F) pco.pixelfly (G) Andor Luca S.

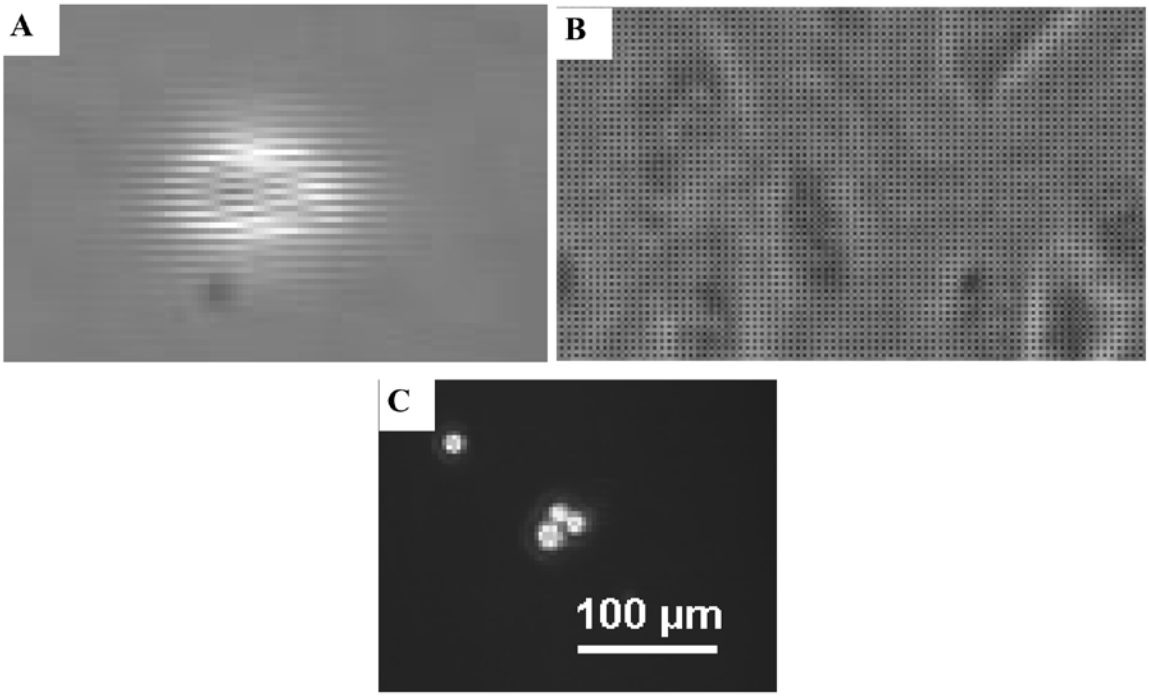

Figure 3.7 Representative screenshots of videos recorded by different cameras. A) Screenshots by Cohu 1322 showing the interlaced video format, which is difficult for cell-tracking software to identify cells. B) Screenshots record by AVT Guppy F-033 showing the unique image quality, which is also difficult for cell-tracking software to identify cells. C) Screenshots recorded by Photometics Evolve that was binned to a resolution of 168 x168 to obtain the necessary high frame rate (70 fps). Cells were too blurry for tracking.

Table 3.1 Summary of tested cameras for cell rolling.

Camera	Price	Pros	Cons
Cohu 1322	NA	Good resolution	Analog output Interlaced videos Poor UI Lack of supported codec
AVT Guppy F-033	NA	Max. 60 fps	Small sensor area 1/3” Hard to use UI
Andor DU-897	$$$$	High pixel size	Low resolution after binning for high frame rate Extremely expensive
Photometrics Evolve 512	$$$$	High pixel size	Low resolution after binning for high frame rate Extremely expensive
Hamamatsu Flash 2.8	$$$	High resolution Relatively inexpensive	Long saving time
pco.pixelfly	$	Very Inexpensive	Unable to perform extended period of video recording Poor UI Poor interface
Andor Luca S	$$	High speed Good resolution Relatively inexpensive	NA

Figure 3.8 Image of flow chamber setup for cell rolling study . A 10 mL syringe without the plunger was used as cell reservoir as shown in Figure 3.5B. Cell reservoir was placed in a 50 mL centrifuge tube that served as a water jacket to control temperature at 37°C by a water bath. Cells were withdrawn from the cell reservoir through the flow chamber by a syringe pump on the left. The chamber setup was placed on the microscope stage that was connected to a high speed camera for video recording.

Chapter 4 Development of an Optical Cell Tracking Analysis Using a Straight-forward Approach to Minimize Processing Time for High Frame Rate Data

4.1 Introduction

Cell tracking and analysis of rolling cells under flow has provided important insights into the understanding of mechanisms involved in inflammation and wound healing. This process has been historically labor intensive and time consuming (Dow, Lackie, & Crocket, 1987). To obtain the instantaneous cell velocity, one had to first manually identify the position of each cell on a frame-by-frame basis in the video recording (Acton, Wethmar, & Ley, 2002). Then the displacement for each cell between sequential frames can be obtained and used in calculating cell velocity. However, as the number of cells increases, the time required to carry out this tracking procedure also subsequently tremendously increases. In addition, as the speed of the camera, or, more specifically, the maximum frame rate or frames per second (fps) able to be acquired, increases, the amount of data increases, and, therefore, the time needed to analyze the recorded data becomes unmanageable.

Tracking and analysis of rolling cells via *in vitro* experiment has evolved from the traditional manual tracking methods to more recent computer tracking approaches. With the development of computer program algorithms for cell identification, the position of each cell can be found automatically. Similar to the steps in manual tracking, computer-aided tracking first involves cell identification, then cell position tracking on a frame-by-frame basis, and final analysis (Cheezum, Walker, & Guilford, 2001). Besides eliminating the need for tedious manual cell tracking, computer program algorithms also avoid bias

that can be introduced by an investigator during manual analysis (DiVietro et al., 2001; E. Y. H. Park et al., 2002; Smith, Berg, & Lawrence, 1999).

Nevertheless, there are inherent challenges to automated cell tracking and analysis that cannot be solved easily with standard computer program image analysis algorithms. There are two critical problems: 1) long computation time due to the complexity of tracking algorithms, and 2) frequent confusion caused by cells that come in close proximity to each other or come in contact with each other. Here we developed a sophisticated tracking algorithm that implements ImageJ and MATLAB to address these two problems. The advantages of both software can be combined to achieve a simple and highly effective solution.

4.2 Concept

The approach described in this manuscript for tracking rolling cells under flow is divided into two main processes (Figure 4.1). The first process employs ImageJ, a public domain image analysis software by National Institutes of Health (NIH), to identify the cells and document their geometric and position information on each frame. The second process takes the frame-by-frame information generated by ImageJ processing and uses this data to correlate identified cells between frames using MATLAB. Finally, the tracked data are output to Excel spreadsheets.

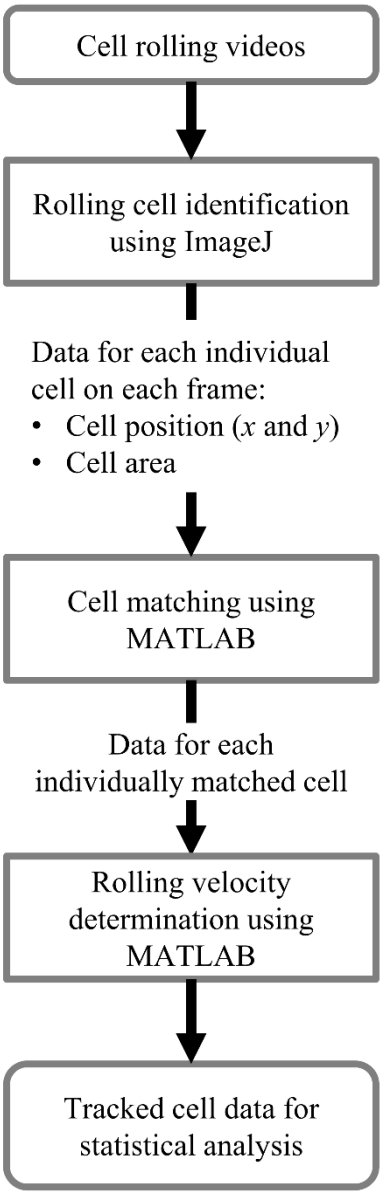

Figure 4.1 Work flow of cell tracking using ImageJ and MATLAB. Supplemental Video 1 shows Image J rolling cell identification and Supplemental Video 2 shows cell matching using MATLAB.

4.3 Cell Identification using ImageJ

ImageJ is a public domain image analysis software and is specifically chosen for rolling cell identification in this manuscript. This Java-based image processing software was first developed at NIH in 1997 and it is now widely embraced by the research community. As of May 2012, more than 20,000 search results on ImageJ could be found in Pubmed Central (Schneider, Rasband, & Eliceiri, 2012). ImageJ has been extensively used by researchers due to its powerful features that resemble commercially available image-processing programs (e.g. Adobe Photoshop), easy-to-use nature, and high compatibility with myriads of image file formats.

The advantage of using ImageJ for identifying cell position, besides those mentioned above, is that ImageJ has preset thresholding methods that can efficiently and rapidly identify the edge of each cell. Each of these preset methods determines an optimal threshold level using its specific thresholding method. ImageJ also allows the user to manually set the threshold when these methods cannot provide the best result. In most cases, these thresholding methods are able to identify the edge of each cell. The ImageJ thresholding methods that were used frequently in this study were Intermodes, IsoData, and MaxEntropy. The optimal thresholding method for a given recording or set of recordings was found to depend on the light intensity, camera settings, cell type, the material used for the bottom plate of the chamber, and other specific experimental conditions; in most cases, using MaxEntropy as the threshold method gave the best results. The steps developed in this study to identify cell positions are as follows (Supplemental Video 1):

1. Load a cell rolling video (~8000 frames) into ImageJ (Approximate time: 1 min)

2. Convert each frame into 8-bit (Figure 4.2A, approximate time: 10 s)
3. Apply thresholds to each frame and convert them into black and white images so that each cell appears to be a white ring object with black background (Figure 4.2B, approximate time: 10 s)
4. Fill in the hole of each white ring to obtain solid white objects (Figure 4.2C, approximate time: 10 s)
5. Find the position of each cell (solid white objects) with respect to the preset parameters including size and circularity (Figure 4.2D, approximate time: 3 min)
6. Export data of all identified cells to tab delimited text file.

Multiple ImageJ parameters were used to insure that only single cells were tracked. To avoid inaccuracies during tracking caused by cells that come in contact, only single cells were considered. Cells that come in contact have a larger area and a much lower circularity when compared to single cells, thus identification parameters, such as the acceptable range for cell area and circularity, were set in ImageJ to prevent tracking of these cells. The identification parameters also served to exclude tracking of undesired objects, such as cell debris (size of debris $\ll$ size of cell) and cell clumps (size of clumps $\gg$ size of cell) that occasionally appeared in the flow media. Settings for cell size and circularity may require optimization depending on experimental conditions and cell type being analyzed. To make certain only single cells were tracked, objects appearing along the edge of the field of view were also excluded by settings in ImageJ.

Details for each identified cell, including cell position in Cartesian coordinates, cell area, cell circularity, cell index and frame number, were imported to MATLAB for matching. A custom ImageJ macro was written to run all the ImageJ processing steps for each video file (macro file available upon request and provided as supplemental file). This ImageJ macro also features the ability to output and save videos of outlined cells to provide visual confirmation of identified cells (Supplemental Video 3). These outlined cells are indexed in the video, making it possible to easily correlate an individual cell observed in the video with the tracking information for that cell provided subsequently by MATLAB matching and with the final analyzed individual cell rolling data.

To avoid confusion during tracking caused by cells that come in contact, only single cells were considered. For cells that come in contact, they have a larger area and a much lower roundness when compared to single cells, so identification parameters, such as the acceptable range for cell area and roundness, were set in ImageJ to prevent tracking of these cells. The identification parameters also served to exclude tracking of undesired objects including small debris and big cell clumps that occasionally appeared in the flow media. To make sure only single cells were tracked, objects appearing along the edge of the field of view were also excluded. Details for each identified cell, including x and y coordinates, cell area, cell roundness, and frame number, were output into an Excel spreadsheet for matching using MATLAB. A custom ImageJ macro (Appendix B) was written to run all these steps for each video file.

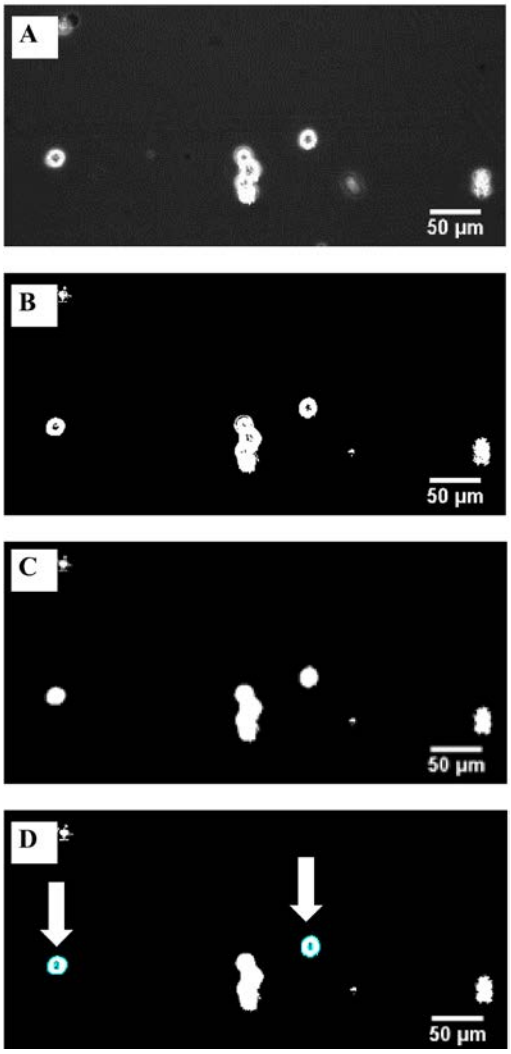

Figure 4.2 Representative images of rolling ECFC identification process by ImageJ. a) Image converted to 8-bit from 16-bit. b) ImageJ filter was applied to produce black and white image. c) Internal holes were filled. d) Image showing the tracked ECFCs with index label (white arrows). Indexed cells from this ImageJ identification process are used for visual confirmation of appropriate identification and index labels are transposed onto the original video recording for later correlation with the final MATLAB processed data on a cell-by-cell basis (Supplemental Video 2).

4.4 Matching Cells with Custom Developed MATLAB Code

After using ImageJ to identify the positions of all cells on each frame, the geometric and position information are imported to MATLAB for matching. The matching process correlates this information for each individual cell in a given frame with the data for each cell identified in the next frame. Using this process, the frame-by-frame positions of each individual cell are output in sequential order; this data can then be used to determine the rolling velocity of each cell. MATLAB code (Appendix C) was established to implement the following steps. First, a cell list was initiated by including all cells in the first frame ($frame_{i=1}$) for matching. Then, each of the cells appearing in the next frame ($frame_{i+1}$) were matched to a cell in the cell list based on three major criteria. To accomplish this, first the difference in *y*-position between the cell from the new frame and the cell from the cell pool must be equal or less than a specified distance for them to be considered as potentially matching. Since the cells are flowing horizontally across the flow chamber (in the *x*-direction), the *y* coordinate of a cell in consecutive frames should not be substantially different. For example, in our previous study of endothelial colony forming cell (ECFC) rolling (W J Seeto et al., 2013), most ECFCs were founds to have an average diameter of 15 to 20 μm in suspension, so the cutoff for difference in *y*-position was set at 10 μm, which is approximately half of the ECFC diameter. Second, cell area between frames cannot differ more than 30% between consecutive frames, which corresponds to a change of 15% in cell diameter. This restriction on change in cell area was implemented to exclude cells on a higher focal plane that commonly appear to be larger than the cells in focus on the bottom of the flow chamber. Based on our observations and testing, most cells exhibit a 1-5% change in their area between consecutive frames during rolling and some may change

up to 25%. Thus, using a cutoff of 30% for cell area was found to be optimal for our application. This cutoff would need adjustment depending on image resolution, frame rate and cell type being used. Third, the displacement of a given cell must not be greater than the distance physically possible for it to have moved at the fluid flow velocity being tested. A cutoff on displacement distance between frames was, therefore, used to prevent potentially mismatched cells. This distance is dependent on both the fluid flow velocity one cell diameter away from the wall, which changes with the shear rate that was being tested, and the rate of data acquisition, i.e. frames per second. In the process of matching, an upper limit on *x* displacement, Δx_{max}, was calculated by EQUATION 23.

$$\Delta x_{max} = \frac{\text{Estimated fluid velocity at one cell diameter away from the bottom of the flow chamber}}{\text{Frame rate}} \qquad (23)$$

The fluid velocity at one cell diameter above the bottom of the flow chamber (the focal plane), estimated based on calculations for laminar flow of a Newtonian fluid between parallel plates, was determined to be an effective upper limit cutoff for cell velocity and is calculated by the MATLAB code based on the input experimental parameters. This estimate was divided by the acquired frames per second, to set the upper limit on *x* displacement, Δx_{max}. Important to consider is that the frame rate of the high speed camera fluctuates over the course of experiments due to the increase in camera temperature. Therefore, dividing by the acquired fps (versus using the theoretical or upper setpoint for fps) was used to account for differences in frame rate between videos (EQUATION 23).

Cells streaming above the focal plane can obscure a rolling cell below, making the area of the rolling cell appear too large and causing it to fall outside of the ImageJ thresholds for cell identification in that frame. The obscured cell will therefore not be included in the ImageJ data for one or more frames and then will be re-included when it is no longer obscured, meaning not all cells are included for every consecutive frame in the data passed from ImageJ to MATLAB. If a cell was not included in the data for the immediately prior frame, the MATLAB code will mistakenly treat these cells as new cells and add them to cell list for matching, even if the cell was included in the data two or more frames earlier. In order to avoid this mistake in cell matching, a tolerance mechanism was established to allow the matching process to skip up to a certain number of frames ($\Delta Frame_{max}$) for cells that are not identified in every frame. Given the high frame rate and, therefore, small displacement per frame, accurate cell matching is still possible in these cases. Starting with the assumption that the space occupied by a particular cell can never be simultaneously occupied any other cell, any object (cell) that is identified within the same space (within one cell diameter from the center of an identified cell) in subsequent frames and, also, fulfills the $\Delta Area<30\%$ criterion is, theoretically, the same cell. The maximum number of frames that can be skipped, $\Delta Frame_{max}$, is determined by the number of frames required for the cell to travel a distance of one cell diameter (as shown in EQUATION 24). To assess this, it is also necessary to know the speed at which the cell is traveling. To evaluate the cell's traveling speed, its average x displacement over the number of frames matched, $\Delta x_{avg,\,\Delta Frame}$, is calculated using EQUATION 3, where x_1 is the

initial x-position of the cell on the first matched frame (Frame_1) and x_k is the x-position of the cell on the last matched frame (Frame_k).

$$\Delta\text{Frame}_{max} = \left(\frac{\text{Cell diameter}}{\Delta x_{\Delta\text{Frame}}}\right) \tag{24}$$

$$\Delta x_{avg,\,\Delta\text{Frame}} = \frac{\Delta(x_k - x_1)}{\Delta(\text{Frame}_k - \text{Frame}_1)} \tag{25}$$

Both ΔFrame_{max} and $\Delta x_{avg,\,\Delta\text{Frame}}$ are constantly updated whenever a new frame is matched for each cell. When matching cells that are more than one frame apart, the upper limit on x-displacement over a number of skipped frames ($\Delta x_{max,\,\Delta\text{Frame}}$) is calculated using EQUATION 4 and 5 instead of EQUATION 1. When $\Delta x_{max,\,\Delta\text{Frame}}$ (calculated using EQUATION 26) is less than one cell diameter, $\Delta x_{max,\,\Delta\text{Frame}}$ equals Δx_{max} multiplied by the number of frames that have been skipped, ΔFrame. On the other hand, when $\Delta x_{max,\,\Delta\text{Frame}}$ is larger than one cell diameter, $\Delta x_{max,\,\Delta\text{Frame}}$ is capped at one cell diameter (EQUATION 27). A representative example showing how this matching tolerant mechanism works to match cells between skipped frames is illustrated in Figure 4.3. Using this matching tolerance mechanism, accurate cell matching is achieved for cells that are not identified in all consecutive frames with minimal risk of compromising the data by inaccurate matching.

$$\text{For } \Delta\text{Frame}>1,\ \Delta x_{max,\,\Delta\text{Frame}} = \Delta x_{max} \times \Delta\text{Frame} \tag{26}$$

$$\text{For } \Delta\text{Frame}>1 \text{ and } \Delta x_{max,\,\Delta\text{Frame}} \geq \text{Cell Diameter},\ \Delta x_{max,\,\Delta\text{Frame}} = \text{Cell Diameter} \tag{27}$$

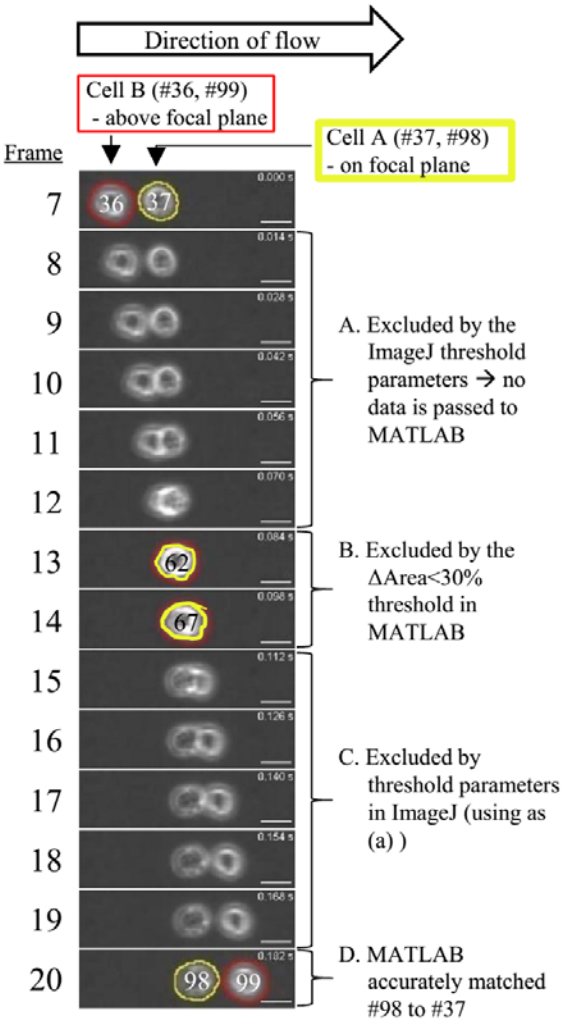

E.

k^{th}	$Frame_k$	Cell Index	$Area_k$ (μm^2)	x_k (μm)	$\frac{\Delta x_{avg.}}{\Delta Frame}$ (μm)	$\Delta Frame_{max}$	$\Delta Frame$	Δx_{max}
1	2	7	518.1	181.8	–	1 *	–	—
2	3	12	507.5	183.2	1.48	16	1	Δx_{max}
3	4	18	496.0	184.8	1.54	16	1	Δx_{max}
4	5	24	495.0	186.7	1.65	15	1	Δx_{max}
5	6	31	479.6	188.3	1.65	15	1	Δx_{max}
6	7	37	472.9	190.3	1.70	14	1	Δx_{max}
7	20	98	549.8	214.8	1.83	13	13	Cell Diameter
8	21	105	536.3	216.5	1.83	13	1	Δx_{max}
9	22	112	543.1	218.5	1.84	13	1	Δx_{max}
10	23	120	539.2	220.6	1.85	13	1	Δx_{max}
⋮	⋮	⋮	⋮	⋮	⋮	⋮	⋮	⋮

Figure 4.3 Illustration of accurately matching a rolling cell (Cell A) that is temporarily obscured by a cell flowing above the focal plane (Cell B). Cells are identified by ImageJ in Frames 7, 13, 14, and 20 and assigned indices. Cell #37 in Frame 7 and #98 in Frame 20 are the same cell (Cell A) that is rolling on the surface, whereas cell #36 in Frame 7 and cell #99 in Frame 20 is another cell (Cell B) that is flowing above Cell A. Data from Frames 8-19 is excluded to prevent mismatching and Cell A in Frame 20 (#37) is then accurately re-matched to Cell A (#98) in Frame 20 using Equations 24-27. A) Touching or

overlapping cells do not meet the size threshold in ImageJ; therefore these cells are excluded and no data is passed to MATLAB. B) Cell #62 and #67 did not meet the ΔArea<30% threshold and are therefore not matched to Cell A by MATLAB. C) Based on the same criteria as in frames 8-12 described in part A), cells in frames 15-19 are excluded by the ImageJ threshold parameters and data is not passed to MATLAB. D) Cell #98 was accurately matched to cell #37 where the number of obscured frames (ΔFrame) was less than the maximum number of frames that can be skipped ($\Delta Frame_{max}$ — calculated using Equation 2 and 3) and the *x*-displacement (Δx) during the obscured frames is less than the maximum allowed *x*-displacement during the obscured frames ($\Delta x_{max,\ \Delta frame}$ — calculated using Equations 4 and 5). E) Table showing the Cell A's matching data. Highlighted portion of the table is the results exported from MATLAB cell matching code. *The first $\Delta Frame_{max}$ is set to 1 by default. A video of these sequential images is shown in Supplemental Video 4.

This matching process was repeated until the last frame of each video; the matching logic is shown as a flow chart in Figure 4.4. After data for each cell was matched, displacement distance and instantaneous velocity were calculated. Following processing using the MATLAB code, important data for each cell, including average rolling velocity and the percentage of frames in which the cell was rolling, can be obtained for analysis and comparison.

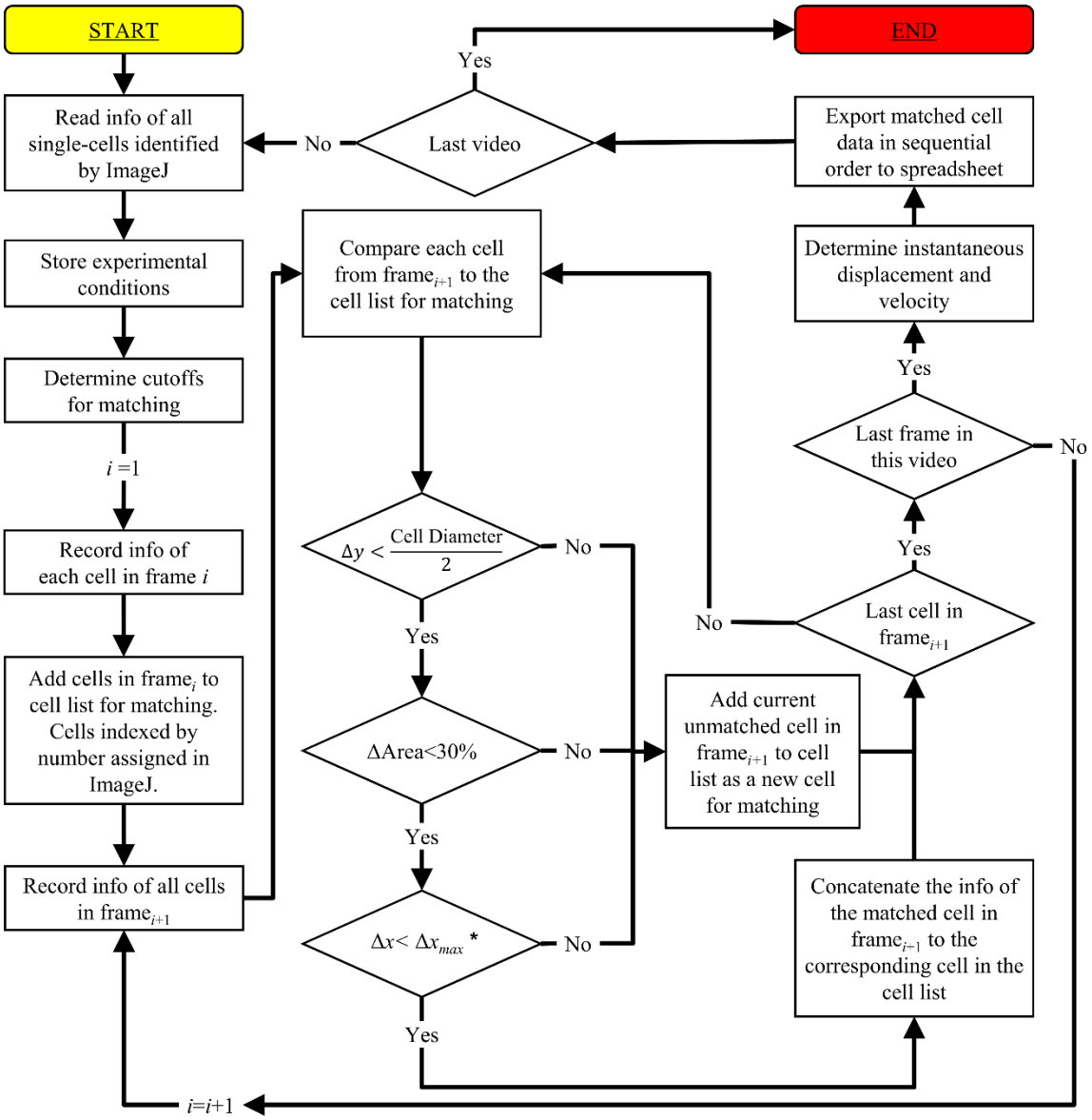

Figure 4.4 Flow chart of the matching process using MATLAB. Multiple nested loops were used to run through all conditions, shear rates, frames, and cells on each frame. Three major matching parameters were Δy, ΔArea, and Δx. *When matching cells that are not in consecutive frames, Δx_{max} is replaced by $\Delta x_{max,\Delta Frame}$ as defined by EQUATION 26 and EQUATION 27.

4.5 Analysis

The study of leukocyte rolling provides useful information in understanding the pathology of inflammation and wound healing. Rolling velocity is an excellent parameter to predict the magnitude of the inflammatory response (Jung, Norman, Scharffetter-Kochanek, Beaudet, & Ley, 1998). A parallel plate flow chamber is generally used to study cell rolling *in vitro* (Konstantopoulos, Kukreti, & McIntire, 1998; Lawrence & Springer, 1991; Rinker et al., 2001). A variety of ligands can be immobilized onto the bottom of the flow chamber and cells are perfused through the chamber (Angelos et al., 2010; Shirure, Henson, Schnaar, Nimrichter, & Burdick, 2011; Taite et al., 2006). By assessing the velocity of rolling cells, the role of different cell surface receptors and their corresponding ligands in influencing cell velocity under flow conditions can then be evaluated.

The novel rolling cell tracking algorithm reported here has been previously used in understanding the effect of immobilized peptides on ECFC rolling under shear (W J Seeto et al., 2013). ECFC rolling events at different shear rates were recorded by Andor Luca S high speed camera at 70 fps, and the NIS Elements (Nikon) was used as the acquisition software. The recording videos were saved in the NIS Elements' nd2 file format and loaded into ImageJ using the Bio-Formats ImageJ plug-in. The nd2 file format was chosen because it maintains all acquisition parameters (including pixel size and fps) in the file as metadata; these acquisition parameters were used in cell identification and matching. After matching, instantaneous rolling velocities for each individual tracked cell at all instances were obtained using EQUATION 28, where displacement is the distance traveled by the cell over some number of frames (ΔFrame). ΔFrame equals from 1 frame up to $\Delta Frame_{max,k}$ if a cell does not appear in every consecutive frame.

$$\text{Instantaneous rolling velocity} = \text{Displacement} \times \frac{\text{Frame rate}}{\Delta\ \text{Frame}} \quad (28)$$

Next, the average rolling velocity for each ECFC was obtained using EQUATION 29, where N is the total number of instantaneous velocities being averaged:

$$\text{Average rolling velocity of individual cell} = \frac{\sum_{i=1}^{N} \text{Instantaneous velocity}}{N} \quad (29)$$

Data obtained through the use of this cell tracking analysis method can be reported on an individual cell basis or data from groups of tracked cells can be averaged for comparison between tested conditions. Figure 4.5A shows example instantaneous rolling velocity data from representative cells over a range of tested shear rates. Average rolling velocities of individual ECFCs found using EQUATION 29 in shown in Figure 4.5B; in this case three separate trials were carried out on separately prepared RGDS peptide-grafted hydrogels at various shear rates (W J Seeto et al., 2013) and each data point on the graph represents one tracked cell. Furthermore, by combining the average velocity data from all rolling ECFCs in each of the three separate trials, average ECFC velocity on RGDS-grafted hydrogels was obtained as shown in Figure 4.5C.

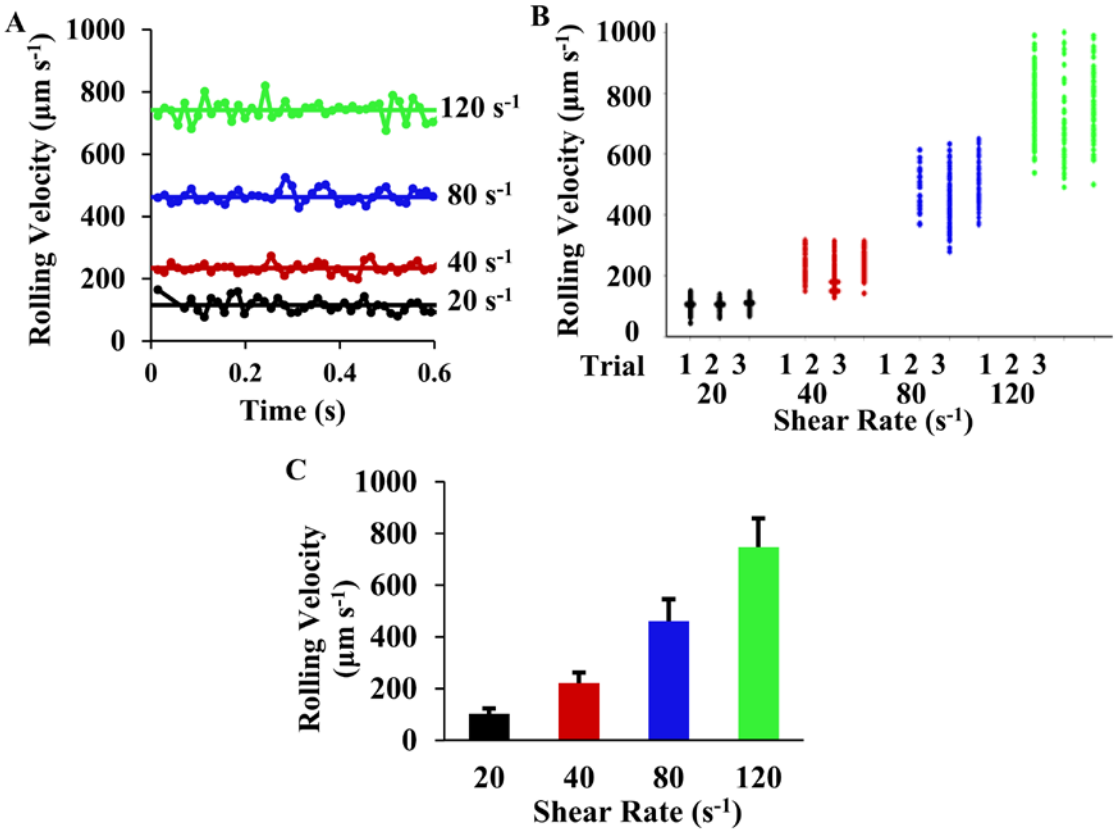

Figure 4.5 Analyzed data obtained using this rolling cell tracking system can be used for further comparative analysis and visualization through generation of multiple types of data plots. a) Instantaneous rolling velocity of representative cells at each tested shear rate can be plotted over time, in this case rolling on RGDS-grafted hydrogels., b) The distribution of rolling velocities for each rolling cell can be visulaized by plotting the individual average rolling velocities; plot shows the distribution of rolling velocities for rolling ECFCs where each marker represents one rolling cell. c) Comparative analysis between multiple replicates of conditions can also be done; here the average rolling velocity of all rolling ECFCs on RGDS-grafted hydrogels at each tested shear rate are shown. Data represent mean ± SD (n=3 separately prepared peptide-grafted hydrogels with 30-100 cells per trial).

4.6 Discussion

The rolling cell tracking system described here has provided a simple, yet highly effective, solution to challenges that commonly appear in typical cell tracking software. Most cell tracking systems require relatively long computation times for cell identification. Using ImageJ for cell identification substantially decreases the time required to track rolling cells, an improvement which can be attributed to use of the preset automatic thresholding methods. ImageJ's straight-forward interface allows users to readily adjust the identification parameters for their specific applications. This minimizes the depth of knowledge and skill in image analysis required to obtain accurate results. Besides decreasing the time required for cell tracking, ImageJ also delivers additional advantageous features that are essential to researchers. One is the capability of outlining and labeling cells in a video showing the identified cells. This provides users a visual verification of the identified cells (Supplemental Video 3). Another is the efficient cell identification process which results in a lower requirement on high-level computational power, which correlates to lower cost. A third advantage of ImageJ is the ability to install various plugins and codecs, reducing the need for time-consuming video conversion between different operating systems or software. Therefore, using ImageJ as cell identification software results in reduced tracking time.

By using MATLAB for cell matching, cell data output from ImageJ can be further processed for data analysis. Accuracy in rolling cell tracking is commonly hampered by frequent confusion of cells that come in close proximity to each other or come in contact with each other (Cheezum et al., 2001; Schmidt, Paschall, Guilford, & Lawrence, 2007). Based on the different approaches developed by Dr. Lawrence's research group (Cheezum

et al., 2001; Schmidt et al., 2007), we have employed both ImageJ and MATLAB in this custom matching algorithm to enhance tracking accuracy. Cells that come close together are compared to themselves in a previous frame using geometric and positional information, i.e. area, *x*-, and *y*-coordinates. For cells that come in contact, their apparent area will either exceed thresholds set in ImageJ for cell identification or set by MATLAB for cell matching. This custom matching algorithm has been validated with extensive testing to deliver repeatability.

The algorithm system reported here was developed to track endothelial cells with approximate spherical cell shape. For cells with a different geometry, cell identification parameters used in this method may need to be optimized for accurate tracking. For example, platelets have a disc shape morphology meaning that they may appear to be an elongated oval depending on viewing angle. In such cases, some cells could be inappropriately excluded during the identification step. Therefore, further testing and optimization would be necessary to ensure accurate tracking of non-spherical objects.

Besides cell types, manipulation of shear conditions is another area of interest in typical cell rolling research. Although laminar flow is most commonly used to mimic flow in blood vessels, more complex flow conditions are common in physiological situations, including unsteady flow caused by the pulsatile nature of blood flow and reversed flow caused by expansion or contraction of blood vessels. Cell matching described in this tracking algorithm has not been optimized for these flow conditions, so further modification is anticipated to be required for analysis of such data.

4.7 Conclusion

A sophisticated cell tracking system that is needed to support *in vitro* experimental analysis was established. The cell rolling tracking algorithm in this study was developed to decrease the computation time and eliminate the issue of incorrect cell tracking due to cells that come into close proximity or contact with each other. Using this tracking system, the average time needed to track a 2 min cell rolling video at 70 fps is less than 20 min, which is a dramatic decrease as compared to currently available systems, and the issue of excluding interacting cells from the tracking data was also resolved.

Chapter 5 Evaluation of the Ability of Known Peptides to Slow EPC Rolling

5.1 Introduction

Endothelial progenitor cells (EPCs) are an important autologous cell source for many tissue engineering applications (Levenberg, 2005). Understanding the interactions of these cells with materials will, however, be critical, in taking advantage of their usefulness. Endothelial cells (ECs) form the lining of blood vessels, making them vital for the prevention of thrombosis in established vessels as well as for new blood vessel formation. Therefore, EPCs could prove useful for endothelializing small-diameter vascular grafts, for vascularizing tissue-engineered constructs, for repairing areas of the vasculature damaged by atherosclerosis, and for preventing restenosis, or the re-narrowing of vessels, following balloon angioplasty.

EPCs are a subpopulation of monocytes that are derived from myeloid cells, which are one type of leukocyte (Moldovan, 2003). EPCs that have been isolated from blood and expanded *in vitro* are frequently called late outgrowth or endothelial colony forming cells (ECFCs) (Timmermans et al., 2009). Expression of surface receptors on these cells differs from other types of monocytes, "early outgrowth" EPCs, and mature endothelial cells (Fadini et al., 2012). Advantages of ECFCs for tissue engineering applications include the relative ease and lack of comorbidity in obtaining autologous cells, the highly proliferative nature of ECFCs, and the ability of ECFCs to yield mature endothelial cells (Obi et al., 2009, 2012). To exploit their potential, however, it is necessary to first understand whether ECFCs behave similarly to ECs in their abilities to interact with engineered biomimetic materials and which cell surface receptors mediate these interactions.

To understand the interactions of specific material-bound ligands with cell surface receptors on ECFCs, it is important to eliminate the confounding effects of adsorbed proteins on the surface with which the cells are interacting. Poly(ethylene glycol) diacrylate (PEGDA) hydrogels have been demonstrated to be an effective "blank slate" material *in vivo* for this purpose (Gonzalez, Gobin, West, McIntire, & Smith, 2004). Using a grafting technique, peptides of interest can be immobilized on PEG hydrogels. These peptide-grafted PEG hydrogels can then be used to evaluate the peptides' potential to support ECFC adhesion and rolling. Other types of ECs are known to interact preferentially with the peptide YIGSR (Graf et al., 1987), which is recognized by the 67kDa laminin binding protein cell adhesion receptor, and the peptide REDV, which is recognized by the $\alpha_4\beta_1$ integrin receptor (Hubbell, Massia, Desai, & Drumheller, 1991; Massia & Hubbell, 1992). ECs have been shown to bind REDV selectively over smooth muscle cells, fibroblasts, and platelets (Hubbell et al., 1991). YIGSR is known to enhance EC migration (Graf et al., 1987) and has been shown to promote endothelialization (Genové, Shen, Zhang, & Semino, 2005), EC adhesion, and spreading (H. Jun & West, 2003). Research has shown that YIGSR modified PEG/polyurethaneurea gels support EC adhesion but not platelet adhesion (H.-W. Jun & West, 2004). In addition, ECs are known to interact with the peptide RGDS, which is widely used in tissue engineering as a cell adhesion ligand because it is recognized by many integrin receptors (Ruoslahti, 1996). RGDS is present in various ECM proteins including fibronectin, vitronectin, laminin, and collagen (West, 2004).

PEG-peptide can be coated on the interior surface of blood vessels and vascular grafts through interfacial photopolymerization (M J Slepian, Massia, Weselcouch,

Khosravi, & Roth, 1995; West & Hubbell, 1996) and can also be used as matrices for tissue engineering (Charles R Nuttelman et al., 2008). Specific applications include vascular grafts (Ruoslahti, 1996), vascularization of synthetic biomaterial (Moon et al., 2010), and next generation stenting (Marvin J Slepian & Hubbell, 1997; Wei et al., 2013). To support vascular re-endothelialization, biomimetic materials should be able to maintain adherent cells on their surfaces under physiological shear stress, support migration and proliferation of mature ECs from the ends of the lesion, and provide appropriate ligands for the rolling and eventual firm adhesion of ECFCs.

Using a parallel-plate flow chamber, we characterized the ability of PEG-RGDS grafted hydrogels to support adherent ECFCs when subjected to superphysiological shear stresses. Dextran has been used to increase the viscosity of the fluid to achieve superphysiological shear (Brown et al., 2009; Stroncek et al., 2009). Detailed characterization of dextran viscosity has shown that the addition of dextran up to 30 wt.% shows Newtonian viscosity behavior (Tirtaatmadja, 2001). Also, research has shown that 5% dextran did not affect cell expression of Mono Mac 6 cells (Rinker et al., 2001). Finally, ECFC rolling velocity on PEG-RGDS, PEG-YIGSRG, and PEG-REDV was quantified.

5.2 Materials and Methods

5.2.1 Comparison on Glass Cleaning Method for Hydrogel Formation

Peptide residues were suspected to be left on the glass surface after grafting of acryloyl-PEG-peptides on PEG hydrogels. To make sure the peptide residuals were not carried over to the rest of the hydrogels, the effect of glass cleaning method was investigated. Glasses that were used to graft acryloyl-PEG-RGDS were cleaned with three

methods and then they were used to form PEG hydrogel as suggested in Section 2.9 The three methods included wiping with 70% ethanol, brushing with glass soap, and soaking in 1M KOH base bath. PEG hydrogels formed with these glasses were seeded with ECFCs and cultured for 24 hours as shown in Section 2.10. Non adherent cells were gently rinsed with PBS before imaging.

5.2.2 Evaluation on Grafting Time for Successful Peptide Grafting

The rating of UV lamp was first validated with a radiometer (International Light Technologies, ILT1400BL). UV lamp was warmed up for 15 min and the sensor of the radiometer was placed at 2.5 cm away from the UV lamp. Intensity at different locations was recorded along the UV lamp.

PEG-RGDS (1.4 and 2.8 μmol/mL) was grafted on PEG hydrogels following the methods shown in Section 2.9 using three different UV crosslinking times: 30 s, 2 min, and 7 min. After grafting the acryloyl-PEG-RGDS (1.4 μmol/mL) on PEG hydrogel with different UV exposure time, ECFCs were seeded on the surfaces and allowed to adhere for 1.5 hr. Then the number of adherent cells per area was counted. These cells were allowed to proliferate and counted after 40 hr.

5.2.3 6X Histidine Tag Characterization

To confirm peptide grafting, HHHHHH-tagged peptide was grafted onto the PEGDA hydrogels and its presence verified by immunostaining. An automated peptide synthesizer APEX396 SC (aapptec) was used to synthesize the HHHHHHRGDSG peptide by solid phase chemistry. Peptide synthesis was confirmed by mass spectrometry. Details of peptide synthesis and mass spectrometry are shown in Section 2.4 and 2.5.

After HHHHHHRGDSG was conjugated to acryloyl-PEG-SVA, PEG-HHHHHHRGDSG (0.7 mM, 2.8 mM, and 5.6 mM) was grafted onto the PEGDA hydrogels and the hydrogels were swollen in PBS. The minimum concentration of 0.7 μmol/mL of acryloyl-PEG-RGDS was selected based on the observation that this was the lowest concentration able to support ECFCs spreading. Round disks of the PEG-peptide grafted hydrogels were cut using a punch and placed into wells of a flat bottom black 96-well plate. To detect the HHHHHHRGDSG, the hydrogels were incubated with blocking buffer (3% FBS in PBS) for 1 hr and then incubated with anti-HHHHHH-FITC antibody (Abcam, 1:200) for 4 hrs at room temperature. After incubation, the antibody solution was removed and the hydrogels were rinsed 3 times over the course of 3 hrs in blocking buffer (3% FBS in PBS) and then rinsed twice with PBS, after which 100 μL of PBS was added to each well. PEGDA hydrogels without grafted PEG-peptide were used as the negative control. Fluorescence intensity was measured using a microplate reader (Synergy HT, Biotek). Optics position was set to read from the top and the excitation and emission wavelengths were set at 485 and 528 nm, respectively. The normalized fluorescence intensity in each condition was determined by subtracting the value of the control.

5.2.4 Characterization of Peptide-grafting using X-ray Photoelectron Spectroscopy

RGDS-grafted and ungrafted PEG hydrogels were dried by subjecting to an increasing concentrations of ethanol (50%, 70%, 90%, 95%, 100%) Then hexamethyldisilazane was added to dry the hydrogels. One hydrogel sample from each condition was subjected to XPS analysis. ECFC adhesion on dried samples was accessed 4 hours after seeding.

5.2.5 ECFC Rolling under Shear

To test the ability of RGDS-, REDV-, and YIGSRG- to slow EPC rolling, the system developed in Chapter 3 was used here. Briefly, peptide-grafted PEG hydrogels were formed using the method shown in Section 2.8 and 2.9. Cell rolling experiments and tracking were performed following the setup shown in Section 3.2 and Chapter 4.

5.2.6 ECFC Retention under Shear

When ECFCs reached 90% confluence, ECFCs were detached from the culture flask and resuspended at a final concentration of 3×10^6 cells/mL. A RGDS-grafted hydrogel was placed on a 2 in x 3 in glass slide and the parallel plate flow chamber (Glycotech) was then placed on top of the peptide-grafted hydrogel. The chamber and hydrogel were separated by a silicone gasket. Use of this parallel plate chamber for cell rolling experiments has been previously described (E. Y. H. Park et al., 2002). Two metal plates and screws were used to secure the flow chamber on top of the hydrogel and glass slide. The assembled flow chamber was then placed on the phase contrast microscope (Ti Eclipse, Nikon). Cell suspension was introduced into the flow chamber and cells were allowed to settle onto to the surface of RGDS-grafted hydrogels for 7 min. To create the superphysiological wall shear stresses, the viscosity of the fluid used to shear the cells was increased by making 3% solution of high molecular weight dextran (2×10^6 MW) in PBS as has been previously described (Brown et al., 2007). A syringe pump (Legato 180, KD Scientific) was then used to withdraw the 3% dextran (2×10^6 MW) solution in PBS through the flow chamber. Wall shear stress, τ_{yx}, was calculated using Equation (21) while shear rate, $\dot{\gamma}$, is calculated by the Equation (20).

The viscosity of the 3% dextran solution was found to be 0.063 P by using a capillary viscometer. Non-adherent cells were gently rinsed by PBS at a shear stress of 0.04 dyn/cm^2, The adherent cells were sheared for 1 min and the number of cells in a 10X objective field of view was counted before and after shear to determine the percentage of adherent cells remaining at each shear stress from 86 dyn/cm^2 to 347 dyn/cm^2. Two concentrations of grafted PEG-RDGS (0.7 mM and 5.6 mM) were tested at (n= 3 per condition). A minimum of three PEG-peptide grafted hydrogels, each prepared separately, were tested for each condition.

5.3 Results and Discussion

5.3.1 The Effect of Glass Cleaning Method on PEG Hydrogels Formation

During grafting of peptides on PEG hydrogels, a small amount of peptide residues was suspected to be left on the glass surface. Wiping with ethanol alone may not be enough to clean the glass, so a qualitative study was performed to determine whether there were peptide residues left on the glass surface. Three methods were used to clean the glass surface such as wiping with ethanol, brushing with glass soap and soaking in base bath. After cleaning with one of the methods, the glass slides were used to prepare PEG hydrogel and ECFCs were seeded on the PEG hydrogels. Results showed that ECFCs were fully adhered and spread on PEG hydrogels that were prepared by using ethanol cleaned glass (Figure 5.1A). ECFCs on PEG hydrogels prepared by glass soap washed glass showed minimal adhesion and slight spreading (Figure 5.1B). For PEG hydrogels that were prepared by the glass that were soaked in base bath, there were minimal ECFC adhesion, but no spreading (Figure 5.1C). This was very surprising on how the acryloyl-PEG-peptide

were left on non-acrylated glass surface and then the residues were able to be transferred onto PEG hydrogel surfaces. Therefore, soaking glass slides with base bath is critical in the preparation of clean glass surface for PEGDA crosslinking in order to avoid compromising the grafting quality.

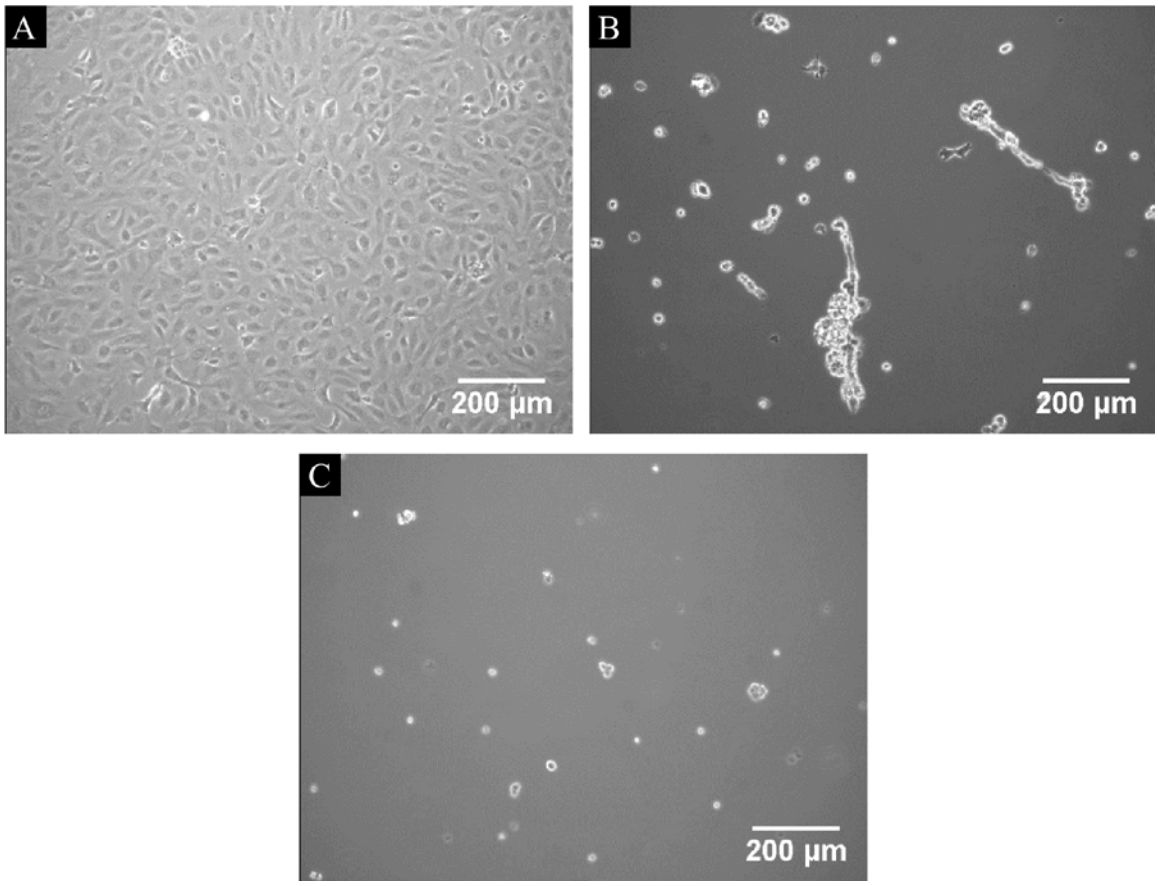

Figure 5.1 PEG hydrogels were made by glass that were cleaned with different methods. A) ECFCs were able to adhere and spread on PEG hydrogels made with ethanol cleaned glass. B) Some spreading was shown on PEG hydrogels made with glass cleaned with glass soap. C) No spreading and only minimal ECFC adhesion was shown on PEG hydrogels made with glass cleaned with base bath.

5.3.2 The Effect of Grafting Time for Successful Peptide Grating on PEG Hydrogels

To evaluate the success of PEG-peptide grafting, the rating of UV lamp was first validated using a radiometer. The distance between the UV lamp and the radiometer sensor was maintained at 2.5 cm, which was the distance between the UV lamp and the hydrogel crosslinking mold. UV intensity was found to vary according to location. UV intensity was found to be maximum at 3.0 mW/cm^2 in the center region as indicated by the yellow arrow region in Figure 5.2. The intensity gradually decreased to 1.8 mW/cm^2 at the ends of the UV lamp. As a result, hydrogel crosslinking mold were only placed under the maximum intensity region of the UV lamp to maintain consistency.

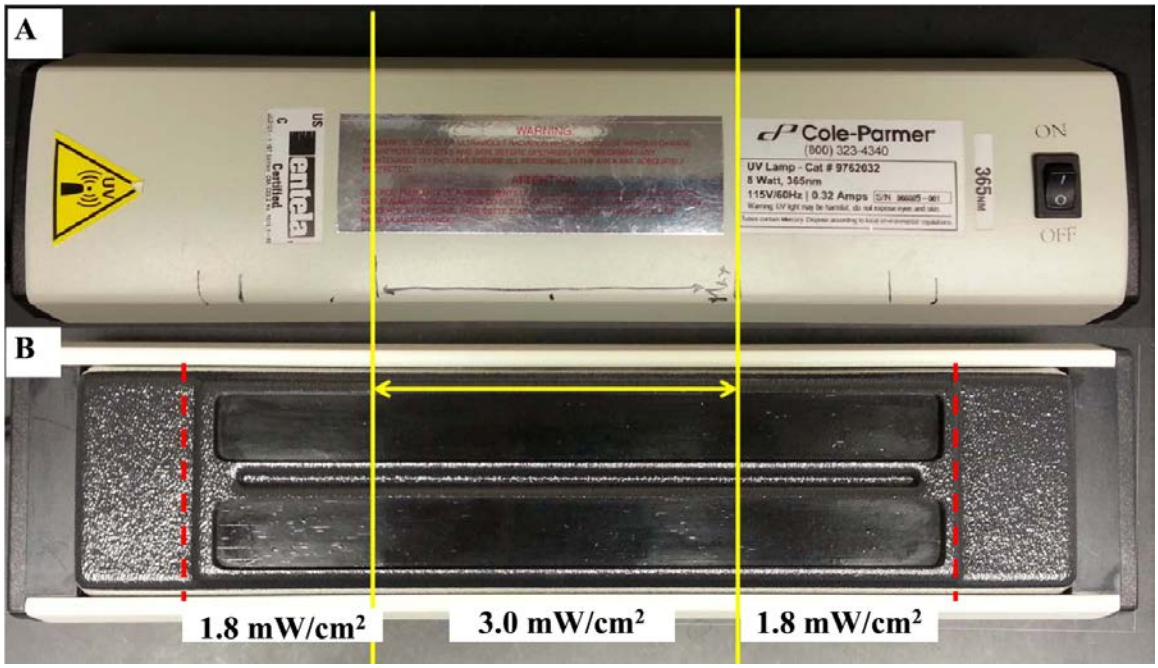

Figure 5.2 PEG Area of maximum UV intensity of UV lamp. UV lamp is rated for 3 mW/cm^2. A) Top view of the UV lamp. B) Bottom view of the UV lamp. Using a radiometer, the region indicated within the yellow arrow is confirmed to maintain an intensity of 3.0 mW/cm^2 at a distance of 2.5 cm while the region outside the yellow arrow gradually decreases to 1.8 mW/cm^2 as indicated by the red dotted lines. Therefore, hydrogel formation was performed within the region indicated by the yellow arrow.

The effect of UV crosslinking time for grafting of PEG-peptides on PEG hydrogel was studied. As shown by Taite *et al.*, an UV exposure of 1 min was used with an UV lamp having 10 mW/cm^2 at 365 nm (Taite et al., 2006). However, this time of UV exposure was found to be insufficient to graft acryloyl-PEG-peptides on PEG hydrogel in this study. Three different UV exposure times were studied: 30 s, 2 min, and 7 min. After grafting the acryloyl-PEG-RGDS (1.4 μmol/mL) on PEG hydrogel with different UV exposure time, ECFCs were seeded on the surfaces and allowed to adhere for 1.5 hr. Then the number of adherent cells was counted. These cells were allowed to proliferate and counted after 40 hr. The number of ECFCs on the PEG hydrogels decreased significantly as expected; PEG is known to resist protein adsorption and cell adhesion, so the loosely adherent ECFCs were washed off during the PBS rinsing. The number of ECFCs on the hydrogels grafted showed a decreased in number for 30 s and 2 min. This was probably because of incomplete grafting of the acryloyl-PEG-RGDS. On the hydrogel with the grafting time of 7 min, ECFCs showed spreading at 1.5 hr after seeding and the number of ECFCs increased significantly 40 hr later (Figure 5.3). Therefore, a grafting time of 7 min was necessary to show complete grafting. Another study was performed, using 2.8 μmol/mL of acryloyl-PEG-RGDS, to evaluate whether a higher grafting solution concentration requires a longer grafting time. Figure 5.4 shows no significant differences in the number of cells on the hydrogels grafted with two different concentrations of peptide solution at time equals 41.5 hr. There was no significant difference. Therefore, a grafting time of 7 min was used for all conditions.

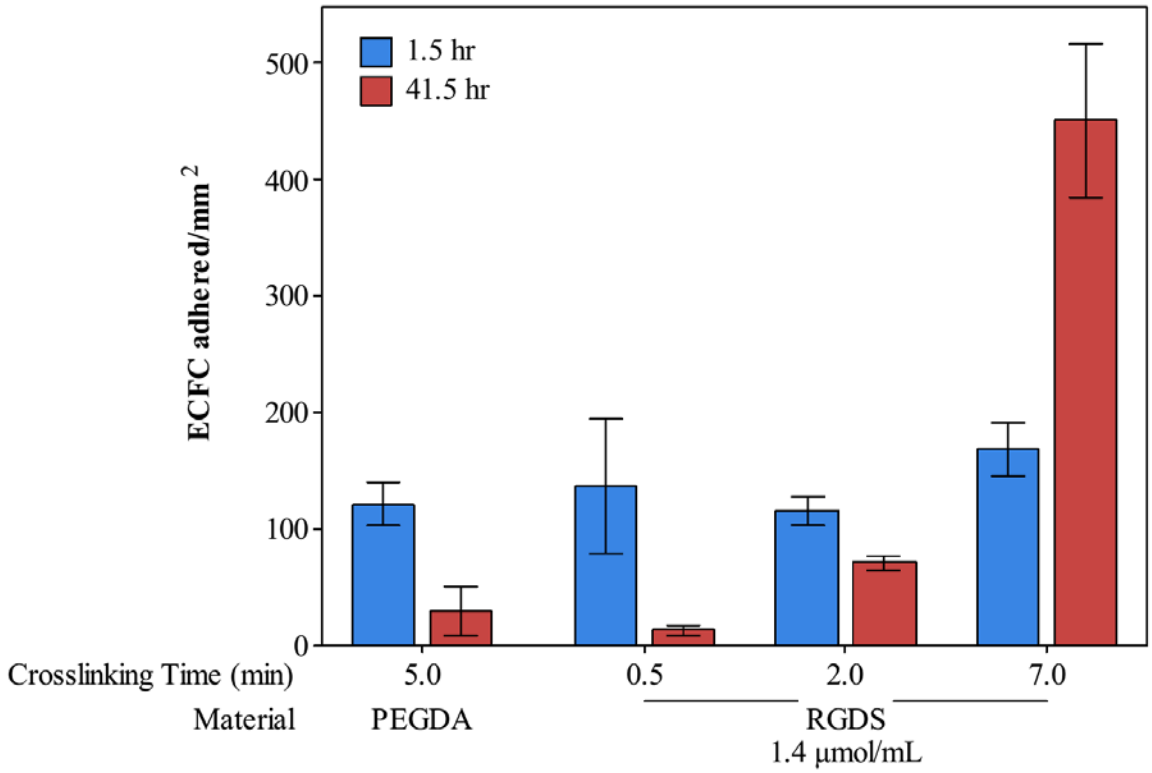

Figure 5.3 The effect of UV time on successful grafting of RGDS peptide. The number of ECFCs adhered significantly decreased on the RGDS-grafted hydrogel with 0.5 and 2 min grafting time after 40 hours whereas the number of ECFCs increased significantly on the RGDS-grafted hydrogel with 7 min grafting time after 40 hours. This showed that grafting of RGDS was completed with a grafting time of 7 min in terms of number of ECFCs adhered on the hydrogels.

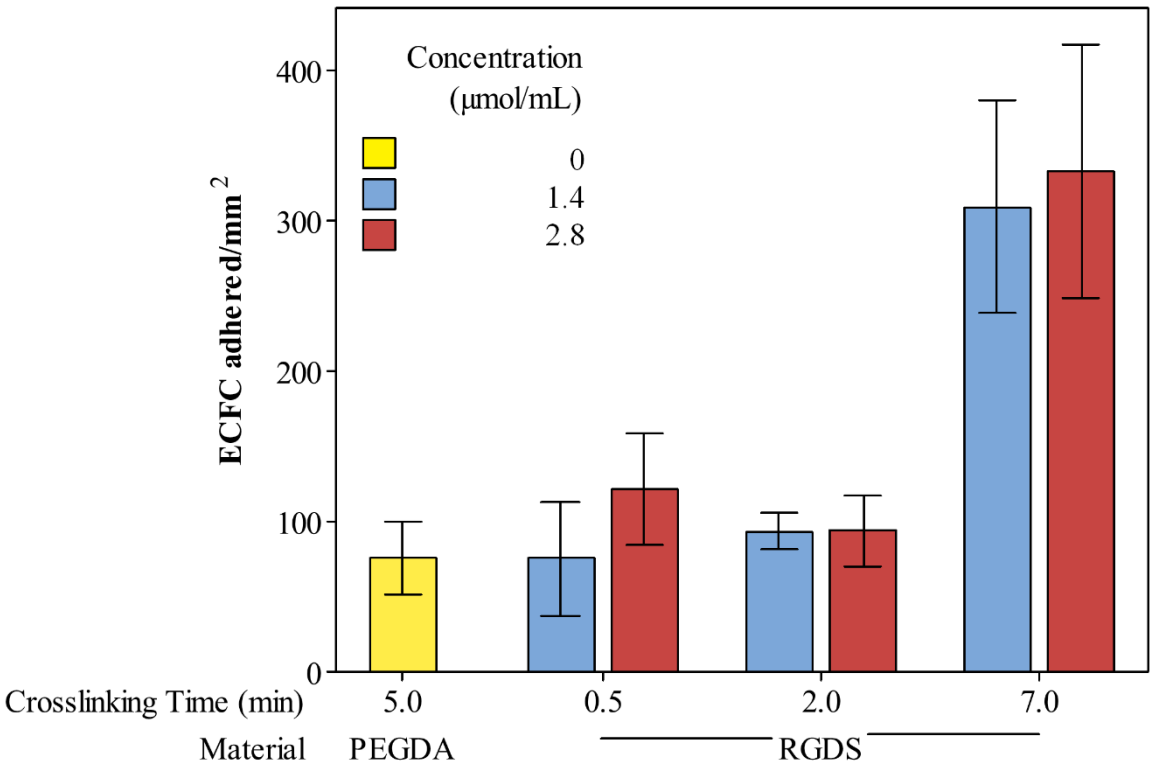

Figure 5.4 The effect of UV time on different concentrations of grafting RGDS peptide. The number of ECFCs adhered on RGDS-grafted hydrogel using after 40 hours showed no significant difference between using 1.4 μmol/mL or 2.8 μmol/mL acryloyl-PEG-RGDS solution. This showed that the increase in the concentration of acryloyl-PEG-RGDS solution did not affect the grafting of RGDS with a grafting time of 7 min in terms of number of ECFCs adhered on the hydrogels.

5.3.3 Confirmation of Peptide-Grafting by 6x Histidine Tagged Immunostaining

RGDS-grafted PEGDA hydrogels were shown to support ECFC adhesion and spreading in static culture at grafted peptide concentrations as low as 0.7 μmol/mL (Figure 5.5A), whereas control PEG hydrogels did not (Figure 5.5B). To demonstrate successful peptide grafting, a HHHHHH tagged RGDS peptide was employed and detected by immunolabeling. Due to the use of free radical chemistry in grafting the peptides onto the PEGDA hydrogels, the termination step could cause the joining of CH_2· on PEG and limit the availability of acrylate end groups on the PEG hydrogels for grafting. Therefore, it was important to verify the success of PEG-peptide grafting and to determine the relationship between PEG-peptide concentration in the grafting solution and the amount of grafted PEG-peptide on the PEG hydrogel surface.

PEG-peptide was confirmed to be grafted onto the PEG hydrogel based on the fluorescence intensity readings of PEG-HHHHHHRGDSG grafted PEG hydrogels being significantly higher than the control non-grafted PEG hydrogels. In addition, the concentration of grafted PEG-HHHHHHRGDSG was found to be dependent on the concentration of the acryloyl-PEG-HHHHHHRGDSG in the grafting solution (Figure 5.6). The average normalized fluorescence intensity increased with increasing concentration of acryloyl-PEG-peptide in the peptide grafting solution. The fluorescence intensity was found to be significantly higher for hydrogels grafted with 5.6 μmol/mL acryloyl-PEG-HHHHHHRGDSG than with 0.7 μmol/mL acryloyl-PEG-HHHHHHRGDSG ($p < 0.05$). This increase in fluorescence intensity was nonlinear with respect to the increase in concentration of PEG-peptide grafting solution; the relative intensities for hydrogels grafted with 2.8 and 5.6 μmol/mL acryloyl-PEG-HHHHHHRGDSG were on average

approximately 3-fold and 4.5-fold higher than for 0.7 μmol/mL, respectively. These results confirm that PEG-peptide can be grafted on the surface of PEG hydrogels in a concentration-dependent fashion using photopolymerization and that grafted peptide supports ECFC adhesion under static conditions.

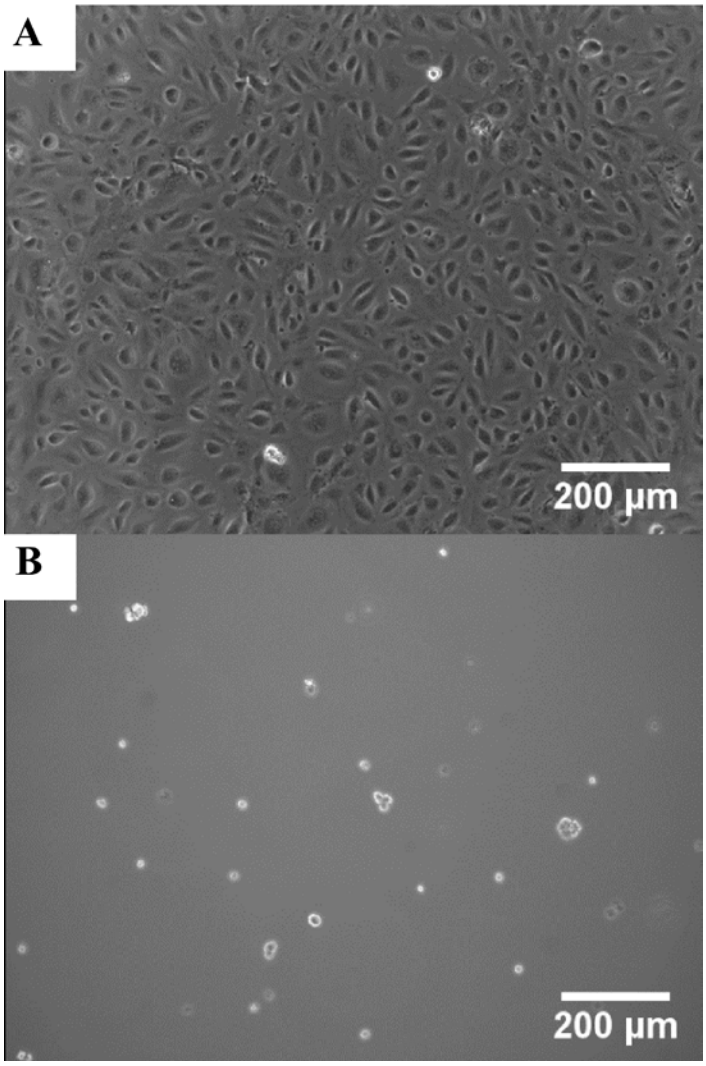

Figure 5.5 ECFCs were seeded on hydrogels to evaluate the ability of hydrogels to support cell adhesion after 1 hr of incubation. (A) Control PEG hydrogels did not support ECFC adhesion. (B) ECFCs adhered and spread on RGDS-grafted (0.7 µmol/mL) PEG hydrogels.

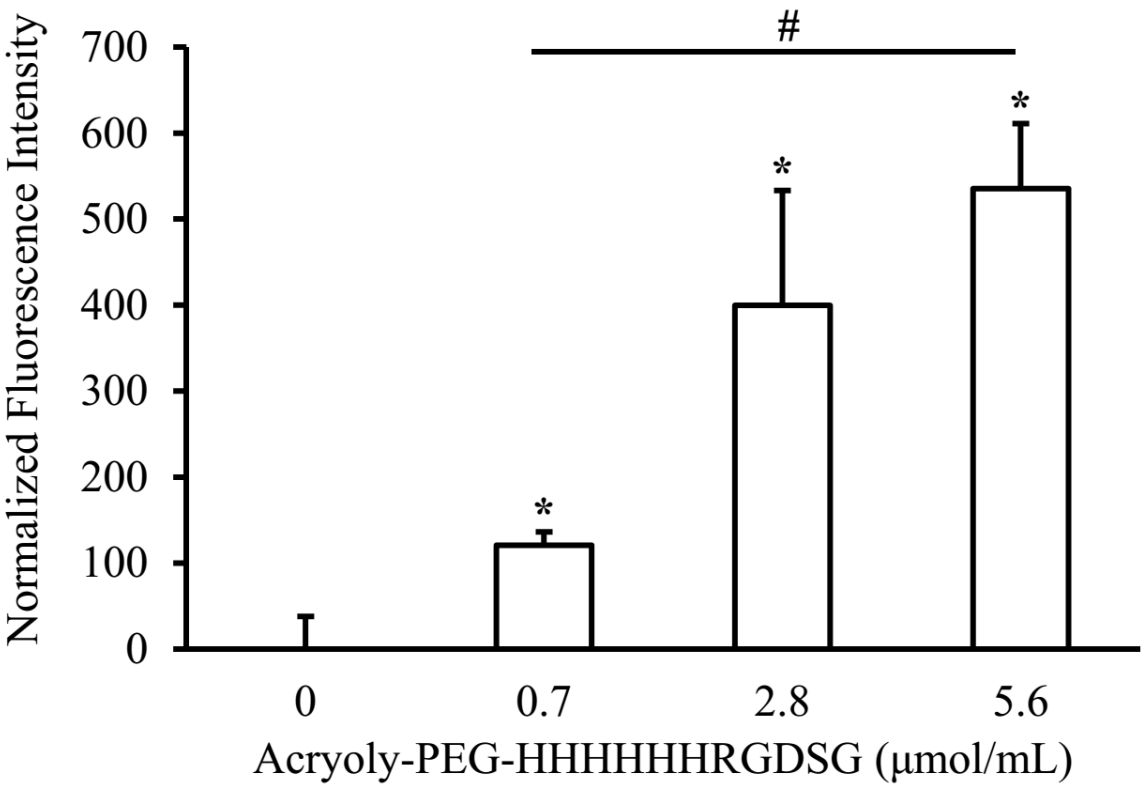

Figure 5.6 Grafting of HHHHHH-tagged RGDS peptide on PEG hydrogels was verified by immunostaining. The fluorescence intensity increased with increasing concentration of acryloyl-PEG-HHHHHHRGDSG in the grafting solution. Data represent mean ± SD (n=3). (*$p<0.05$ compared to control, #$p<0.05$ between 0.7 and 5.6 μmol/mL).

5.3.4 Inconclusive Confirmation of Peptide-Grafting by XPS

General XPS survey scan of RGDS-grafted hydrogels was attempted to estimate the amount of RGDS that was grafted on PEG hydrogels. Results showed that there was 0.7% nitrogen (N_{1s} peak) present on both RGDS-grafted and ungrafted hydrogels (Figure 5.7A and C). In order to verify this result, ECFCs were also seeded on the surface of the same batch of hydrogels that had also been through the chemical drying process. After 4 hours, ECFCs spread on the RGDS-grafted hydrogels (Figure 5.7B), but not on the ungrafted PEG hydrogels (Figure 5.7D). Since the ungrafted PEG hydrogels were still able to resist ECFC adhesion and spreading, the nitrogen that is present could be due to contamination from atmospheric nitrogen. From this experiment, the confirmation of peptide-grafting by XPS is inconclusive.

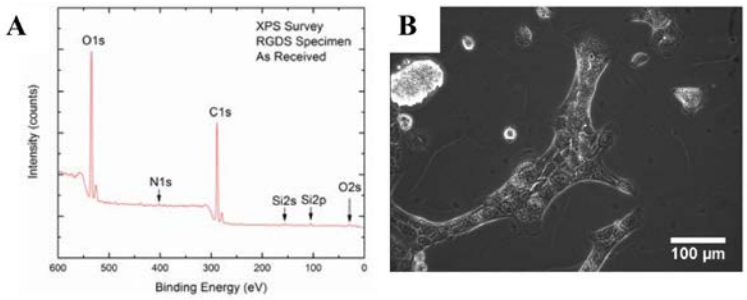

XPS Surface Elemental Composition (at %)

O	N	C	Si
29	0.7	68	2

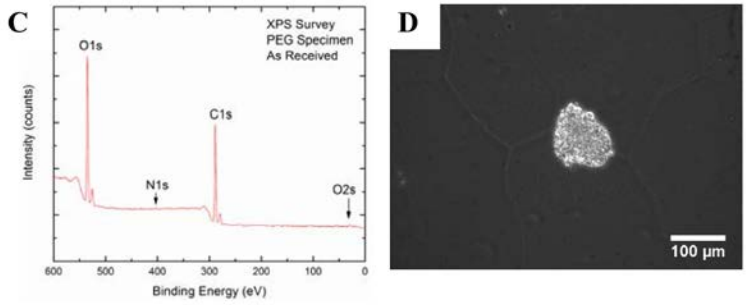

XPS Surface Elemental Composition (at %)

O	N	C	Si
29	0.7	70	0

Figure 5.7 Quantification of peptide grafting using XPS. A) General XPS survey scan of RGDS-grafted hydrogels. Results showed the presence of 0.7% of nitrogen which represented the potential presence of RGDS. B) ECFCs spread on the RGDS-grafted hydrogels after chemical drying. C) General XPS survey scan of ungrafted PEG hydrogels (control). Results showed the presence of 0.7% nitrogen which may represent the potential contamination from atmospheric nitrogen. D) No ECFCs spread on the PEG hydrogels after chemical drying.

5.3.5 Validation of Cutoff Rolling Velocity for ECFC Rolling on Hydrogels

To identify whether a cell is rolling, the upper velocity cutoff was determined by flowing ECFCs across the surface of control PEG hydrogels at different shear rates. Using video recordings, ECFC rotation on the focal plane of PEG hydrogels was observed. As shown in Figure 5.8, cell tracking showed that ECFCs' average velocity on PEG hydrogels fell between estimated fluid flow velocity at a distance of approximately one cell diameter (i.e. 15 μm, the average diameter of ECFCs in suspension) above the hydrogel surface and the estimated fluid flow velocity at a distance of approximately one cell radius (i.e. 7.5 μm) above the hydrogel surface. Therefore, based on these experiments, 40% of average fluid flow velocity was used as the cutoff velocity for cell rolling as is shown in Figure 5.8.

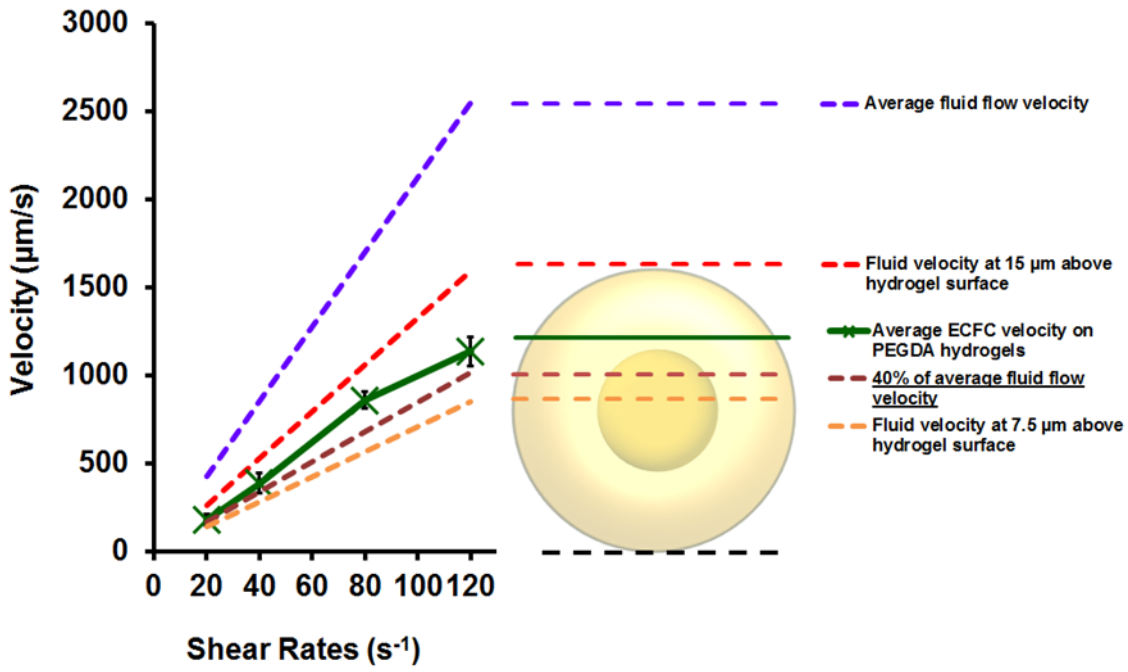

Figure 5.8 Comparison between calculated fluid velocities and ECFC velocity. The velocity of ECFCs on the surface of PEG hydrogels was less than the calculated fluid velocity at approximately one cell diameter (15 μm) and greater than the calculated fluid velocity at approximately one cell radius (7.5 μm) above the hydrogel surface. Data represent mean ± SD (n=3). Therefore, to eliminate any ECFCs that might be non-specifically interacting with the PEG hydrogel surface, the cutoff for identification of rolling cells was set at 40% of the average fluid velocity.

5.3.6 PEG-RGDS Grafted PEG Hydrogels Support Adherent ECFCs under Superphysiological Shear

As a first step in evaluating the potential of using peptide-grafted hydrogels as an intravascular material for supporting ECFCs, the strength of adhesion of ECFCs on the surface of RGDS-grafted hydrogels was studied under superphysiological shear stresses. PEGDA hydrogels were also tested as a control, but no ECFCs remained adhered after the initial PBS rinse (shear stress of the rinse was 0.04 dyn/cm^2, more than two orders of magnitude below the lowest experimental conditions). PEGDA hydrogels grafted with the low (0.7 μmol/mL) and the high concentration of acryloyl-PEG-RGDS (5.6 μmol/mL) were tested. Results showed that ECFCs remained firmly adhered on the RGDS-grafted hydrogels at shear stresses up to approximately 350 dyn/cm^2 for both concentrations (Figure 5.9A). Cell retention percentages on 0.7 μmol/mL acryloyl-PEG-RGDS grafted hydrogels were 90±4%, 96±3%, 87±2%, and 85±6% at shear stresses of 86 dyn/cm^2, 174 dyn/cm^2, 261 dyn/cm^2, and 347 dyn/cm^2, respectively. Cell retention percentages on 5.6 μmol/mL acryloyl-PEG-RGDS grafted hydrogels were 94±5%, 90±8%, 90±8%, and 97±2% at shear stresses of 86 dyn/cm^2, 174 dyn/cm^2, 261 dyn/cm^2, and 347 dyn/cm^2, respectively (Figure 5.9A). No significant difference in the percentage of retained cells was found between the two concentrations at any of the tested shear stresses. Based on these results, a grafting concentration of 0.7 μmol/mL was chosen for use in the subsequent dynamic adhesion experiments. Representative images of adhered ECFC before and after shear are shown in Figure 5.9B and C.

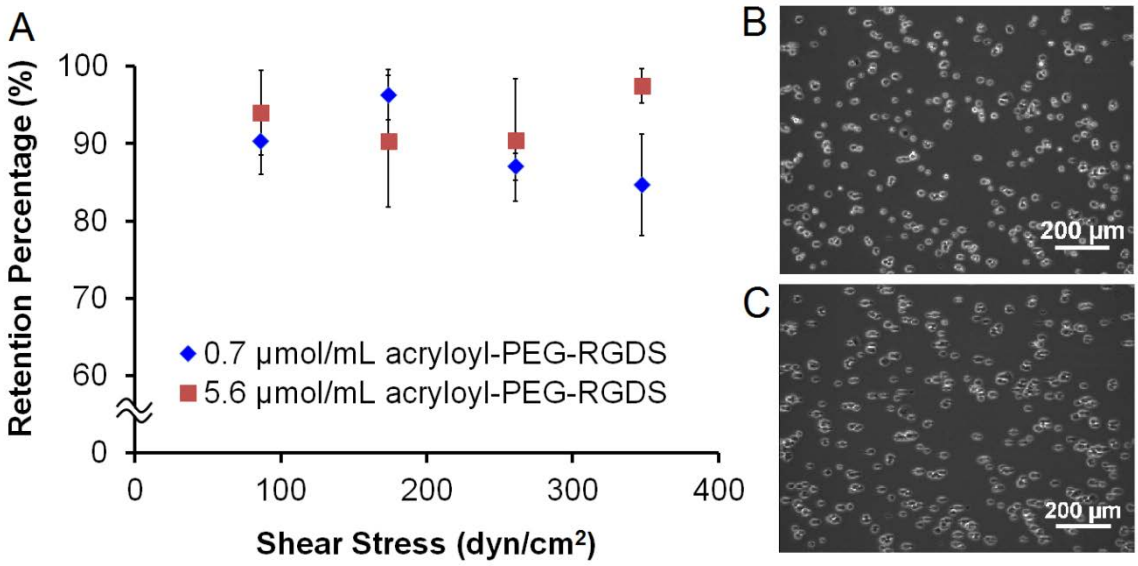

Figure 5.9 Retention of ECFCs on RGDS-grafted hydrogels. A) Retention percentage of ECFCs did not differ between 0.7 and 5.6 µmol/mL RGDS-coupled hydrogels after 1 min of superphysiological shear. Data represent mean ± SD (n=3). B) Representative image of ECFCs on a 5.6 µmol/mLof acryloyl-PEG-RGDS grafted hydrogel before shear. C) Image of ECFCs after shear for 1 min at 347.4 dyn/cm^2 on hydrogel shown in B).

5.3.7 PEG-RGDS Grafted PEGDA Hydrogels Support Rolling of ECFCs

ECFC rolling on RGDS-grafted hydrogels was performed and compared to both PEG hydrogels and RGES-grafted hydrogels. RGDS is a ubiquitous cell adhesion peptide, whereas RGES does not support cell adhesion and served as a control peptide. Velocities of ECFCs on RGES showed no significant difference as compared to control PEGDA hydrogels. On the other hand, velocities of ECFCs on RGDS-grafted hydrogels were significantly decreased as compared to ECFC velocities on RGES-grafted hydrogels at all shear rates. As shown in Figure 5.10A, the rolling velocities of ECFCs on RGDS-grafted hydrogels were 103±3 μm/s, 223±14 μm/s, 469±38 μm/s, and 741±28 μm/s at 20 s^{-1}, 40 s^{-1}, 80 s^{-1}, and 120 s^{-1}, respectively. Representative traces of individual cells' instantaneous velocities on RGDS-grafted, RGES-grafted, and control PEGDA surfaces are shown in Figure 5.10B and C. For each tested surface, a series of extracted frames following a representative ECFC moving through the flow chamber is presented in Figure 5.11. Some ECFC capture events were observed on RGDS-grafted hydrogels at 20 s^{-1}; the total number of capture events at this shear rate was far less than the number of rolling cells, however, and, therefore, insufficient for analysis (data not shown). In summary, the RGDS-grafted hydrogels supported ECFC rolling at all shear rates whereas RGES-grafted hydrogels did not support ECFC rolling. Specific transient binding between ECFCs and RGDS was demonstrated.

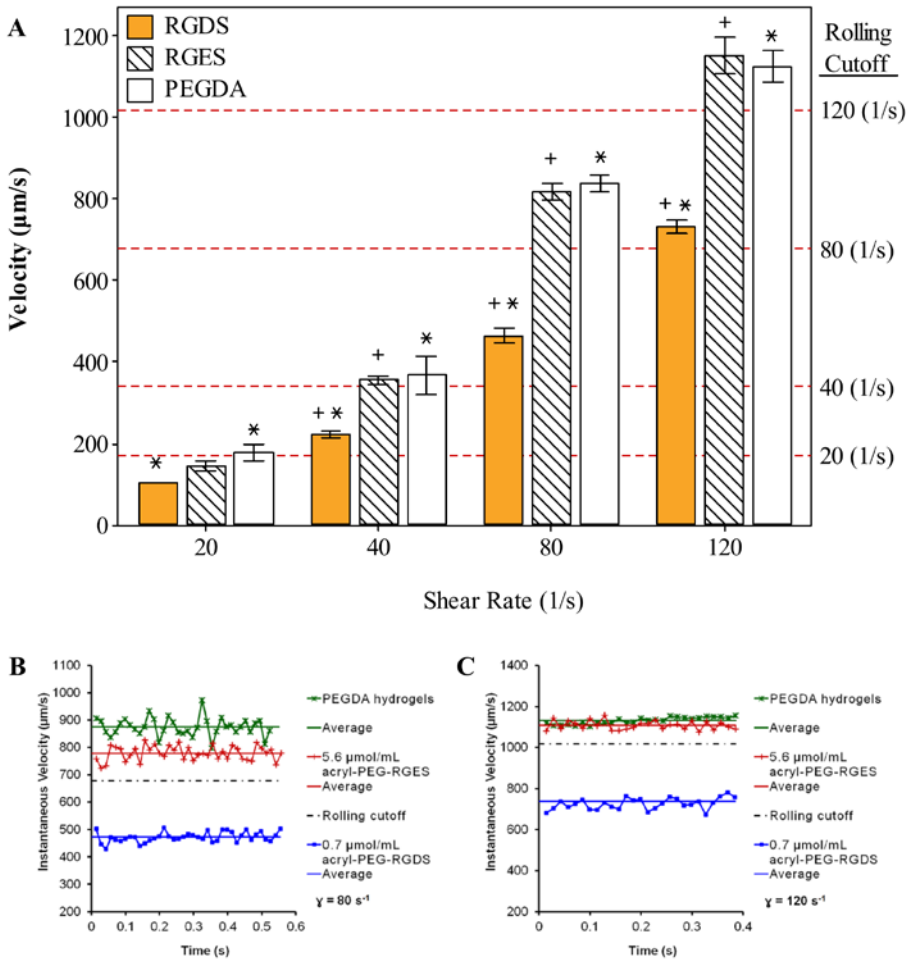

Figure 5.10 Grafting PEG hydrogels with RGDS significantly slowed ECFC velocity. A) The ECFCs velocity on RGES-grafted hydrogels was similar to the velocity on ungrafted PEGDA hydrogels, while ECFC rolling velocity on RGDS-grafted hydrogel showed a significant decrease compared to RGES-grafted and PEGDA hydrogels at all shear rates. Data represent mean ± SD (n=3). (*p<0.05 between RGDS-grafted hydrogels and ungrafted PEGDA hydrogels. +p<0.05 between RGDS- and RGES-grafted hydrogels). B,C) Instantaneous velocity, average rolling velocity and 40% of average fluid velocity of representative ECFCs on PEG, PEG-RGES, and PEG-RGDS hydrogels at shear rates of 80 s^{-1} and 120 s^{-1}, respectively.

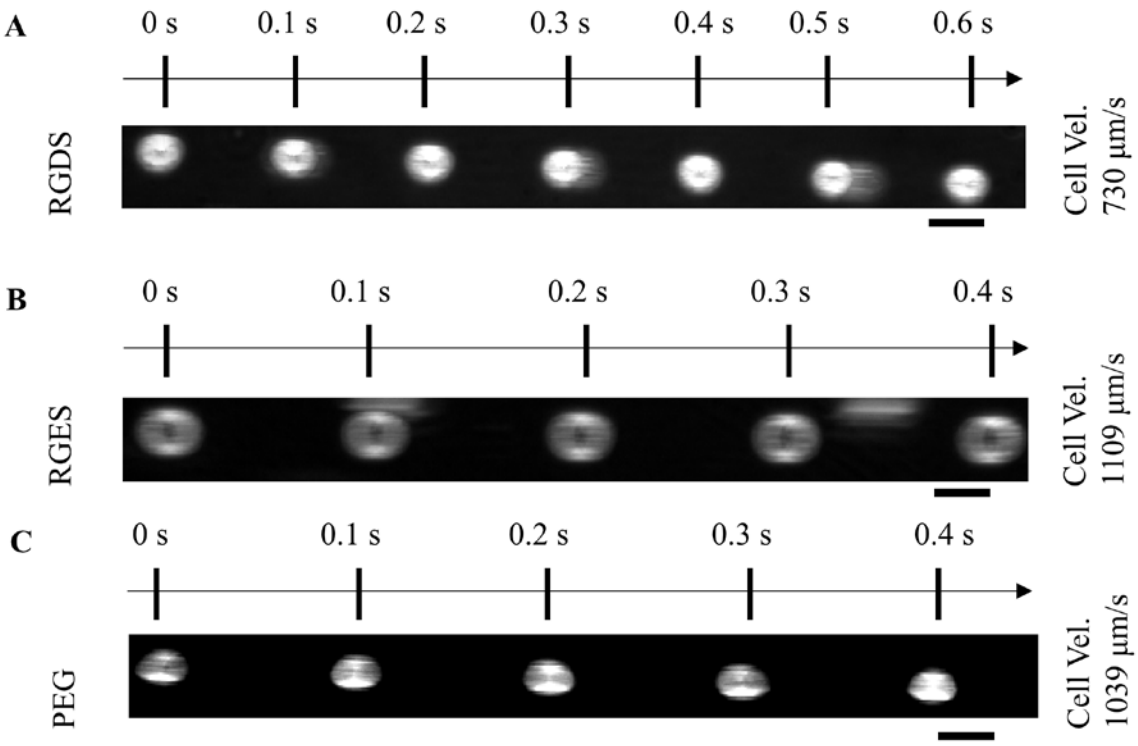

Figure 5.11 Series of extracted frames following a representative ECFC through the flow chamber on A) PEG, B) 5.6 µmol/mL RGES-grafted, C) 0.7 µmol/mL RGDS-grafted hydrogels. Scale bar = 30µm.

5.3.8 PEG-REDV Slows ECFC Rolling Velocity more than PEG-RDGS and PEG-YIGSRG

In addition to PEG-RGDS, PEG-YIGSRG and PEG-REDV grafted hydrogels also supported ECFC rolling. YIGSR and REDV are peptides known to preferentially interact with ECs (Graf et al., 1987; Hubbell et al., 1991; Massia & Hubbell, 1992). Rolling velocities on YIGSRG were similar to rolling velocities on RGDS; specifically, the ECFC rolling velocities on PEG-YIGSRG grafted hydrogels were 102±9 μm s^{-1}, 223±22 μm s^{-1}, 484±12 μm s^{-1}, and 740±10 μm s^{-1} at 20 s^{-1}, 40 s^{-1}, 80 s^{-1}, and 120 s^{-1}, respectively. Surprisingly, PEG-REDV grafted hydrogels reduced ECFC rolling velocities substantially more than either RGDS- or YIGSRG- grafted hydrogels (Figure 5.12A). ECFC rolling velocities on PEG-REDV grafted hydrogels were 79±4 μm s^{-1}, 181±6 μm s^{-1}, 357±6 μm s^{-1}, and 560±15 μm s^{-1} at 20 s^{-1}, 40 s^{-1}, 80 s^{-1}, and 120 s^{-1}, respectively ($p < 0.05$ for shear rates at 80 s^{-1}, and 120 s^{-1} compared to RGDS and YIGSRG). Representative plots of instantaneous rolling velocities for ECFCs that were tracked across the field of view at 80 s^{-1} and 120 s^{-1} are shown in Figure 5.12B and C. For each tested surface, a series of extracted frames following a representative ECFC moving through the flow chamber is presented in Figure 5.13. To visualize the distribution of ECFC rolling velocities, each tracked ECFC is plotted against its rolling velocity in Figure 5.14. To allow for better visualization of the data points and for visual comparison of ECFC velocity distributions between trials, cells are separated by trial, where each trial was performed using a separately prepared peptide-grafted hydrogel. At all shear rates, it can observed that on the REDV-grafted hydrogels a large number of ECFCs are grouped at lower rolling velocities with a more sparse distribution of ECFCs at higher rolling velocities, whereas on the

RGDS- and YIGSRG-grafted hydrogels, the distribution of ECFCs is more even across all the observed rolling velocities, with more ECFCs tending to have higher rolling velocities. Upon closer examination, rolling velocities on REDV-grafted hydrogels at all shear rates were found to be significantly and positively skewed toward lower velocities at all shear rates (Figure 5.14). These results show that multiple peptides are able to support ECFC rolling, including RDGS, YIGSRG, and REDV. In addition, RDGS and YIGSRG supported ECFCs rolling at similar velocities, whereas REDV slowed ECFC rolling velocity to a significantly greater extent. This significant decrease demonstrates that ECFC rolling velocity on the hydrogels depends on the particular grafted PEG-peptide and suggests that the integrin bound by REDV, $\alpha_4\beta_1$ may be important in ECFC rolling.

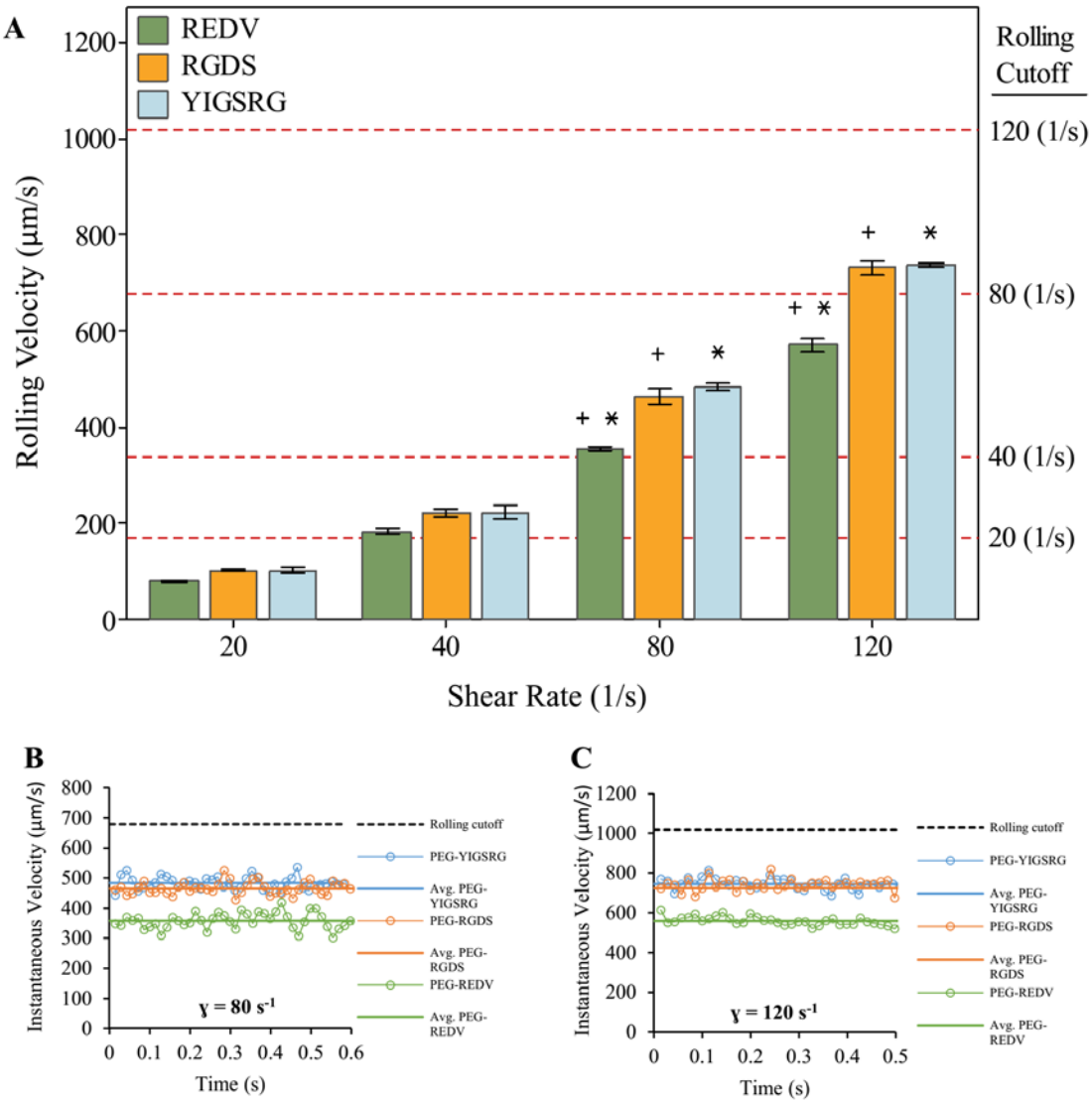

Figure 5.12 Comparison of ECFC rolling on REDV-, RGDS-, and YIGSRG-grafted hydrogels. A) ECFC rolling velocity was lower on REDV-grafted hydrogels as compared to RGDS-grafted hydrogels and YIGSRG-grafted hydrogels at all shear rates. Data represent mean ± SD (n=3). (* and + $p<0.05$ within groups of 80 s^{-1} and 120 s^{-1}). B,C) Instantaneous velocity, average rolling velocity and 40% of average fluid velocity of representative ECFCs on REDV-, RGDS-, and YIGSRG-grafted hydrogels at 80 s^{-1} and 120 s^{-1}, respectively.

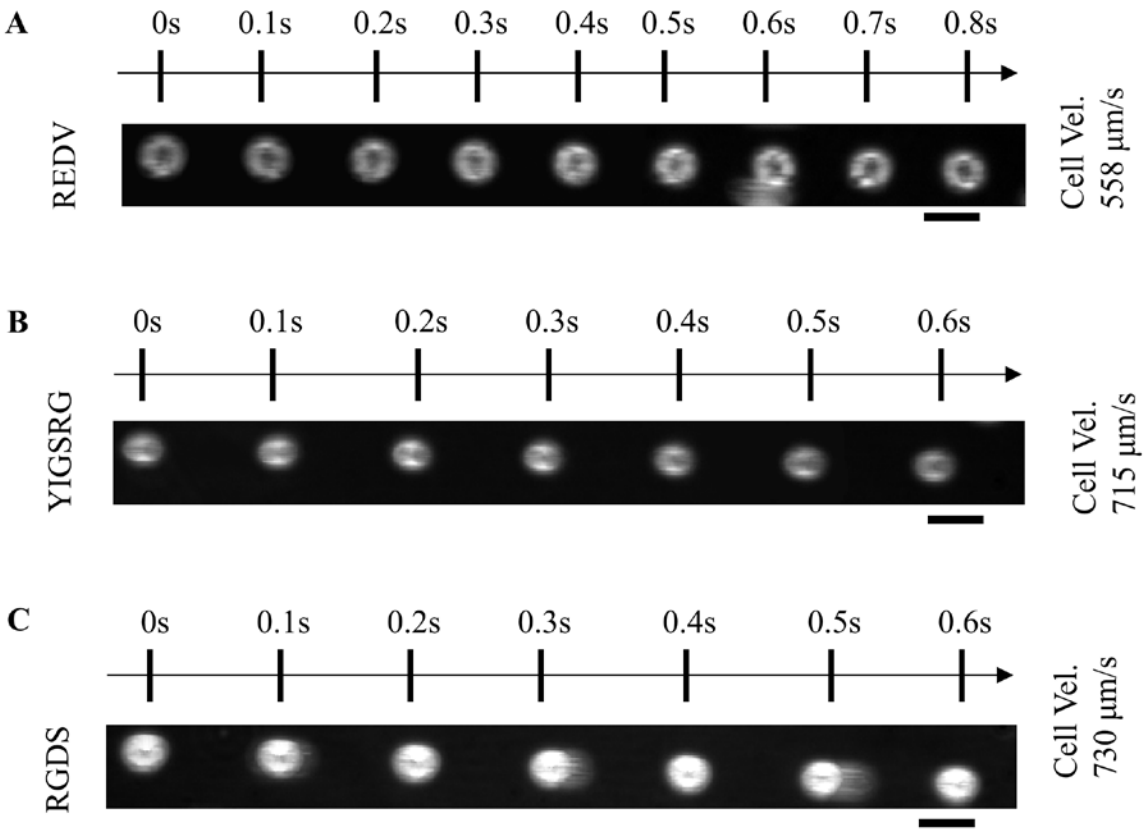

Figure 5.13 Series of extracted frames following a representative ECFC through the flow chamber on A) REDV-, B) RGDS-, and C) YIGSRG-grafted hydrogels. Scale bar = 30μm.

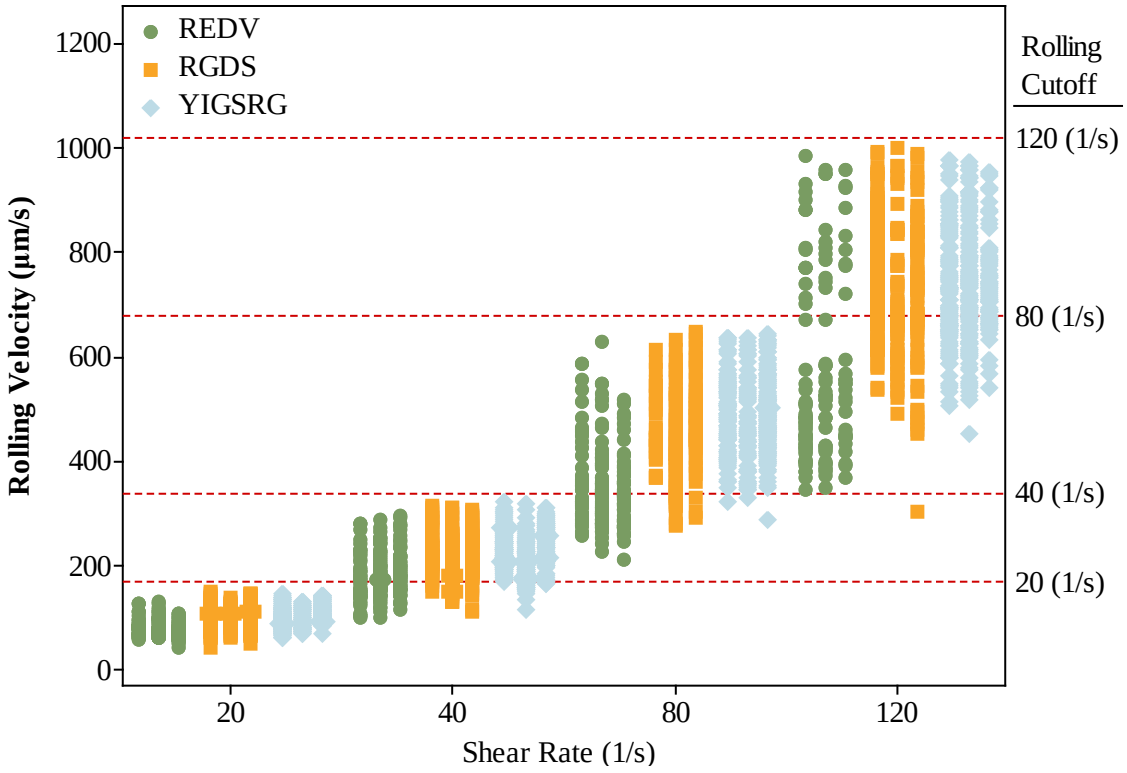

Figure 5.14 Individual data plot showing the distribution of rolling velocities for tracked ECFCs on the peptide-grafted hydrogels at each tested shear rate. Each marker represents one tracked cell. Separately prepared peptide-grafted hydrogels were used for each trial. At shear rates of 80 s^{-1} and 120 s^{-1}, more cells are grouped at the lower rolling velocities for REDV-grafted hydrogels than for RGDS- and YISGRG-grafted hydrogels.

Table 5.1 Skewness of rolling velocities on the three bioactive peptide-grafted hydrogels. Data is considered significantly skewed when skewness is larger than two times of SES. Rolling velocities on REDV-grafted hydrogels at all shear rates were found to be significantly and positively skewed toward lower velocities at all shear rates.

Shear rates (s^{-1})	Peptides	Skewness	Standard error of skew (SES)	SES x 2	Significantly skewed
20	REDV	1.06	0.17	0.35	Yes
	RGDS	0.21	0.15	0.30	No
	YIGSRG	0.19	0.13	0.26	No
40	REDV	0.62	0.18	0.36	Yes
	RGDS	0.24	0.14	0.28	No
	YIGSRG	0.21	0.12	0.24	No
80	REDV	1.06	0.18	0.37	Yes
	RGDS	0.12	0.20	0.39	No
	YIGSRG	0.10	0.13	0.26	No
120	REDV	1.01	0.21	0.42	Yes
	RGDS	0.16	0.15	0.31	No
	YIGSRG	0.25	0.14	0.27	No

5.4 Discussion

In this parallel plate flow chamber setup, ECFC rolling on peptide-grafted hydrogels was studied under laminar flow conditions. Therefore, by assuming laminar flow, the velocity profile in the chamber can be approximated as parabolic, which is necessary in estimating the fluid flow velocity at specific distances from the hydrogel surfaces. In justifying the velocity cutoff for ECFC rolling, the parabolic velocity profile was used in estimating maximum fluid velocity at a distance of one cell diameter (i.e. 15 μm) and at one cell radius (i.e. 7.5 μm) from the hydrogel surface. Due to the parabolic nature of the velocity profile, non-adherent cells near the hydrogel surface are expected to have an average velocity between these local slower fluid flow velocities, rather than the much higher average fluid flow velocity further from the hydrogel surface.

Although PEG-peptide grafting has been used previously in the literature to examine rolling of other cell types, the quantification of grafted peptide on the hydrogel surfaces post-grafting has not been reported. This study validated the peptide grafting method by immunostaining acryloyl-PEG-HHHHHHRGDSG grafted hydrogels. These results demonstrated that peptides can be grafted on PEGDA hydrogels in a nonlinear, concentration dependent manner using photopolymerization. The use of PEG as a spacer may also provide an advantage for capturing cells from flow; for example, use of PEG spacer arms to couple binding ligands to microparticles increased the affinity of the ligands for their target receptors under flow conditions, resulting in more particles adhered to the sheared surfaces (Ham, Klibanov, & Lawrence, 2009). Future investigations could examine the effect of grafted-peptide concentration on the rolling velocity of ECFCs.

This study investigated ECFC interactions with peptide-grafted hydrogels under shear stress with the long-term goal of informing the design of biomaterials for improved intravascular endothelialization. PEGDA was chosen as the backbone hydrogel material due to its good biocompatibility, which is important for future applications, and its ability to resist protein adsorption, which allows it to serve as a "blank slate" for investigating the specific interactions of coupled peptides with ECFCs. In the absence of peptide grafting, PEGDA was unable to support ECFC adhesion (Figure 5.5). In addition, ECFC velocities on PEG hydrogels were higher than the cutoff of 40% average fluid flow velocity and were comparable to velocities on hydrogels grafted with the nonbinding peptide RGES. Therefore, results of experiments using peptide-grafted PEGDA hydrogels provide insight into the interactions of ECFCs with the grafted peptides during cell rolling.

The effect of shear is one of the most important factors on the dynamic adhesion of ECFCs. Although the range of typical arterial shear stress is 6-40 dyn/cm^2 (Patrick & McIntire, 1995), leukocyte rolling has been reported to occur primarily at shear stresses below 1 dyn/cm^2 (Finger et al., 1996). In this study, ECFC rolling was investigated at shear rates ranging from 20 s^{-1} to 120 s^{-1}, which corresponded to shear stresses of 0.2 dyn cm^{-2} to 1.0 dyn cm^{-2}.

Improved clinical outcomes through EPC capture has been an elusive goal. Vascular grafts designed to capture EPCs using antibodies against CD34 demonstrated enhanced re-endothelialization during *in vivo* testing, but neointimal hyperplasia was still observed (Rotmans et al., 2005). Similarly, although the Genous stent employing this antibody approach to EPC capture does not suffer from the stent thrombosis issues

observed with drug-eluting stents, it has also been reported to have late-lumen loss (Beijk et al., 2010). One drawback to the antibody approach is that multiple types of cells are CD34+, including smooth muscle progenitor cells, which potentially led to the lackluster clinical results (Garg et al., 2010; Wendel, Avci-Adali, & Ziemer, 2010). Peptide library screening has been also used to identify peptides that uniquely bind EPCs expanded from human blood over other cell types, including human umbilical vein endothelial cells, HL60 promyelocytic cells, lymphocytes, and neutrophils (Veleva, Cooper, & Patterson, 2007). CGRGDS has been incorporated into a non-fouling fibrous scaffold and has been shown to support cell capture (Wang & Cooper, 2013), although the shear rates tested were much lower than those used in this study. The results demonstrate, however, that peptides hold promise as the binding ligands for ECFC capture, assuming that cell rolling velocity can slowed sufficiently.

The prevalence and nature of EPCs differs based on multiple factors, not the least of which is the health status of person from whom they are isolated; people with metabolic and cardiovascular disease have been shown to have lower numbers of circulating EPCs (Fadini et al., 2012; Xia et al., 2012) As described in the introduction, ECFCs, also known as late outgrowth EPCs, are isolated and expanded from blood. For this study, human umbilical cord blood-derived ECFCs were employed. These cells may, however, differ somewhat from human adult peripheral blood-derived ECFCs; differences in source-dependent ECFC behavior on biomaterial surfaces has been previously reported (Wang & Cooper, 2013). The potential clinical use of EPCs in the endothelialization of vascular grafts and stented vessels will require further study of source-dependent cell properties.

Rolling of ECFCs on extracellular matrix proteins has been reported previously (Angelos et al., 2010), but the current study is the first to our knowledge to report ECFC rolling on a peptide-grafted PEG hydrogel surface. Since PEGDA resists protein adsorption, the peptide-grafted PEG hydrogels employed in this study provide a good platform for specifically investigating the ability of one peptide or a combination of peptides to support ECFC rolling, capture, and adhesion. Due to its additive nature, this peptide-grafted PEG hydrogel system tests not only whether specific peptide-ECFC interactions are necessary, but also whether these interactions are sufficient to support the ECFCs under shear stress. ECFC rolling and strength of adhesion have been examined here, whereas future studies could test the incorporation of additional cell receptor-specific peptide ligands to support capture of rolling ECFCs at these shear rates. This knowledge is essential to recapitulate this natural process for endothelium repair on the surface of intravascular biomaterials.

ECFC rolling was successfully observed on the peptide-grafted hydrogels; ECFC rolling velocity was dependent on the shear rate employed and on the particular peptide that had been grafted. ECFC rolling was attributed to interactions between ECFC surface receptors and grafted peptides. Since some non-specific interactions are potentially occurring between PEGDA hydrogels and ECFCs, based on the observation that ECFC velocity on PEGDA hydrogels was lower than the calculated fluid velocity at a distance of one cell diameter from the hydrogel surface, a rolling velocity cutoff was employed to ensure that reported results were the result of specific ligand-receptor interactions. Taking into consideration both the average rolling velocity and the instantaneous velocities of ECFCs on PEGDA hydrogels, 40% of the average flow velocity was determined to provide

a reasonable cutoff (Figure 5.8). Further study could be undertaken to more carefully examine cells moving at the higher velocities observed across PEG hydrogels to determine the nature of interactions and the potential dependence on the properties of the PEG hydrogel surface; this was not, however, the subject of this investigation, since interactions with grafted peptides resulted in ECFC rolling at significantly lower velocities.

ECFC rolling in this research was examined across hydrogels grafted with three bioactive peptides, RGDS, REDV, and YIGSRG, in addition to the control peptide RGES. All three bioactive peptides supported a significant decrease in ECFC rolling velocity comparing to control PEG hydrogels and PEG-RGES grafted hydrogels, demonstrating that the peptide-grafted hydrogels are able to specifically interact with the surface receptors on ECFCs while rolling. Rolling velocities on RGDS- and YIGSRG-grafted hydrogels were similar, resulting in the conclusion that not only integrins, but also the 67kDa laminin binding receptor participate in ECFC rolling. This is in agreement with other research that suggests this receptor has great potential as a biomaterial for homing of ECFCs (Choi, Bae, Joung, & Park, 2009). Furthermore, REDV-grafted hydrogels supported significantly lower ECFC rolling velocities; REDV has a high binding affinity for the integrin $\alpha_4\beta_1$ (Massia & Hubbell, 1992). Although other cell types, including leukocytes, smooth muscle cells, and tumors, also express $\alpha_4\beta_1$ (Barry, Ludbrook, Murrison, & Horgan, 2000), it has been reported that only ECs adhered to REDV, whereas fibroblasts, vascular smooth muscle cells and platelets did not adhere (Hubbell et al., 1991). In addition, although firm adhesion of ECFCs on REDV-grafted hydrogels was not observed in this study, previous research has shown that REDV is able to capture ECFCs under flow when coated on PDMS

in a microfluidic device (Vickers & Murthy, 2010). This difference may be due to the high resistance of PEGDA to protein adsorption and therefore the absence of other ligands on the REDV-grafted PEGDA that could have been present on the REDV-coated PDMS. However, a small number of firm adhesion events were observed on the RGDS-grafted hydrogels at 20 s^{-1} where lower rolling velocity occurs. Since RGDS recognizes a wide range of integrins, RGDS-grafted hydrogels have a higher probability of forming multiple bonds with ECFCs during rolling than REDV-grafted hydrogels. It has been previously reported that ECFCs interact with the integrins $\alpha_v\beta_3$ and $\alpha_5\beta_1$ during cell rolling (Angelos et al., 2010); both of these integrins bind RGDS. For comparison, platelets have $\alpha_v\beta_3$, $\alpha_{IIb}\beta_3$, $\alpha_{II}\beta_1$, $\alpha_v\beta_1$, $\alpha_{vI}\beta_1$ (Bennett, Berger, & Billings, 2009; Bennett, 2005). We, therefore, conclude that peptide-grafted PEGDA hydrogels can support ECFC rolling and have the capability to capture rolling ECFCs when both low rolling velocity and multiple bond formation are attained.

5.5 Conclusions

In conclusion, a system has been developed to study specific interaction of peptides with ECFCs using PEG hydrogel system. An appropriateglass cleaning method was first identified and was followed by the verification of PEG-peptide grafting technique by cell adhesion assay and 6X histidine immunolabeling assay. Using the flow chamber system that was developed in Chapter 3, rolling ECFCs can be identified and specific interaction between peptides with ECFCs can be studied.

This study has demonstrated that peptide-grafted PEG hydrogels facilitate investigation of the interactions between specific material-bound ligands and cell surface

receptors on ECFCs. The use of a parallel plate flow chamber system has successfully aided in studying the effect of peptides on ECFC rolling velocity under shear stress. Whereas PEG hydrogels and hydrogels grafted with the non-bioactive peptide RGES did not support ECFC rolling, hydrogels grafted with one of the bioactive peptides RGDS, REDV, or YIGSRG all supported ECFC rolling, significantly reducing the velocity of the ECFCs. Furthermore, REDV-grafted hydrogels reduced ECFC rolling velocity to a significantly greater extent than RGDS- and YIGSRG-grafted hydrogels.

Understanding ECFC rolling on biomaterial surfaces will inform the design of future small diameter vascular grafts and next generation stenting materials. Improved ability to promote re-endothelialization is essential to enhancing healing damaged and diseased blood vessels. The peptide-grafted PEGDA hydrogel system used in this study possesses unique experimental advantages for informing synthetic biomaterial design, enabling it to augment knowledge found using materials that are coated with extracellular matrix proteins.

Chapter 6 Identification of Novel Peptides for Slower ECFC Rolling and Enhanced ECFC Capture Ability

6.1 Introduction

In the previous chapter, peptides, including REDV, RGDS, and YIGSRG, that were grafted on PEG hydrogels have been shown to support EPC rolling under shear. Despite the fact that REDV-grafted hydrogels reduced EPC rolling velocity the most, it does not support firm adhesion even at low shear rate. To identify peptides that are capable of slowing and capturing EPCs, more peptides should be evaluated.

Pepbank is a useful text mining tool that was developed to identify peptide sequences in MEDLINE abstracts and two public sources ASPD and UniProt (Shtatland, Guettler, Kossodo, Pivovarov, & Weissleder, 2007). With this searching tool, peptides that are relevant to target integrins can be researched. According to Angelos *et al.*, when both integrins $\alpha_5\beta_1$ and $\alpha_v\beta_3$ are blocked, EPC adhesion was significantly reduced (Angelos et al., 2010). Therefore, this chapter focuses in searching for peptides that bind to these integrins. At the time of preparation of this document, there were 47 and 88 hits for $\alpha_5\beta_1$ and $\alpha_v\beta_3$, respectively. We next excluded almost all RGD- and PHSRN- containing peptides from the results since RGD is a ubiquitous peptide while PHSRN is a well-known synergistic peptide that works together with RGD. For peptides that bind $\alpha_5\beta_1$, VILVLF (A5-1) (Kim, Bang, Chang, & Kang, 2008), CRRETAWAC (Larsen, Kligman, Tang, Kottke-Marchant, & Marchant, 2007), and -$(C_{16})_2$-Glu-C2-KSSPHSRNSGSGSGSGSGRGDSP (PR_b) (Mardilovich, Craig, McCammon, Garg, & Kokkoli, 2006) were selected for further testing. HSDVHK (P11) (Lee, Kang, Chang, Han,

& Kang, 2004) and NCKHQCTCIDGAVGCIPLCP (V2) (Chen, Leu, Todorovic, Lam, & Lau, 2004) were selected for $\alpha_v\beta_3$ testing.

6.1.1 Novel Peptides for $\alpha_5\beta_1$

VILVLF (A5-1)

Kim *et al.* have used ProteoChip to screen through a hexapeptide positional scanning synthetic peptide combinatorial library (PS-SPCL) and have found that A5-1 has a high affinity for $\alpha_5\beta_1$ (Kim et al., 2008). This screening strategy has been previously used to identify peptides for $\alpha_v\beta_3$ (Lee et al., 2004) and plant extracts for $\alpha_5\beta_1$ (Bang, Kim, Seong, Shin, & Kang, 2007). Furthermore, the binding affinity of VILVLF to $\alpha_5\beta_1$ was found to be higher than RGD. Briefly, an initial screening of a hexapeptide PS-SPCL was first performed using a competitive inhibition assay to narrow down to a reasonable number of peptides for further evaluation. As shown in Figure 6.1, peptides with valine, V, at Position 1 showed the lowest fluorescent intensity (as highlighted by the blue box) meaning these peptides were highly competitive for $\alpha_5\beta_1$ and inhibited binding of the fluorescently labeled fibronectin (FN) to $\alpha_5\beta_1$. On the other hand, more than one amino acid showed similar result at Position 2, 3, and 4. Using this logic, 8 hexapeptides with sequence VXXXLF were synthesized where X represents isoleucine/glutamic acid at Position 2, leucine/valine at Position 3, and valine/asparagine at Position 4. These 8 hexapeptides (VILVLF, VILNLF, VIVVLF, VIVNLF, VELVLF, VELNLF, VEVVLF, and VEVNLF) were further screened using the same competitive inhibition assay and VILVLF was found to be the most competitive for $\alpha_5\beta_1$. Thus, A5-1 has a high specificity and affinity for $\alpha_5\beta_1$ and it has high potential in capturing $\alpha_5\beta_1$-expressing EPCs.

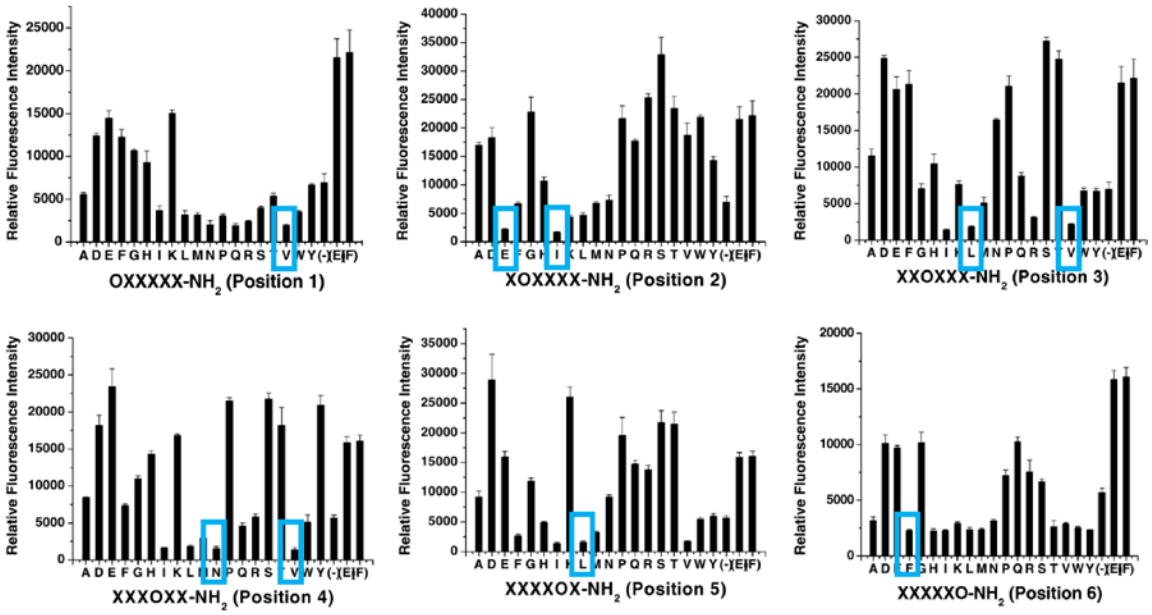

Figure 6.1 Inhibition of integrin $\alpha_5\beta_1$-FN interaction by a hexapeptide PS-SPCL. The *y*–axis represents the relative fluorescence intensity of fluorescently-labeled FN that was bound to the integrin $\alpha_5\beta_1$ coated ProteoChip. The *x*–axis represents the peptides with different amino acids at the corresponding position. The amino acids at each position of the hexapeptide that substantially inhibited the binding of the fluorescently labeled FN to $\alpha_5\beta_1$ are highlighted by blue boxes. The lower the relative fluorescence intensity, the higher the binding affinity of the peptide to $\alpha_5\beta_1$. Adapted from reference (Kim et al., 2008).

CRRETAWAC

Koivunen *et al*. identified the peptide CRRETAWAC which has a high binding affinity and selectivity for integrin $\alpha_5\beta_1$. They constructed a heptapeptide library by ligating a synthetic oligonucleotide into fUSE 5 vector (Koivunen, Wang, & Ruoslahti, 1994). The oligonucleotide has a core sequence of TGT(NNK)$_7$TGT where N represents an equal molar mixture of A, C, G, T while K represents G or T. TGT was coded for cysteine and NNK was coded for all amino acid. The cysteines on each side of the peptide were designed to form disulfide bond and to form cyclic peptides. Thus, the oligonucleotide produces a library of cyclic peptides with seven random amino acids.

The peptide library was screened with $\alpha_5\beta_1$ coated wells to identify the peptide with high binding affinity with $\alpha_5\beta_1$. The first two pannings were performed with 5 μg of $\alpha_5\beta_1$ per well while the third and fourth pannings with 10 and 1 ng/well, respectively. The bound phages were rescued and sequenced at the end of the pannings. Among the non-RGD containing peptides, CRRETAWAC showed the highest affinity to $\alpha_5\beta_1$.

Larsen *et al*. have implemented CREETAWAC in endothelialization of expanded polytetrafluoroethylene (ePTFE) surfaces by incorporating GSSSCRRETAWAC (Figure 6.2) (Larsen et al., 2007). When ePTFE was modified with GSSSCRRETAWAC, it supported EC attachment and proliferation. Furthermore, a significant lower coverage of the surface by platelets was observed comparing to RGD surface and FN-coated glass.

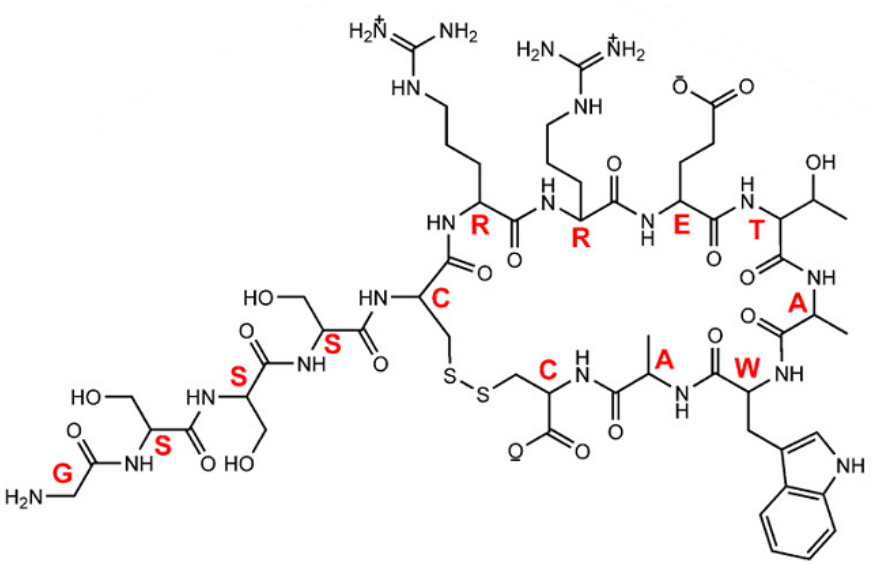

Figure 6.2 CREETAWAC-containing cyclic peptide for use in modification of ePTFE. This peptide allowed high EC binding through $\alpha_5\beta_1$ integrin and showed low platelet adhesion. Adapted from reference (Larsen et al., 2007).

-(C_{16})$_2$-Glu-C2-KSSPHSRNSGSGSGSGSGRGDSP (PR_b) for *$\alpha_5\beta_1$*

Despite the fact that PR_b contained the ubiquitous RGD peptide and the synergistic PHSRN peptide, this peptide is chosen to test for the capability on EPC rolling due to the its superior design in accurately mimicking FN's binding affinity for $\alpha_5\beta_1$. This peptide has been shown to mimic FN through HUVEC adhesion, spreading, and extracellular FN production (Mardilovich et al., 2006). In native FN, the distance between PHSRN and RGD is 30 – 40 Å which is a critical factor for PHSRN to perform its synergistic role in adhesion. With the length for each amino acid being 3.7 Å, the Kokkoli Lab used SGSGSGSGSG, which is a total of 10 amino acids to give a linker distance of 37 Å, to match the distance between PHSRN and RGD. In addition, study have shown that the ratio of hydrophilic to hydrophobic residues in between PHSRN and RGD in FN is almost 1:1 (Mardilovich & Kokkoli, 2004). The repeating SG sequence was chosen to mimic this ratio. Therefore, PR_b was able to mimic the adhesion property of FN for $\alpha_5\beta_1$.

6.1.2 Novel Peptides for $\alpha_v\beta_3$

HSDVHK (P11)

P11 was discovered by screening through PS-SPCL using protein-protein competitive inhibition assay (Lee et al., 2004). The PS-SPCL that was studied was comprised of 114 types of hexapeptide mixture and this library was divided into 6 groups with each group has various amino acids residues at each position. The PS-SPCL together with fluorescently labeled vitronectin (VN) were added onto $\alpha_v\beta_3$-coated surface and allowed to compete for the $\alpha_v\beta_3$ integrin. As shown in Figure 6.3, peptides with histidine, H, at Position 1 (as highlighted by the blue box) showed the lowest fluorescent intensity

meaning it was highly competitive for $\alpha_v\beta_3$ and inhibited the fluorescently labeled VN to bind $\alpha_v\beta_3$. Similarly, histidine at Position 5 and lysine, K, at position 6 showed the same result. On the other hand, more than one amino acid showed similar result at Position 2, 3, and 4. Therefore, 12 hexapeptides with sequence HXXXHK were synthesized where X represents glycine/histidine/serine at Position 2, aspartic acid/leucine at Position 3, and leucine/valine at Position 4. These 12 hexapeptides were further screened using the same competitive inhibition assay and HSDVHK was found to be the most competitive for $\alpha_v\beta_3$. Thus, HSDVHK has a high specificity and affinity for $\alpha_v\beta_3$ and it has high potential in capturing $\alpha_v\beta_3$-expressing EPCs.

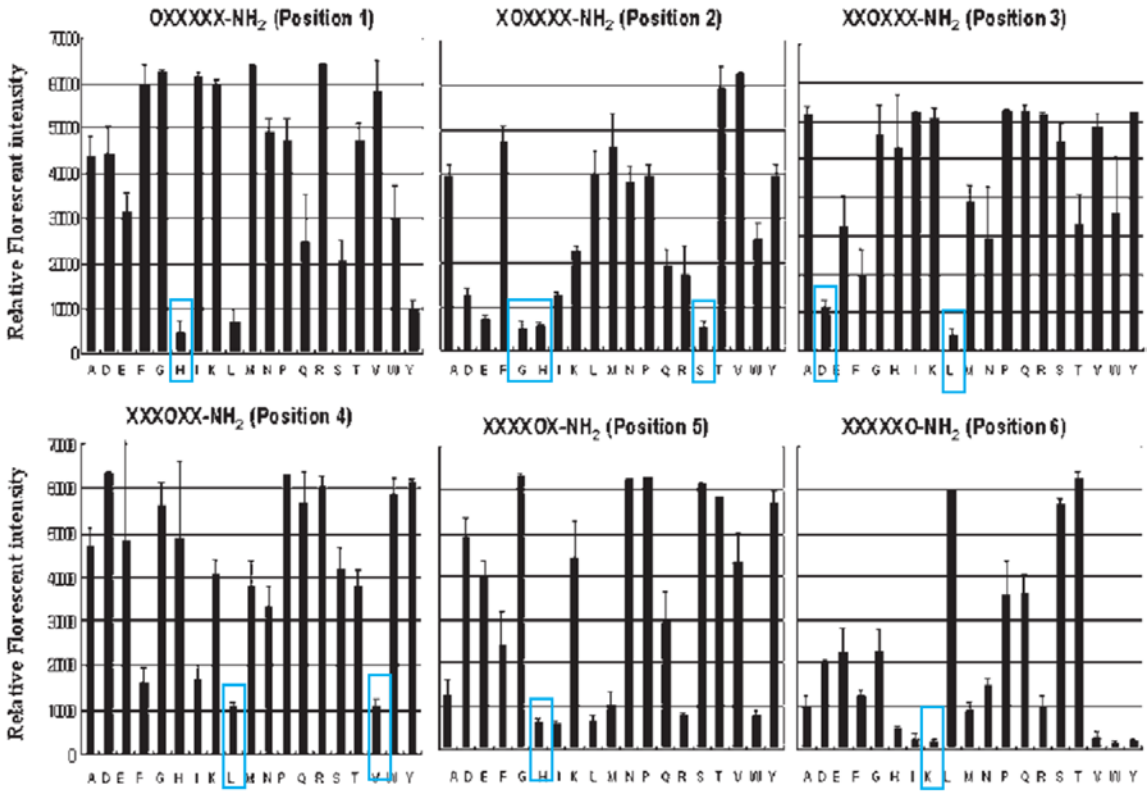

Figure 6.3 Inhibition of integrin $\alpha_v\beta_3$-VN by a hexapeptide PS-SPCL. The *y*–axis represents the relative fluorescence intensity of fluorescently-labeled VN bound to the integrin $\alpha_v\beta_3$ coated ProteoChip. The *x*–axis represents the peptides with different amino acids at the corresponding position. The amino acids at each position of the hexapeptide that substantially inhibited the binding of the fluorescently labeled VN to $\alpha_v\beta_3$ are highlighted by blue boxes. Adapted from reference (Lee et al., 2004)

NCKHQCTCIDGAVGCIPLCP (V2)

V2 is a peptide representing the 116-135 residues of the cysteine-rich heparin-binding protein (CCN1). The functions of CCN1 include regulating cell adhesion, migration, proliferation, survival and differentiation in mesenchymal cells (Chen et al., 2004). Studies have shown that CCN1 binds directly to $\alpha_v\beta_3$ and mediates pro-angiogenic activities (Kireeva, Lam, & Lau, 1998; Leu, Lam, & Lau, 2002). Chen *et al.* reported evaluated peptides of different portion of CCN1 and reported that V2 was responsible portion for HUVEC adhesion specifically through $\alpha_v\beta_3$ (Chen et al., 2004). They have also shown that when the D residue was altered into A, the altered V2 peptide lost the capability to bind HUVEC through $\alpha_v\beta_3$ integrin. Furthermore, shorter versions of V2 have also shown similar results meaning V2 is the exact peptide required to bind $\alpha_v\beta_3$. Therefore, V2 is a potential peptide to capture EPCs due to its specific binding to $\alpha_v\beta_3$.

Additional analyses on EPC rolling were performed to evaluate the effect of novel peptides in the dynamic adhesion of EPC under shear. As the novel peptides have high binding affinity to $\alpha_5\beta_1$ and $\alpha_v\beta_3$, there may be high potential for these peptides to capture EPCs.

6.2 Materials and Methods

6.2.1 Peptide Synthesis

VILVLFG

VILVLFG was synthesized under standard procedure as shown in Section 2.4. Mass spectrometry was used to confirm the synthesis (Appendix D.11).

CRRETAWAC

Some alterations in the sequence of the peptide and extra reactions were involved in the testing of CRRETAWAC. According to Larsen *et al.*, the peptide sequence GSSS was added at the N-terminus of CRRETAWAC to extend the peptide further away from the substrate interface. In this project, all peptides were coupled to the acryloyl-PEG that serves as the spacer arm, so GSSS may not be necessary. Therefore, the original peptide CRRETAWAC was synthesized for testing, instead of GSSSCRRETAWAC. In order to create the disulfide bridge to form the cyclic CREETAWAC peptide, Fmoc-S-acetaminomethyl-L-cysteine (Fmoc-Cys(Acm)) was used during the peptide synthesis because the Acm protection group is stable during TFA cleavage. The disulfide bridge can be formed subsequent to cleavage with iodine oxidation as suggested by aapptec. The peptide was dissolved in 2 mg/mL of 50% acetic acid. Then the peptide solution was added into 50 mL of 0.1 M iodine solution in acetic acid. The mixture was then stirred until the yellow color persists. Aqueous ascorbic acid was added drop-wise to quench the excess iodine until the mixture is colorless. The mixture was placed in rotavap to concentrate by evaporation to approximately one third of the original volume. Mass spectrometry was used to confirm the production of the peptide and the cyclic CRRETAWACG should have a molecular weight of 1150 g/mol. However, as shown in Appendix D.12, the cyclized CRRETAWACG (1150 g/mol) was only the minor product whereas the major products were shown to be 1221 g/mol and 1292 g/mol which correspond to the peptide with a single and double Acm protection groups present. After extra iodine oxidation procedures were followed, similar results were obtained. Therefore, the peptide CRRETAWAC (instead of

CRRETAWACG) was purchased from American Peptide with >95% purity. Formation of disulfide bonds between the cysteine residues was completed by manufacturer as requested.

PHSRNSGSGSGSGSGRGDSG (PRb)

Regarding to the original PR_b peptide, the C_{16} hydrophobic tail, glutamic acid tail connector, and the -C_2-tail spacer will be discarded to reduce peptide synthesis complexity. As a result, PHSRNSGSGSGSGSGRGDSG (PRb) was synthesized under standard procedure as shown in Section 2.4. Mass spectrometry was used to confirm the synthesis (Appendix D.13).

HSDVHKG

HSDVHKG was synthesized under standard procedure as shown in Section 2.4. Mass spectrometry was used to confirm the synthesis (Appendix D.14).

NCKHQCTCIDGAVGCIPLCPG

NCKHQCTCIDGAVGCIPLCPG (V2) was synthesized under standard procedure as shown in Section 2.4. Mass spectrometry was used to confirm the synthesis (Appendix D.15). However, the peptide was not readily to be dissolved in aqueous injection solution for mass spectrometry analysis. Furthermore, many unexpected by-products were present. Therefore, the V2 peptide was excluded in this study due to the inability to accurately synthesize the peptide.

6.2.2 PEG-Peptide Conjugation and Confirmation through Mass Spectrometry

CRRETAWAC, PRb, and HSDVHKG was conjugated to PEG in the exact same fashion as described in Section 2.8. Mass spectrometry was used to confirm the conjugation

as shown inAppendix D.16, Appendix D.17, and Appendix D.18. Unfortunately, while attempting with the PEG-peptide conjugation under organic solvents as suggested in literature (Bahney et al., 2011; Culver et al., 2012; Nemir, Hayenga, & West, 2010), A5-1 peptide precipitated immediately after the addition of DIPEA, which acts as a base catalyst. Therefore, A5-1 was excluded in this study due to the inability to conjugate to acryloyl-PEG for grafting.

6.2.3 ECFC Rolling on Novel Peptide-grafting PEG Hydrogels

ECFC rolling was carried out as described previously in Section 2.9

6.3 Results and Discussion

6.3.1 Adhesion of ECFCs on Novel Peptide-grafted PEG Hydrogels

Adhesion of ECFCs on CRRETAWAC-, PRb-, P11-grafted hydrogels was first accessed. Both CRRETAWAC and PRb supported ECFC adhesion and spreading. ECFCs were also able to form a monolayer and maintain their cobble stone morphology (as shown in Figure 6.4A and B). However, P11-grafted hydrogels were only able to support ECFC adhesion, but not spreading (Figure 6.4C). On P11-grafted hydrogels, ECFCs aggregated to form adherent cell clumps. This suggests that although P11 was found to have high specificity for $\alpha_v\beta_3$ (Lee et al., 2004), it may not support regular cellular activities other than cell adhesion. Without the ability to support cell spreading and the formation of monolayer, P11 alone could not support ECFC endothelialization which is critical for healing damaged and diseased blood vessels.

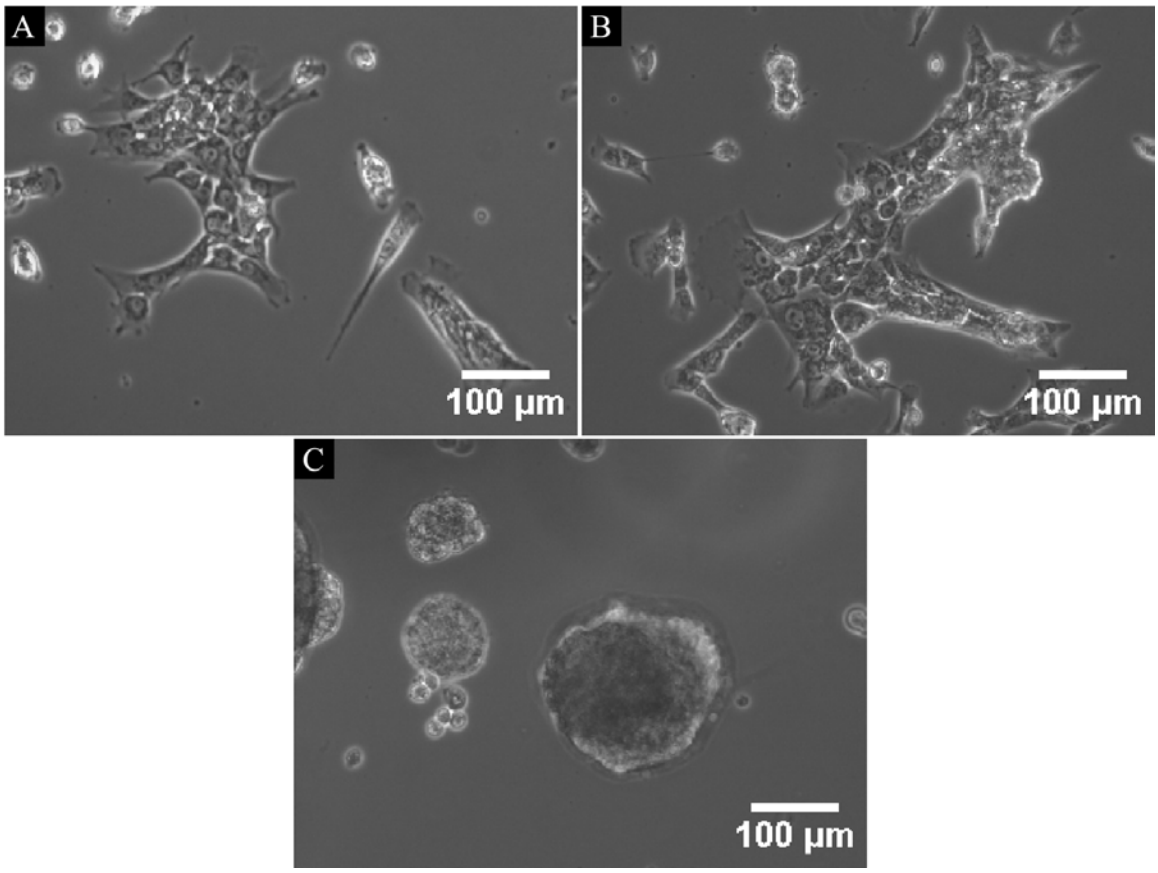

Figure 6.4 Adhesion of ECFCs on novel peptides-grafted PEG hydrogels after 24 hours. ECFC adhesion on A) CRRETAWAC- B) PRb- C) P11-grafted PEG hydrogels.

6.3.2 Similar ECFC Rolling Velocity Exhibited by Novel Peptides Comparing to RGDS

ECFC rolling was performed on novel peptide-grafted hydrogels and the results were compared to RGDS, REDV, and YIGSRG-grafted hydrogels (Figure 6.5 and Figure 6.6). All novel peptides supported ECFC rolling as the velocities were well below the cutoff for rolling velocity. Regarding the novel peptide, P11 showed the lowest rolling velocity whereas CRRETAWAC showed the highest rolling velocity at all shear rates. Comparing to RGDS and YIGSRG, both P11 and PRb showed similar rolling velocities and CRRETAWAC showed significantly higher rolling velocities at all shear rates. ECFC rolling velocities of all three novel peptides were significantly higher than REDV at 40 s^{-1}, 80 s^{-1}, and 120 s^{-1}. Some ECFC capture events were observed on CRRETAWAC and PRb-grafted hydrogels at 20 s^{-1}, and this will be further analyzed in Section 6.3.3. In summary, the all tested novel peptides support ECFC rolling.

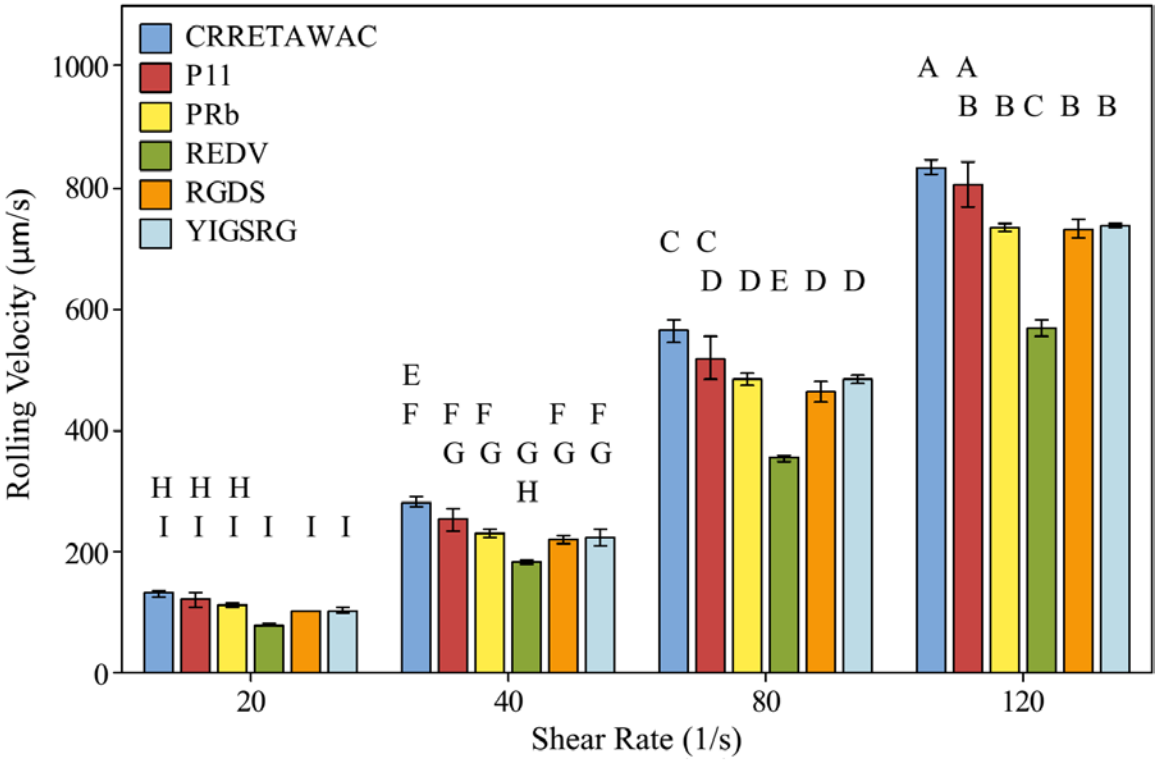

	Shear Rate (1/s)			
Peptide	20	40	80	120
CRRETAWAC	131.6±16.3	278.4±28.6	550.6±64.1	828.4±82.7
P11	127.5±18.4	251.0±41.2	508.0±86.5	787.6±102.1
PRb	110.3±17.7	235.0±36.1	485.7±67.5	735.1±102.6
REDV	78.6±15.8	183.3±43.4	353.8±82.0	564.3±177.0
RGDS	102.2±20.1	218.7±42.4	455.8±86.7	739.7±121.9
YIGSRG	103.2±18.9	223.2±38.0	487.6±72.5	737.0±107.9

Figure 6.5 Comparison of ECFC rolling velocity between novel peptides and known ECM peptides. As each shear rate, conditions that do not share the same letter are significantly different (p<0.05) from each other based on Tukey's test. Data represent mean ± SD (n=3).

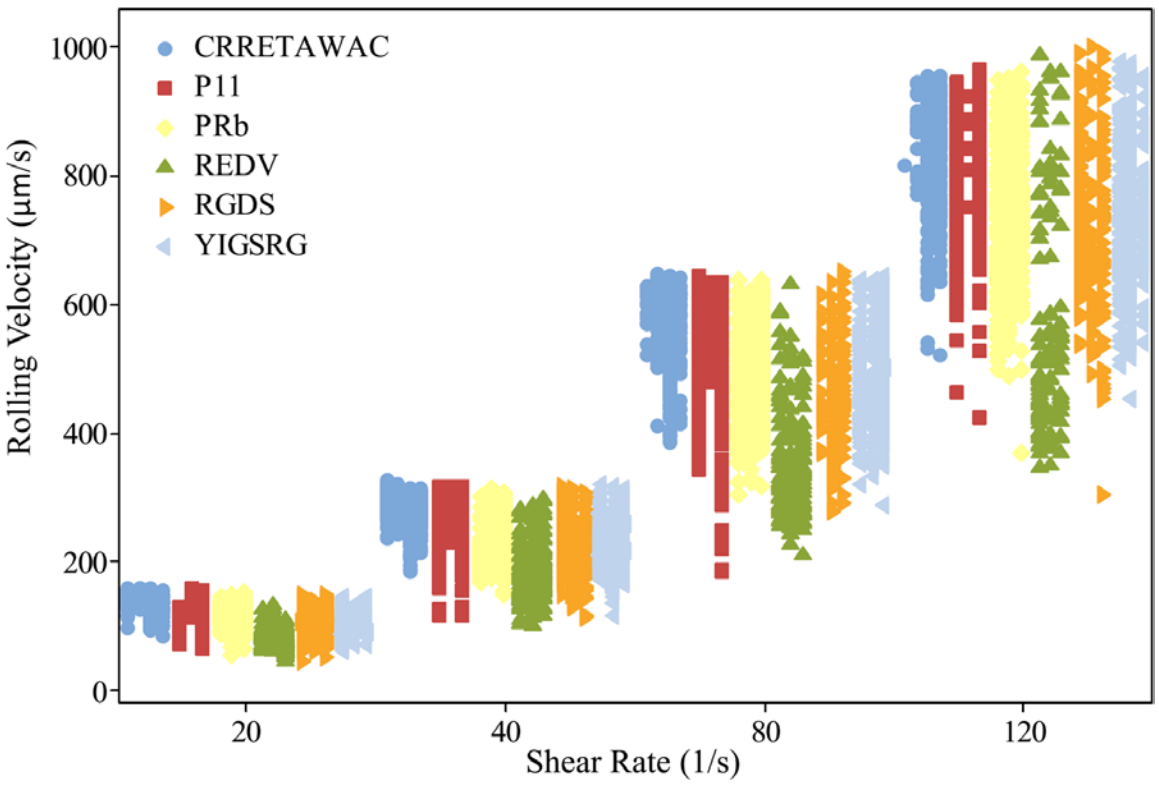

Figure 6.6 Individual data plot showing the distribution of rolling velocities for rolled ECFCs on the peptide-grafted hydrogels at each tested shear rate. Each marker represents one tracked cell. Separately prepared peptide-grafted hydrogels were used for each trial and each trial is shown as a separate column.

6.3.3 Capture of ECFC by CRRETAWAC and Enhanced Capture of ECFC by Combination of REDV and CRRETAWAC

ECFC Capture on CRRETAWAC- and PRb-grafted Hydrogels

Cell capture events were consistently observed on CRRETAWAC- and PRb-grafted hydrogels at 20 s^{-1}. Number of captured cells were counted and normalized to the total number of cells interacted with each hydrogel surface. During each of the 2 min recordings, 3.74%±1.0% of ECFCs were captured on CRRETAWAC-grafted hydrogels and 1.14%±0.2% of ECFCs were captured on PRb-grafted hydrogels Figure 6.7. Since both of these novel peptides are specific for the integrin $\alpha_5\beta_1$, the result of this study strongly supports that $\alpha_5\beta_1$ is responsible for cell capture. This is in agreement with Angelos *et al*. who have suggested that initial capture of EPCs is directly dependent on integrin $\alpha_5\beta_1$ (Angelos et al., 2010).

Increased ECFC Capture on REDV/CRRETAWAC-grafted Hydrogels

To further evaluate the potential use of CRRETAWAC and PRb in the ECFC capture for endothelialization, ECFC rolling on hydrogels that were grafted with combinations of CRRETAWAC or PRb with REDV was assessed. In order to maintain consistent grafting of peptides, a final concentrations of 0.7 μmol/mL of equal molar mixtures of acryloyl-PEG-peptides precursors were grafted onto the surface of PEG hydrogels. Hydrogels grafted with REDV/CRRETAWAC combination (0.35 μmol/mL of REDV/0.35 μmol/mL of CRRETAWAC) had significantly increased ECFC capture of 13.4%±2.3% as compared to CRRETAWAC alone (Figure 6.7). This increased ECFC capture may be due to the contribution from REDV which has shown that it significantly reduces the rolling velocity. This theory was supported by the observation of lower rolling

velocity on REDV/CRRETAWAC-grafted hydrogels (Figure 6.8), although no significant difference was found between the rolling velocities on CRRETAWAC and REDV/CRRETAWAC at all tested shear rates.

No ECFC Capture on REDV/PRb-grafted Hydrogels

As REDV has a significantly positive effect on enhancing the ability of CRRETAWAC to support ECFC capture, it has a negative effect on PRb's ability to support ECFC capture (Figure 6.7). The implementation of REDV in combination with PRb has completely eliminated PRb's capability for ECFC capture (from 1.14%±0.2% to 0%). This unforeseen result was probably due to the significant difference in length of the two peptides. Unlike CRRETAWAC, PRb has no Cys that forms internal disulfide bridge, so it is considered as a linear peptide. While REDV has four amino acids, PRb has 20 amino acids, which is five times longer than REDV. The much longer PRb may have shielded the shorter REDV which restricted the access of integrin $\alpha_4\beta_1$ on ECFCs to REDV. This hypothesis is also supported by the increase in ECFC rolling velocity on REDV/PRb-grafted hydrogels compared to PRb alone as shown in Figure 6.8 and Figure 6.9.

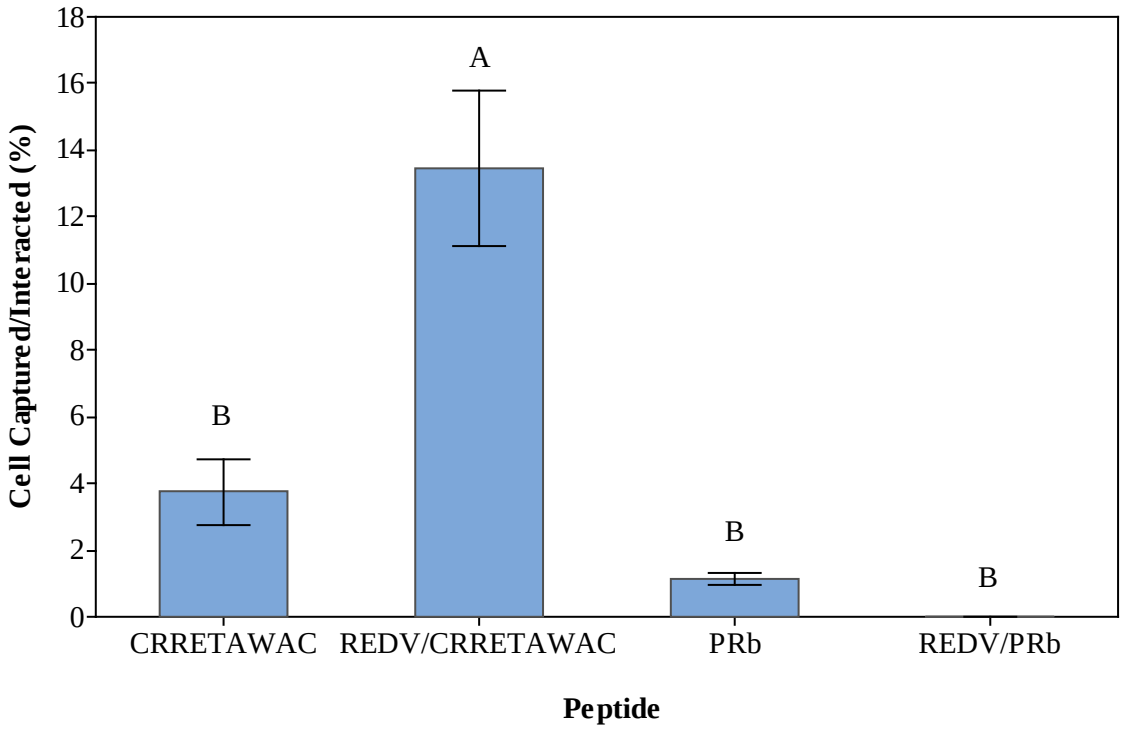

Figure 6.7 Number of ECFC captured Comparison of ECFC rolling velocity between novel peptides and known ECM peptides. Conditions that do not share the same letter are significantly different (p<0.05) based on Tukey's test. Data represent mean ± SD (n=3).

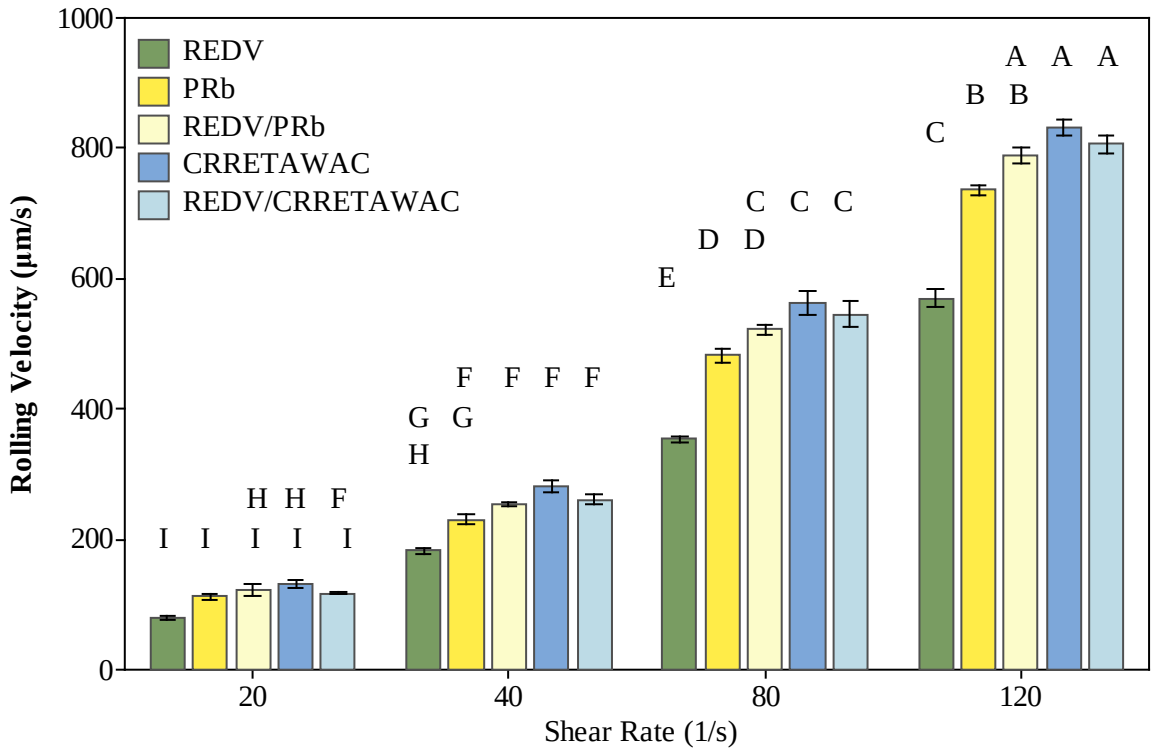

Figure 6.8 Comparison of ECFC rolling velocity between novel peptides, known ECM peptides, and combinations thereof. Conditions that do not share the same letter are significantly different (p<0.05) from Tukey's test. Data represent mean ± SD (n=3).

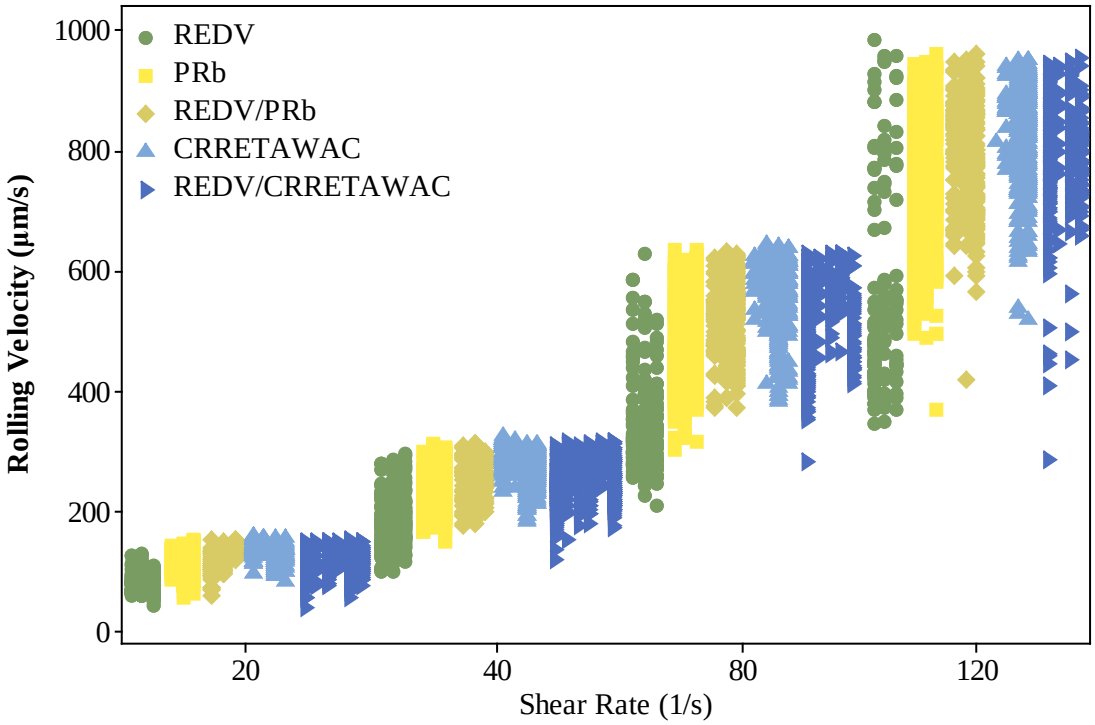

Figure 6.9 Individual data plot showing the distribution of rolling velocities for rolled ECFCs on the peptide-grafted hydrogels at each tested shear rate. Each marker represents one tracked cell. Separately prepared peptide-grafted hydrogels were used for each trial and each trial is shown as a separate column.

6.4 Conclusions

Novel peptides were selected to evaluate their capability in slowing and capturing EPCs. Pepbank was used to identify peptides that have high affinity and/or selectivity for the integrins $\alpha_5\beta_1$ and $\alpha_v\beta_3$. Although these peptides have shown great promise in cell adhesion, their performance in cell rolling and capture under shear is yet to be evaluated. Although five peptides were identified, three were assessed due to the success in synthesis and conjugation to acryloyl-PEG. Using the flow system developed in Chapter 3 together with the rolling cell tracking algorithm developed in Chapter 4, assessment on CRRETAWAC and PRb showed that $\alpha_5\beta_1$ is the major integrin that is responsible for ECFC capture under shear whereas previously tested ECM peptides were not. CRRETAWAC was found to be superior in capturing rolling ECFCs under shear, and this effect was enhanced by the implementation of REDV, which is specific for $\alpha_4\beta_1$. Although PRb also has potential in capturing ECFCs, its capturing ability was not observed when implementing REDV. This illustrates the importance of the peptide length in biomaterial design. To conclude, this chapter has provided the rationale for testing the proposed peptides and has led to a better understanding in which cell surface receptors can be used to mediate ECFC rolling and capture under shear.

Chapter 7 Isolation of ECFCs for Potential Veterinary Clinical Uses

7.1 Introduction

Besides the clinical relevance of EPC in human, the benefits of EPCs may also be used in veterinary species. EPC study has been done in various species of animals including mice, rabbits (Ma et al., 2009), dogs (Wu et al., 2005), pigs (Achneck et al., 2011; Jantzen et al., 2011), sheep, baboons (Ensley, 2006), and rhesus macaques (Hu et al., 2002). The isolated EPCs in these animal studies have shown promising potential for applications in tissue engineering and vascular therapy. As EPCs have been used therapeutically to treat non-healing wounds, limb ischemia, and cardiovascular ischemia (E Chavakis & Dimmeler, 2011; Nagano et al., 2007), the concept of EPC therapy could be applied in veterinary medicine to treat common diseases that lack vasculature. However, currently isolation of EPCs from horses has yet to be studied. To investigate the potential applications of EPCs in horses, it was first necessary to determine whether EPCs could indeed be successfully isolated from healthy horses and to verify the identity of the cells obtained. This study sought to isolate, culture, and characterize one specific subtype of EPCs, ECFCs, from healthy horses. Characterization included analysis of cell morphology, *in vitro* tubule formation, uptake of acetylated low density lipoprotein, and endothelial and hematopoietic cell marker expression.

EPC isolation method depends on two major categories: location of cell source and purification method. EPCs have been shown to be present in different part of the body, peripheral blood, bone marrow (Asahara et al., 1999), umbilical cord blood (Murohara et al., 2000), vessel walls (D. A. Ingram et al., 2005), and fetal liver (Cherqui et al., 2006; Rafii & Lyden, 2003). Depending on the location of cell source, EPCs showed some varied

phenotypic characteristics. EPCs can also be isolated with different purification methods, including media and substrate culture, density gradient technique (Achneck et al., 2011; Jantzen et al., 2011; Ma et al., 2009), and magnetic bead sorting. Media and substrate culture is used in this preliminary study due to its simple and cost effective nature (Hofmann, Reinisch, & Strunk, 2009). Density gradient centrifugation is a common monocyte isolation technique, but it requires a certain level of skill in order to achieve consistent results. Magnetic sorting was used in the initial discovery of EPCs (Asahara et al., 1997), but it may cause low cell viability (Shirota, Hongbing, Yasui, & Matsuda, 2003). Hence, this method was not considered in this study.

In order to validate the success of EPC isolation, three common assays can be used to identify EPCs from mixed cell populations. The first one is uptake of 1,1'-dioctadecyl-3,3,3',3'-tetramethyl-indocarbocyanine perchlorate labeled acetylated low density lipoprotein (DiI-Ac-LDL). Endothelial cells and microglial cells possess "scavenger" receptors that specifically uptake the Ac-LDL. When the lipoprotein is degraded by lysosomal enzymes, the DiI (fluorescent probe) accumulates in the intracellular membranes. This labeling technique is shown to have no effect on cell viability according to the manufacturer. Although microglial cells, a type of macrophage, may also uptake Ac-LDL and fluoresce, these cells can be easily distinguished from endothelial cells with the fact that they are more brightly labeled. The second characterization assay is the Matrigel tubule formation assay where ECs form tubular networks on Matrigel, which is a gelatinous protein mixture derived from Engelbreth-Holm-Swarm (EHS) mouse. This assay is very common for studying *in vitro* angiogenesis

(Arnaoutova & Kleinman, 2010). ECs can form tubule networks on Matrigel in 6-12 hr (Kleinman & Martin, 2005). The third assay to identify EPCs is immunocytochemistry. As previously mentioned in Section 1.2 there are common surface markers (phenotype) between ECFCs and ECs, so surface markers are also critical in the identification of EPCs (D. A. Ingram et al., 2004; Wood et al., 2012; Yoder et al., 2007). ECFCs are typically positive for endothelial markers: CD31, CD34, CD105, VEGFR-2, and vWF; and are typically negative for the expression of hematopoietic markers: CD14, CD45 and CD133 (Asahara et al., 1997; Kovacic et al., 2008; Richardson & Yoder, 2011; Timmermans et al., 2009).

Evaluation of the angiogenic capabilities of the isolated equine ECFCs in three dimensional environment could also provide insights in assessing their potentials for clinical use. As described in Section 1.3, PEG hydrogels possess great properties to serve as a 3D tissue engineered scaffolds for ECFCs. In order for angiogenesis to take place, modification of PEG hydrogels is necessary for ECFCs to degrade and tunnel through the polymer network. PEG-fibrinogen was chosen as the biomaterial due to its adhesive and degradable properties. This hybrid polymer has been previously shown to support extension formation of encapsulated smooth muscle cells (Almany & Seliktar, 2005; Dikovsky, Bianco-Peled, & Seliktar, 2006). In this Chapter, the vascularization of 3D PF hydrogels by the isolated equine ECFCs will also be illustrated.

7.2 Materials and Methods

7.2.1 Isolation and Culture of Equine ECFCs

All procedures involving animals were approved by the Auburn University Animal Care and Use Committee. Blood draw was performed by our collaborator Dr. Wooldridge and her students in Department of Clinical Sciences at Auburn University College of Veterinary Medicine.

Ten mL of peripheral blood from the jugular vein were collected into lithium heparin tubes from 24 adult horses from the Auburn University College of Veterinary Medicine teaching and reproduction herds and from the Auburn University Equestrian Team herd. Blood samples were transported on ice to the lab for processing within 1 hour.

Whole Blood Isolation Method

EPC isolation was performed using a protocol published by Hofmann *et al.* with some modifications (Hofmann et al., 2009). Five mL of blood was collected from the adult horses of similar age and body condition from their jugular vein and transferred to lithium-heparin blood vacutainer tube. All blood samples were processed within an hour. Each blood sample was placed in a T-75 tissue culture polystyrene flask (BD) together with 20 mL of pre-warmed defined horse media and incubated at 37°C. Horse media consist of Endothelial Growth Medium-2 (EGM-2), hydrocortisone, hFGF, VEGF, IGF, ascorbic acid, hEGF, GA-1000, heparin, and 10% horse serum. After 24 hours, blood and media mixture was removed and cells were rinsed three times with warm PBS. Then 20 mL of fresh horse media was added and returned to incubation. Six mL of media were changed

twice a week and flasks were screened every other day to look for colonies. Once colonies were found, cells were passaged the same as human ECFCs either for expansion or storage.

Colony Harvest, Subculture, and Cryopreservation

Once colonies developed, day of appearance and colony number were noted, and colony morphology was recorded via light microscopy. Colonies were harvested using trypsin/EDTA (0.25 mg/mL) at 37°C for 1 min. Trypsin was neutralized by the addition of fresh media, followed by centrifugation at 200 x g for 5 min. Cells were re-seeded onto a collagen-coated T75 cm^2 cell culture flask for cell expansion. To coat the flask with collagen, 7.5 mL of 50 µg/mL rat-tail type I collagen in 0.02 N acetic acid was added to the T75 flasks and incubated for 30 min at room temperature. The collagen solution was then aspirated, and the flask was rinsed with 7.5 mL of PBS. Once the cells reached 80%-90% confluency, they were subcultured at a cell density of 3,000 cells/cm^2 to be used for characterization assays, and the remaining cells were cryopreserved at 337,500 cells/mL in a freezing medium containing 95% horse serum and 5% dimethyl sulfoxide for future experiments.

7.2.2 In Vitro Tubule Formation Assay

When EPCs reached 90% confluency, cells were detached from culture flask and resuspended in EGM-2 media. Cells were seeded onto Matrigel (BD) coated 96-well plate at 5000, 7500, and 10,000 cells/well. Well plates were coated with 50 µl of Matrigel per well and incubated at 37°C prior cell seeding. Tubule formation was observed every 2 hours under microscope. Human ECFCs (P9-P11) served as the positive control while mouse fibroblast cells served as the negative control. Both cell types were seeded at the

same cell density as the equine ECFCs. The tubule formation assay was repeated 3 times for each horse, with each assay performed in duplicate.

7.2.3 Uptake of Acetylated-Low Density Lipoprotein

When EPCs reached 90% confluence, cells were detached and seeded in collagen-I coated 24-well plate at 16,000 cells/well. Cells were allowed to adhered and incubate at 37°C for 24 hours. Cell culture medium was removed and cells were rinsed twice with PBS. 500 μL of 10 μg/mL of DiI-Ac-LDL (Biomedical Technologies) in cell culture medium and cells were allowed to incubate for 6 hours. DiI-Ac-LDL containing medium was removed and washed with PBS three times for 15 s each. Cells were fixed with 4% paraformaldehyde in PBS solution for 20 min at room temperature covered in aluminum foil. Then cells were rinsed with water three times for 5 s each. Lastly, DAPI was added to counter stain the nuclei for 25 min at room temperature. DAPI solution was removed and cells were rinsed with PBS three times for 2 min each. Fluoromount was added before imaging under fluorescent microscope. Human ECFCs and bovine aortic endothelial cells (BAECs) were used as positive controls while mouse 3T3 fibroblasts were used as negative control.

Equine ECFCs (P1-P3), human ECFCs (P11-P14), and mouse fibroblast cells were seeded at a cell density of 8,000 cells/cm^2 using 24-well cell culture plates that had been pre-coated with collagen (50 μg/mL) as described above. All cells were incubated for 24 hr at standard cell culture conditions. After 24 hr, DiI-Ac-LDL was added at a concentration of 50 μg/mL, diluted in pre-warmed supplemented media appropriate for the cell type, and the cells were incubated for 4 hr at standard cell culture conditions. After incubation, the

cells were washed with probe-free media, fixed with 4% paraformaldehyde for 20 min, and counter stained with DAPI for 25 min. The cells were then mounted and imaged. Images were analyzed for the percentage of positive cells using two separate fields of view per well at 10x (1.26 mm^2) magnification and using two separate wells for a total of 4 images per horse. Assays were repeated 3 times for each horse and all cell samples were assayed in duplicate. Overlaid images showing DAPI staining and uptake of DiI-Ac-LDL at 10x (1.26 mm^2) magnification were used for analysis. The percentage of cells positive for DiI-Ac-LDL uptake was determined by dividing the total number of DAPI stained cells per field of view by the number of cells taking up DiI-Ac-LDL.

7.2.4 Cell Senescence and Cell Growth after Subculture

To evaluate cell senescence and cell growth, cells were continually subcultured, and in vitro tubule formation and DiI-Ac-LDL uptake assays performed at each passage. The tubule formation assay was performed as described above, for each cell passage for each individual horse, using a seeding density of 10,000 cells/cm^2. The time until tubule appearance and tubule quality score (1-4 score) were recorded. The scoring system for vascular tubule formation (Figure 7.3) was: 1) no tubule formation, 2) projecting tubules from cells but no connections between any cells, 3) vascular tubule formation with connecting tubules in 50% or less of the field and 4) high level of vascular tubule formation with connecting tubules greater than 50% of the field. At the 24 hr time point, 3 fields of view at 10x (1.1 mm^2) magnification were acquired from the samples from all 3 horses at each passage. These images were scored twice by a blinded observer (MMS), and, if any discrepancy, the scores were averaged prior to statistical analysis. The median score of the

3 fields from each horse was compared between passages for a single observation for each horse (n=3) at each passage.

The DiI-Ac-LDL uptake assay was performed in duplicate as described above on samples from every horse at each passage. Four fields of view at 10x (1.26 mm^2) magnification were acquired and analyzed, for a total of 4 images per passage per horse. Images were analyzed to determine the percentage of cells positive for DiI-Ac-LDL uptake as described above. The mean of the percentages for all images for each horse was used for statistical analysis for a single observation for each horse (n=3) at each passage.

Cell seeding density after each subculture, cell number at time of subculture, and time (hr) between subcultures were recorded and used to determine the number of cell doublings per 24 hr period as well as the PDT. These were calculated using the following equations:

$$\text{NCD} = \frac{Log_2 \frac{C_H}{C_S}}{\text{Number of days}} \tag{30}$$

$$\text{PDT} = \frac{\text{NCD}}{\text{Total number of hours}} \tag{31}$$

NCD is the number of cell doublings, C_H is the number of cells at time of subculture, and C_S is the number of cells at seeding. PDT was the total time taken, in hours, for the population to double.

7.2.5 Isolation of Equine Carotid Endothelial Cells

For use as a positive control for flow cytometry and indirect immunofluorescence staining, ECs were harvested from an adult horse that was submitted for necropsy

examination according to previous protocols (MacEachern, Smith, & Nolan, 1997). Briefly, isolated carotid arteries were digested with Type II collagenase and plated in DMEM with 25 mM 4-(2-hydroxyethyl)-1-piperazineethanesulfonic acid (HEPES), 10% FBS, penicillin/streptomycin, and 10% calf serum. Cells were subcultured when they reached 80% confluency and plated on collagen coated flasks with horse serum supplemented EGM-2 (the same medium used for equine ECFCs). The isolated cells were then sorted by flow cytometry based on their ability to uptake DiI-Ac-LDL to obtain a more pure EC population and eliminate any contaminating smooth muscle cells. When the cells reached 70% confluency, they were incubated with DiI-Ac-LDL using the same protocol as described above. The brightest 22% of cells were gated, sorted at 65 lb/in^2 into medium, and then maintained at standard culture conditions. The ECs were further characterized by phenotypic appearance and vascular tubule formation *in vitro*.

7.2.6 Indirect Immunofluorescence Staining

Equine ECFCs (P3 to P5) and ECs (P4 to P6) were evaluated for expression of EC markers vWF, VEGFR-2, CD34 and CD105 and expression of the hematopoietic marker CD14 using IF. Equine ECFCs or ECs were seeded on collagen-coated glass coverslips at a cell density of 6700 cells/cm^2 and allowed to expand until 80 to 90% confluency was reached. Cells were then fixed with 4% paraformaldehyde, washed, and blocked with 3% FBS for 30 min. To detect the intracellular protein vWF, cells were permeabilized with 0.1% Triton X-100 for 30 min prior to blocking. Following blocking, the equine ECFCs and equine ECs were incubated with the primary antibodies followed by the appropriate secondary antibodies. All antibodies were diluted in 3% FBS and incubated at room

temperature at the following dilutions: vWF, 1:200 for 3 hr; VEGFR-2, 1:200 for 3 hr; CD34, 1:100 for 3 hr; CD105, 1:100 for 3 hr; CD14, 1:100 for 1 hr. Secondary antibodies were all used at a concentration of 1:400 and incubated 12-18 hr at 4°C. Coverslips containing stained cells were mounted on slides and imaged using fluorescence microscopy. Visualization of red and green fluorescence was in tetramethylrhodamine isothiocyanate spectrum (TRITC, excitation: 562 nm, emission 576 nm) and fluorescein isothiocyanate spectrum (FITC, excitation: 498 nm, emission 520 nm), respectively.

7.2.7 Flow Cytometry

Equine ECFCs (P3-P5) were characterized for expression of the endothelial cell surface marker CD105 and the hematopoietic surface marker CD14 using flow cytometry. Cultured ECs served as the positive control for evaluation of CD105 expression, and monocytes from equine whole blood served as the positive control for evaluation of CD14 expression. Cultured cells were trypsinized as described above, centrifuged and re-suspended in supplemented EBM-2 media and allowed to incubate for 30 min at room temperature for cell surface marker regeneration. For staining, 5×10^5 cultured cells in 100 µL media were used per condition. Whole equine blood was collected in lithium-heparin tubules and aliquots of 100 µL were used for the staining protocol. Serum present in the whole blood provided natural blocking of the monocytes prior to the addition of the primary antibody. Following the 30 min incubation for cell marker regeneration, equine ECFCs and ECs were blocked with 10% horse serum for 30 min. The primary antibody (same CD105 and CD14 antibodies described above) was added at concentrations of 0.02 µg/µL for CD105 and 0.01 µg/µL for CD14 for both cultured cells and whole blood

samples and allowed to incubate at room temperature for 1 hr (CD105) or 30 min (CD14). After incubation with the primary antibody, the red blood cells were lysed with 3 mL of lysis buffer (200 mM NH4Cl, 3 mM KHCO3, 0.002 mM EDTA, pH= 7.3) before staining with the secondary. All cells were washed with 1 mL of PBS and then stained with the appropriate secondary antibody (1:400). All cells were filtered through 35 μm mesh to prepare for flow analysis. A total of 10,000 events were collected for all samples looking at forward scatter versus side scatter plots for imaging. Gates were set to select for live cultured cells, eliminating doubled cells, dead cells, and debris. Gates for whole blood samples were gated to only include monocytes. The percentage of cells positive for the expression of CD14 and CD105 was determined for 2 separate samples of cultured ECFCs from each of the 3 horses.

7.2.8 Evaluation of Photoinitiator on Cell Viability

Photoinitiators, including I-2959, DMPA, and I-184, were dissolved into concentrations of 0.03, 0.05, and 0.1 g/mL in 70% ethanol. Eosin Y was dissolved into concentrations of 0.003, 0.007, and 0.014 g/mL in 70% ethanol. ECFCs were suspended in media and diluted to 20,000 cells/mL. 500 μL of ECFC suspension was added into each well of 48-well plates. The prepared photoinitiators were added to the ECFC suspension at a concentration of 5 μL/well. Control was set up with only the addition of 70% ethanol but not any photoinitiators. After 1 hour of incubation at 37°C, ECFCs that were incubated with I-2959, DMPA, I-184, and control were exposed to UV light at 365 nm for 5 min while ECFCs that were incubated with eosin Y and control without eosin Y were exposed to visible light for 5 min. Another control to study the effect of UV or visible light exposure

was setup by covering the plates with foil to keep the plates from exposing to UV or visible light.

After a 48-hour incubation, ECFCs were assayed for viability using WST-1 metabolic indicator (Fisher). ECFCs were rinsed with 250 μL PBS and 500 μL of ECFC media was added. 50 μL of WST-1 was added per well and incubated at 37°C for 2 hours. Cell viability was quantified by measuring the absorbance at 420 nm with a Biotek Synergy HT microplate reader. The effect of background was accounted by subtracting the average empty well reading from all values. Sample values were scaled linearly from 0 to 1. Wells with media only had a value of 0 while wells with the addition of 70% ethanol to ECFCs had a value of 1.

7.2.9 Synthesis of PEG-fibrinogen

PEG-fibrinogen was prepared as previously described (Dikovsky et al., 2006). First, 10,000 MW PEGDA was synthesized from 10,000 PEG using the method shown in Section 2.2. Tris (2-carboxyethyl) phosphine hydrochloride (TCEP-HCl) was combined with 7 mg/ml fibrinogen in PBS with 8 M urea (1.5:1 TCEP to fibrinogen molar ratio). Next, for PEGylation of fibrinogen, PEG-DA was reacted with fibrinogen (4:1 molar ratio) for 3 h, precipitated in acetone and dissolved in PBS with 8 M urea. The reacted PEG-fibrinogen was dialyzed against PBS at 4ºC for 48 h followed by lyophilization. To characterize the PEGylated product, fibrinogen content was measured using Pierce BCA assay.

7.2.10 Encapsulation of Isolated Equine EPCs in PEG-fibrinogen Hydrogels

PF precursor solution was prepared by combining PF (21 mg/mL of PEGDA and 9.94 mg/mL of fibrinogen) with 1.5% triethanolamine (TEOA), 3.96 µl/ml N-vinyl pyrrolidone (NVP), and 10 mM eosin Y (Fisher Scientific) photoinitiator (in PBS). Equine ECFCs were resuspended in PF precursor solution at 12 million cells/mL and 8 µL of the mixture was crosslinked under a LED light for 1 min to form a 200 µm thick disc on acrylated glass. The PF hydrogels were placed in a 6-well plate with 2 mL of horse media and incubated at 37°C and 5% CO_2.

7.2.11 Visualization of 3D Tubule Formation

F-actin was stained with Alexa Fluor 568-Phalloidin (Molecular Probes) as described by the manufacture protocol. The PF hydrogels was rinsed with PBS and fixed in 4% paraformaldehyde for 15 min at room temperature. The hydrogels was rinsed with PBS and blocked with 3% FBS overnight at 4°C. Then the hydrogels was incubated with the Alexa Fluor 568-Phalloidin overnight at 4°C. Nuclei were counter stained with DAPI. The hydrogels was rinsed with PBS and mounted with Fluoromount G. Tubular networks was visualized using confocal microscopy.

7.2.12 Statistical Analysis

All continuous data are presented as mean ± standard deviation. Ordinal score data are presented as median and interquartile range. The percentage of DiI-Ac-LDL positive cells, number of cell doublings, and population doubling times after serial subculture were analyzed using a one-way analysis of variance with Tukey's post-hoc comparison. The tubule formation assay scores at each passage were analyzed with a Kruskal-Wallis test

and Dunn's post hoc comparison, and grouped early (P1-P4) and late (P5-P10) passages were compared with a two-tailed Mann-Whitney U test. All analyses were performed with a commercial statistics package, and $P<0.05$ was considered significant.

7.3 Results

7.3.1 Equine ECFCs Isolated from Peripheral Blood of Horses

To develop a method to isolate and culture equine EPCs, the media and substrate culture method was used. Colonies appeared on day 9 at which time 16 colonies were observed. Colonies were circular in shape and showed a confluent monolayer which is similar to human ECFCs. A representative image of the isolated equine EPCs is shown in Figure 7.1. In Figure 7.2A, a 10x magnification image shows the edge of the colony. Although cells were very dense closer to the center of the colony, cells were able to maintain a confluent monolayer which is a crucial evidence of being endothelial-like cells. In Figure 7.2B, the cobble stone morphology of the cells can be clearly observed. The isolated EPCs retained their endothelial morphology up to passage 6 in culture which is the highest passage that this preliminary study has used.

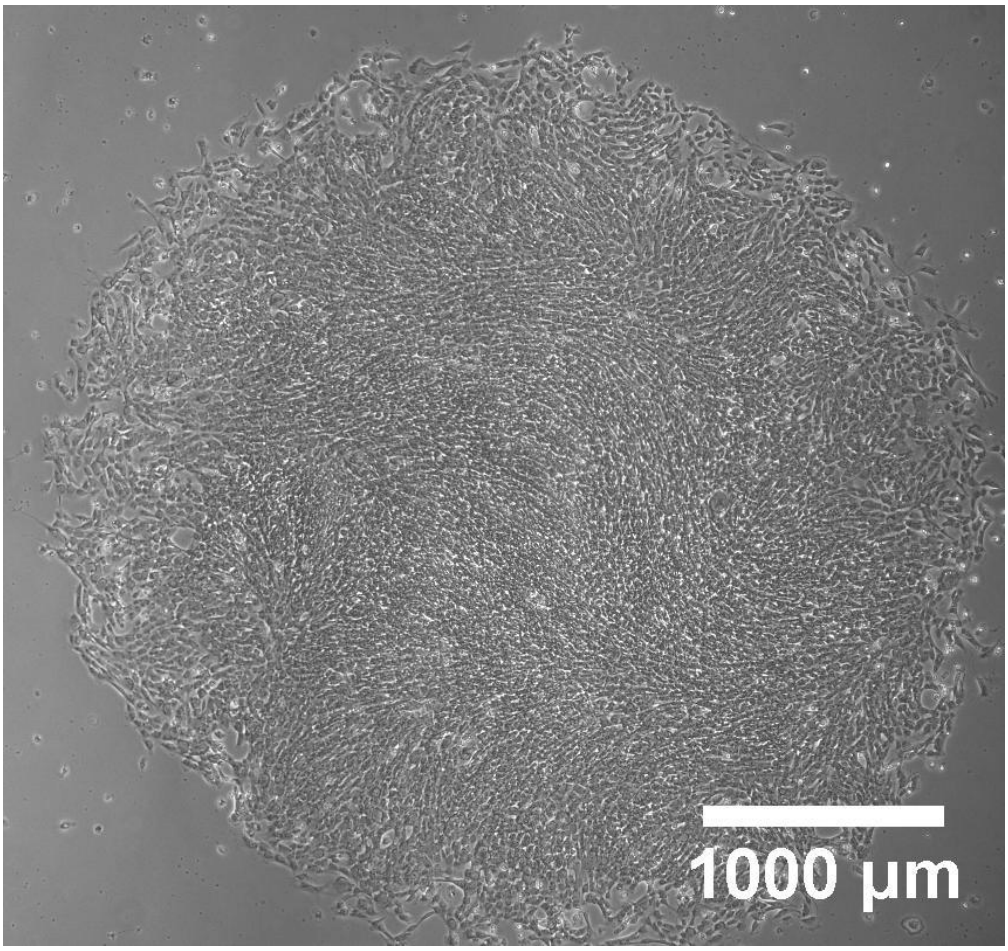

Figure 7.1 Representative colony of horse EPC after isolation on day 9. 16 colonies have been observed.

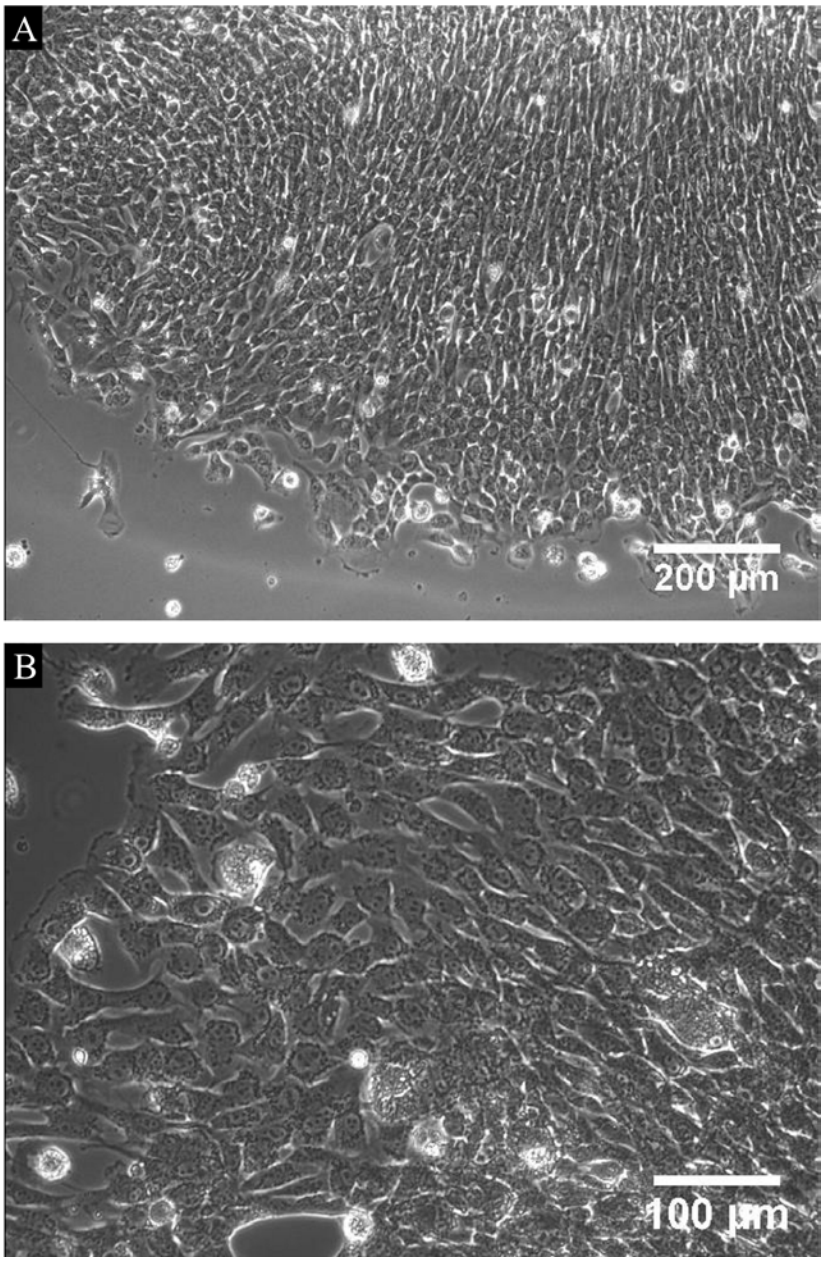

Figure 7.2 Outgrowth of horse EPC colony after isolation on day 9. A) 10x magnification of the edge of colony. B) 20x magnification of the edge of colony showing cobble stone morphology.

The equine EPC colonies appeared on day 9 which is similar to the day 12 suggested by the protocol optimized for human EPC isolation (Hofmann et al., 2009). According to Ingram *et al*., EPCs derived from human umbilical cord were able to sustain up to 100 doublings in culture (D. A. Ingram et al., 2004).

In this study, ECFCs were successfully isolated from peripheral blood samples of adult horses. A total of 24 horses were sampled, and 3 of the 24 blood samples produced colonies exhibiting characteristic ECFC phenotype appearance of cobblestone morphology and significant outgrowth after subculture which are characteristic of ECFCs isolated from in other species. Breeds of the 24 horses sampled included 15 warmbloods, 8 quarter horses, 1 paint, and 1 Arabian. The age range of horses sampled was 4 to 23 years of age, with a mean of 10.9 ± 4.4 years of age. There were 20 geldings and 4 mares. The blood samples from the 3 horses that successfully produced colonies had colony appearance at 12 ± 2.5 days with 2.8 ± 1.5 colonies per mL of blood, which is similar to other studies (Hofmann et al., 2009; Kaushal et al., 2001). Of the three horses that produced cell colonies, all were geldings aged 23 yr (horse 1), 18 yr (horse 2), and 10 yr (horse 3). Breeds of the horses with colony production included an American Quarter horse (horse 1) and two warmbloods (horse 2 and 3).

7.3.2 Functional Characterization of Equine ECFCs: *In Vitro* Tubule Formation Assay

Equine ECFCs exhibited vascular tubule formation in vitro, an endothelial function that is characteristic of ECFCs that have been isolated from other species3. Equine ECFCs (P1-P3) from all 3 horses had formed vascular tubules in vitro by 24 hr post cell seeding onto basement membrane and maintained tubule structure until 48 hr post seeding (Figure

7.3). The positive control for assay conditions, human ECFCs, showed vascular tubule formation by 5 hr post cell seeding and maintained tubule structures until 48 hr post cell seeding (Figure 7.3). The negative control cell type, mouse fibroblasts, was used to distinguish the ECFCs from other progenitor cell types found circulating in peripheral blood. The fibroblast cells failed to form vascular tubules at any time point and aided in validating that the isolated equine cells had phenotypic and functional characteristics of true ECFCs (Figure 7.3). Images of tubule formation at 4x magnification were recorded, allowing the visualization of the branching networks that formed at 24 hr post-seeding throughout the entire well (Figure 7.3). The ability of equine ECFCs to successfully form vascular tubule structures in vitro confirmed that they were phenotypically and functionally similar to ECFCs and not early EPCs or other circulating progenitor cells.

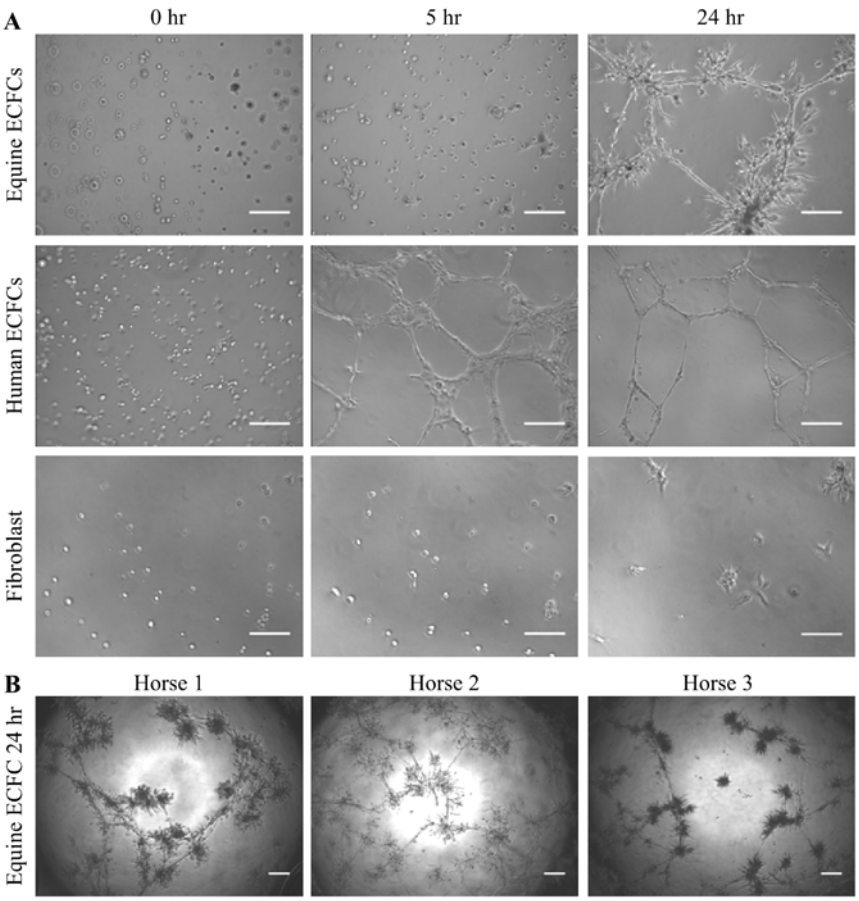

Figure 7.3 Equine ECFCs form vascular tubules *in vitro*. A) Representative images of equine ECFCs, human ECFCs, and mouse fibroblasts on basement membrane at 0, 5 and 24 hr respectively. All cells were seeded at 10,000 cells/well. Tubule formation of equine ECFCs was seen at 24 hr and persisted up to 48 hr, while tubule formation of human ECFCs, as the positive control, was seen by 5 hr and persisted up to 48 hr. Mouse fibroblasts served as a negative control and as expected, did not form tubules. Scale bars represent 100 μm. B) Representative images of horse 1, 2 and 3 ECFCs on basement membrane at 24 hr. Tubule networks were seen at 24 hr post seeding at 4x (7.09 mm2) magnification. Seeding density was 21,000 cells/well. Scale bars represent 200 μm. Endothelial colony forming cell (ECFC).

7.3.3 Functional Characterization of Equine ECFCs: Uptake of Acetylated Low Density Lipoprotein

Equine ECFCs exhibited uptake of DiI-Ac-LDL. The ability of endothelial cells and endothelial progenitor cells to uptake DiI-Ac-LDL is an established functional assay to characterize these cell types (Voyta, Via, Butterfield, & Zetter, 1984). Isolated equine ECFCs (P1-P3) from all 3 horses were able to uptake DiI-Ac-LDL with 74.9% ± 14.7% positive cells (Figure 7.4). The positive control used in the assay, human ECFCs, exhibited a 100% positive uptake of DiI-Ac-LDL (Figure 7.4). The negative control cells, mouse fibroblasts, did not exhibit any uptake of DiI-Ac-LDL (Figure 7.4), demonstrating the specificity of the assay for endothelial-type cells.

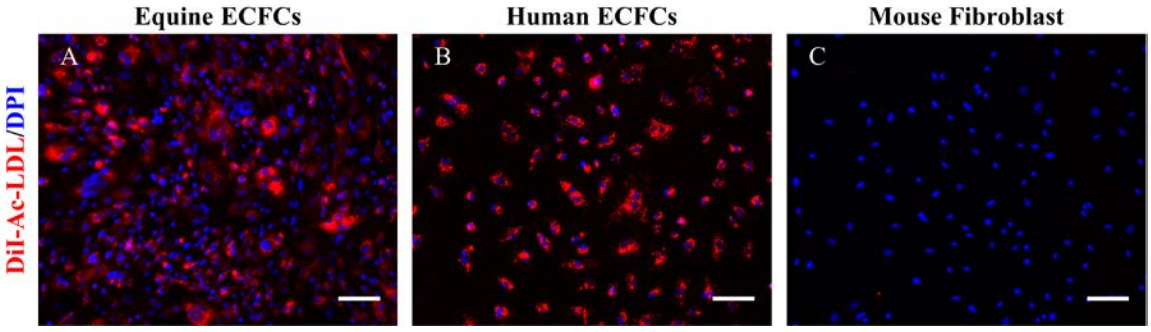

Figure 7.4 Uptake of DiI-Ac-LDL by Equine ECFCs. A) Equine ECFCs showed an 85% uptake of DiI-Ac-LDL (red). B) Human ECFCs showed a 100% uptake of DiI-Ac-LDL. C) Mouse fibroblast cells as the negative control did not uptake any DiI-Ac-LDL. Nuclei are counter-stained with DAPI (blue). Scale bars represent 100 μm. DiI-labeled acetylated low density lipoprotein (DiI-Ac-LDL); Endothelial colony forming cell (ECFC).

7.3.4 Cell Senescence and Cell Growth of Equine ECFCs:

The ability of equine ECFCs to form vascular tubules significantly decreased in later passages (P5-P10) versus earlier passages (P1-P4), and the ability of equine ECFCs to uptake DiI-Ac-LDL decreased as the number of passages increased. Equine ECFC growth also slowed down after multiple subcultures, as evidenced by the number of cell doublings per time trending downward and the population doubling time trending upward with passage number (both changes non-significant).

The median score of tubule quality was significantly different ($P=0.0098$) between earlier passages (P1-P4) and later passages (P5-P10, Figure 7.5). No passage of ECFCs from any horse completely lost the ability to uptake LDL; however, a significant ($P<0.0001$) decrease in the percentage of cells positive for LDL uptake was identified in higher passages (Figure 7.5). As passage number increased from P3 to P9, cell doubling rate trended downward, whereas population doubling time trended upward (Figure 7.5). Additionally, cells lost their characteristic cobblestone morphology and became more spindle-shaped after multiple cell subcultures, and an increase in the presence of cytoplasmic vacuoles in the cytoplasm of the cell was observed (Figure 7.5).

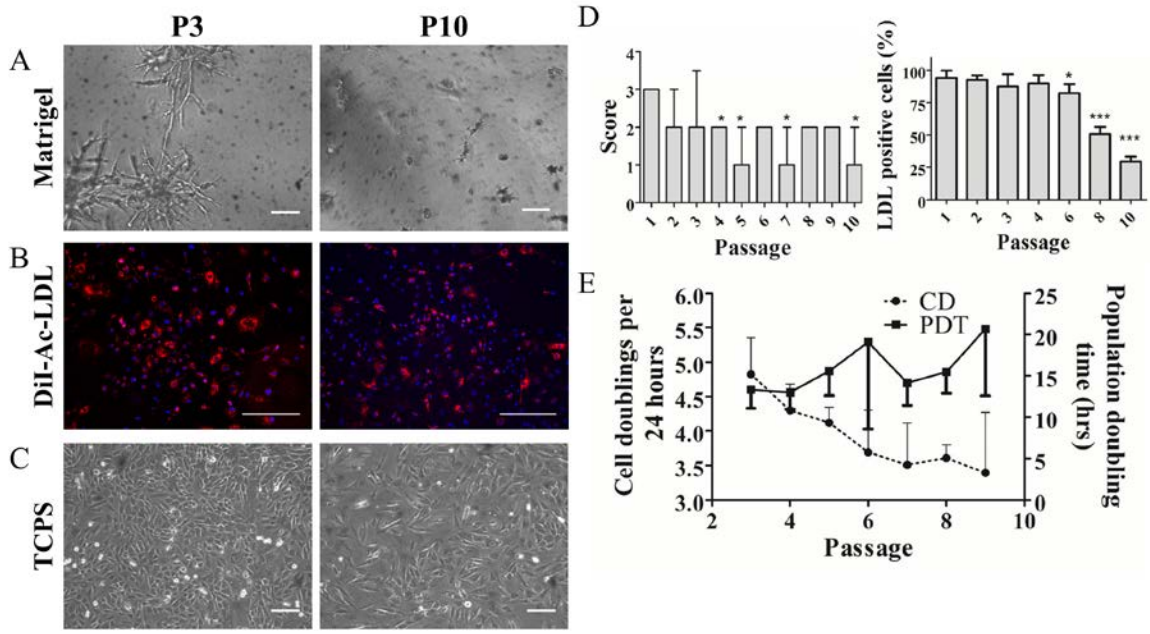

Figure 7.5 Growth and functional activity of equine ECFCs decrease with increasing passage number. A) Equine ECFCs at passage (P) 3 and P10 respectively showing a decrease in tubule formation in the higher passage. P3 has a score of 3/4 and P10 has a score of 1/4. B) Uptake of DiI-Ac-LDL (red) at P3 and P10 showing a decrease in uptake at higher passages. C) Equine ECFCs from P3 and P10 showing the loss of cobblestone morphology and increase in vacuolated, spindle shaped cells in the later passage. D) The qualitative score of tubule formation also decreased as passage increased. Bars represent the median and whiskers are the interquartile range. *Indicates significant difference at $P<0.05$. DiI-Ac-LDL uptake decreased significantly from P1 in higher passages at *P<0.05 or ***P<0.001. E) Cell doublings (CD) trended down as passage increased while population doubling time (PDT) trended up.

7.3.5 Analysis of Equine ECFC Marker Expression:

Equine ECFCs from all 3 horses were positive through IF staining for expression of the endothelial markers vWF, VEGFR-2, CD34, and CD105 (Figure 7.6). Equine ECFCs from all 3 horses were positive for expression of the hematopoietic marker CD14 and the endothelial/stem cell marker CD105 through flow cytometry analysis (Figure 7.7). Since many of the antibodies used were not specific for equine proteins, all cells were stained with the secondary antibody only to verify specific staining versus background for IF (data not shown). The positive control equine ECs were also positive for vWF, VEGFR-2, CD34, and CD105 using IF (Figure 7.6). Staining for CD14 using IF was unsuccessful; conclusive evidence could not be obtained, since the only equine CD14 antibody available to our laboratory was optimized for flow cytometry and not for IF. Flow cytometry was only performed using the antibody for the endothelial marker CD105 and the antibody for the hematopoietic marker CD14 because the other antibodies were unsuccessful (no fluorescently labeled cells detected) when tested for flow cytometry on the positive control equine ECs and the equine ECFCs. Equine ECFCs stained positively for CD105 with flow cytometry in all 3 horses (83.1 ± 13.6% positive cells). ECFCs from horse number 2 showed the lowest percent positive staining (67.4%); whereas ECFCs from horse 1 and 3 were 90.7% and 91.2% positive, respectively. The positive control for CD105 of equine ECs were 99.6% percent positive (Figure 7.7). ECFCs from all 3 horses were positive for CD14 (83.3% ± 1.5). The positive control cells for CD14 expression of whole blood monocytes were 24.6% positive as expected based on results from other groups (Kabithe, Hillegas, Stokol, Moore, & Wagner, 2010), and ECs were negative for CD14 as expected (Figure 7.7).

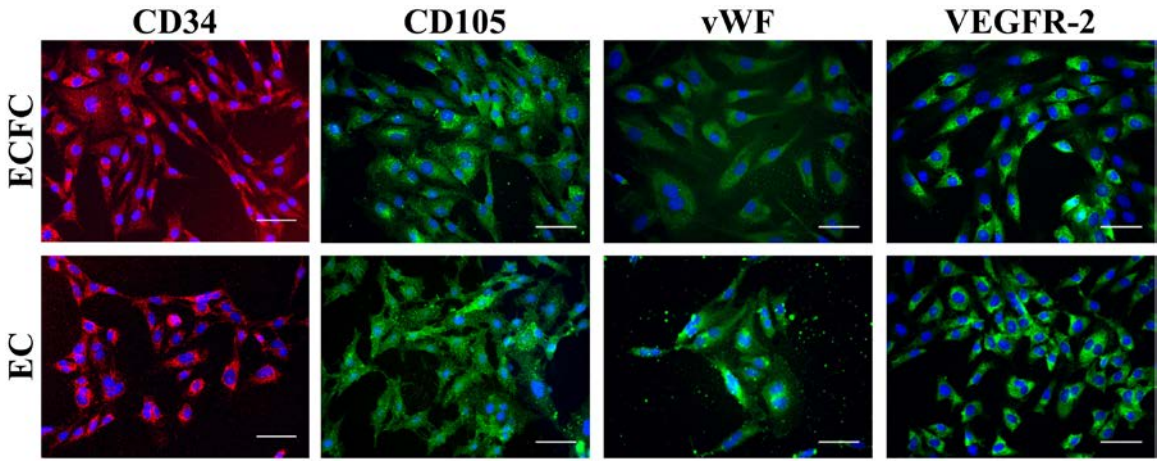

Figure 7.6 Endothelial marker expression in equine ECFCs. Equine ECFCs and equine carotid ECs were positive for CD34 (red), CD105 (green), vWF (green), and VEGFR-2 (green) expression using indirect immunofluorescence. Nuclei are stained with DAPI (blue). Scale bars represent 50 μm. Endothelial colony forming cell (ECFC); equine carotid endothelial cell (EC).

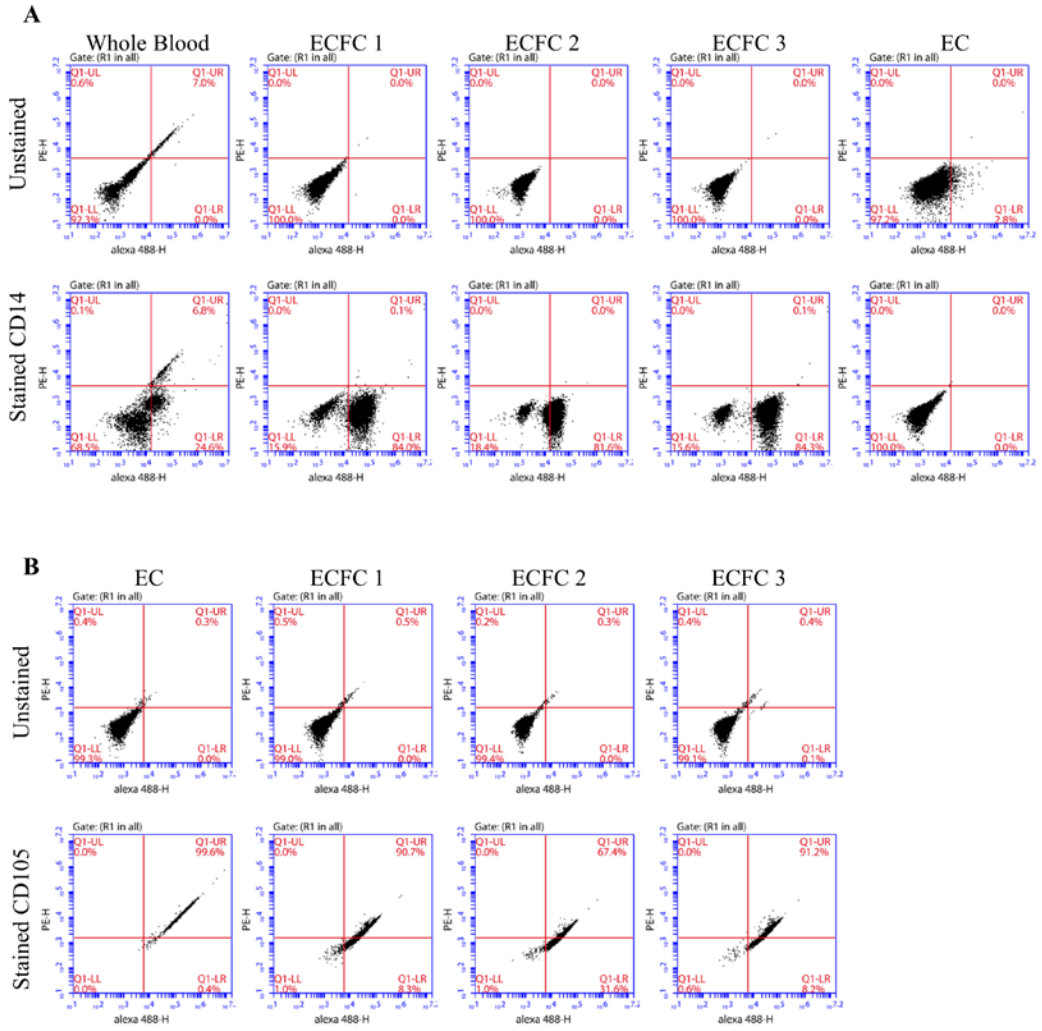

Figure 7.7 Flow cytometric analysis of cell surface marker expression in equine ECFCs from three horses. A) CD14 expression shown in dot plot distribution. Equine whole blood gated (R1) for monocyte size is shown as a positive control with 24.6% staining. Equine carotid ECs did not stain for CD14. ECFCs from all horses stained positive for CD14: horse 1 (84%), horse 2 (81.6%), and horse 3 (84.3%). B) CD105 expression shown in dot plot distribution. The positive control ECs stained positive for CD105 (99.6%). Equine ECFCs from all horses stained positive for CD105: horse 1 (90.7%), horse 2 (67.4%), and horse 3 (91.2%).

7.3.6 Photoinitiator Selection

Photopolymerization uses photoinitiator to induce polymerization of monomers and this process creates high-energy radicals that may cause oxidative damage to cell populations (Williams, Malik, Kim, Manson, & Elisseeff, 2005). Characterizing the effect of photoinitiators on EPC viability is critical in photoinitiator selection. There are four major choices of photoinitiators that are seen frequently in literature in crosslinking PEGDA, and they are 1-Hydroxy-cyclohexyl-phenyl-ketone (I-184), I-651 (which is DMPA), 1-[4-(2-Hydroxyethoxy)-phenyl]-2-hydroxy-2-methyl-1-propane-1-one (I-2959), and eosin Y. I-184 and DMPA have cell viability issues, so they are commonly not suggested for use in cell encapsulation applications. I-2959 has been shown in study with cell encapsulation due to the minimal effect in cell viability, but it is only strongly sensitive to 305 nm light (Figure 7.8) (Williams et al., 2005). This wavelength is not FDA approved because it falls into the mutagenic UVB spectrum. Therefore, it is not the best option to work with. On the other hand, Eosin Y is also proved to have minimal effect on cell viability and it is readily able to crosslink PEGDA from 450 nm to 550 nm.

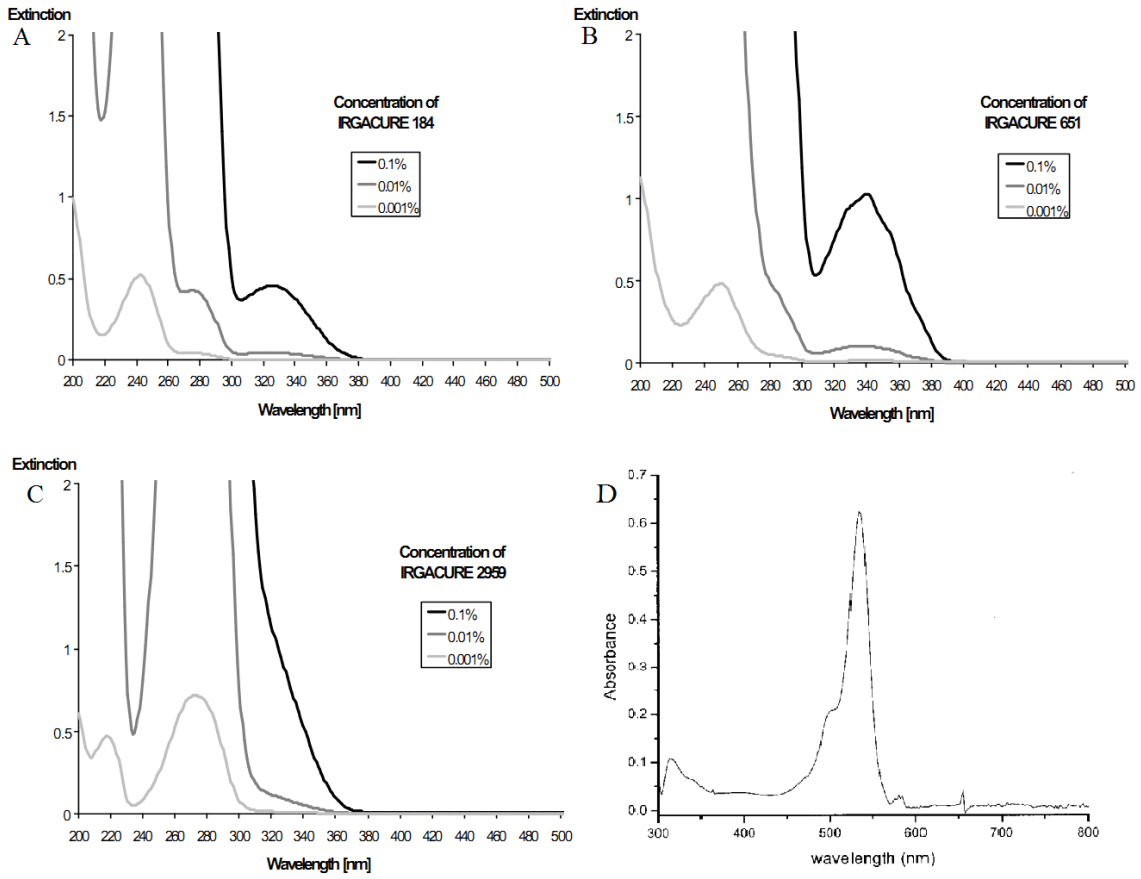

Figure 7.8 Absorbance spectrum of I-184, I-651, I-2959, and eosin Y. A-C) Reprinted from specification data sheet. D) Reprinted with permission from Ref (Padon & Scranton, 2001).

7.3.7 The Effect of Photoinitiator on ECFC Viability

In order to select the optimal photoinitiator to for cell encapsulation, a cell viability assay of four photoinitiators was performed on ECFCs. Since cell viability was quantified based on absorbance, the absorbance of WST-1 metabolic indicator on ECFCs that were cultured with media only was used as reference. The effect of UV at 365 nm or light exposure for 5 min on the ECFC viability is negligible as shown in Figure 7.9 Same amount of ethanol that was used in dissolving the photoinitiators was added to the media in order to show the effect of ethanol on cell viability. There is a significant decrease in ECFC viability by the addition of ethanol in the dark and a non-significant decrease after exposure to UV. Both I-184 and I-651 (DMPA) resulted in extremely poor ECFC viability regardless of the concentrations and UV exposure (Figure 7.9A and B). Exposure to I-2959 significantly reduced ECFC viability at all concentrations and with or without UV exposure, but viability was still far better than for either I-184 or DMPA (Figure 7.9C). Compared to the other three photoinitiators, Eosin Y yielded the best result. Without light exposure, there is a slight decrease in viability at concentrations of 0.007% and 0.014% Eosin Y, whereas a greater, but still non-significant, decrease in viability is shown with light exposure (Figure 7.9D). Therefore, Eosin Y produced the best result in terms of maintaining ECFC viability.

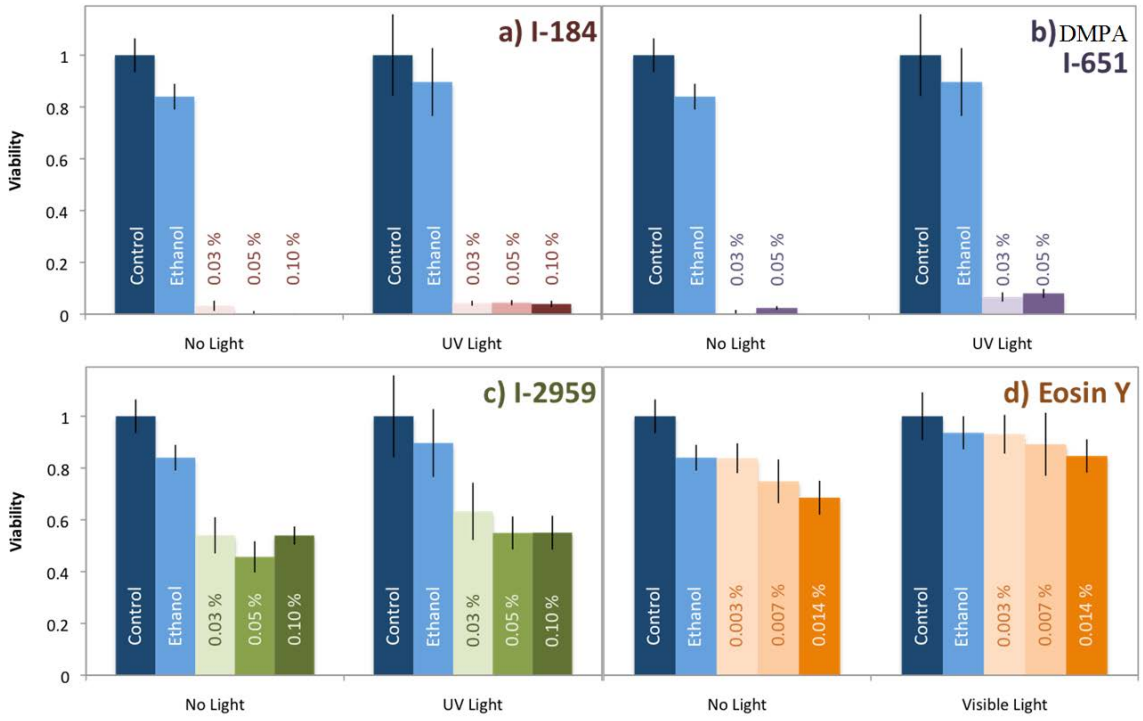

Figure 7.9 ECFCs in culture with exposure to photoinitiators. A decreased viability is shown when ECFCs are exposed to A) I-184 or B) DMPA. The decrease in viability was alleviated when ECFCs are exposed C) I-2959 and D) Eosin Y.

7.3.8 Encapsulation of Isolated Equine EPCs in PEG-fibrinogen Hydrogels

To evaluate of the angiogenic capabilities of the isolated equine ECFCs in three dimensional environment, equine ECFCs were encapsulated in PEG-fibrinogen (PF). Through BCA assay, stock PEG-fibrinogen was found to have a PEGDA concentration of and a fibrinogen content of 9.94 mg/mL. Equine ECFCs were encapsulated using various concentrations of PF precursor solutions. As summarized in Table 7.1, tubule formation occurs sooner as PF precursor solution is more diluted, until PF concentration reaches 25% where PF hydrogels could not be formed. When using 50% of PF precursor solution, cells started to degrade the surrounding PF hydrogels and tunneling through the PF hydrogels (Figure 7.10). To better visualize the tubule formation within the hydrogels, equine ECFCs were stained with Phalloidin. Figure 7.10 shows a continuous tubular network of equine ECFCs within the PF hydrogels.

Table 7.1 Timeline of tubule formation of equine ECFCs in various concetrations of PEG-fibrinogen precursor solution.

PEG-Fb	**100%**	**75%**	**50%**	**25%**
Tubule formation	> 2 wks	~ 2 wks	24 hr	Incomplete hydrogel formation

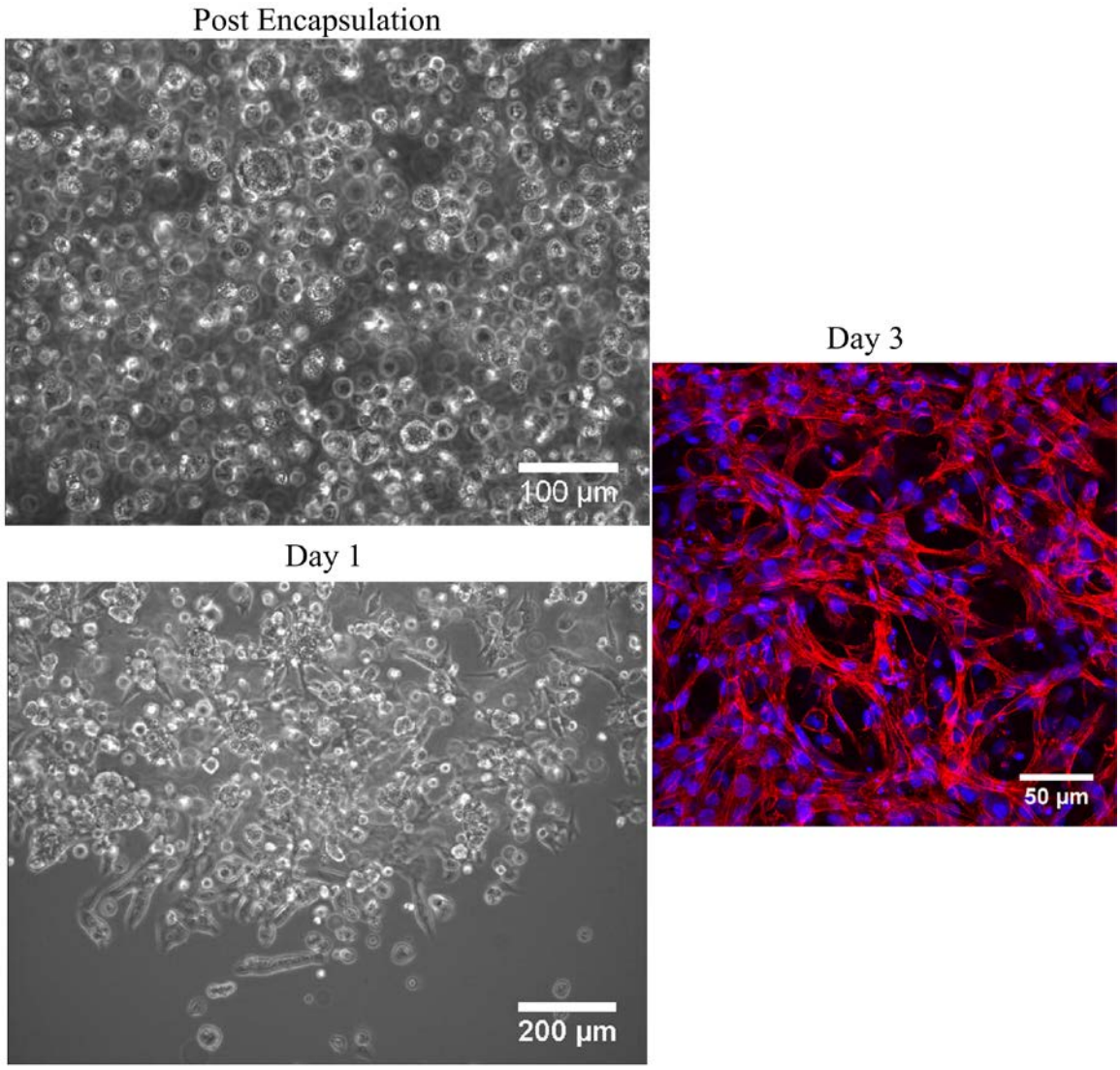

Figure 7.10 Representative images of encapsulated equine ECFCs. Equine ECFCs were encapsulated in PF at a cell density of 12 million cells/mL. ECFCs remained spherical post encapsulation and started to spread within the 50% PF hydrogels on Day 1. On Day 3, continuous tubular network is observed using confocal microscopy where the F-actin was stained with Phalloidin (red) and nuclei were counter stained with the DAPI (blue).

7.4 Discussion

In this study, equine ECFCs, a subtype of EPCs, were successfully isolated from and characterized in the peripheral blood of adult horses. The potential relevance of EPCs in the clinical treatment of diseases associated with decreased vascularization such as complicated wounds, non-union fractures, tendon and ligament repair, infectious corneal disease, chronic laminitis, and intestinal ischemia is evident. Therefore, the therapeutic potential for EPCs in the future of regenerative medicine is exciting. This study demonstrates that EPCs can be isolated non-invasively from the peripheral blood of healthy horses, and the ability to isolate and accurately characterize these cells will allow for further research, including in vivo characterization and therapeutic use of equine EPCs.

Although ECFCs were successfully isolated, only 3 of 24 horses sampled produced cell colonies. This protocol was specifically developed to reduce the need for foreign animal proteins which could interfere with future human therapeutic applications (example FBS and collagen) (Reinisch et al., 2009). The protocol also only called for 5 mL of blood to be used for cell isolation. The larger cross-sectional size of the horse's jugular vein when compared to a human vein could account for the low yield of equine ECFCs seen in this study. This difference in the size of the vessels between the two species could have potentially affected the uniformity of the cell sample obtained during the blood draw, since circulating cells are not evenly distributed between the vessel wall and the center. A proportionally larger blood sample may be needed from the horse to obtain similar cell populations with each blood draw, analogous to results in people. Although one modification to the established human EPC isolation protocol was to supplement with horse serum, it is important to note that the growth factors added to the EBM-2 media were

optimized for the human cells. EPCs are known to be rare in circulation and studies in other species report various cell yields ranging from 4 to 6 colonies/ml (Hofmann et al., 2009). Modifications of the isolation protocol, including utilization of a larger sample volume, concentration of mononuclear cells with density gradient centrifugation, and collection from smaller diameter veins are currently under investigation in our laboratories. Bone marrow sampling, although more invasive, is the standard protocol for collection of MSCs, and EPCs and EPC subtypes could be isolated from this source as well, or could be differentiated from MSCs as was recently shown in dogs (Kabithe et al., 2010).

The isolated equine ECFCs exhibited the characteristic cobblestone cell morphology with a single layer of growth, which is a key feature used to distinguish ECFCs from other cell types. The equine ECFCs formed colonies after 7 days in culture and displayed significant outgrowth upon colony harvest and cell expansion. These observations of colony appearance, cell morphology, and expansion further aided in the determination that the cells being isolated were ECFCs and not early EPCs, circulating endothelial cells, or other types of adult stem cells found in peripheral blood (Richardson & Yoder, 2011; Timmermans et al., 2009). All three equine ECFC samples formed vascular tubules when tested using the in vitro tubule formation assay. The appearance of the equine tubules was quite similar to those of tubule formations observed in other species (Escudero, González, Acurio, Valenzuela, & Sobrevia, 2013). This characteristic demonstrates the potential of these cells to aid in the tissue vascularization and establishes the ability of this assay to evaluate cell function if ECFCs are to be used as a biomarker in the equine species. The ECFCs from these 3 horses formed tubules by 24 hr post cell seeding whereas human

ECFCs exhibited tubule formation by 5 hr post cell seeding. Tubules were seen in one horse at 8.5 hr when extra images were obtained, so the timing of tubule formation of equine ECFCs in vitro may be slightly different than that of human cells or may have inter-horse variation. Samples from more horses need to be analyzed to determine when tubule formation truly occurs in the horse. The EGM-2 media is optimized for human cells, so this may affect how rapidly the equine cells formed tubules versus the human cells. The vascularization potential may also differ between equine and human EPCs, but more direct comparisons between multiple horses and humans would need to be investigated. The uptake of DiI-Ac-LDL is a common method used to characterize EPCs since uptake of LDL is a trait of endothelial cells (Asahara et al., 1997; Bai et al., 2012; Kovacic et al., 2008; Voyta et al., 1984). All three equine ECFCs samples in the study reliably up took DiI-Ac-LDL with 85% positive cells.

Results of the IF staining showed that equine ECFCs were positive for the endothelial markers vWF, VEGFR-2, CD34 and CD105. Characterization of stem and progenitor cells with cell surface markers is a standard approach, but it presents specific challenges in horses because of a lack of available antibodies. The antibodies that were chosen for this study either had evidence from the literature of potential cross reactivity or were anti-equine protein (CD14). Cells were stained with the secondary antibody only to account for any background staining. A positive control cell was included (equine ECs), leading to the conclusion that the equine ECFCs were staining positive for endothelial markers which characterized them as ECFCs. The selected proteins are not only important endothelial cell markers, but also play important roles in the function of EPCs and ECs.

The glycoprotein vWF functions in hemostasis and endothelial cell adhesion (Dejana et al., 1989; McEver & Cummings, 1997). The presence of the vWF protein on EPCs and ECs not only allows for proper cell function and adhesion during vascular repair, but also facilitates *in vitro* characterization of EPCs and ECs against other cell types lacking vWF (e.g. smooth muscle cells)(Dejana et al., 1989). VEGFR-2 is critical for endothelial cell development and is the key receptor for VEGF. VEGFR-2 intracellular signaling effectively promotes the survival, proliferation, permeability, and migration of EPCs and ECs (Holmes, Roberts, Thomas, & Cross, 2007). Expression of VEGFR-2 by equine ECFCs is critical for their successful isolation and sustained culture. CD34 is a glycophosphoprotein found on lymphohematopoetic and early stem/progenitor cells, endothelial cells and embryonic fibroblast cells. Early studies showed CD34+/VEGFR-2+ cells isolated from umbilical cord blood, bone marrow and peripheral blood differentiated into endothelial cells when cultured in vitro, hence the presence of CD34 is commonly seen as a way to distinguish EPCs from non EPC and stem cell progenitors(Timmermans et al., 2009). CD105 is a homodimeric transmembrane protein that is associated with proliferation through transforming growth factor beta (TGF-β) signaling and is predominately found on endothelial cells (Duff, Li, Garland, & Kumar, 2003). The positive staining of equine ECFCs for vWF, VEGFR2, CD34, and CD105 provides additional evidence that these cells are true ECFCs.

One unexpected result from this study was that most of the isolated equine cells expressed CD14. CD14 is a receptor for the binding of lipopolysaccharide (LPS) complex and allows for the initiation of the immune response to bacteria and is a cell surface marker

for macrophages and hematopoietic cells (Jersmann, Hii, Hodge, & Ferrante, 2001; Kabithe et al., 2010). CD14 expression is not limited to cells of myeloid lineage, and is expressed on early EPCs in humans and at low levels in vascular endothelial cells (Jersmann, 2005). ECFCs have been extensively characterized in humans, and much controversy has existed regarding nomenclature and marker expression. There is no single marker or group of markers that can distinguished ECFCs from terminally differentiated endothelial cells, which makes specific identification rely on both markers and other characteristics such as growth and function (Richardson & Yoder, 2011). One difference between early EPCs and ECFCs in humans is that early EPCs express the hematopoietic markers CD14 and CD45, and ECFCs do not. This suggests hematopoietic origin of early EPCs. We do not believe, however, that the cells isolated in this study are early EPCs because early EPCs do not form vascular tubules *in vitro*, they appear in culture at <7 days, and they have very different cell morphology (Richardson & Yoder, 2011; Timmermans et al., 2009). Since we were unable to isolate cells fitting the description of early EPCs in the horse, we do not know if that cell type circulates in the horse or if the lineages for the ECFCs are the same in the horse as in the human. It is unlikely that cross-reactivity of the CD14 antibody caused a false positive since the equine ECs were negative for CD14, and the peripheral blood stained positive in a manner similar to that of previous work done on equine monocytes (Kabithe et al., 2010). The positive staining of equine ECFCs for CD14 is likely a species difference or possibly indicates more than one cell type in the isolated population. The expression of cell surface markers of ECFCs in species other than humans or rodents is not as fully characterized, which is likely in part due to lack of antibodies. As

an example, protein expression of CD34, vWF, CD146, VEGFR-2, CD31 and eNOS has been evaluated in EPCs from the dog (Wills, Heaney, Jane Wardrop, & Haldorson, 2009; Wu et al., 2005), but CD14 or CD45 expression have not. Other types of equine cells (such as MSCs) have also been shown to differ slightly in their gene expression from their human counterparts, making this result, although not necessarily anticipated, also not completely unexpected. Previous work in equine MSCs has shown that they are positive for CD14 suggesting that equine MSCs derive from CD14 positive cells, which differs from MSCs in other species (Hackett, Flaminio, & Fortier, 2011). This work in MSCs used the same equine anti-CD14 antibody as was used in the current study and disputes the definition of MSCs as being derived from non-hematopoietic precursor cells in the horse. Interestingly, the CD14 in the equine MSC study was trypsin labile which was not the case in our study (Hackett et al., 2011). More work on cell surface marker characterization over a range of passages, and isolating single colonies or separating and characterizing the CD14+/CD14- cells would answer these questions more specifically, but the ability to form vascular tubes is characteristic that many other cell types would not have. Other studies have shown ECFCs from peripheral blood to be positive for CD14 (Kalka et al., 2000). This leads back to the conclusion that no single marker is capable of identifying EPCs and EPCs subcategories, and that a combination of characterization methods is needed to characterize EPCs and EPC subtypes.

There is good clinical evidence that stem cell therapy improves clinical outcomes in equine tendon and ligament injuries (Godwin, Young, Dudhia, Beamish, & Smith, 2012), but questions remain concerning whether or not clinical effects are due to stem cell

engraftment and tissue regeneration or paracrine mechanisms. The use of biomaterial scaffolds to optimize the function of stem cells is becoming more and more common. Work in this area in horses has begun with the investigation of equine MSC migration out of fibrin hydrogels, treatment of meniscal lacerations with MSCs and fibrin glue, 3-dimensional culture conditions and chondrogenesis, and creation of a decellularized tendon as scaffold for regenerative therapy (Ferris, Frisbie, Kisiday, & McIlwraith, 2012; Watts, Ackerman-yost, & Nixon, 2013; Youngstrom, Barrett, Jose, & Kaplan, 2013). Promoting rapid vascularization is one of the biggest challenges in using engineered tissues for enhancing wound healing and treating disease (Moon et al., 2010). Combining EPCs with engineered biomaterials could allow the direct delivery and retention of EPCs, as well as the appropriate growth factors and signaling molecules needed, in the area of interest. Although engineering complex tissues may not be an immediate clinical goal in the horse, in order to continue to advance the field of equine regenerative medicine, understanding and development of methods to promote equine vascularization is essential, and ready access to equine EPCs is a key part of that process.

In standard 2-dimensional cell culture conditions, cells are not in their native environment; they are exposed to trypsinization, grown on surfaces not necessarily optimized for cell performance, and not provided with the same environmental stimuli that are present *in vivo* (e.g. shear stress). When investigating cells for use in therapeutic applications, it is imperative to evaluate how long cells can remain in culture before losing their functional properties. The quality of equine ECFC tubules was diminished by P4, and ECFCs had a significant decrease in uptake of DiI-Ac-LDL between P6 and P8. Based on

the results of this study, we recommend that equine ECFCs be used for research at P5 or lower. Future studies to validate these findings in vivo will be required prior to clinical use. This lifespan of the cells' performance is similar to that of other studies with human ECFCs in that cells can undergo about 100 cell doublings before reaching cell senescence(D. a Ingram, Caplice, & Yoder, 2005).

Encapsulation of EPCs in PEG-fibrinogen (PF) hydrogels has great potential in tissue engineering and clinical applications. PF was developed to create a controllable, degradable, and biofunctional 3D scaffold for cell culture (Almany & Seliktar, 2005). While PEG provides high biocompatibility and versatile physical structure, fibrinogen provides biological cues including protease degradation capability (Werb, 1997) and cell-adhesion motifs (Herrick, Blanc-Brude, Gray, & Laurent, 1999). For tissue engineering application, encapsulation of EPCs in PF hydrogels may serve as an *in vitro* platform to study EPC angiogenesis in 3D environment. For clinical applications, cell delivery of encapsulated cells has the advantage of being minimally invasive while supporting high cell survival. Compared to cell or polymer implantation therapy that may cause large incisions, encapsulated cells can be delivered by injection which could reduce costs and surgical trauma (Williams et al., 2005). Injection of cells encapsulated within PF has also shown to enhance cell survival and differentiation compare to injection of cell suspended in aqueous saline solution (Fuoco et al., 2012). Therefore, investigation of the encapsulation of isolated equine EPCs may provide a platform for better understanding of EPC-mediated angiogenesis as well as facilitate successful translation for EPC therapy in veterinary regenerative medicine.

In conclusion, equine ECFCs can be isolated from peripheral blood samples of healthy horses. Equine ECFCs formed vascular tubules *in vitro*, demonstrated receptor mediated uptake of DiI-Ac-LDL, were positive for expression of CD34, CD105, VEGFR-2 and vWF through IF staining, and were positive for CD14 and CD105 expression through flow cytometry. Cells exhibited decreased ability to form vascular tubule structures in later passages (P5-P9) and had decreased uptake of DiI-Ac-LDL between P6 and P9. Cells also lost their characteristic phenotypic appearance of cobblestone morphology and single monolayer, contact-inhibited growth at higher passages. It is recommended that equine ECFCs be used at a P5 or less. By furthering the understanding of the basic biology of these cells, we move closer to advancing the opportunities for their application in equine regenerative medicine. A source of equine EPCs and the ability to encapsulate them in a biomaterial carrier will be invaluable.

References

Achneck, H. E., Jamiolkowski, R. M., Jantzen, A. E., Haseltine, J. M., Lane, W. O., Huang, J. K., … Lawson, J. H. (2011). The biocompatibility of titanium cardiovascular devices seeded with autologous blood-derived endothelial progenitor cells: EPC-seeded antithrombotic Ti implants. *Biomaterials*, *32*(1), 10–8. doi:10.1016/j.biomaterials.2010.08.073

Acton, S. T., Wethmar, K., & Ley, K. (2002). Automatic tracking of rolling leukocytes in vivo. *Microvascular Research*, *63*(1), 139–48. doi:10.1006/mvre.2001.2373

Almany, L., & Seliktar, D. (2005). Biosynthetic hydrogel scaffolds made from fibrinogen and polyethylene glycol for 3D cell cultures. *Biomaterials*, *26*(15), 2467–77. doi:10.1016/j.biomaterials.2004.06.047

Angelos, M. G., Brown, M. A., Satterwhite, L. L., Levering, V. W., Shaked, N. T., & Truskey, G. A. (2010). Dynamic adhesion of umbilical cord blood endothelial progenitor cells under laminar shear stress. *Biophysical Journal*, *99*(11), 3545–54. doi:10.1016/j.bpj.2010.10.004

Arnaoutova, I., & Kleinman, H. K. (2010). In vitro angiogenesis: endothelial cell tube formation on gelled basement membrane extract. *Nature Protocols*, *5*(4), 628–35.

Asahara, T., Masuda, H., Takahashi, T., Kalka, C., Pastore, C., Silver, M., … Isner, J. M. (1999). Bone marrow origin of endothelial progenitor cells responsible for postnatal vasculogenesis in physiological and pathological neovascularization. *Circulation Research*, *85*(3), 221–228. doi:10.1161/01.RES.85.3.221

Asahara, T., Murohara, T., Sullivan, A., Silver, M., van der Zee, R., Li, T., … Isner, J. M. (1997). Isolation of putative progenitor endothelial cells for angiogenesis. *Science (New York, N.Y.)*, *275*(5302), 964–7. Retrieved from http://www.ncbi.nlm.nih.gov/pubmed/9020076

Avci-Adali, M., Paul, A., Ziemer, G., & Wendel, H. P. (2008). New strategies for in vivo tissue engineering by mimicry of homing factors for self-endothelialisation of blood contacting materials. *Biomaterials*, *29*(29), 3936–45. doi:10.1016/j.biomaterials.2008.07.002

Avci-Adali, M., Ziemer, G., & Wendel, H. P. (2010). Induction of EPC homing on biofunctionalized vascular grafts for rapid in vivo self-endothelialization--a review of current strategies. *Biotechnology Advances*, *28*(1), 119–29. doi:10.1016/j.biotechadv.2009.10.005

Bahney, C. S., Lujan, T. J., Hsu, C. W., Bottlang, M., West, J. L., & Johnstone, B. (2011). Visible light photoinitiation of mesenchymal stem cell-laden bioresponsive hydrogels. *European Cells and Materials*, *22*, 43–55.

Bai, C., Hou, L., Zhang, M., Pu, Y., Guan, W., & Ma, Y. (2012). Characterization of vascular endothelial progenitor cells from chicken bone marrow. *BMC Veterinary Research*, *8*, 54. doi:10.1186/1746-6148-8-54

Bang, J. I. Y., Kim, E.-Y., Seong, N. S., Shin, Y. S., & Kang, I.-C. (2007). ProteoChip-based library screening of integrin alpha5beta1 antagonists from Korean medicinal plant extracts. *Archives of Pharmacal Research*, *30*(12), 1584–9. Retrieved from http://www.ncbi.nlm.nih.gov/pubmed/18254246

Barry, S. T., Ludbrook, S. B., Murrison, E., & Horgan, C. M. (2000). Analysis of the alpha4beta1 integrin-osteopontin interaction. *Experimental Cell Research*, *258*(2), 342–51. doi:10.1006/excr.2000.4941

Beijk, M. A. M., Klomp, M., Verouden, N. J. W., van Geloven, N., Koch, K. T., Henriques, J. P. S., … de Winter, R. J. (2010). Genous endothelial progenitor cell capturing stent vs. the Taxus Liberte stent in patients with de novo coronary lesions with a high-risk of coronary restenosis: a randomized, single-centre, pilot study. *European Heart Journal*, *31*(9), 1055–64. doi:10.1093/eurheartj/ehp476

Bennett, J. S. (2005). Review series Structure and function of the platelet integrin αIIbβ3. *The Journal of Clinical Investigation*, *115*(12), 3363–9. doi:10.1172/JCI26989.ligand-binding

Bennett, J. S., Berger, B. W., & Billings, P. C. (2009). The structure and function of platelet integrins. *Journal of Thrombosis and Haemostasis*, *7 Suppl. 1*, 200–5. doi:10.1111/j.1538-7836.2009.03378.x

Brown, M. A., Wallace, C. S., Anamelechi, C. C., Clermont, E., Reichert, W. M., & Truskey, G. A. (2007). The use of mild trypsinization conditions in the detachment of endothelial cells to promote subsequent endothelialization on synthetic surfaces. *Biomaterials*, *28*(27), 3928–35. doi:10.1016/j.biomaterials.2007.05.009

Brown, M. A., Wallace, C. S., Angelos, M., & Truskey, G. A. (2009). Late outgrowth endothelial progenitor cells exposed to laminar shear stress. *Tissue Engineering. Part A*, *15*(11).

Carter, A. J., Aggarwal, M., Kopia, G. A., Tio, F., Tsao, P. S., Kolata, R., … Falotico, R. (2004). Long-term effects of polymer-based, slow-release, sirolimus-eluting stents in a porcine coronary model. *Cardiovascular Research*, *63*(4), 617–24. doi:10.1016/j.cardiores.2004.04.029

Chan, L. Y., Gunasekera, S., Henriques, S. T., Worth, N. F., Le, S.-J., Clark, R. J., … Daly, N. L. (2011). Engineering pro-angiogenic peptides using stable, disulfide-rich cyclic scaffolds. *Blood*, *118*(25), 6709–17. doi:10.1182/blood-2011-06-359141

Chavakis, E., Aicher, A., Heeschen, C., Sasaki, K., Kaiser, R., El Makhfi, N., … Dimmeler, S. (2005). Role of beta2-integrins for homing and neovascularization capacity of endothelial progenitor cells. *The Journal of Experimental Medicine*, *201*(1), 63–72. doi:10.1084/jem.20041402

Chavakis, E., & Dimmeler, S. (2011). Homing of progenitor cells to ischemic tissues. *Antioxidants & Redox Signaling*, *15*(4), 967–80.

Cheezum, M. K., Walker, W. F., & Guilford, W. H. (2001). Quantitative comparison of algorithms for tracking single fluorescent particles. *Biophysical Journal*, *81*(4), 2378–88. doi:10.1016/S0006-3495(01)75884-5

Chen, N., Leu, S.-J., Todorovic, V., Lam, S. C.-T., & Lau, L. F. (2004). Identification of a novel integrin alphavbeta3 binding site in CCN1 (CYR61) critical for pro-angiogenic activities in vascular endothelial cells. *The Journal of Biological Chemistry*, *279*(42), 44166–76. doi:10.1074/jbc.M406813200

Cherqui, S., Kurian, S. M., Schussler, O., Hewel, J. A., Yates, J. R., & Salomon, D. R. (2006). Isolation and angiogenesis by endothelial progenitors in the fetal liver. *Stem Cells*, *24*(1), 44–54. doi:10.1634/stemcells.2005-0070

Choi, W. S., Bae, W. J., Joung, Y. K., & Park, K. D. (2009). Fabrication of EC-Specific PU surfaces co-immobilized with GRGDS and YIGSR Peptides. *Macromolecular Research*, *17*(7), 458–463.

Culver, J. C., Hoffman, J. C., Poche, R. A., Slater, J. H., West, J. L., & Dickinson, M. E. (2012). Three-Dimensional Biomimetic Patterning in Hydrogels to Guide Cellular Organization. *Advanced Materials*, *24*(17), 2344–2348. doi:10.1002/adma.201200395.Three-Dimensional

Dejana, E., Lampugnani, M. G., Giorgi, M., Gaboli, M., Federici, A. B., Ruggeri, Z. M., & Marchisio, P. C. (1989). Von Willebrand factor promotes endothelial cell adhesion via an Arg-Gly-Asp-dependent mechanism. *The Journal of Cell Biology*, *109*(1), 367–75. Retrieved from http://www.pubmedcentral.nih.gov/articlerender.fcgi?artid=2115492&tool=pmcentrez&rendertype=abstract

DeLong, S. A., Gobin, A. S., & West, J. L. (2005). Covalent immobilization of RGDS on hydrogel surfaces to direct cell alignment and migration. *Journal of Controlled Release*, *109*(1-3), 139–48. doi:10.1016/j.jconrel.2005.09.020

Dikovsky, D., Bianco-Peled, H., & Seliktar, D. (2006). The effect of structural alterations of PEG-fibrinogen hydrogel scaffolds on 3-D cellular morphology and cellular migration. *Biomaterials*, *27*(8), 1496–506. doi:10.1016/j.biomaterials.2005.09.038

Dimmeler, S., & Zeiher, A. M. (2004). Vascular repair by circulating endothelial progenitor cells: the missing link in atherosclerosis? *Journal of Molecular Medicine (Berlin, Germany)*, *82*(10), 671–7. doi:10.1007/s00109-004-0580-x

DiVietro, J. A., Smith, M. J., Smith, B. R., Petruzzelli, L., Larson, R. S., & Lawrence, M. B. (2001). Immobilized IL-8 triggers progressive activation of neutrophils rolling in vitro on P-selectin and intercellular adhesion molecule-1. *Journal of Immunology (Baltimore, Md. : 1950)*, *167*(7), 4017–25. Retrieved from http://www.ncbi.nlm.nih.gov/pubmed/11564821

Dow, J. A., Lackie, J. M., & Crocket, K. V. (1987). A simple microcomputer-based system for real-time analysis of cell behaviour. *Journal of Cell Science*, *87 (Pt 1)*, 171–82. Retrieved from http://www.ncbi.nlm.nih.gov/pubmed/3667712

Duff, S. E., Li, C., Garland, J. M., & Kumar, S. (2003). CD105 is important for angiogenesis: evidence and potential applications. *The Journal of the Federation of American Societies for Experimental Biology*, *17*(9), 984–92. doi:10.1096/fj.02-0634rev

Ensley, A. E. (2006). *Functional evaluation of circulating endothelial progenitor cells for vascular tissue engineering*. Georgia Institute of Technology.

Escudero, C., González, M., Acurio, J., Valenzuela, F., & Sobrevia, L. (2013). The Role of Placenta in the Fetal Programming Associated to Gestational Diabetes. In L. Sobrevia (Ed.), *Gestational Diabetes - Causes, Diagnosis and Treatment*.

Fadini, G. P., Losordo, D., & Dimmeler, S. (2012). Critical reevaluation of endothelial progenitor cell phenotypes for therapeutic and diagnostic use. *Circulation Research*, *110*(4), 624–37. doi:10.1161/CIRCRESAHA.111.243386

Ferris, D., Frisbie, D., Kisiday, J., & McIlwraith, C. W. (2012). In vivo healing of meniscal lacerations using bone marrow-derived mesenchymal stem cells and fibrin glue. *Stem Cells International*, *2012*, 1–9. doi:10.1155/2012/691605

Finger, E. B., Puri, K. D., Alon, R., Lawrence, M. B., von Andrian, H. U., & Springer, T. (1996). Adhesion through L-selectin requires a threshold hydrodynamic shear. *Nature*, *379*(18), 266–9.

Fischman, D. L., Leon, M. B., Baim, D. S., Schatz, R. A., Savage, M. P., Penn, I., … Veltri, L. (1994). A randomized comparison of coronary-stent placement and

balloon angioplasty in the treatment of coronary artery disease. *The New England Journal of Medicine*, *331*(8), 496–501.

Frangos, J. A., Eskin, S. G., McIntire, L. V, & Ives, C. L. (1985). Flow effects on prostacyclin production by cultured human endothelial cells. *Advancement Of Science*, *227*(4693), 1477–1479.

Fuoco, C., Salvatori, M. L., Biondo, A., Shapira-Schweitzer, K., Santoleri, S., Antonini, S., … Gargioli, C. (2012). Injectable polyethylene glycol-fibrinogen hydrogel adjuvant improves survival and differentiation of transplanted mesoangioblasts in acute and chronic skeletal-muscle degeneration. *Skeletal Muscle*, *2*(1), 24. doi:10.1186/2044-5040-2-24

Garg, S., Duckers, H. J., & Serruys, P. W. (2010). Endothelial progenitor cell capture stents: will this technology find its niche in contemporary practice? *European Heart Journal*, *31*(9), 1032–5. doi:10.1093/eurheartj/ehp591

Genové, E., Shen, C., Zhang, S., & Semino, C. E. (2005). The effect of functionalized self-assembling peptide scaffolds on human aortic endothelial cell function. *Biomaterials*, *26*(16), 3341–51. doi:10.1016/j.biomaterials.2004.08.012

Giancotti, F. G. (1999). Integrin Signaling. *Science*, *285*(5430), 1028–1033. doi:10.1126/science.285.5430.1028

Glagov, S., Zarins, C., Giddens, D. P., & Ku, D. N. (1988). Hemodynamics and atherosclerosis - Insights and perspectives gained form studies of human arteries. *Archives of Pathology & Laboratory Medicine*, *112*(10), 1018.

Godwin, E. E., Young, N. J., Dudhia, J., Beamish, I. C., & Smith, R. K. W. (2012). Implantation of bone marrow-derived mesenchymal stem cells demonstrates improved outcome in horses with overstrain injury of the superficial digital flexor tendon. *Equine Veterinary Journal*, *44*(1), 25–32. doi:10.1111/j.2042-3306.2011.00363.x

Gonzalez, A. L., Gobin, A. S., West, J. L., McIntire, L. V, & Smith, C. W. (2004). Integrin interactions with immobilized peptides in polyethylene glycol diacrylate hydrogels. *Tissue Engineering*, *10*(11-12), 1775–86. doi:10.1089/ten.2004.10.1775

Graf, J., Ogle, R. C., Robey, F. A., Sasaki, M., Martin, G. R., Yamada, Y., & Kleinman, H. K. (1987). A pentapeptide from the laminin B1 chain mediates cell adhesion and binds the 67,000 laminin receptor. *Biochemistry*, *26*(22), 6896–900. Retrieved from http://www.ncbi.nlm.nih.gov/pubmed/2962631

Hackett, C. H., Flaminio, M. J. B. F., & Fortier, L. A. (2011). Analysis of CD14 expression levels in putative mesenchymal progenitor cells isolated from equine bone marrow. *Stem Cells and Development*, *20*(4), 721–35. doi:10.1089/scd.2010.0175

Ham, A. S., Klibanov, A. L., & Lawrence, M. B. (2009). Action at a distance: lengthening adhesion bonds with poly(ethylene glycol) spacers enhances mechanically stressed affinity for improved vascular targeting of microparticles. *Langmuir : The ACS Journal of Surfaces and Colloids*, *25*(17), 10038–44. doi:10.1021/la900966h

Herold, D. A., Keil, K., & Bruns, D. (1989). Oxidation of polyethylene glycols by alcohol-dehydrogenase. *Biochemical Pharmacology*, *38*(1), 73–76.

Herrick, S., Blanc-Brude, O., Gray, A., & Laurent, G. (1999). Fibrinogen. *The International Journal of Biochemistry & Cell Biology*, *31*(7), 741–746. doi:10.1016/S1357-2725(99)00032-1

Hill-West, J. L., Chowdhury, S. M., Sawhney, A. S., Pathak, C. P., Dunn, R. C., & Hubbell, J. A. (1994). Prevention of postoperative adhesions in the rate by in-situ photopolymerization of bioresorbable hydrogel barriers. *Obstetrics and Gynecology*, *83*(1), 59–64.

Hirschi, K. K., Ingram, D. A., & Yoder, M. C. (2008). Assessing identity, phenotype, and fate of endothelial progenitor cells. *Arteriosclerosis, Thrombosis, and Vascular Biology*, *28*(9), 1584–95. doi:10.1161/ATVBAHA.107.155960

Hoffmann, R., Mintz, G. S., Dussaillant, G. R., Popma, J. J., Pichard, A. D., Satler, L. F., … Leon, M. B. (1996). Patterns and mechanisms of in-stent restenosis: a serial intravascular ultrasound study. *Circulation*, *94*(6), 1247–1254. doi:10.1161/01.CIR.94.6.1247

Hofmann, N. A., Reinisch, A., & Strunk, D. (2009). Isolation and large scale expansion of adult human endothelial colony forming progenitor cells. *Journal of Visualized Experiments*, *32*. doi:10.3791/752

Holmes, K., Roberts, O. L., Thomas, A. M., & Cross, M. J. (2007). Vascular endothelial growth factor receptor-2: structure, function, intracellular signalling and therapeutic inhibition. *Cellular Signalling*, *19*(10), 2003–12. doi:10.1016/j.cellsig.2007.05.013

Hristov, M., Erl, W., & Weber, P. C. (2003). Endothelial progenitor cells isolation and characterization. *Trends in Cardiovascular Medicine*, *13*(5), 201–206.

Hristov, M., Zernecke, A., Liehn, E. A., & Weber, C. (2007). Regulation of endothelial progenitor cell homing after arterial injury. *Thrombosis and Haemostasis*, *98*(2), 274–277. doi:10.1160/TH07

Hu, J., Takatoku, M., Sellers, S. E., Agricola, B. A., Metzger, M. E., Donahue, R. E., & Dunbar, C. E. (2002). Analysis of origin and optimization of expansion and transduction of circulating peripheral blood endothelial progenitor cells in the rhesus macaque model. *Human Gene Therapy*, *13*(17), 2041–50. doi:10.1089/10430340260395893

Hubbell, J. A., Massia, S. P., Desai, N. P., & Drumheller, P. D. (1991). Endothelial cell-selective materials for tissue engineering in the vascular graft via a new receptor. *Bio/technology (Nature Publishing Company)*, *9*(6), 568–72. Retrieved from http://www.ncbi.nlm.nih.gov/pubmed/1369319

Humphries, M. J. (2000). Integrin Structure. *Biochemical Society*, *28*(4), 311–340.

Hur, J., Yoon, C.-H., Kim, H.-S., Choi, J.-H., Kang, H.-J., Hwang, K.-K., … Park, Y.-B. (2004). Characterization of two types of endothelial progenitor cells and their different contributions to neovasculogenesis. *Arteriosclerosis, Thrombosis, and Vascular Biology*, *24*(2), 288–93. doi:10.1161/01.ATV.0000114236.77009.06

Ingram, D. a, Caplice, N. M., & Yoder, M. C. (2005). Unresolved questions, changing definitions, and novel paradigms for defining endothelial progenitor cells. *Blood*, *106*(5), 1525–31. doi:10.1182/blood-2005-04-1509

Ingram, D. A., Mead, L. E., Moore, D. B., Woodard, W., Fenoglio, A., & Yoder, M. C. (2005). Vessel wall-derived endothelial cells rapidly proliferate because they contain a complete hierarchy of endothelial progenitor cells. *Blood*, *105*(7), 2783–6. doi:10.1182/blood-2004-08-3057

Ingram, D. A., Mead, L. E., Tanaka, H., Meade, V., Fenoglio, A., Mortell, K., … Yoder, M. C. (2004). Identification of a novel hierarchy of endothelial progenitor cells using human peripheral and umbilical cord blood. *Blood*, *104*(9), 2752–2760. doi:10.1182/blood-2004-04-1396.Supported

Jantzen, A. E., Lane, W. O., Gage, S. M., Jamiolkowski, R. M., Haseltine, J. M., Galinat, L. J., … Achneck, H. E. (2011). Use of autologous blood-derived endothelial progenitor cells at point-of-care to protect against implant thrombosis in a large animal model. *Biomaterials*, *32*(33), 8356–63. doi:10.1016/j.biomaterials.2011.07.066

Jersmann, H. P. A. (2005). Time to abandon dogma: CD14 is expressed by non-myeloid lineage cells. *Immunology and Cell Biology*, *83*(5), 462–7. doi:10.1111/j.1440-1711.2005.01370.x

Jersmann, H. P. A., Hii, C. S. T., Hodge, G. L., & Ferrante, A. (2001). Synthesis and Surface Expression of CD14 by Human Endothelial Cells Synthesis and Surface Expression of CD14 by Human. *Infection and Immunity*, *69*(1), 479–85. doi:10.1128/IAI.69.1.479

Jun, H., & West, J. L. (2003). Development of a YIGSR-peptide-modified polyurethaneurea to enhance endothelialization. *Journal of Biomaterials Science. Polymer Edition*, *15*(1), 73–94.

Jun, H.-W., & West, J. L. (2004). Modification of polyurethaneurea with PEG and YIGSR peptide to enhance endothelialization without platelet adhesion. *Journal of Biomedical Materials Research. Part B, Applied Biomaterials*, *72*(1), 131–9. doi:10.1002/jbm.b.30135

Jung, U., Norman, K. E., Scharffetter-Kochanek, K., Beaudet, A. L., & Ley, K. (1998). Transit time of leukocytes rolling through venules controls cytokine-induced inflammatory cell recruitment in vivo. *The Journal of Clinical Investigation*, *102*(8), 1526–33. doi:10.1172/JCI119893

Kabithe, E., Hillegas, J., Stokol, T., Moore, J., & Wagner, B. (2010). Monoclonal antibodies to equine CD14. *Veterinary Immunology and Imunopathology*, *138*(1-2), 149–53. doi:10.1016/j.vetimm.2010.07.003

Kalka, C., Masuda, H., Takahashi, T., Kalka-Moll, W. M., Silver, M., Kearney, M., … Asahara, T. (2000). Transplantation of ex vivo expanded endothelial progenitor cells for therapeutic neovascularization. *Proceedings of the National Academy of Sciences of the United States of America*, *97*(7), 3422–7. doi:10.1073/pnas.070046397

Kaushal, S., Amiel, G. E., Guleserian, K. J., Shapira, O. M., Perry, T., Sutherland, F. W., … Mayer, J. E. (2001). Functional Small Diameter Neovessels using Endothelial Progenitor Cells Expanded Ex Vivo. *Kaushal, S., Amiel, G. E., Guleserian, K. J., Shapira, O. M., Perry, T., Sutherland, F. W., Rabkin, E., et Al. (2010). Functional Small Diameter Neovessels Using Endothelial Progenitor Cells Expanded Ex Vivo, 7(9), 1035–1040. doi:10.1038/nm0901-1035.Funct*, *7*(9), 1035–1040. doi:10.1038/nm0901-1035.Functional

Kiemeneij, F., Serruys, P. W., Macaya, C., Rutsch, W., Heyndrickx, G., Albertsson, P., … Morel, M. A. (2001). Continued benefit of coronary stenting versus balloon angioplasty: five-year clinical follow-up of Benestent-I trial. *Journal of the*

American College of Cardiology, *37*(6), 1598–603. Retrieved from http://www.ncbi.nlm.nih.gov/pubmed/11345371

Kim, E.-Y., Bang, J. Y., Chang, S.-I., & Kang, I.-C. (2008). A novel integrin alpha5beta1 antagonistic peptide, A5-1, screened by Protein Chip system as a potent angiogenesis inhibitor. *Biochemical and Biophysical Research Communications*, *377*(4), 1288–93. doi:10.1016/j.bbrc.2008.10.166

Kireeva, M. L., Lam, S. C., & Lau, L. F. (1998). Adhesion of human umbilical vein endothelial cells to the immediate-early gene product Cyr61 is mediated through integrin alphavbeta3. *The Journal of Biological Chemistry*, *273*(5), 3090–6. Retrieved from http://www.ncbi.nlm.nih.gov/pubmed/9446626

Kleinman, H. K., & Martin, G. R. (2005). Matrigel: basement membrane matrix with biological activity. *Seminars in Cancer Biology*, *15*(5), 378–86. doi:10.1016/j.semcancer.2005.05.004

Koivunen, E., Wang, B., & Ruoslahti, E. (1994). Isolation of a highly specific ligand for the α5β1 integrin from a phage display library. *The Journal of Cell Biology*, *124*(3), 373–80. Retrieved from http://www.pubmedcentral.nih.gov/articlerender.fcgi?artid=2119941&tool=pmcentrez&rendertype=abstract

Konstantopoulos, K., Kukreti, S., & McIntire, L. V. (1998). Biomechanics of cell interactions in shear fields. *Advanced Drug Delivery Reviews*, *33*(1-2), 141–64. Retrieved from http://www.ncbi.nlm.nih.gov/pubmed/10837657

Kopp, H.-G., Ramos, C. A., & Rafii, S. (2006). Contribution of endothelial progenitors and proangiogenic hematopoietic cells to vascularization of tumor and ischemic tissue. *Current Opinion in Hematology*, *13*(3), 175–81. doi:10.1097/01.moh.0000219664.26528.da.Contribution

Kovacic, J. C., Moore, J., Herbert, A., Ma, D., Boehm, M., & Graham, R. M. (2008). Endothelial progenitor cells, angioblasts, and angiogenesis--old terms reconsidered from a current perspective. *Trends in Cardiovascular Medicine*, *18*(2), 45–51. doi:10.1016/j.tcm.2007.12.002

Ku, D. N. (1997). Blood Flow in Arteries. *Annual Review of Fluid Mechanics*, *29*(1), 399–434. doi:10.1146/annurev.fluid.29.1.399

Larsen, C. C., Kligman, F., Tang, C., Kottke-Marchant, K., & Marchant, R. E. (2007). A biomimetic peptide fluorosurfactant polymer for endothelialization of ePTFE with limited platelet adhesion. *Biomaterials*, *28*(24), 3537–48. doi:10.1016/j.biomaterials.2007.04.026

Lawrence, M. B., & Springer, T. A. (1991). Leukocytes roll on a selectin at physiologic flow rates: distinction from and prerequisite for adhesion through integrins. *Cell*, *65*(5), 859–73. Retrieved from http://www.ncbi.nlm.nih.gov/pubmed/1710173

Lee, Y., Kang, D.-K., Chang, S.-I., Han, M. H., & Kang, I.-C. (2004). High-throughput screening of novel peptide inhibitors of an integrin receptor from the hexapeptide library by using a protein microarray chip. *Journal of Biomolecular Screening*, *9*(8), 687–94. doi:10.1177/1087057104268125

Leu, S.-J., Lam, S. C.-T., & Lau, L. F. (2002). Pro-angiogenic activities of CYR61 (CCN1) mediated through integrins alphavbeta3 and alpha6beta1 in human umbilical vein endothelial cells. *The Journal of Biological Chemistry*, *277*(48), 46248–55. doi:10.1074/jbc.M209288200

Levenberg, S. (2005). Engineering blood vessels from stem cells: recent advances and applications. *Current Opinion in Biotechnology*, *16*(5), 516–23. doi:10.1016/j.copbio.2005.08.007

Ley, K., Gaehtgens, P., Fennie, C., Singer, M. S., Lasky, L. A., & Rosen, S. D. (1991). Lectin-like cell adhesion molecule 1 mediates leukocyte rolling in mesenteric venules in vivo. *Blood*, *77*(12), 2553–5. Retrieved from http://www.ncbi.nlm.nih.gov/pubmed/2043760

Ma, Z.-L., Mai, X.-L., Sun, J.-H., Ju, S.-H., Yang, X., Ni, Y., & Teng, G.-J. (2009). Inhibited atherosclerotic plaque formation by local administration of magnetically labeled endothelial progenitor cells (EPCs) in a rabbit model. *Atherosclerosis*, *205*(1), 80–6. doi:10.1016/j.atherosclerosis.2008.07.048

MacEachern, K. E., Smith, G. L., & Nolan, A. M. (1997). Methods for the isolation, culture and characterisation of equine pulmonary artery endothelial cells. *Research in Veterinary Science*, *62*(2), 147–52. Retrieved from http://www.ncbi.nlm.nih.gov/pubmed/9243714

Mardilovich, A., Craig, J. A., McCammon, M. Q., Garg, A., & Kokkoli, E. (2006). Design of a novel fibronectin-mimetic peptide-amphiphile for functionalized biomaterials. *Langmuir : The ACS Journal of Surfaces and Colloids*, *22*(7), 3259–64. doi:10.1021/la052756n

Mardilovich, A., & Kokkoli, E. (2004). Biomimetic peptide-amphiphiles for functional biomaterials: the role of GRGDSP and PHSRN. *Biomacromolecules*, *5*(3), 950–7. doi:10.1021/bm0344351

Massia, S. P., & Hubbell, J. A. (1992). Vascular endothelial cell adhesion and spreading promoted by the peptide REDV of the IIICS region of plasma fibronectin is

mediated by integrin alpha 4 beta 1. *The Journal of Biological Chemistry*, *267*(20), 14019–26. Retrieved from http://www.ncbi.nlm.nih.gov/pubmed/1629200

McEver, R. P., & Cummings, R. D. (1997). Perspectives series: cell adhesion in vascular biology. Role of PSGL-1 binding to selectins in leukocyte recruitment. *The Journal of Clinical Investigation*, *100*(3), 485–91. doi:10.1172/JCI119556

Mellick, A. S., Plummer, P. N., Nolan, D. J., Gao, D. G., Bambino, K., Hahn, M., … Mittal, V. (2010). Using the transcription factor inhibitor of DNA binding 1 to selectively target endothelial progenitor cells offers novel strategies to inhibit tumor angiogenesis and growth. *Cancer Research*, *70*(18), 7273–82.

Mellott, M. B., Searcy, K., & Pishko, M. V. (2001). Release of protein from highly cross-linked hydrogels of poly(ethylene glycol) diacrylate fabricated by UV polymerization. *Biomaterials*, *22*(9), 929–41. Retrieved from http://www.ncbi.nlm.nih.gov/pubmed/11311012

Moldovan, N. I. (2003). Current priorities in the research of circulating pre-endothelial cells. In N. I. Moldovan (Ed.), *Novel angiogenic mechanisms: role of circulating progenitor endothelial cells* (1st ed.). New York: Kluwer Academic/Plenum Publisher.

Moon, J. J., Saik, J. E., Poché, R. A., Leslie-Barbick, J. E., Lee, S.-H., Smith, A. A., … West, J. L. (2010). Biomimetic hydrogels with pro-angiogenic properties. *Biomaterials*, *31*(14), 3840–7. doi:10.1016/j.biomaterials.2010.01.104

Murohara, T., Ikeda, H., Duan, J., Shintani, S., Sasaki, K. I., Eguchi, H., … Imaizumi, T. (2000). Transplanted cord blood-derived endothelial precursor cells augment postnatal neovascularization. *The Journal of Clinical Investigation*, *105*(11), 1527–36. doi:10.1172/JCI8296

Mutin, M., Canavy, I., Blann, A., Bory, M., Sampol, J., & Dignat-George, F. (1999). Direct evidence of endothelial injury in acute myocardial infarction and unstable angina by demonstration of circulating endothelial cells. *Blood*, *93*(9), 2951–8. Retrieved from http://www.ncbi.nlm.nih.gov/pubmed/10216090

Nagano, M., Yamashita, T., Hamada, H., Ohneda, K., Kimura, K., Nakagawa, T., … Ohneda, O. (2007). Identification of functional endothelial progenitor cells suitable for the treatment of ischemic tissue using human umbilical cord blood. *Blood*, *110*(1), 151–60. doi:10.1182/blood-2006-10-047092

Nemir, S., Hayenga, H. N., & West, J. L. (2010). PEGDA hydrogels with patterned elasticity: Novel tools for the study of cell response to substrate rigidity. *Biotechnology and Bioengineering*, *105*(3), 636–44. doi:10.1002/bit.22574

Nguyen, K. T., & West, J. L. (2002). Photopolymerizable hydrogels for tissue engineering applications. *Biomaterials*, *23*(22), 4307–14. Retrieved from http://www.ncbi.nlm.nih.gov/pubmed/12219820

Nuttelman, C. R., Henry, S. M., & Anseth, K. S. (2002). Synthesis and characterization of photocrosslinkable, degradable poly(vinyl alcohol)-based tissue engineering scaffolds. *Biomaterials*, *23*(17), 3617–26. Retrieved from http://www.ncbi.nlm.nih.gov/pubmed/12109687

Nuttelman, C. R., Mortisen, D. J., Henry, S. M., & Anseth, K. S. (2001). Attachment of fibronectin to poly(vinyl alcohol) hydrogels promotes NIH3T3 cell adhesion, proliferation, and migration. *Journal of Biomedical Materials Research*, *57*(2), 217–23. Retrieved from http://www.ncbi.nlm.nih.gov/pubmed/11484184

Nuttelman, C. R., Rice, M. A., Rydholm, A. E., Salinas, C. N., Shah, D. N., & Anseth, K. S. (2008). Macromolecular monomers for the synthesis of hydrogel niches and their application in cell encapsulation and tissue engineering. *Progress in Polymer Science*, *33*(2), 167–79. doi:10.1016/j.progpolymsci.2007.09.006

Obi, S., Masuda, H., Shizuno, T., Sato, A., Yamamoto, K., Ando, J., … Asahara, T. (2012). Fluid shear stress induces differentiation of circulating phenotype endothelial progenitor cells. *American Journal of Physiology - Cell Physiology*, *303*(6), 595–606. doi:10.1152/ajpcell.00133.2012

Obi, S., Yamamoto, K., Shimizu, N., Kumagaya, S., Masumura, T., Sokabe, T., … Ando, J. (2009). Fluid shear stress induces arterial differentiation of endothelial progenitor cells. *Journal of Applied Physiology*, *106*(1), 203–11. doi:10.1152/japplphysiol.00197.2008

Padon, K. S., & Scranton, A. B. (2001). A mechanistic investigation of the three-component radical photoinitiator system Eosin Y spirit soluble,N-methyldiethanolamine, and diphenyliodonium chloride. *Journal of Polymer Science Part A: Polymer Chemistry*, *39*(5), 715–723. doi:10.1002/1099-0518(20010301)39:5<715::AID-POLA1043>3.0.CO;2-O

Park, E. Y. H., Smith, M. J., Stropp, E. S., Snapp, K. R., DiVietro, J. A., Walker, W. F., … Lawrence, M. B. (2002). Comparison of PSGL-1 microbead and neutrophil rolling: microvillus elongation stabilizes P-selectin bond clusters. *Biophysical Journal*, *82*(4), 1835–47. doi:10.1016/S0006-3495(02)75534-3

Park, S.-W., Park, H.-K., Hong, M.-K., Lee, S.-G., Lee, I.-S., Kim, J.-W., … Park, S.-J. (1998). Comparison of slotted tube versus coil stent implantation for ostial left anterior descending coronary artery stenosis: initial and late clinical outcomes. *Journal of Korean Medical Science*, *13*, 483–7.

Patrick, C. W., & McIntire, L. V. (1995). Shear stress and cyclic strain modulation of gene expression in vascular endothelial cells. *Blood Purification*, *13*(3-4), 112–24.

Peichev, M., Naiyer, A. J., Pereira, D., Zhu, Z., Lane, W. J., Williams, M., … Oz, M. C. (2000). Expression of VEGFR-2 and AC133 by circulating human CD34 + cells identifies a population of functional endothelial precursors Expression of VEGFR-2 and AC133 by circulating human CD34 ♀ cells identifies a population of functional endothelial precursors. *Blood*, *95*, 952–958.

Peppas, N. A., Hilt, J. Z., Khademhosseini, A., & Langer, R. (2006). Hydrogels in biology and medicine: from molecular principles to bionanotechnology. *Advanced Materials*, *18*(11), 1345–1360. doi:10.1002/adma.200501612

Peppas, N. A., & Merrill, E. W. (1977). Development of semicrystalline poly(vinyl alcohol) hydrogels for biomedical applications. *Journal of Biomedical Materials Research*, *11*(3), 423–34. doi:10.1002/jbm.820110309

Rafii, S., & Lyden, D. (2003). Therapeutic stem and progenitor cell transplantation for organ vascularization and regeneration. *Nature Medicine*, *9*(6), 702–12. doi:10.1038/nm0603-702

Reinisch, A., Hofmann, N. A., Obenauf, A. C., Kashofer, K., Rohde, E., Schallmoser, K., … Strunk, D. (2009). Humanized large-scale expanded endothelial colony-forming cells function in vitro and in vivo. *Blood*, *113*(26), 6716–25. doi:10.1182/blood-2008-09-181362

Richardson, M. R., & Yoder, M. C. (2011). Endothelial progenitor cells: quo vadis? *Journal of Molecular and Cellular Cardiology*, *50*(2), 266–72. doi:10.1016/j.yjmcc.2010.07.009

Rinker, K. D., Prabhakar, V., & Truskey, G. A. (2001). Effect of contact time and force on monocyte adhesion to vascular endothelium. *Biophysical Journal*, *80*(4), 1722–32. doi:10.1016/S0006-3495(01)76143-7

Roger, V. L., Go, A. S., Lloyd-Jones, D. M., Benjamin, E. J., Berry, J. D., Borden, W. B., … Turner, M. B. (2011). Heart disease and stroke statistics--2012 update: a report from the american heart association. *Circulation*, *125*, 12–230. doi:10.1161/CIR.0b013e31823ac046

Ross, R. (1999). Atherosclerosis - an inflammatory disease. *The New England Journal of Medicine*, *340*, 115–126.

Ross, R., & Glomset, J. A. (1973). Atherosclerosis and the arterial smooth muscle cell of smooth muscle. *Advancement Of Science*, *180*(4093), 1332–1339.

Rotmans, J. I., Heyligers, J. M. M., Verhagen, H. J. M., Velema, E., Nagtegaal, M. M., de Kleijn, D. P. V, … Pasterkamp, G. (2005). In vivo cell seeding with anti-CD34 antibodies successfully accelerates endothelialization but stimulates intimal hyperplasia in porcine arteriovenous expanded polytetrafluoroethylene grafts. *Circulation*, *112*(1), 12–8. doi:10.1161/CIRCULATIONAHA.104.504407

Ruoslahti, E. (1991). Integrins. *Journal of Clinical Investigation*, *87*(January), 1–5.

Ruoslahti, E. (1996). RGD and other recognition sequences for integrins. *Cancer Research*, *12*, 697–715.

Schmedlen, R. H., Masters, K. S., & West, J. L. (2002). Photocrosslinkable polyvinyl alcohol hydrogels that can be modified with cell adhesion peptides for use in tissue engineering. *Biomaterials*, *23*(22), 4325–32. Retrieved from http://www.ncbi.nlm.nih.gov/pubmed/12219822

Schmidt, B. J., Paschall, C. D., Guilford, W. H., & Lawrence, M. B. (2007). High resolution optical tracking to identify adhesive events in vitro. *Conference Proceedings of the Asilomar Conference on Signals, Systems, and Computers*, 1856–1860.

Schneider, C. A., Rasband, W. S., & Eliceiri, K. W. (2012). NIH Image to ImageJ: 25 years of image analysis. *Nature Methods*, *9*(7), 671–5. doi:10.1038/nmeth.2089

Scott, R. A., & Peppas, N. A. (1999). Highly crosslinked, PEG-containing copolymers for sustained solute delivery. *Biomaterials*, *20*(15), 1371–80. Retrieved from http://www.ncbi.nlm.nih.gov/pubmed/10454008

Seeto, W. J. (2012). *Peptide grafted poly(ethylene glycol) hydrogel as biomaterial for endothelial colony forming cells*. Auburn University.

Seeto, W. J., Tian, Y., & Lipke, E. A. (2013). Peptide-grafted poly(ethylene glycol) hydrogels support dynamic adhesion of endothelial progenitor cells. *Acta Biomaterialia*, *9*, 8279–89. doi:10.1016/j.actbio.2013.05.023

Sen, S., McDonald, S. P., Coates, P. T. H., & Bonder, C. S. (2011). Endothelial progenitor cells: novel biomarker and promising cell therapy for cardiovascular disease. *Clinical Science*, *120*(7), 263–83. doi:10.1042/CS20100429

Serruys, P. W., Jaegere, P. De, & Kiemeneij, F. K. (1994). A comparison of balloon expandable-stent implantation with balloon angioplasty in patients with coronary artery disease. *The New England Journal of Medicine*, *331*(8), 489–495.

Shirota, T., Hongbing, H., Yasui, H., & Matsuda, T. (2003). Human endothelial progenitor cell-seeded hybrid graft: proliferative and antithrombogenic potentials in vitro and fabrication processing. *Tissue Engineering*, *9*(1), 127–36.

Shirure, V. S., Henson, K. A., Schnaar, R. L., Nimrichter, L., & Burdick, M. M. (2011). Gangliosides expressed on breast cancer cells are E-selectin ligands. *Biochemical and Biophysical Research Communications*, *406*(3), 423–9. doi:10.1016/j.bbrc.2011.02.061

Shtatland, T., Guettler, D., Kossodo, M., Pivovarov, M., & Weissleder, R. (2007). PepBank--a database of peptides based on sequence text mining and public peptide data sources. *BMC Bioinformatics*, *8*, 280. doi:10.1186/1471-2105-8-280

Slaughter, B. V, Khurshid, S. S., Fisher, O. Z., Khademhosseini, A., & Peppas, N. A. (2009). Hydrogels in regenerative medicine. *Advanced Materials*, *21*(32-33), 3307–29. doi:10.1002/adma.200802106

Slepian, M. J., & Hubbell, J. A. (1997). Polymeric endoluminal gel paving: hydrogel systems for local barrier creation and site-specific drug delivery. *Advanced Drug Delivery Reviews*, *24*, 11–30.

Slepian, M. J., Massia, S. P., Weselcouch, E., Khosravi, F., & Roth, L. (1995). In-situ photopolymerized hydrogel barriers applied following porcine arterial stenting reduce intra-stent neointimal thickening. *Circulation*, *92*(8), 1823–1823.

Smith, M. J., Berg, E. L., & Lawrence, M. B. (1999). A direct comparison of selectin-mediated transient, adhesive events using high temporal resolution. *Biophysical Journal*, *77*(6), 3371–83. doi:10.1016/S0006-3495(99)77169-9

Stone, G. W., Moses, J. W., Ellis, S. G., Schofer, J., Dawkins, K. D., Morice, M.-C., … Leon, M. B. (2007). Safety and efficacy of sirolimus- and paclitaxel-eluting coronary stents. *The New England Journal of Medicine*, *356*(10), 998–1008. doi:10.1056/NEJMoa067193

Stroncek, J. D., Grant, B. S., Brown, M. A., Povsic, T. J., Truskey, G. A., & Reichert, W. M. (2009). Comparison of endothelial cell phenotypic markers of late-outgrowth endothelial progenitor cells isolated from patients with coronary artery disease and healthy volunteers. *Tissue Engineering. Part A*, *15*(11), 3473–86. doi:10.1089/ten.TEA.2008.0673

Tabachnick, B. G., & Fidell, L. S. (1996). *Using multivariate statistics* (3rd ed.). New York: Harper Collins. Retrieved from http://jalt.org/test/bro_1.htm

Taite, L. J., Rowland, M. L., Ruffino, K. A., Smith, B. R. E., Lawrence, M. B., & West, J. L. (2006). Bioactive hydrogel substrates: probing leukocyte receptor-ligand interactions in parallel plate flow chamber studies. *Annals of Biomedical Engineering*, *34*(11), 1705–11. doi:10.1007/s10439-006-9173-x

Timmermans, F., Plum, J., Yöder, M. C., Ingram, D. A., Vandekerckhove, B., & Case, J. (2009). Endothelial progenitor cells: identity defined? *Journal of Cellular and Molecular Medicine*, *13*(1), 87–102. doi:10.1111/j.1582-4934.2008.00598.x

Tirtaatmadja, V. (2001). Rheology of dextran solutions. *Journal of Non-Newtonian Fluid Mechanics*, *97*(2-3), 295–301. doi:10.1016/S0377-0257(00)00226-3

Truskey, G. A., Yuan, F., & Katz, D. F. (2004). *Transport phenomena in biological systems*. New Jersey.

Urbich, C., & Dimmeler, S. (2004). Endothelial progenitor cells: characterization and role in vascular biology. *Circulation Research*, *95*(4), 343–53. doi:10.1161/01.RES.0000137877.89448.78

Vajkoczy, P., Blum, S., Lamparter, M., Mailhammer, R., Erber, R., Engelhardt, B., … Hatzopoulos, A. K. (2003). Multistep nature of microvascular recruitment of ex vivo-expanded embryonic endothelial progenitor cells during tumor angiogenesis. *The Journal of Experimental Medicine*, *197*(12), 1755–65. doi:10.1084/jem.20021659

Veleva, A. N., Cooper, S. L., & Patterson, C. (2007). Selection and initial characterization of novel peptide ligands that bind specifically to human blood outgrowth endothelial cells. *Biotechnology and Bioengineering*, *98*(1), 306–12. doi:10.1002/bit

Vickers, D. A. L., & Murthy, S. K. (2010). Receptor expression changes as a basis for endothelial cell identification using microfluidic channels. *Lab on a Chip*, *10*(18), 2380–6. doi:10.1039/c004870d

Voyta, J. C., Via, D. P., Butterfield, C. E., & Zetter, B. R. (1984). Identification and isolation of endothelial cells based on their increased uptake of acetylated-low density lipoprotein. *The Journal of Cell Biology*, *99*(6), 2034–40. Retrieved from http://www.pubmedcentral.nih.gov/articlerender.fcgi?artid=2113570&tool=pmcentrez&rendertype=abstract

Wang, X., & Cooper, S. L. (2013). Adhesion of endothelial cells and endothelial progenitor cells on peptide-linked polymers in shear flow. *Tissue Engineering Part A*, *19*(9), 1–9. doi:10.1089/ten.tea.2011.0653

Watts, A. E., Ackerman-yost, J. C., & Nixon, A. J. (2013). A Comparison of Three-Dimensional Culture Systems to Evaluate In Vitro Chondrogenesis. *Tissue Engineering Part A*, *19*(19), 2275–83. doi:10.1089/ten.tea.2012.0479

Wei, Y., Ji, Y., Xiao, L.-L., Lin, Q.-K., Xu, J.-P., Ren, K.-F., & Ji, J. (2013). Surface engineering of cardiovascular stent with endothelial cell selectivity for in vivo re-endothelialisation. *Biomaterials*, *34*(11), 2588–99. doi:10.1016/j.biomaterials.2012.12.036

Wendel, H. P., Avci-Adali, M., & Ziemer, G. (2010). Endothelial progenitor cell capture stents--hype or hope? *International Journal of Cardiology*, *145*(1), 115–7. doi:10.1016/j.ijcard.2009.06.020

Werb, Z. (1997). ECM and cell surface proteolysis : regulating cellular ecology. *Cell*, *91*, 439–442.

West, J. L. (2004). Biofunctional Polymers. In G. E. Wnek (Ed.), *Encyclopedia of Biomaterials and Biomedical Engineering* (1st ed., Vol. 7, pp. 89–95). New York: Marcel Dekker, Inc. doi:10.1081/E-EBBE

West, J. L., & Hubbell, J. A. (1996). Separation of the arterial wall from blood contact using hydrogel barriers reduces intimal thickening after balloon injury in the rat: the roles of medial and luminal factors in arterial healing. *Proceedings of the National Academy of Sciences of the United States of America*, *93*(23), 13188–193. Retrieved from http://www.pubmedcentral.nih.gov/articlerender.fcgi?artid=24068&tool=pmcentrez&rendertype=abstract

Wijelath, E. S., Rahman, S., Murray, J., Patel, Y., Savidge, G., & Sobel, M. (2004). Fibronectin promotes VEGF-induced CD34 cell differentiation into endothelial cells. *Journal of Vascular Surgery*, *39*(3), 655–60. doi:10.1016/j.jvs.2003.10.042

Williams, C. G., Malik, A. N., Kim, T. K., Manson, P. N., & Elisseeff, J. H. (2005). Variable cytocompatibility of six cell lines with photoinitiators used for polymerizing hydrogels and cell encapsulation. *Biomaterials*, *26*(11), 1211–8. doi:10.1016/j.biomaterials.2004.04.024

Wills, T., Heaney, A., Jane Wardrop, K., & Haldorson, G. (2009). Immunomagnetic isolation of canine circulating endothelial and endothelial progenitor cells. *Veterinary Clinical Pathology*, *38*(4), 437–42.

Wood, J. A., Colletti, E., Mead, L. E., Ingram, D., Porada, C. D., Zanjani, E. D., … Almeida-Porada, G. (2012). Distinct contribution of human cord blood-derived

endothelial colony forming cells to liver and gut in a fetal sheep model. *Hepatology*, *56*(3), 1086–1096.

Working, P. K., Newman, M. S., Johnson, J., & Cornacoff, J. B. (1997). Safety of poly(ethylene glycol) and poly(ethylene glycol) derivatives. *ACS Symposium Series*, *680*, 45–57. Retrieved from http://apps.webofknowledge.com.spot.lib.auburn.edu/full_record.do?product=WOS&search_mode=Refine&qid=52&SID=4ELIlANL5GKG4bGH8Ie&page=1&doc=2

Wu, H., Riha, G. M., Yang, H., Li, M., Yao, Q., & Chen, C. (2005). Differentiation and proliferation of endothelial progenitor cells from canine peripheral blood mononuclear cells. *The Journal of Surgical Research*, *126*(2), 193–8. doi:10.1016/j.jss.2005.01.016

Xia, W. H., Yang, Z., Xu, S. Y., Chen, L., Zhang, X. Y., Li, J., … Tao, J. (2012). Age-related decline in reendothelialization capacity of human endothelial progenitor cells is restored by shear stress. *Hypertension*, *59*(6), 1225–31. doi:10.1161/HYPERTENSIONAHA.111.179820

Yoder, M. C., Mead, L. E., Prater, D., Krier, T. R., Mroueh, K. N., Li, F., … Ingram, D. A. (2007). Redefining endothelial progenitor cells via clonal analysis and hematopoietic stem/progenitor cell principals. *Blood*, *109*(5), 1801–9. doi:10.1182/blood-2006-08-043471

Youngstrom, D. W., Barrett, J. G., Jose, R. R., & Kaplan, D. L. (2013). Functional characterization of detergent-decellularized equine tendon extracellular matrix for tissue engineering applications. *PloS ONE*, *8*(5), e64151. doi:10.1371/journal.pone.0064151

Zeng, L., Chen, C., Song, G., Yan, Z., Xu, S., Jia, L., … Xu, K. (2012). Infusion of endothelial progenitor cells accelerates hematopoietic and immune reconstitution, and ameliorates the graft-versus-host disease after hematopoietic stem cell transplantation. *Cell Biochemistry and Biophysics*, *64*(3), 213–22. doi:10.1007/s12013-012-9387-5

Appendix A Sample Calculation on Yield of PEGDA Acrylation

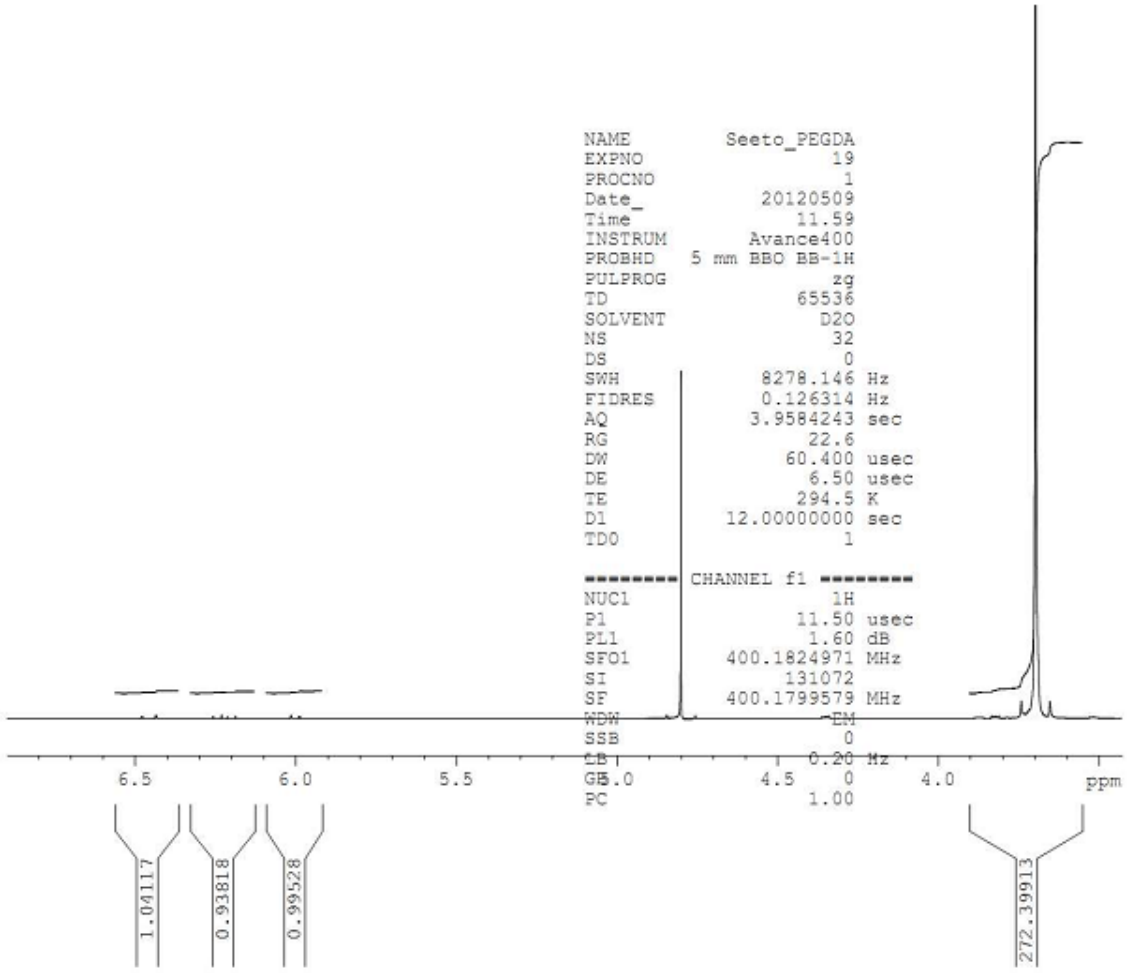

Appendix A.1 NMR diagram showing the integrated intensity of protons on acrylate groups and PEG of PEGDA chain.

PEG Acrylation Sample Calculations

$$MW_{PEGmonomer} = 44.053 g/mol$$

$$MW_{PEG} = 6000 g/mol$$

$$n_{monomer} = \frac{MW_{PEG}}{MW_{PEGmonomer}} = \frac{6000}{44.053} = 136.2$$

$$n_{proton/monomer} = 4$$

Integrated intensity of PEG peak

$$(I_{PEG}) = 268.08$$

Integrated intensity of acrylate single proton peaks

$$I_{acrylate1}, I_{acrylate2}, I_{acrylate3} = 0.970, 0.920, 0.960$$

$$n_{PEG} = \frac{I_{PEG}}{n_{proton/monomer} \times n_{monomer}} = \frac{I_{PEG}}{4 \times 136.2} = 0.492$$

$$n_{tacrylate} = n_{PEG} \times 2 = 0.492 \times 2 = 0.984$$

$$n_{acrylate} = \frac{I_{acrylate1} + I_{acrylate2} + I_{acrylate3}}{3} = \frac{0.970 + 0.920 + 0.960}{3} = 0.950$$

Acrylation percentage

$$= \frac{n_{acrylate}}{n_{tacrylate}} \times 100\% = \frac{0.950}{0.984} \times 100\% = 96.5\%$$

Appendix B ImageJ Cell Identification Code

```
//Video file names should be in this format: "CellType Material Concentration ExperimentDate Trial ShearRate FileNumber"

Dialog.create("");
Dialog.addCheckbox("Use same parameters for all videos?", true);
Dialog.show();

SameParameters=Dialog.getCheckbox();

if (SameParameters==1){
Dialog.create("Initialize parameters for all videos:");
Dialog.addNumber("How long are your videos in seconds?", 20);
Dialog.addMessage("If manual threshold, please select the following checkbox and enter threshold range");
Dialog.addCheckbox("Manual threshold?", false);
Dialog.addNumber("Threshold-lower boundary", 0);
Dialog.addNumber("Threshold-upper boundary", 10000);
Dialog.addMessage("If automatic threshold, please choose threshold method");
Dialog.addChoice("Threshold:", newArray("MaxEntropy dark", "Intermodes dark", "IsoData dark"));
Dialog.addString("Cell size (microns):","200-700");
Dialog.addString("Circularity:","0.82-1");
Dialog.addCheckbox("Check if you want to use custom scale",false);
Dialog.addNumber("Custom scale (px/um)", 1.020);
Dialog.show();

//set particle analysis parameter==================
VideoLength=Dialog.getNumber();
ThresholdManual=Dialog.getCheckbox();
ThresholdSettingL=Dialog.getNumber();
ThresholdSettingH=Dialog.getNumber();
ThresholdSetting=Dialog.getChoice();
SizeSetting=Dialog.getString();
CircularitySetting=Dialog.getString();
CustomScale=Dialog.getCheckbox();
Scale=Dialog.getNumber();
}

SourceDir = getDirectory("Choose rolling video directory. Folder can ONLY contain video files.");
FolderList = getFileList(SourceDir);
FileNameList=newArray("");
```

```
for (k=0; k<FolderList.length; k++) {
filepath=SourceDir+FolderList[k];
run("Bio-Formats Importer", "  open=filepath color_mode=Default view=Hyperstack stack_order=XYCZT");

if (SameParameters==0){
Dialog.create("Initialize parameters for current videos:");
Dialog.addMessage("Analyzing "+FolderList[k]);
Dialog.addNumber("How long is this video in seconds?", 20);
Dialog.addMessage("If manual threshold, please select the following checkbox and enter threshold range");
Dialog.addCheckbox("Manual threshold?", false);
Dialog.addNumber("Threshold-lower boundary", 0);
Dialog.addNumber("Threshold-upper boundary", 10000);
Dialog.addMessage("If automatic threshold, please choose threshold method");
Dialog.addChoice("Threshold:", newArray("MaxEntropy dark", "Intermodes dark", "IsoData dark"));
Dialog.addString("Cell size (microns):","200-700");
Dialog.addString("Circularity:","0.82-1");
Dialog.addCheckbox("Check if you want to use custom scale",false);
Dialog.addNumber("Custom scale (px/um)", 1.020);
Dialog.show();
//set particle analysis parameter==================
VideoLength=Dialog.getNumber();
ThresholdManual=Dialog.getCheckbox();
ThresholdSettingL=Dialog.getNumber();
ThresholdSettingH=Dialog.getNumber();
ThresholdSetting=Dialog.getChoice();
SizeSetting=Dialog.getString();
CircularitySetting=Dialog.getString();
CustomScale=Dialog.getCheckbox();
Scale=Dialog.getNumber();
}

if(CustomScale==1){
run("Set Scale...", "distance=Scale known=1 pixel=1 unit=um");
}

//get time, file directory=========================
getDateAndTime(year, month, dayOfWeek, dayOfMonth, hour, minute, second, msec);
dir=getDirectory("image");
savedirectory=dir;

//get file name, format, frame rate================
```

```
FullFileName=getTitle();
FileNameSub=split(FullFileName, ".");
FileName=FileNameSub[0]+"."+FileNameSub[1];
selectWindow(FullFileName);
FPS=nSlices/VideoLength;
//FPS=Stack.getFrameRate();
fps="_"+FPS;

//start tracking================================
selectWindow(FullFileName);
//run("Rotate... ", "angle=180 grid=1 interpolation=None stack");
run("8-bit");
if (ThresholdManual==0)
setAutoThreshold(ThresholdSetting);
else if (ThresholdManual==1) {
setThreshold(ThresholdSettingL,ThresholdSettingH);
}
setOption("BlackBackground", false);
run("Convert to Mask", "method=Intermodes background=Default");
run("Fill Holes", "stack");
run("Set Measurements...", "area center shape feret's stack display redirect=None
decimal=3");
run("Analyze Particles...", "size=&SizeSetting circularity=&CircularitySetting
show=Outlines display exclude clear add stack");

//save tracked files============================
FileSaveFormat=FileName+fps;
directoryBW=savedirectory+FileSaveFormat;
roiManager("Associate", "true");
roiManager("Centered", "false");

run("Input/Output...", "jpeg=75 gif=-1 file=.txt copy_row save_column save_row");

//Print Time to log================================
    MonthNames                                                                    =
newArray("Jan","Feb","Mar","Apr","May","Jun","Jul","Aug","Sep","Oct","Nov","Dec");
    DayNames = newArray("Sun", "Mon","Tue","Wed","Thu","Fri","Sat");
    TimeString ="Date: "+DayNames[dayOfWeek]+" ";
    if (dayOfMonth<10) {TimeString = TimeString+"0";}
    TimeString = TimeString+dayOfMonth+"-"+MonthNames[month]+"-"+year+" Time:
";
    if (hour<10) {TimeString = TimeString+"0";}
    TimeString = TimeString+hour+":";
    if (minute<10) {TimeString = TimeString+"0";}
```

```
    TimeString = TimeString+minute+":";
    if (second<10) {TimeString = TimeString+"0";}
    TimeString = TimeString+second;
if (ThresholdManual==1){
ThresholdSetting=ThresholdSettingL+","+ThresholdSettingH;
}
ToPrint=FileName+fps+" "+SizeSetting+" "+CircularitySetting+" "+ThresholdSetting+"
"+TimeString;
print(ToPrint);
FileNameList=Array.concat(FileNameList,FileName+fps+".txt");

DrawingFile="Drawing of "+FullFileName;
roiManager("Save", savedirectory+FileSaveFormat+" Roiset.zip");

selectWindow("Results");
saveAs("Text",savedirectory+FileSaveFormat);
beep();

//selectWindow(FileSaveFormat+" Drawing.tif");
selectWindow(DrawingFile);
close();
selectWindow("Results");
run("Close");
selectWindow("ROI Manager");
run("Close");
selectWindow(FolderList[k]);
run("Close");
}
selectWindow("Log");saveAs("Text",savedirectory+"LogCellIdentification");selectWind
ow("Log");run("Close");
for (j=1; j<FileNameList.length; j++) {

print(FileNameList[j]);
}
selectWindow("Log");saveAs("Text",savedirectory+"ListForMATLABCellMatching");s
electWindow("Log");run("Close");
Dialog.create("ImageJ Cell Identification");
Dialog.addMessage("Cell identification is completed. Place MATLAB code into the same
folder and run.");
Dialog.show();
```

Appendix C MATLAB Cell Matching Code

```
%Seeto, Wen Jun (Aaron). Department of Chemical Engineering. Auburn University, Auburn, AL.
clc;clear;CodeVersion='v318';
%Parameters to set:
ListOfImageJTrackingFiles='ListForMATLABCellMatching.txt';
OutputFileName_AnalyzedCells=['Rolling ECFC sample_' CodeVersion '_' ListOfImageJTrackingFiles(1:end-4) '.xlsx'];
OutputSheetName_AnalyzedCells=ListOfImageJTrackingFiles(1:end-4);
%Chamber dimensions
ChamberWidth=2.5;%mm
ChamberLength=15;%mm
ChamberThickness=0.127;%mm
FOVwidth=500;%um
%Cell properties
Cutoff_specific_rolling_velocity=0.4;%percentage
Cutoff_deltaY_coefficient=0.5;%percentage
% Cutoff_deltaY=CellDiameter_average*Cutoff_deltaY_coefficient;
Cutoff_deltaArea_percentage=0.3;%percentage
%MATLAB matching & analysis parameters
Cutoff_trackedframes_percentage=0.7;
% Cutoff_tether_time=0.1;%seconds
% Cutoff_capture_time=3;%seconds
% Cutoff_capture_speed=15;%um/s
Cutoff_rolling_frames=0.8;%percentage of frames that are below rolling cutoff
deltaSlice_cutoff_initial=1;

extraMaxCell=500;
extraMaxCellRow=500;

HorizontalHeadingsExtra={'FPS' 'Displacement (um)' 'Velocity (um/s)' 'Cell Status'};
RollingPercentageTxt1='Rolled <';RollingPercentageTxt2='% of the frames';
RollingPercentageTxt=[RollingPercentageTxt1 num2str(Cutoff_rolling_frames*100) RollingPercentageTxt2];
ToAnalysisSummaryHeadings={'Object';'Material';'ExpDate';'Trial';'Video num';'Shear rates (1/s)';'Rolling (um/s)';'STD';'Max(um/s)';'Min(um/s)';'Matched';'%Rolling';'Rolling cells';'NonRolling'};%;'Captured';'Tethered';'Interacted with Material (Roll+Captured+Tethered)';'%Interacted with Material';'%Captured/Interacted';'Captured Area (um2)';'%Tethered/Interacted'};
ToMinitabHeadings={'Object' 'Material' 'Shear rate(1/s)' 'Trial' 'Video num' 'Video file name' 'Rolling avg (um/s)' 'Rolling %' 'Tracked frames' 'Rolling time (s)'};
ToMinitabAll=[];ToAnalysisSummaryAll=[];
```

```
%================================================================
=========
%Load cell data from ImageJ cell identification
List=importdata(ListOfImageJTrackingFiles);
MaxCell_added=zeros(length(List),1);
MaxCellRow_added=MaxCell_added;
cells_cleared=MaxCell_added;
%Matching
for ListLoop=1:length(List)
   %If you want to pause the code, create and place a "PauseMatching.txt" in the dir
   [status, result] = system('dir PauseMatching');
   if status == 0
      delete('PauseMatching.txt')
      fprintf('\n Code is paused. To continue, click "F5".');
      keyboard
   end
   fprintf('\n \nPreparing file %s (%2.0f/%2.0f) ',List{ListLoop},ListLoop,length(List));

   [celltype,remain]=strtok(List{ListLoop},' ');
   [material,remain]=strtok(remain,' ');
   [concentration,remain]=strtok(remain,' ');
   [exp_date,remain]=strtok(remain,' ');
   [n_num,remain]=strtok(remain,' ');
   [sr,remain]=strtok(remain,' ');
   [file_number,remain]=strtok(remain(2:end),'.');
   [video_format,remain]=strtok(remain,'_');
   [FPS,remain]=strtok(remain,'txt');
   FPS=FPS(2:end-1);
   fps=str2num(FPS);
   [n_numLoop,remain]=strtok(n_num,'n');
   n_num=['n' num2str(n_numLoop)];
   FileName=[celltype ' ' material ' ' concentration ' ' exp_date ' ' n_num  ' ' sr ' ' file_number
video_format '_' FPS '.txt'];
   OutputFileName_Matched=['Matched_' CodeVersion '_' celltype '_' material '_'
concentration '_' exp_date '_' n_num  '_rolling.xlsx'];

   ShearRate=str2num(sr);
   MaxCellRow=3000;MaxCell=5000;%This uses about 2GB of memory for the variable
Cells
   maxcell_exceeded=0;cells_stop_clear=0;

   %Reset viables
   clear SRnumTemp SRtxtTemp SRrawTemp Col_Label_All Col_FileName_All
Cells_FileName rolling_data
```

```
    clear Col_Area_All Col_X_All Col_Y_All Col_circ_All
    clear Col_Slice_All Col_Roundness_All Col_Solidity_All HorizontalHeadings
    clear RolledDistance NonRolledDistance TetheredDistance CapturedDistance
    clear RolledVelocity NonRolledVelocity TetheredVelocity CapturedVelocity

    rolling_data=importdata(FileName);

    Col_Label=1;
    Col_FileName=find(strcmp(rolling_data.textdata(1,:),'Label'));
    Col_Area=find(strcmp(rolling_data.textdata(1,:),'Area'));
    Col_X=find(strcmp(rolling_data.textdata(1,:),'XM'));
    Col_Y=find(strcmp(rolling_data.textdata(1,:),'YM'));
    Col_circ=find(strcmp(rolling_data.textdata(1,:),'Circ.'));
    Col_Slice=find(strcmp(rolling_data.textdata(1,:),'Slice'));
    Col_MinFeret=find(strcmp(rolling_data.textdata(1,:),'MinFeret'));
    Col_Roundness=find(strcmp(rolling_data.textdata(1,:),'Round'));
    Col_Solidity=find(strcmp(rolling_data.textdata(1,:),'Solidity'));

    HorizontalHeadings=rolling_data.textdata(1,:);
    HorizontalHeadings{1}='Cell';
    HorizontalHeadings=[HorizontalHeadings HorizontalHeadingsExtra];

    [rolling_data_textdata_Row,rolling_data_textdata_Col]=size(rolling_data.textdata);

Col_FPS=rolling_data_textdata_Col+1;Col_Displacement=Col_FPS+1;Col_Velocity=C
ol_Displacement+1;Col_CellStatus=Col_Velocity+1;

    clear SRnum TrackedFrames
    rolling_data_data_Row=length(rolling_data.data(:,1));
    rolling_data_filler=NaN(rolling_data_data_Row,1);
    SRnum=[str2double(rolling_data.textdata(2:end,Col_Label))          rolling_data_filler
rolling_data.data];
    [rolling_data_data_Row,rolling_data_data_Col]=size(rolling_data.data);

    SRtxt=cell(rolling_data_textdata_Row,1);
    SRnum=[SRnum repmat(fps,[rolling_data_data_Row 1])];
    %Store shear rate
    SRtxt{1}=sr;

SRtxt(2:rolling_data_textdata_Row)=rolling_data.textdata(2:rolling_data_textdata_Row,
Col_FileName);
    clear rolling_data %To free memory
    ToExportAll_row_num=rolling_data_data_Row+1;
    ToExportAll=cell(ToExportAll_row_num,rolling_data_data_Col);
```

```
    fprintf('\n  Matching:');
    Cell_Diameter_all(ListLoop)=round(median(SRnum(:,Col_MinFeret)));%um
    x_max=max(SRnum(:,Col_X));
    cell_diameter_average=Cell_Diameter_all(ListLoop);
    Cutoff_deltaY=cell_diameter_average*Cutoff_deltaY_coefficient;
    Flow_velocity_average(ListLoop)=ShearRate*(ChamberThickness*1000)/6;%um/s
    b=ChamberThickness/2*1000;%um
    y_cell=b-cell_diameter_average;%mm
    velocity_at_one_cell_diameter=Flow_velocity_average(ListLoop)/b^2*(b^2-y_cell^2);

Cutoff_velocity_percentage_at_one_cell_diameter=velocity_at_one_cell_diameter/Flow_
velocity_average(ListLoop);
    %set cutoff_rolling_percentage for different materials
    if strcmp(material,'PEGDA')||strcmp(material,'RGES') == 1 %for non-specific
interactions
        Cutoff_rolling_percentage=Cutoff_velocity_percentage_at_one_cell_diameter;
    else
        Cutoff_rolling_percentage=Cutoff_specific_rolling_velocity;
    end

Cutoff_velocity_at_one_cell_diameter(ListLoop)=Flow_velocity_average(ListLoop)*Cut
off_velocity_percentage_at_one_cell_diameter;

Cutoff_rolling(ListLoop)=Flow_velocity_average(ListLoop)*Cutoff_rolling_percentage;

Cutoff_trackedframes=fps*FOVwidth/Cutoff_velocity_at_one_cell_diameter(ListLoop)*
Cutoff_trackedframes_percentage;

    clearing_start=-1;

    row_count=1;
    cell_num=0;
    matching_i_start=1;matching_j_start=1;
    row_count_show=0;
    Cells=NaN(MaxCellRow,rolling_data_data_Col,MaxCell);
    last_frame_num_of_each_cell=NaN(MaxCell,1);
    Cells_mean_deltaX=NaN(round(rolling_data_textdata_Row/2),MaxCell);
    deltaSlice_cutoff_max=fps/3;%Max number of frames apart for each cell

    %Repeat to check every row----------------------------------
    total_row=rolling_data_data_Row;
    while row_count<=total_row
        if maxcell_exceeded ==1
```

```
        break
    end
    %Show matching progress
    if floor(row_count/(total_row/10))>row_count_show
        matching_progress=10*(1+row_count_show);
        if matching_progress<100
            fprintf('...%2.0f%%',matching_progress);
        end
        row_count_show=row_count_show+1;
    end

    %Initiate cell list for current video
    %If current row is a new video, store all cells in current slice to array "cell"
    if SRnum(row_count,Col_Label)==1 %1 means new tracking video

        %store all cells in first slice to Cells
        slice_next=SRnum(row_count,Col_Slice);
        slice=slice_next;
        while slice==slice_next
            %Store current slice to cell
            cell_num=cell_num+1;
            Cells_FileName(cell_num,1)=SRtxt(row_count+1);%celltxt(cell#,shear rate)
            SRnumCol=length(SRnum(row_count,:));

Cells(1,1:SRnumCol,cell_num)=SRnum(row_count,:);%cell(sequence,location,cell#)
            last_frame_num_of_each_cell(cell_num)=SRnum(row_count,Col_Slice);
            row_count=row_count+1;
            slice=slice_next;
            slice_next=SRnum(row_count,Col_Slice);
        end
    end

    %Store all cells in new slice to temp and then match
    clear temp temptxt
    temp_num=0;
    slice=slice_next;
    while slice==slice_next
        temp_num=temp_num+1;
        temptxt(temp_num,ListLoop)=SRtxt(row_count+1);
        temp(temp_num,:)=SRnum(row_count,:);
        row_count=row_count+1;
        slice=slice_next;
        if row_count>total_row
            slice_next=0;
```

```
        else
            slice_next=SRnum(row_count,Col_Slice);
        end
    end

    %match cells in new frame to cell list
    for matching_i=1:length(temp(:,1))
        matched=0;clear cells_to_match
        cells_to_match=find(last_frame_num_of_each_cell>=(slice-round(fps)));
        matching_j_times=length(cells_to_match);
        if temp(matching_i,Col_Label)==98
            a=1;
        end
        for matching_j=1:matching_j_times
            matching_cells=cells_to_match(matching_j);
            lastslice_of_matching_cells=find(isnan(Cells(:,Col_Y,matching_cells))        ==
1,1,'first')-1;

            %Determine the maximum of frames apart for matching due to
            %cells being obscured by another
            if lastslice_of_matching_cells==1 %For Cells with only one matched frame
                deltaFrame_max=deltaSlice_cutoff_initial;
            else
                %Equation 3

deltaX_deltaFrame=(Cells(lastslice_of_matching_cells,Col_X,matching_cells)-
Cells(1,Col_X,matching_cells))/(Cells(lastslice_of_matching_cells,Col_Slice,matching_c
ells)-Cells(1,Col_Slice,matching_cells));
                %Equation 2
                deltaFrame_max=floor(cell_diameter_average/deltaX_deltaFrame);
            end


            deltaFrame=temp(matching_i,Col_Slice)-
Cells(lastslice_of_matching_cells,Col_Slice,matching_cells);
            if                    lastslice_of_matching_cells>1                    &&
Cells(lastslice_of_matching_cells,Col_X,matching_cells)+deltaX_deltaFrame*deltaFram
e>x_max %if predicted-x>width of frame, skip to next cell
                continue
            end
            if deltaFrame<=deltaFrame_max && deltaFrame>0%deltaFrame>0 to prevent
matching temp to matched temp
                deltaY=abs(temp(matching_i,Col_Y)-
Cells(lastslice_of_matching_cells,Col_Y,matching_cells));
```

```
            if deltaY<Cutoff_deltaY %compare Y
                deltaX=temp(matching_i,Col_X)-
Cells(lastslice_of_matching_cells,Col_X,matching_cells);
                deltaArea=abs(temp(matching_i,Col_Area)-
Cells(lastslice_of_matching_cells,Col_Area,matching_cells))/Cells(lastslice_of_matchin
g_cells,Col_Area,matching_cells);

                %Adust deltaX_cutoff w.r.t. difference in frame
                if deltaFrame==1

deltaX_max=Cutoff_velocity_at_one_cell_diameter(ListLoop)/fps;%Equation 1
                    deltaX_max_current=deltaX_max;
                elseif deltaFrame>1
                    deltaXmax_deltaFrame=deltaX_max*deltaFrame;%Equation 4
                    if deltaXmax_deltaFrame>=cell_diameter_average
                        deltaXmax_deltaFrame=cell_diameter_average;%Equation 5
                    end
                    deltaX_max_current=deltaXmax_deltaFrame;
                end

                if  deltaX>-(cell_diameter_average/2) && deltaX<deltaX_max_current
&& deltaArea<Cutoff_deltaArea_percentage %compare X and Area
                    tempCol=length(temp(matching_i,:));

Cells(lastslice_of_matching_cells+1,1:tempCol,matching_cells)=temp(matching_i,:);

last_frame_num_of_each_cell(matching_cells)=temp(matching_i,Col_Slice);

                    if      lastslice_of_matching_cells+1==MaxCellRow      %Increase
MaxCellRow
                        Cells(MaxCellRow+1:MaxCellRow+extraMaxCellRow,:,:)=NaN;
                        %
Cells_mean_deltaX(MaxCellRow+1:MaxCellRow+extraMaxCellRow,:)=NaN;
                        MaxCellRow=MaxCellRow+extraMaxCellRow;
                        MaxCellRow_added(ListLoop)=MaxCellRow_added(ListLoop)+1;
                    end

                    matched=1;
                    break
                end
            end
        end
    end
```

```
        %Store unmatched cell to a new "Cells"
        if matched==0
            cell_num=cell_num+1;
            %When the number of cells (cell_num) reaches MaxCell, clear Cells with less
than 5 matched frames
            if cell_num>MaxCell && cells_stop_clear==0
                %If you want to pause the code, create and place a "PauseMatching.txt" in the
dir
                [status, result] = system('dir PauseMatching');
                if status == 0
                    delete('PauseMatching.txt')
                    fprintf('\n Code is paused. To continue, click "F5".');
                    keyboard
                end
                %Find Cells with less than 5 matched frames
                cells_to_clear=[];cells_to_keep=[];

cells_to_clear_tofind=find(last_frame_num_of_each_cell>deltaSlice_cutoff_max,1,'last');
                cells_to_clear=find(isnan(Cells(6,1,1:cells_to_clear_tofind))==1);
                cells_to_keep=find(isnan(Cells(6,1,1:cells_to_clear_tofind))==0);
                Cells(:,:,cells_to_clear)=NaN;
                Cells_FileName_temp(cells_to_keep,1)=Cells_FileName(cells_to_keep);
                Cells_FileName=cell(MaxCell,1);
                Cells_FileName(cells_to_keep,1)=Cells_FileName_temp(cells_to_keep);
                clear Cells_FileName_temp

                last_frame_num_of_each_cell(cells_to_clear)=NaN;
                [~,cells_sortOrder] = sort(Cells(1,1,:),3);
                Cells = Cells(:,:,cells_sortOrder);
                cells_sortOrder1=squeeze(cells_sortOrder);
                Cells_FileName=Cells_FileName(cells_sortOrder1);

last_frame_num_of_each_cell=last_frame_num_of_each_cell(cells_sortOrder1);
                cells_cleared(ListLoop)=cells_cleared(ListLoop)+1;
                if length(cells_to_keep)>MaxCell*0.9 %Do not clear and sort Cells if
cells_to_keep is getting close to MaxCell
                    cells_stop_clear=1;
                end
                cell_num=find(isnan(Cells(1,1,:))==1,1,'first');
            elseif cell_num>MaxCell && cells_stop_clear==1
                last_frame_num_of_each_cell(MaxCell+1:MaxCell+extraMaxCell,1)=NaN;
                Cells(:,:,MaxCell+1:MaxCell+extraMaxCell)=NaN;
```

```
MaxCell=MaxCell+extraMaxCell;MaxCell_added(ListLoop)=MaxCell_added(ListLoop)
+1;
            end

Cells_FileName(cell_num,1)=temptxt(matching_i,ListLoop);%celltxt(cell#,shear rate)
            tempCol=length(temp(matching_i,:));

Cells(1,1:tempCol,cell_num)=temp(matching_i,:);%cell(sequence,location,cell#)
            last_frame_num_of_each_cell(cell_num)=temp(matching_i,Col_Slice);

         end
      end

      if isnan(slice_next)==1 && row_count<total_row
         row_count=row_count+1;
      end
   end
   clear Cells_mean_deltaX %To free memory
   if maxcell_exceeded==0
      fprintf('...100%%');
   end

   %If you want to pause the code, create and place a "PauseMatching.txt" in the dir
   [status, result] = system('dir PauseMatching.txt');
   if status == 0
      delete('PauseMatching.txt')
      fprintf('\n Code is paused. To continue, click "F5".');
      keyboard
   end

   fprintf('\n  Analyzing\n');
   ToExport_Cells_FileName=[];
   AvgVelocity=[];
   analysis_counter=0;
   Inst_counter=0;
   Cells_concatenate=[];
%     Captured=[];    CapturedTxt=[];    CapturedCellStatus=[];
%     Tethered=[];    TetheredTxt=[];    TetheredCellStatus=[];
   Rolled=[];                    RolledTxt=[];                    RolledCellStatus=[];
RolledVelocity=[];Rolled_tracked_frames=[];
   NonRolled=[];   NonRolledTxt=[];   NonRolledCellStatus=[];
   filledCells_FileName=[];tracked_frames=[];
   ToAnalysis=[];Rolled_FileName=[];
```

```
%     Cutoff_capture_frames=floor(Cutoff_capture_time*fps);
%     Cutoff_tether_frames=floor(Cutoff_tether_time*fps);
   cells_to_analyse=find(isnan(Cells(floor(Cutoff_trackedframes),1,:)) == 0);
   analysis_i_end=length(cells_to_analyse);%find(isnan(Cells(1,1,:))      ==      1,1,'first')-
1;%Find the number of tracked cells
   Cells_finalrow=NaN(analysis_i_end,1);
   RollingPercentage=[]; RollingTime=RollingPercentage; %Reset
   num_nonrolled=0;num_rolled=0;
%     num_captured=0;num_tethered=0;
   for analysis_i=1:analysis_i_end
      analysing_cell=cells_to_analyse(analysis_i);
      Cells_finalrow(analysing_cell)=find(isnan(Cells(:,1,analysing_cell)) == 1,1,'first')-1;
      analysis_j_end=Cells_finalrow(analysing_cell);
      %Analyze Cells that meet the minimum tracked frames & determine if
      %rolled
      if analysis_j_end>Cutoff_trackedframes
         clear Inst_Distance Inst_Velocity Inst_VelocityFilled CellsCurrent
         Inst_counter=Inst_counter+1;
         Cells_calculation_counter_start=Inst_counter;
         analysis_counter=analysis_counter+1;

ToExport_Cells_FileName=[ToExport_Cells_FileName;Cells_FileName(analysing_cell,
1)];


Inst_Distance(1,1)=0;Inst_Velocity=Inst_Distance;Inst_VelocityFilled=Inst_Velocity;tra
cked_frames(analysis_counter,1)=0;
         for analysis_j=2:analysis_j_end       %count total tracked frames
            slice_filling_difference=Cells(analysis_j,Col_Slice,analysing_cell)-
Cells(analysis_j-1,Col_Slice,analysing_cell);
            Inst_counter=Inst_counter+1;
            Inst_Distance=[Inst_Distance;           ((Cells(analysis_j,Col_X,analysing_cell)-
Cells(analysis_j-1,Col_X,analysing_cell))^2+(Cells(analysis_j,Col_Y,analysing_cell)-
Cells(analysis_j-1,Col_Y,analysing_cell))^2)^0.5];
            Inst_Velocity=[Inst_Velocity;Inst_Distance(end)*fps/slice_filling_difference;];
            if slice_filling_difference==1
               tracked_frames(analysis_counter,1)=tracked_frames(analysis_counter,1)+1;

Inst_VelocityFilled=[Inst_VelocityFilled;Inst_Distance(end)*fps/slice_filling_difference;
];
            elseif slice_filling_difference>1

tracked_frames(analysis_counter,1)=tracked_frames(analysis_counter,1)+slice_filling_di
fference+1;
```

```
            Inst_VelocityFilled=[Inst_VelocityFilled;
repmat(Inst_Velocity(end),[slice_filling_difference+1 1])];
        end
    end
    rolling_percentage=(length(find(Inst_VelocityFilled<Cutoff_rolling(ListLoop)))-
1)/tracked_frames(analysis_counter)*100;
    rolling_time=tracked_frames(analysis_counter)*rolling_percentage/100/fps;

    fillerCellStatus=cell(analysis_j_end-1,1);

filledCells_FileName=[ToExport_Cells_FileName(analysis_counter);fillerCellStatus];
    cells_current=[Cells(1:Cells_finalrow(analysing_cell),:,analysing_cell)
Inst_Distance Inst_Velocity];
    cells_current=num2cell(cells_current);

    if rolling_percentage/100<Cutoff_rolling_frames%non-rolling
        AvgVelocity{analysis_counter}=RollingPercentageTxt;
        num_nonrolled=num_nonrolled+1;
        clear NonRolledCurrent NonRolledCellStatus
        NonRolledCellStatus=[RollingPercentageTxt;fillerCellStatus;];
        NonRolledCurrent=[cells_current NonRolledCellStatus;];
        NonRolledCurrent(:,Col_FileName)=filledCells_FileName;
        NonRolled=[NonRolled;NonRolledCurrent];

    else
        AvgVelocity{analysis_counter,1}=mean(Inst_VelocityFilled);
        num_rolled=num_rolled+1;
        clear RolledCurrent RolledCellStatus
        RolledCellStatus=[AvgVelocity(analysis_counter);fillerCellStatus;];
        RolledCurrent=[cells_current RolledCellStatus;];
        RolledCurrent(:,Col_FileName)=filledCells_FileName;
        Rolled=[Rolled;RolledCurrent];
        RolledVelocity=[RolledVelocity;mean(Inst_VelocityFilled)];
        RollingPercentage=[RollingPercentage;rolling_percentage];

Rolled_tracked_frames=[Rolled_tracked_frames;tracked_frames(analysis_counter)];
        RollingTime=[RollingTime;rolling_time];

Rolled_FileName=[Rolled_FileName;ToExport_Cells_FileName(analysis_counter)];
    end
  end
end

if isempty(RolledVelocity)==1
```

```
        continue
    end
    RollingAvg(ListLoop)=mean(RolledVelocity);
    RollingStd(ListLoop)=nanstd(RolledVelocity);
    RollingMax(ListLoop)=nanmax(RolledVelocity);
    RollingMin(ListLoop)=nanmin(RolledVelocity);
    RollingNum(ListLoop)=num_rolled;
    Num_nonrolling(ListLoop)=num_nonrolled;
    Num_captured(ListLoop)=0;%num_captured;
    Num_tethered(ListLoop)=0;%num_tethered;

Num_interacted(ListLoop)=RollingNum(ListLoop)+Num_captured(ListLoop)+Num_tet
hered(ListLoop);

Num_matched_cell(ListLoop)=RollingNum(ListLoop)+num_nonrolled+Num_captured(
ListLoop)+Num_tethered(ListLoop);
    RollingRatio(ListLoop)=RollingNum(ListLoop)/Num_matched_cell(ListLoop)*100;

CapturedRollingRatio(ListLoop)=Num_captured(ListLoop)/(RollingNum(ListLoop)+Nu
m_captured(ListLoop)+Num_tethered(ListLoop))*100;

InteractedRatio(ListLoop)=(RollingNum(ListLoop)+Num_captured(ListLoop)+Num_tet
hered(ListLoop))/Num_matched_cell(ListLoop)*100;
    if Num_captured(ListLoop)~=0
        CapturedArea(ListLoop)=sum(captured_lastframe(:,3));
    else
        CapturedArea(ListLoop)=0;
    end

TetheredRollingRatio(ListLoop)=Num_tethered(ListLoop)/(RollingNum(ListLoop)+Nu
m_captured(ListLoop)+Num_tethered(ListLoop))*100;
    Matched_cell_num(ListLoop)=analysis_counter;

    clear to_analysis ToAnalysisSummary ToMinitab ToMinitabCelltype
ToMinitabMaterial ToMinitabShearRate ToMinitabnnum ToMinitabVidNum
    to_analysis_rolling=[RolledVelocity RollingPercentage Rolled_tracked_frames
RollingTime];
    to_analysis_rolling=num2cell(to_analysis_rolling);
    ToAnalysis=[ToAnalysis;Rolled_FileName to_analysis_rolling];

    num_ToAnalysis=length(ToAnalysis(:,1));
    ToMinitabCelltype(1:num_ToAnalysis)={celltype};
    ToMinitabMaterial(1:num_ToAnalysis)={material};
    ToMinitabShearRate(1:num_ToAnalysis)=num2cell(ShearRate);
```

```
   ToMinitabnnum(1:num_ToAnalysis)={n_numLoop};
   ToMinitabVidNum(1:num_ToAnalysis)={file_number};
   ToMinitab=[ToMinitabCelltype' ToMinitabMaterial' ToMinitabShearRate'
ToMinitabnnum' ToMinitabVidNum' ToAnalysis];
   ToMinitabAll=[ToMinitabAll;ToMinitab];


ToAnalysisSummary=[ShearRate;RollingAvg(ListLoop);RollingStd(ListLoop);RollingM
ax(ListLoop);RollingMin(ListLoop);Num_matched_cell(ListLoop);RollingRatio(ListLoo
p);RollingNum(ListLoop);Num_nonrolling(ListLoop)];%;Num_captured(ListLoop);Num
_tethered(ListLoop);Num_interacted(ListLoop);InteractedRatio(ListLoop);CapturedRolli
ngRatio(ListLoop);CapturedArea(ListLoop);TetheredRollingRatio(ListLoop)];
   ToAnalysisSummary=num2cell(round(ToAnalysisSummary*100)/100);
   ToAnalysisSummary=[celltype; material; exp_date; n_numLoop; file_number;
ToAnalysisSummary];
   ToAnalysisSummaryAll=[ToAnalysisSummaryAll ToAnalysisSummary];

   if isempty(Rolled)==0
      sheetname_rolled=[num2str(ShearRate) '_' file_number '_Rolled'
num2str(num_rolled)];
      Rolled=[HorizontalHeadings(1:length(Rolled(1,:))); Rolled;];
      xlswrite(OutputFileName_Matched, Rolled(:,:),sheetname_rolled);
   end
   if isempty(NonRolled)==0
      sheetname_nonrolled=[num2str(ShearRate) '_' file_number '_NonRolled'
num2str(num_nonrolled)];
      NonRolled=[HorizontalHeadings(1:length(NonRolled(1,:))); NonRolled;];
      xlswrite(OutputFileName_Matched, NonRolled(:,:),sheetname_nonrolled);
   end
end

%If you want to pause the code, create and place a "PauseMatching.txt" in the dir
[status, result] = system('dir PauseMatching');
if status == 0
   delete('PauseMatching.txt')
   fprintf('\n Code is paused. To continue, click "F5".');
   keyboard
end

ToMinitabAll=[ToMinitabHeadings;ToMinitabAll];
ToAnalysisSummaryAll=[ToAnalysisSummaryHeadings ToAnalysisSummaryAll];
xlswrite(OutputFileName_AnalyzedCells,
ToMinitabAll,OutputSheetName_AnalyzedCells,'A1');
ToAnalysisSummaryAll=ToAnalysisSummaryAll';
```

```
if length(ToMinitabHeadings)<25
   col_ToAnalysisSummaryAll=char(length(ToMinitabHeadings)+'A'-1+2);
else
   col_ToAnalysisSummaryAll='';
   for i=1:floor(length(ToMinitabHeadings)/26)+1
      col_ToAnalysisSummaryAll=[col_ToAnalysisSummaryAll 'A'];
   end
   col_ToAnalysisSummaryAll=[col_ToAnalysisSummaryAll
char(length(ToMinitabHeadings)-26*i+'A'-1+2)];
end

xlswrite(OutputFileName_AnalyzedCells,
ToAnalysisSummaryAll,OutputSheetName_AnalyzedCells,[col_ToAnalysisSummaryAll
'1']);
fprintf('\n \n Matching done.\n');
```

Appendix D Mass Spectrometry

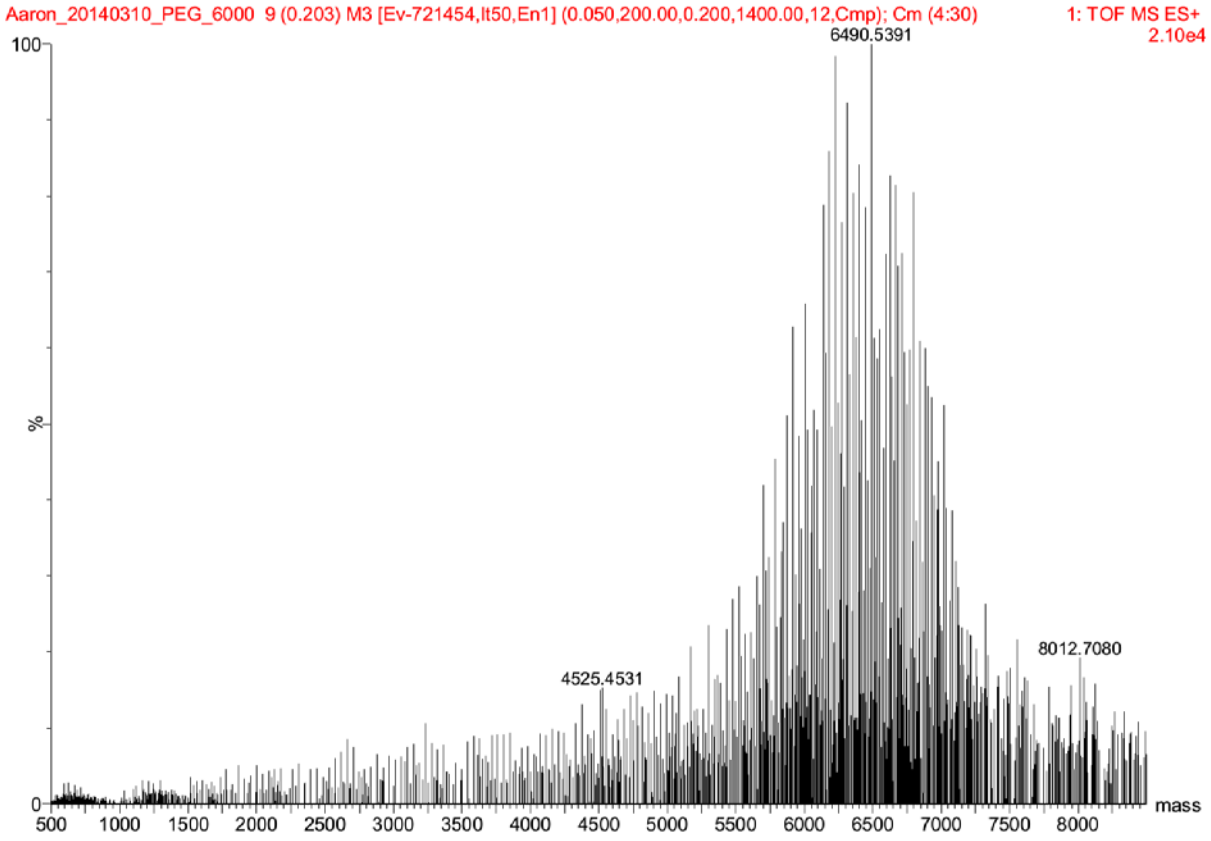

Appendix D.1 Mass spectrometry to confirm the molecular weight of PEG 6000.

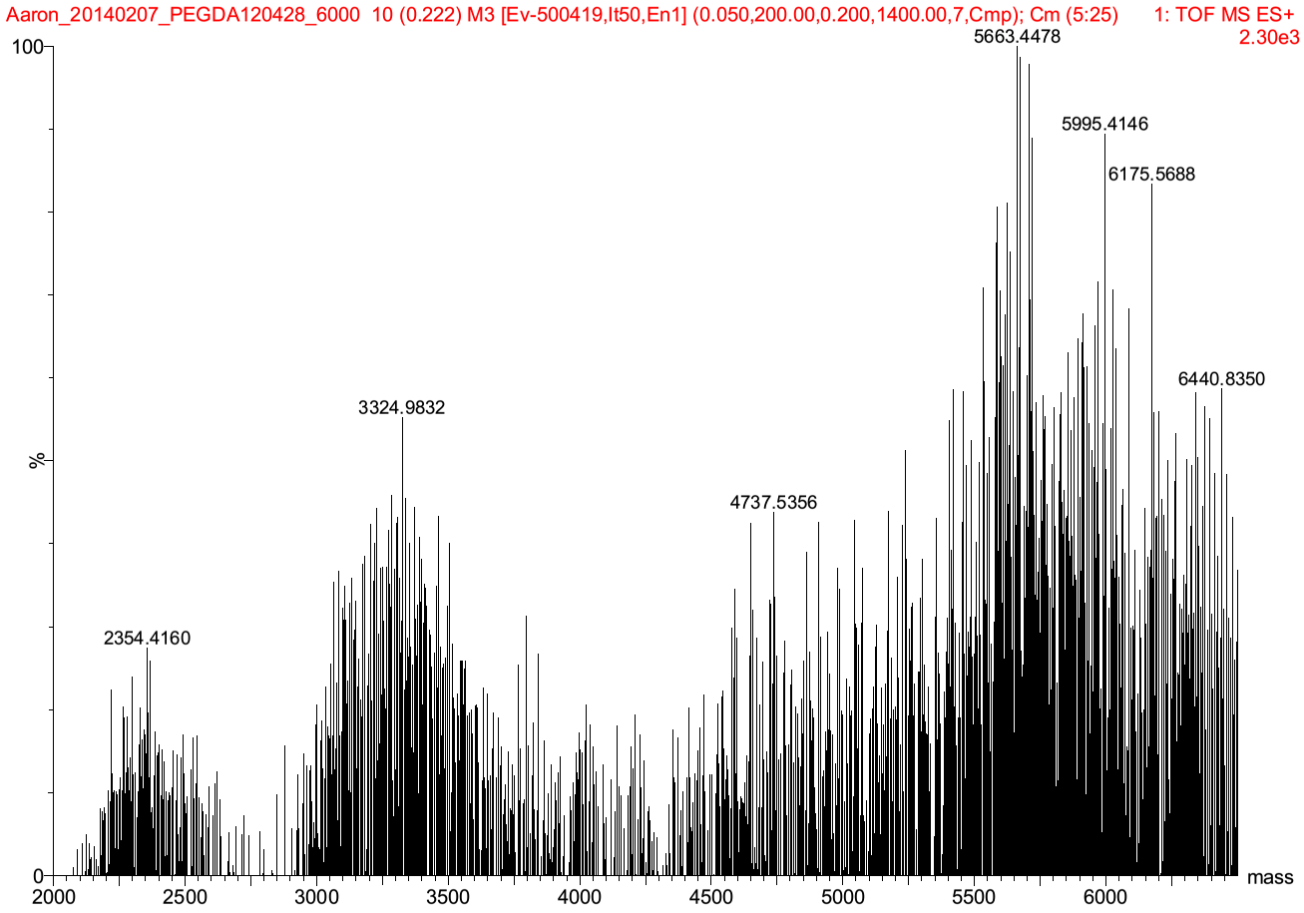

Appendix D.2 Mass spectrometry to confirm the molecular weight of PEGDA 6000.

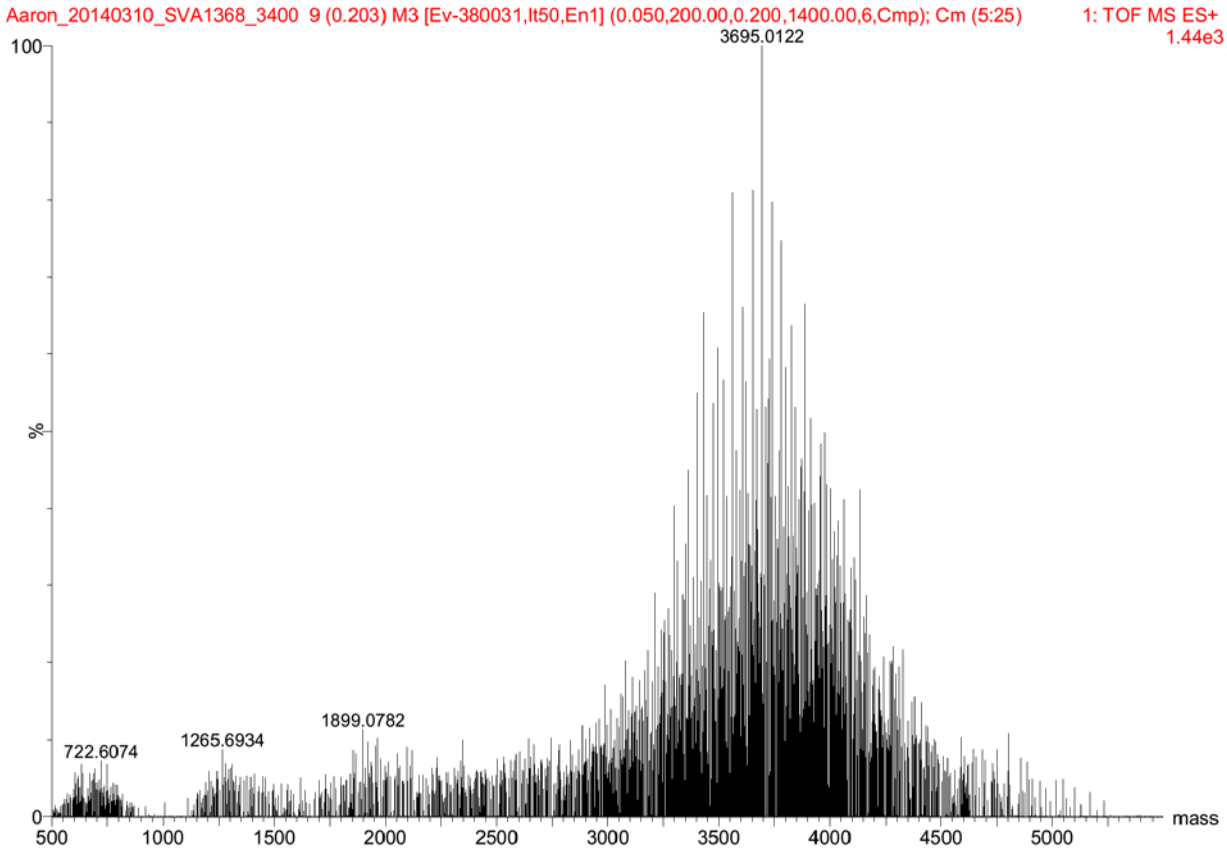

Appendix D.3 Mass spectrometry to confirm the molecular weight of acryl-PEG-SVA.

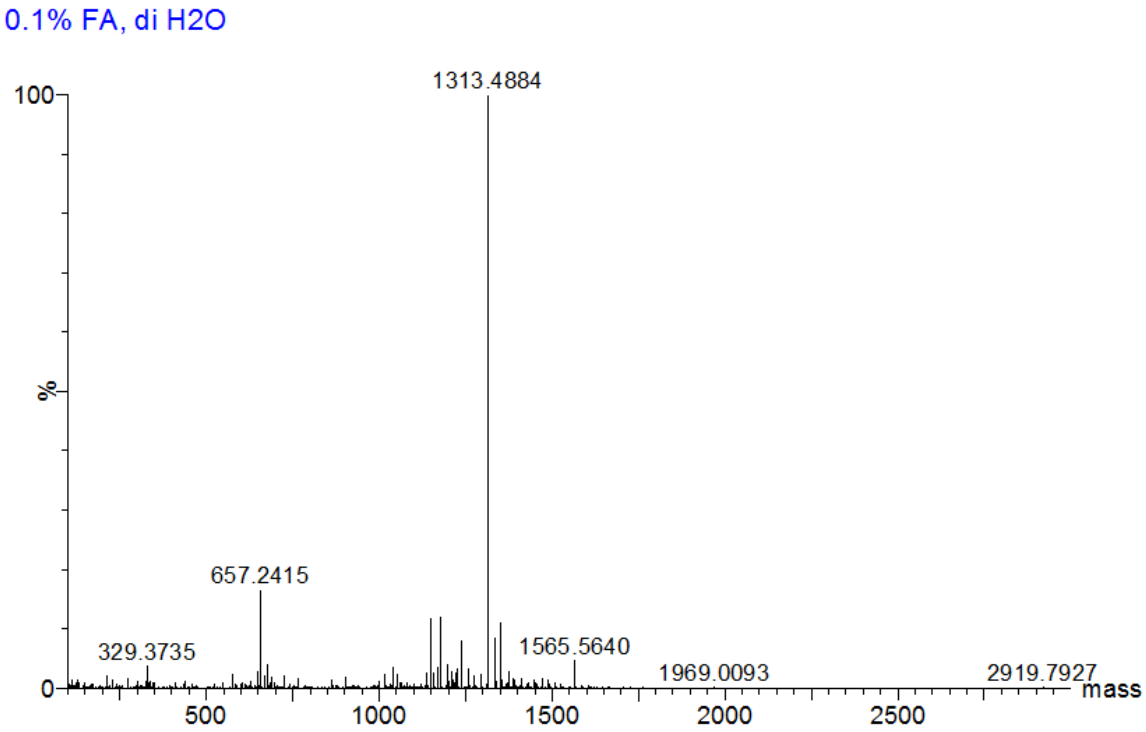

Appendix D.4 Confirmation of the mass of 6HRGDS by mass spectrometry. The peak 1313.4884 represented the protonized 6HRGDS which has a MW of 1312.556.

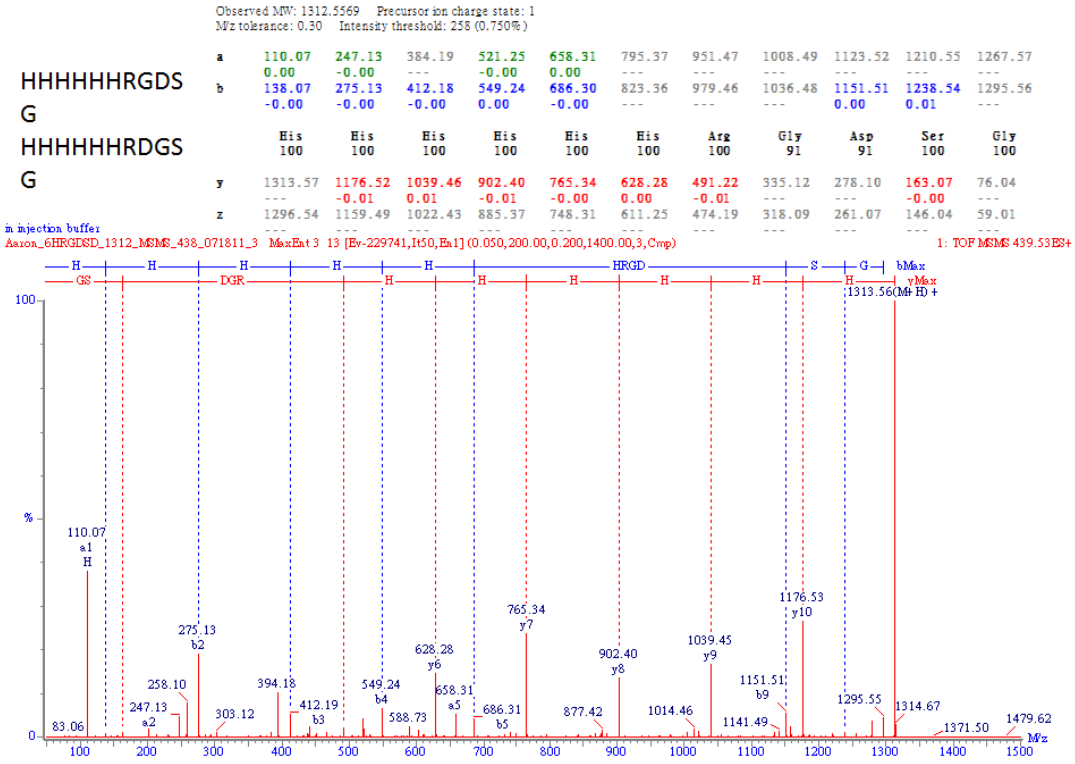

Appendix D.5 Sequencing result showing that the peptide HHHHHHRGDS was synthesized.

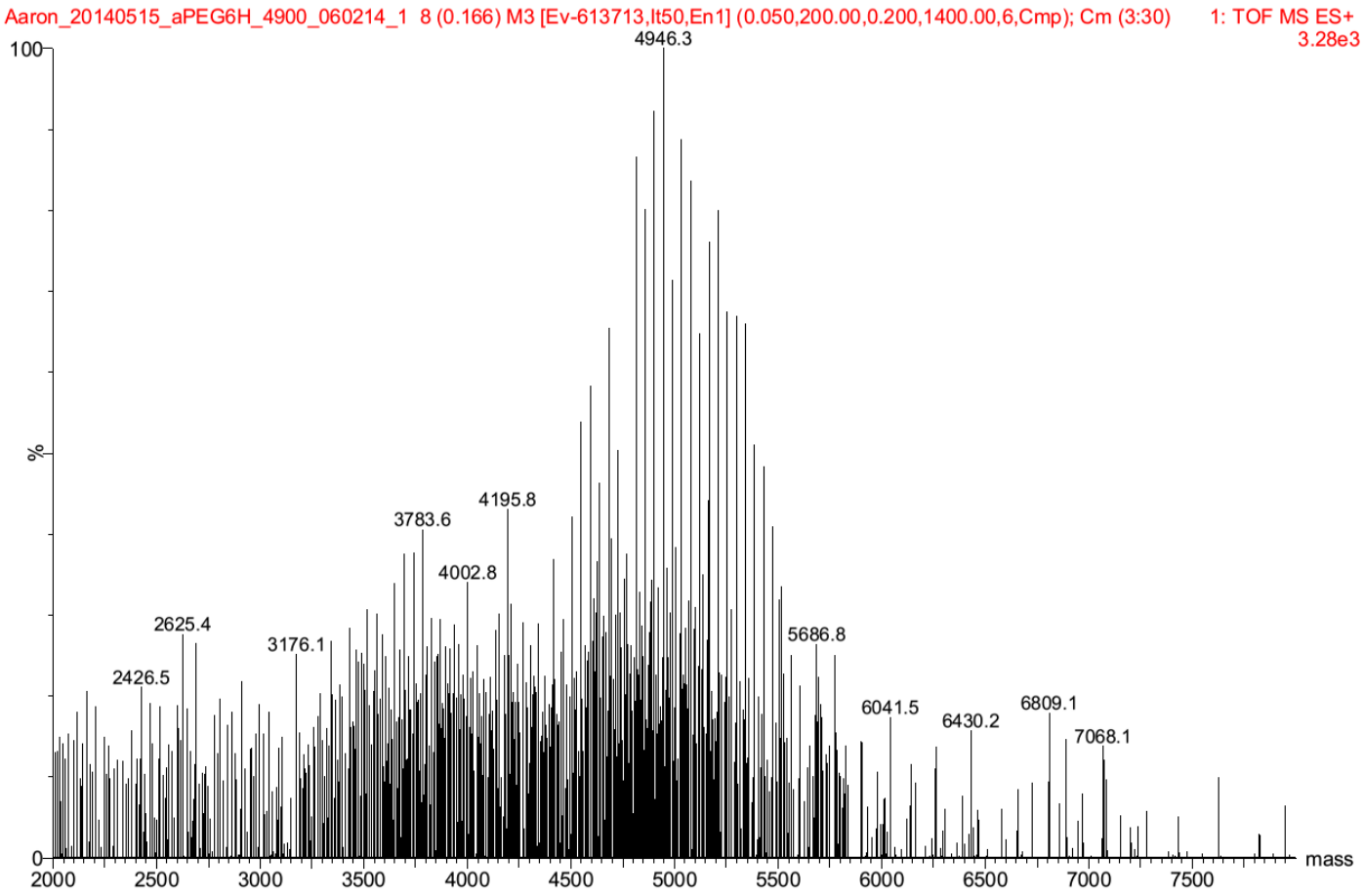

Appendix D.6 Confirmation of the acryloyl-PEG-HHHHHHRGDS conjufation by mass spectrometry.

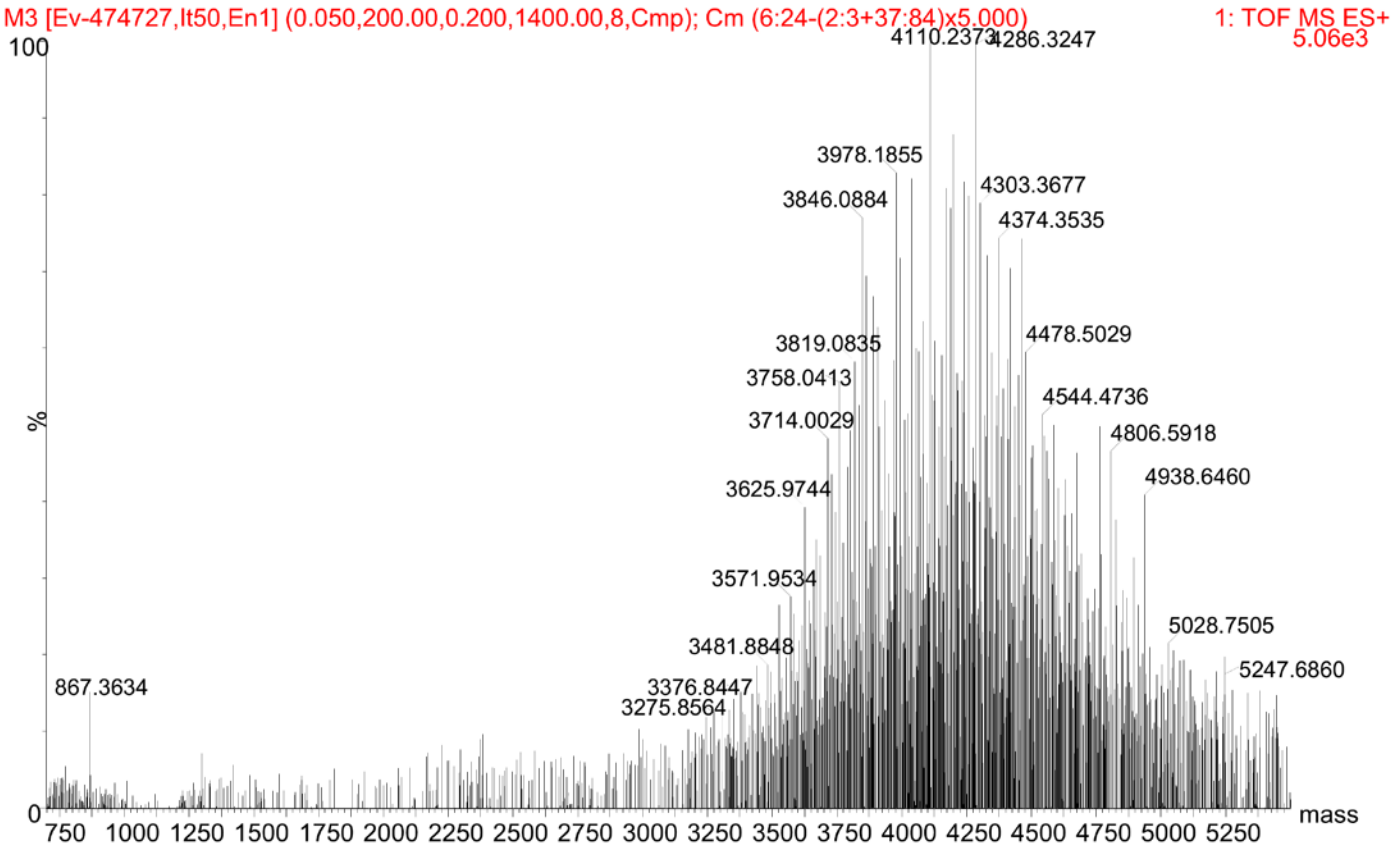

Appendix D.7 Confirmation of the acryloyl-PEG-RGDS conjufation by mass spectrometry.

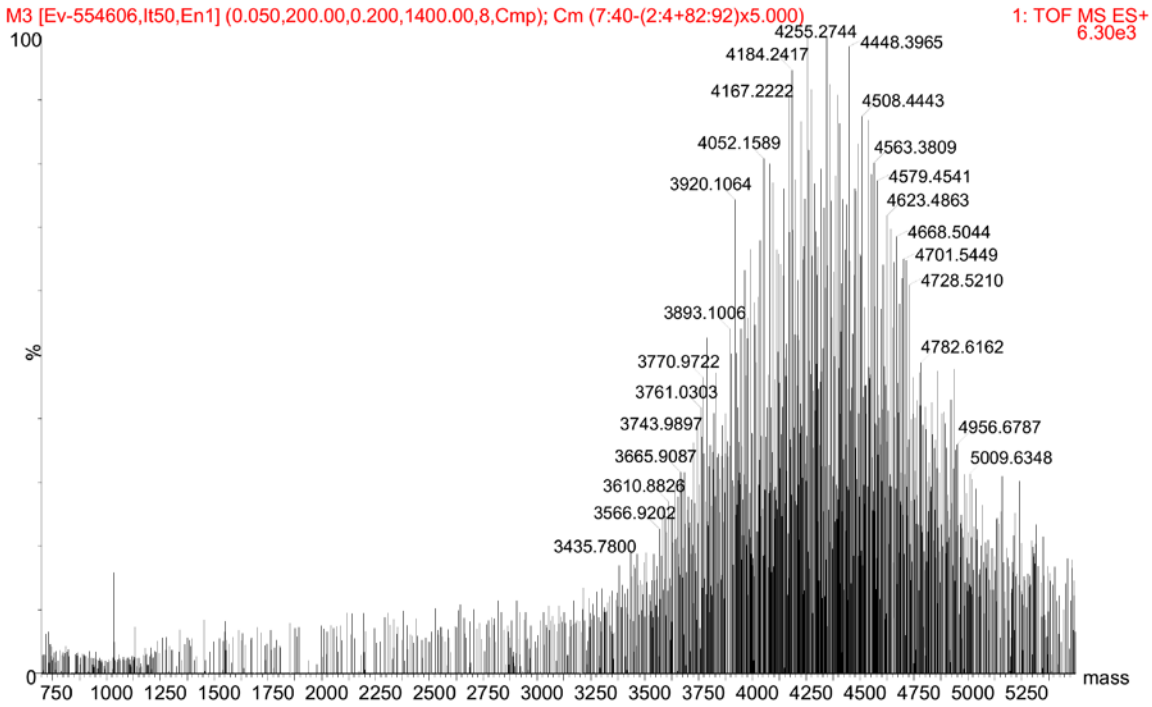

Appendix D.8 Confirmation of the acryloyl-PEG-REDV conjufation by mass spectrometry.

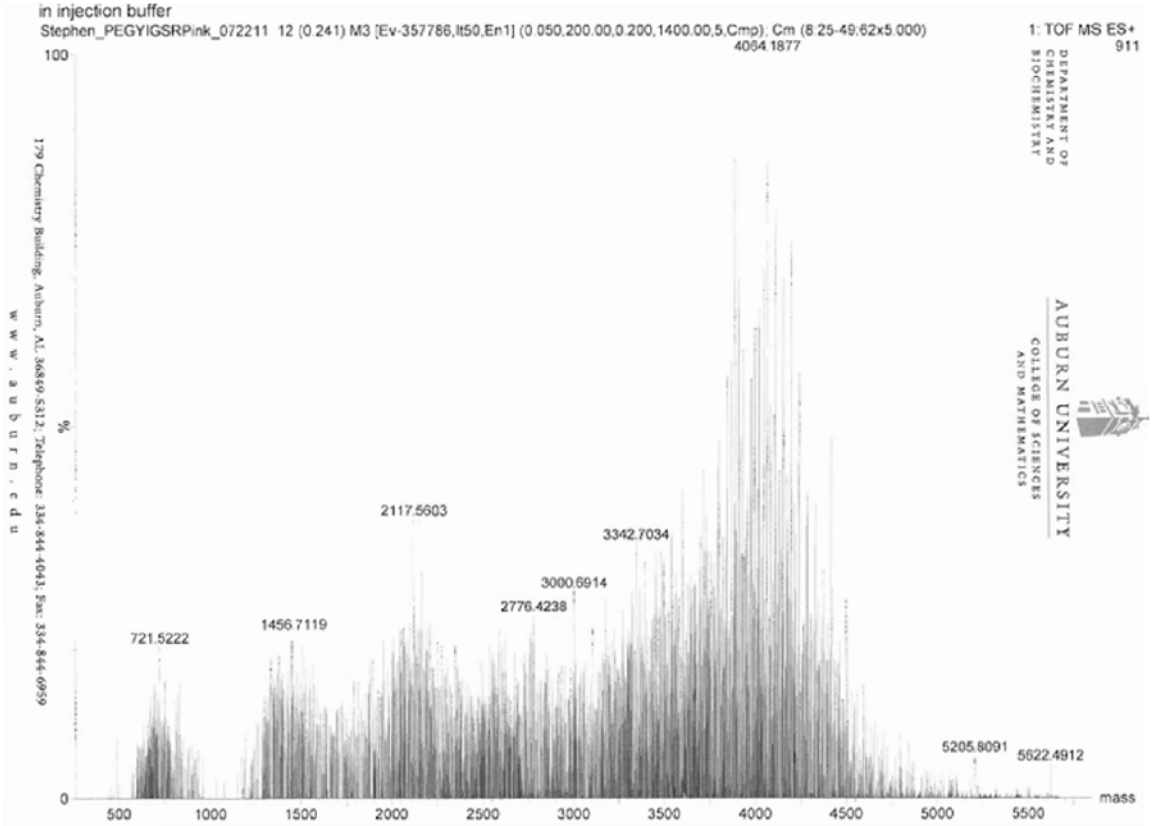

Appendix D.9 Confirmation of the acryloyl-PEG-YIGSRG conjufation by mass spectrometry.

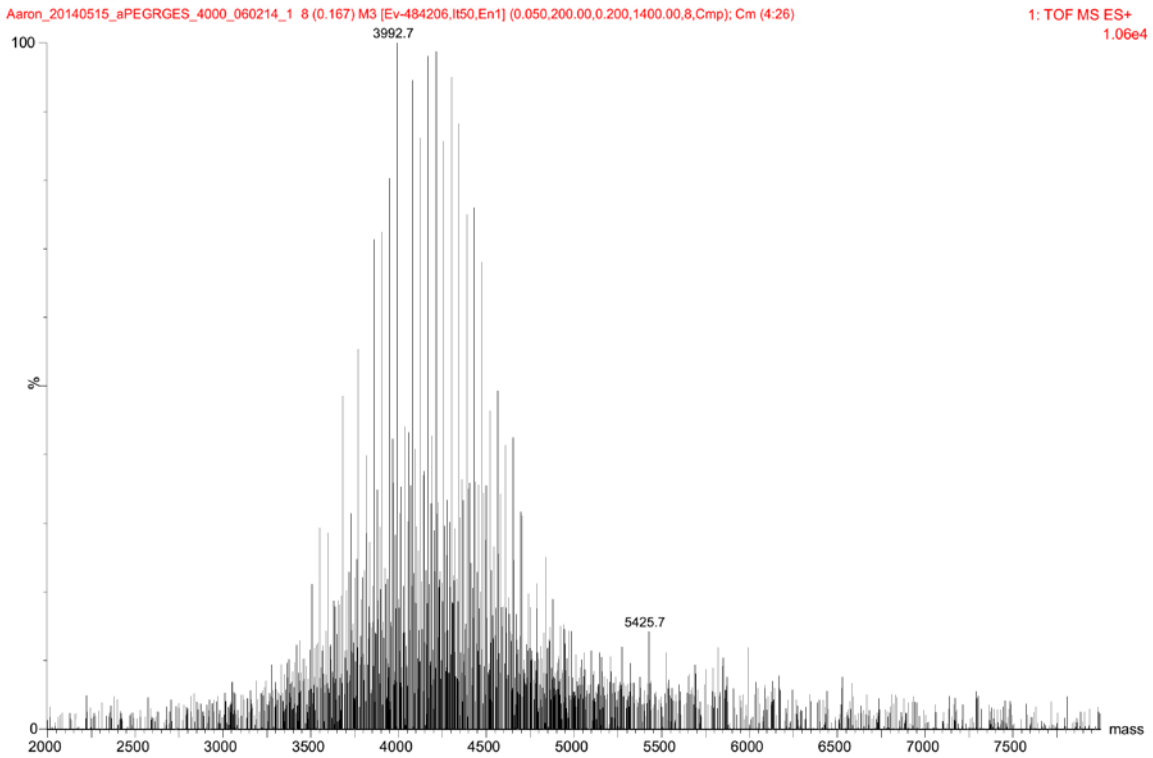

Appendix D.10 Confirmation of the acryloyl-PEG-RGES conjufation by mass spectrometry.

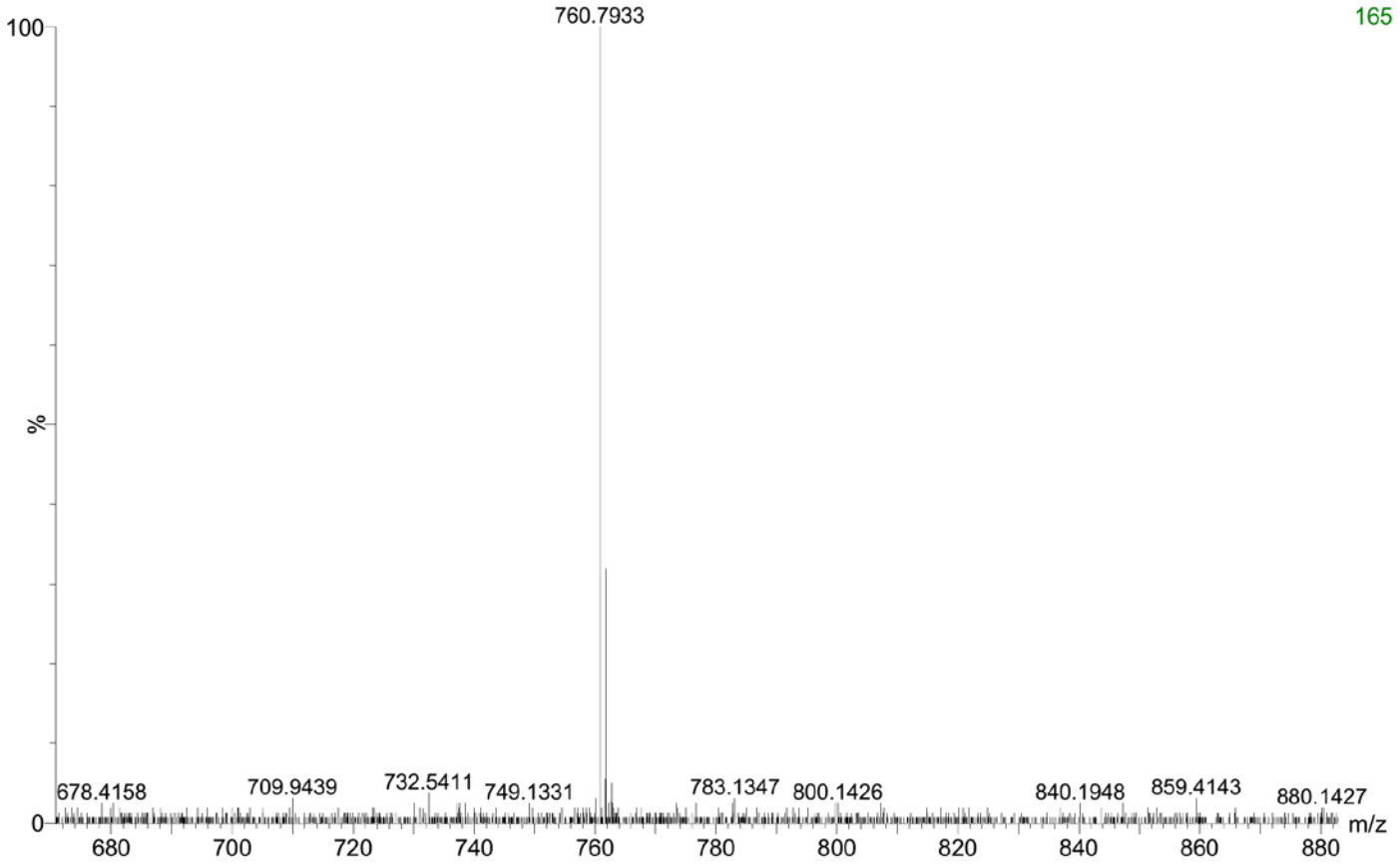

Appendix D.11 Confirmation of the synthesis of VILVLFG (A5-1) by mass spectrometry.

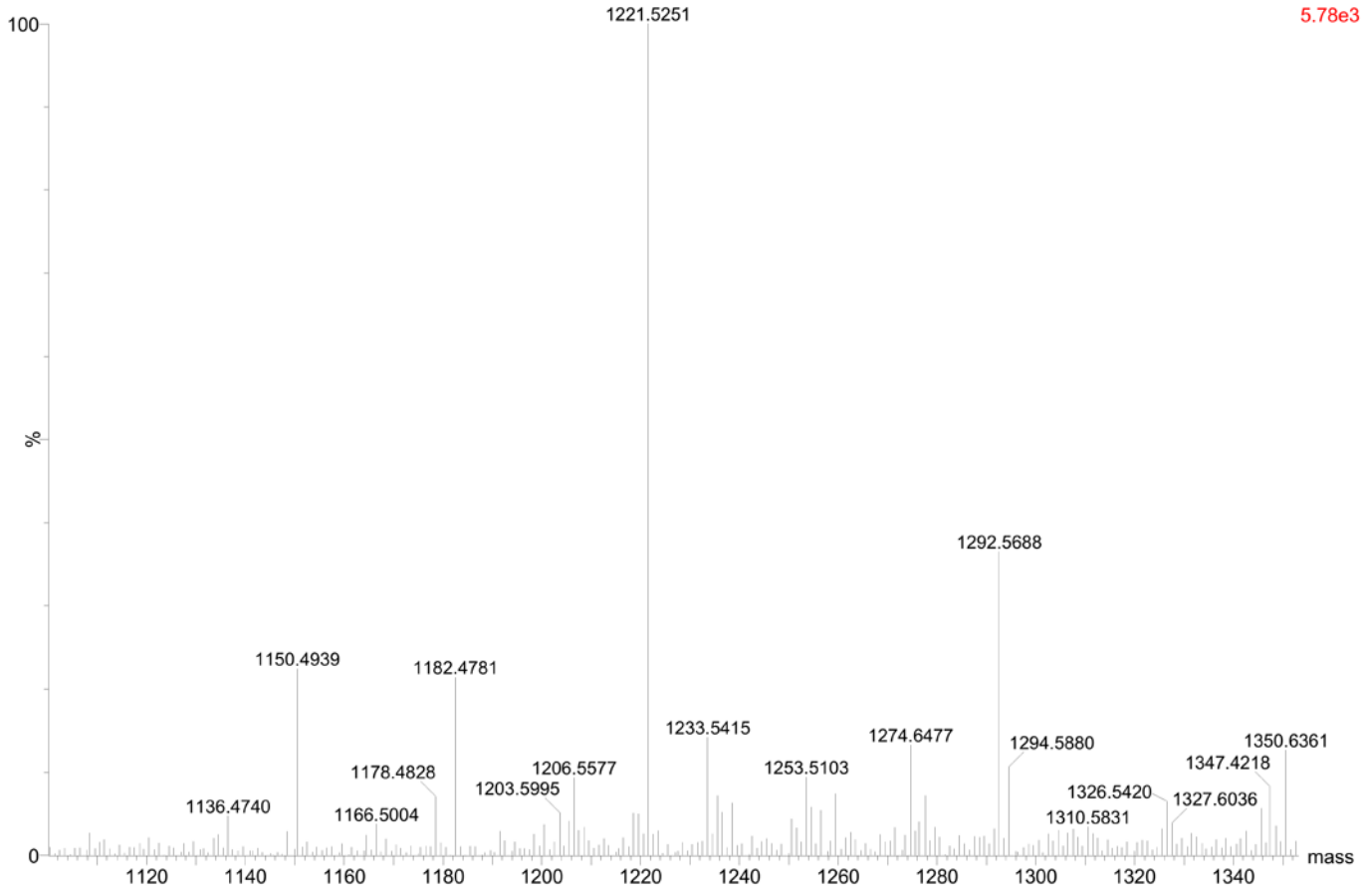

Appendix D.12 Confirmation of the synthesis of CRRETAWACG by mass spectrometry.

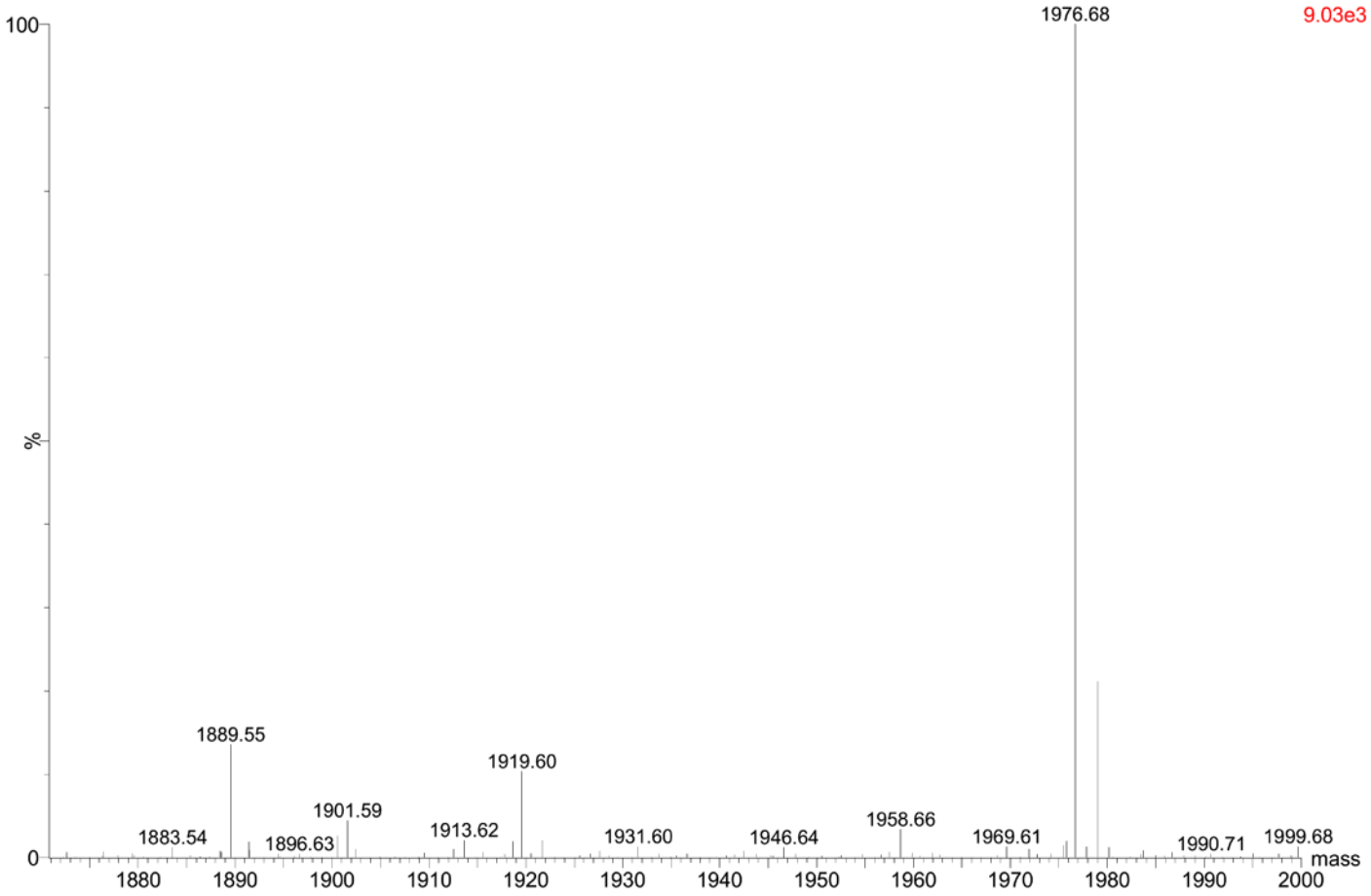

Appendix D.13 Confirmation of the synthesis of PRb by mass spectrometry.

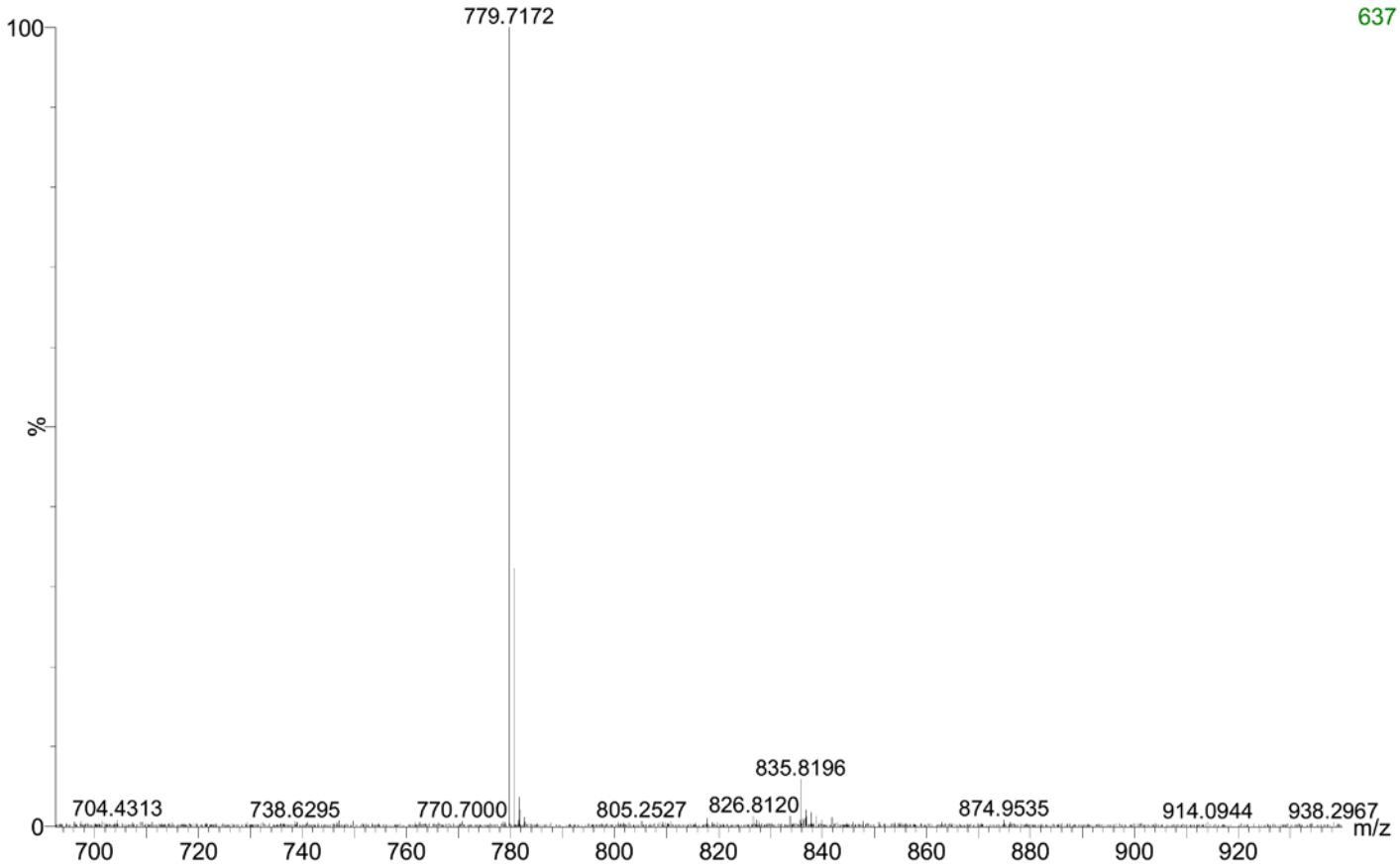

Appendix D.14 Confirmation of the synthesis of P11 by mass spectrometry.

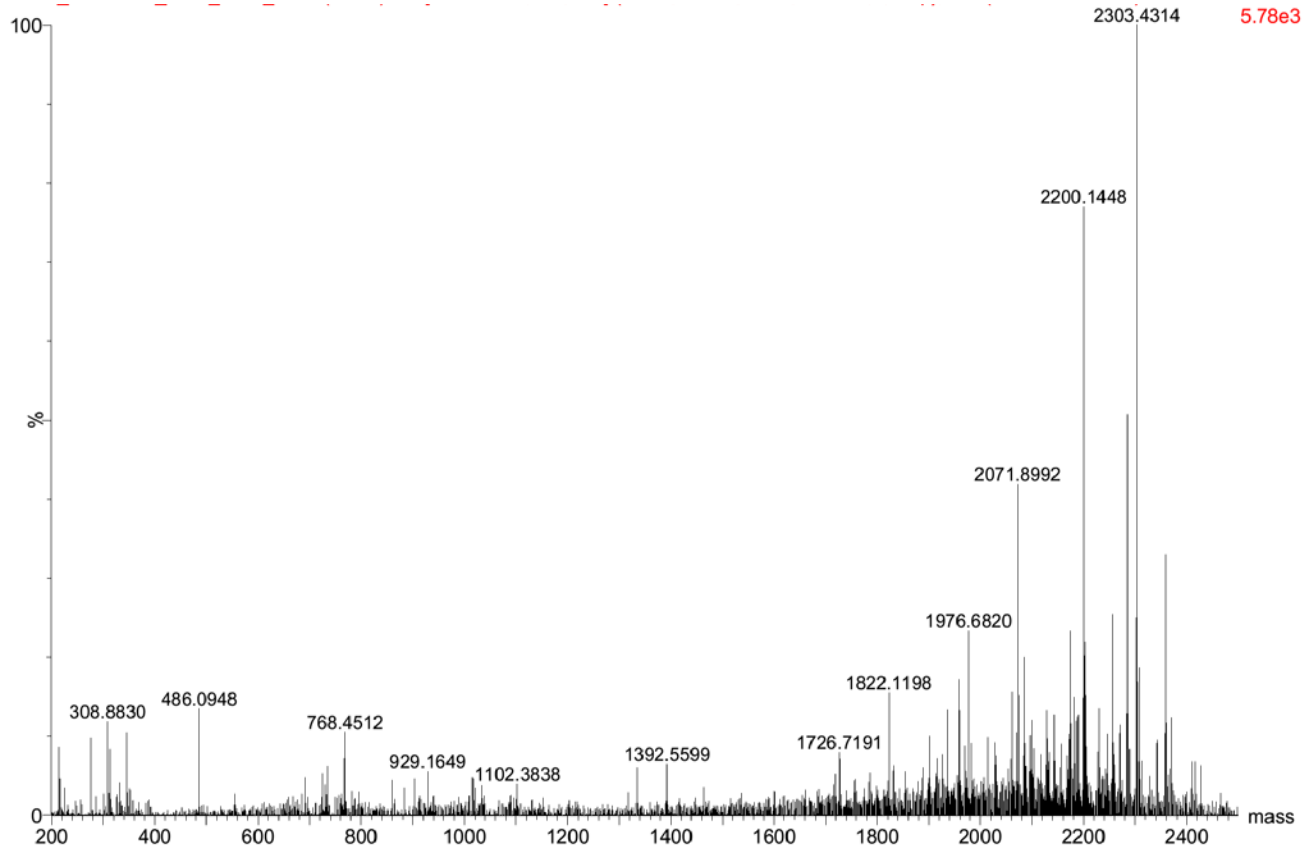

Appendix D.15 Confirmation of the synthesis of V2 by mass spectrometry.

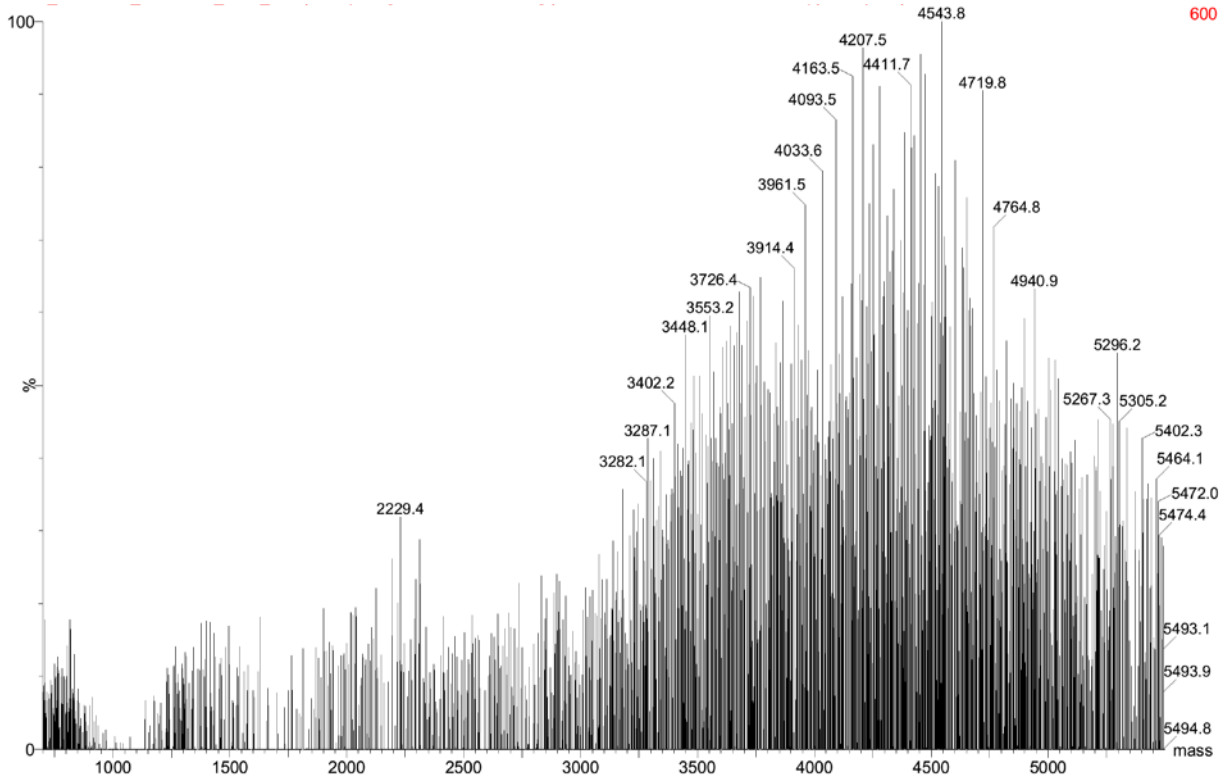

Appendix D.16 Confirmation of the acryloyl-PEG-P11 conjufation by mass spectrometry.

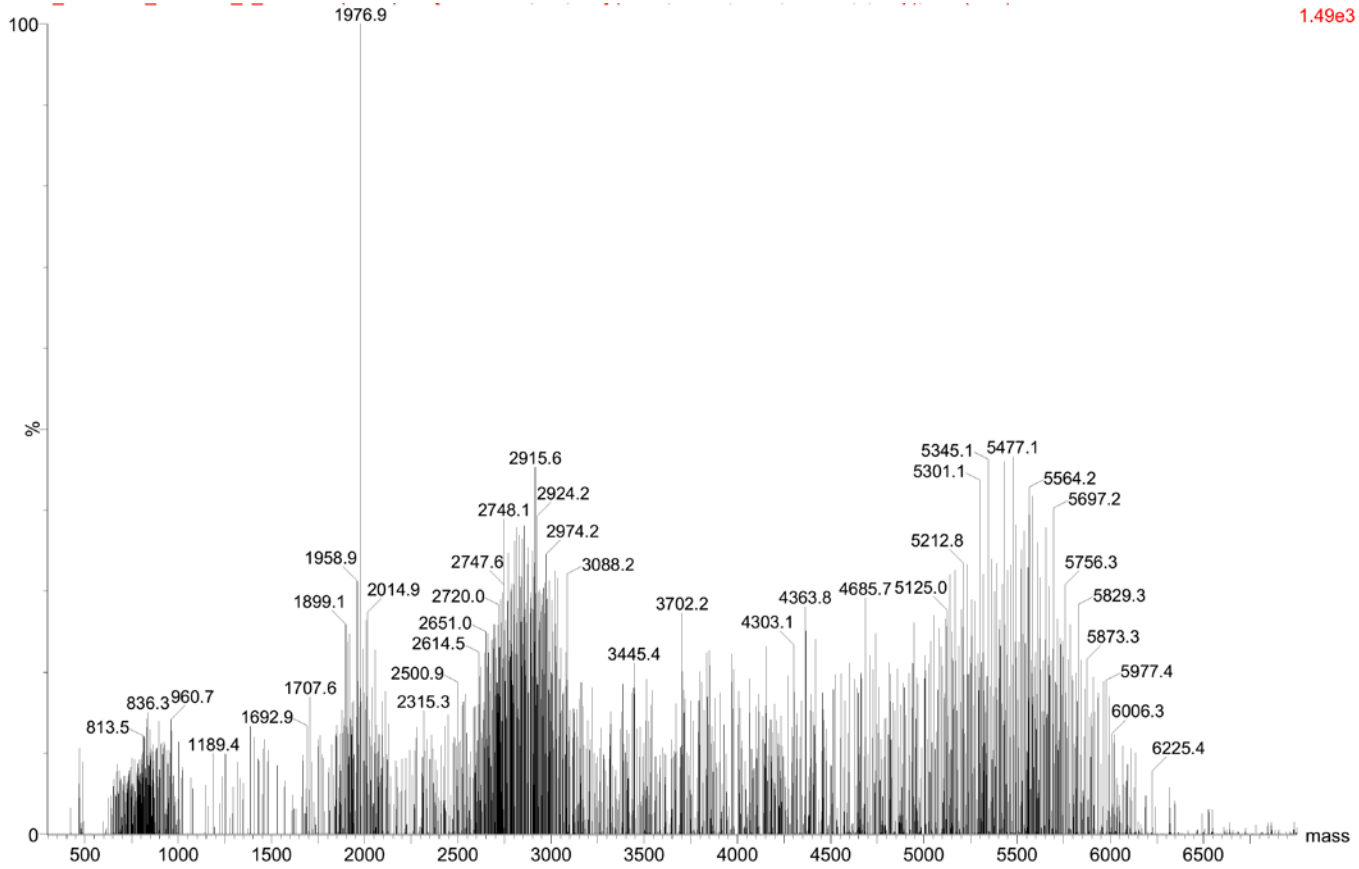

Appendix D.17 Confirmation of the acryloyl-PEG-PRb conjufation by mass spectrometry.

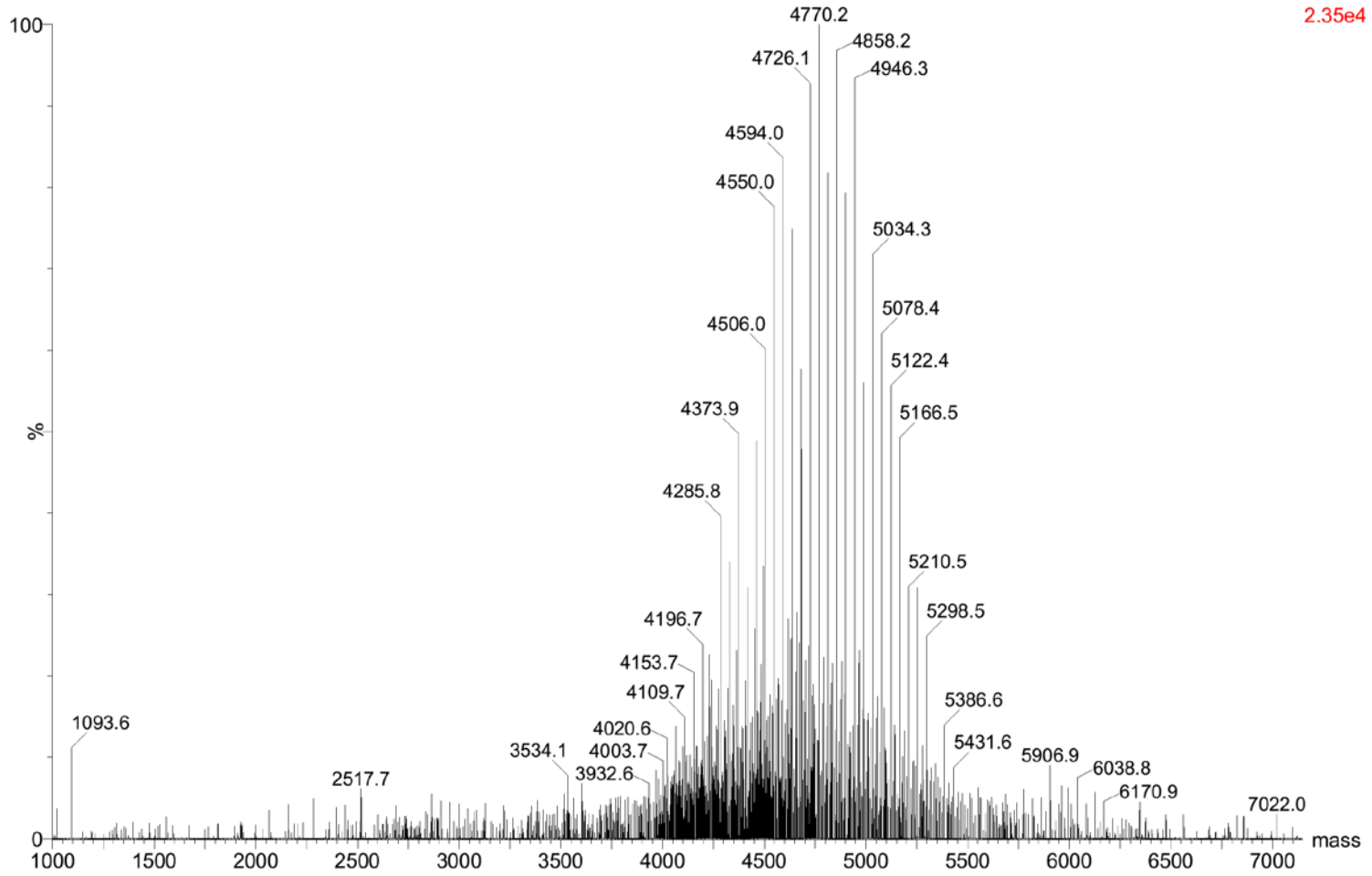

Appendix D.18 Confirmation of the acryloyl-PEG-CRRETAWAC conjufation by mass spectrometry.